DESIGN AND EVALUATION OF WALKING, SIT-TO-STAND, AND STAND-TO-SIT CONTROL STRATEGIES FOR A HIP-KNEE-ANKLE-FOOT PROSTHESIS WITH MOTORIZED HIP JOINT

Farshad Golshan

Thesis submitted to the University of Ottawa
in partial fulfillment of the requirements for the Doctor
of Philosophy in Biomedical Engineering

Ottawa–Carleton Institute for Biomedical Engineering
Faculty of Engineering
University of Ottawa

Abstract

Hip disarticulation (HD) amputation involves the removal of the entire lower limb and the hip joint, adversely affecting mobility and quality of life. Depending on their physical condition and life goals, some people with amputation are prescribed a hip-knee-ankle-foot (HKAF) prostheses to regain mobility. However, HKAF prostheses are known to have a high rejection rate compared to transfemoral and transtibial prostheses, primarily due to their excessive energy demands and the physical fitness required for effective use. Despite advancements in motorized prosthetic joints for the knee and ankle, innovation for HKAF prostheses has stagnated. This thesis addresses this gap by developing and evaluating adaptive control strategies for a motorized HKAF prosthesis to enhance mobility for HD amputees.

Based on preliminary mechanical development of the first viable motorized hip joint (Power Hip), this thesis developed and refined the electronics, sensors, and control system to enable people with hip level amputations to walk, sit, and stand. A prototype Powered Hip prosthesis was tested against a conventional passive prosthesis (Otto Bock Helix hip, C-Leg knee, Terion K2 foot) in a single HD participant. The Theia Markerless motion analysis system and Visual3D were used for kinematic and kinetic analyses. During walking, the Power Hip reduced pelvic tilt range from 22.77° ± 5.76° to 6.72° ± 1.49°, minimizing compensatory pelvic movements. Hip extension range improved from -0.22° ± 0.77° to -7.04° ± 2.85°, enabling a more natural stride by stabilizing the hip throughout the gait cycle. During sit-to-stand, ground reaction forces (GRF) on the prosthetic side increased from 0.30 ± 0.67 N/kg to 2.69 ± 0.34 N/kg, while stand-to-sit GRF rose from 4.28 ± 1.00 N/kg to 5.37 ± 0.52 N/kg. These enhancements improved load distribution, reducing intact-limb forces and aligning kinetic profiles more closely with transfemoral amputee patterns.

By achieving movement biomechanics comparable to transfemoral prosthesis users, this research reimagined what HKAF prostheses can achieve. This research lays the foundation for a new generation of user-friendly prosthesis that prioritize mobility, independence, and quality of life for people with hip-level amputations.

Co-Authorship

This dissertation contains material from four manuscripts (Chapters 4–7). The authorship is as follows:

- Chapter 4: F. Golshan, N. Baddour, H. Gholizadeh, and E. D. Lemaire, "A pelvic kinematic approach for calculating hip angles for active hip disarticulation prosthesis control," J Neuroeng Rehabil, vol. 20, no. 1, p. 152, Nov 9 2023, doi: 10.1186/s12984-023-01273-x.
- Chapter 5: F. Golshan, E. D. Lemaire, H. Gholizadeh, D. Nielen, and N. Baddour, “Design and preliminary evaluation of a gait control strategy for hip-knee-ankle-foot prosthesis with motorized hip joint”.
- Chapter 6: F. Golshan, N. Baddour, H. Gholizadeh, D. Nielen, and E. D. Lemaire, “Comparison of hip-disarticulation prosthesis gait between conventional and motorized hip joints”.
- Chapter 7: F. Golshan, E. D. Lemaire, H. Gholizadeh, D. Nielen, and N. Baddour, “Design and evaluation of stand-to-sit and sit-to-stand control protocols for a hip-knee-ankle-foot prosthesis with a motorized hip joint”

Farshad Golshan completed conceptualization, prototype development, design of the research, participant training, ethics document preparation, data acquisition, data analysis, and writing/revision of the manuscripts. In the thesis, Farshad Golshan is referred to as the author.

Acknowledgements

I would like to express my deepest gratitude to my supervisors, Prof. Edward Lemaire and Prof. Natalie Baddour, for their unwavering support and guidance throughout the years. Their expertise, encouragement, and constructive feedback have been instrumental in shaping this research and helping me navigate the challenges of academic work. I am truly grateful for their mentorship and dedication.

I extend my heartfelt thanks to Dr. Hossein Gholizadeh, whose technical expertise greatly helped this project. His insights and collaboration were invaluable in addressing prosthesis related issues and advancing the research forward. Additionally, I am deeply appreciative of the Power Hip research team; Yousef Bader, Kelly Brannen, Sarah Mroz, and Michael Botros for their tireless efforts in developing the prototype that served as the foundation for my study. Special thanks are also due to Mr. David Langlois from Össur R&D for his thoughtful design input and support in bringing this project to fruition. I am equally grateful to the entire team at Össur for their contributions, which played a critical role in the success of this endeavor.

I would like to acknowledge David Nielen at Nielen Prosthetics & Orthotics Clinic for his assistance with participant recruitment and his ongoing support during the research process. Furthermore, I am indebted to Mitacs and the Natural Sciences and Engineering Research Council of Canada (NSERC) for providing the financial resources necessary to carry out this work. Their funding enabled me to pursue this research with confidence and focus.

My sincere appreciation goes to research assistant Lucas Cho, for his exceptional contributions to optimizing the prototype design. His hard work and innovative thinking significantly enhanced the quality of the research outcomes. I also wish to thank Prof. Adrian Chan for granting access to the Abilities Living Laboratory at Carleton University, which provided an ideal environment for conducting experiments and gathering data. Finally, I would like to offer my most profound thanks to the volunteers who generously donated their time to participate in this research. Their involvement was essential to the success of this project.

To all those mentioned above, your support has been invaluable, and I am deeply grateful for your contributions to this journey.

Table of Contents

List of Figures

List of Tables

List of Abbreviations

AD	Ankle disarticulation
ADC	Analog to digital convertor
AI	Artificial intelligence
APA	Anticipatory postural adjustments
BLE	Bluetooth Low-Energy
COM	Center of mass
CTPAS	Canadian type prosthesis alignment system
DOA	Degree of asymmetry
DOS	Degree of symmetry
EMG	Electromyography
FOC	Field-oriented controller
FSM	Finite state machine
GI	Gait initiation
GRF	Ground reaction force
GT	Gait termination
GUI	Graphical user interface
HD	Hip disarticulation
HKAF	Hip-Knee-Ankle-Foot
HP	Hemipelvectomy
I2C	Inter-integrate circuit
IDS	Initial double support
IMU	Inertial measurement unit
PID	Proportional-integral-derivative
RMSE	Root means square error
ROM	Range of motion
SI	Symmetry index
SPI	Serial peripheral interface
SS	Single support
TDS	Terminal double support
TF	Transfemoral
TT	Transtibial
UART	Universal asynchronous receiver transmitter

Chapter 1: Introduction

1.1 Background

Lower extremity amputation is a surgical procedure that removes partial or major segments of lower limbs, hindering the person's ability to walk [1, 2]. Lower limb amputations include ankle disarticulation (AD), transtibial amputation (TT), transfemoral amputation (TF), hip disarticulation (HD), and hemipelvectomy (HP) [3]. HD and HP are the most extreme types of lower limb amputation and are achieved by complete removal of the foot, shank, thigh, hip joint, and a portion of the pelvis [4].

Compared to other lower-level amputations, people with HD or HP often have a much higher degree of disability [5]. The lack of neuromuscular control can make the rehabilitation and prosthetic fitting process difficult, especially for the elderly [5]. Due to major lower extremity muscle removal, the extent of HD amputee control over their Hip-Knee-Ankle-Foot (HKAF) prosthesis is often limited to the pelvis and lumbar spine motion. Therefore, HKAF prosthetic users must expend much greater energy (>80%) to ambulate, climb stairs, or stand up from a chair when compared to other lower-level prosthetic users and able-bodied individuals [6]. In addition, before complications that lead to amputation, people with HD and HP amputations often have malignant tumours, ischemia, diabetes, or severe infections that adversely affect their health and physical fitness, further affecting their ability to operate a prosthesis [4, 6, 7].

Over the years, various fitting processes and prostheses have been introduced to help people with HD and HP regain their ability to walk [5]. Ottobock Helix3D is the most advanced hip joint for HD and HP currently available [8]. Paired with a microprocessor-controlled prosthetic knee, the passive Helix3D provides hydraulic control of hip flexion during swing and some control during stance [9]. Compared to existing hip prostheses in the market, which are all passive joints, Helix3D prostheses have greater hip angle extension to flexion range and reduced sagittal pelvic tilt required to swing the hip [10].

Despite these advancements, Helix3D users exhibit significant functional limitations relative to other lower-limb amputees and able-bodied individuals [10-12]. These include heightened metabolic demands during ambulation, reduced endurance for long-distance walking, challenges navigating sloped surfaces, and restricted hip range of motion, culminating in abbreviated stride lengths and slower gait velocities. Furthermore, the prosthesis offers no functional support during sit-to-stand or stand-to-sit transitions, necessitating complete reliance on the intact limb [13].

1.2 Motivation

People with HD or HP amputations require greater physical fitness levels to use a prosthesis and have limited prosthetic options, which can often lead to prosthesis rejection [14]. However, new studies inspired by recent advancements in prosthetic actuation technologies are emerging to address limitations of hip prostheses by replacing hydraulic and mechanical prosthetic joints with active actuators [15-17]. Unlike fully mechanical (passive) or microprocessor controller dampening (semi-active) prostheses, motorized (active) prostheses can reduce the physical demand required to operate prostheses by providing the necessary joint torque for stable walking [18].

Although the active prosthesis research field is yet to mature fully, early studies demonstrated that, despite the added weight, active transfemoral prostheses have significant advantages over passive and semi-passive prostheses [19-21]. These advantages include fewer falls and stumble recovery [19], more symmetrical loading during ascending and descending ramps and stairs [20], and improved walking biomechanics that closely resembles able-bodied biomechanics [21, 22]. Even though both semi-active and active knee prostheses are controlled by microcontrollers, unlike semi-active prostheses that operate on a net negative torque control principal, active prostheses operate by inducing both net negative and positive torque at the joint. Therefore, semi-active prosthesis control methods can not be directly applied to active prostheses [16].

The control strategy is the method that enables prosthetic users to interact with and control the active prosthesis with consideration for their capabilities and limitations. A control strategy is implemented by software installed on a prosthetic microcontroller [23]. This software can monitor user and prosthesis states using real-time sensors and then process the needed joint actuation. As prosthetic and rehabilitation actuation technologies become more common, several studies have presented different control strategies for TF motorized prostheses and exoskeleton rehabilitation robotics [24-29]. However, despite the benefits of these advancements, a similar research trend is absent in the active hip prosthesis control field.

The lack of robust control strategies for active hip prostheses has hindered both research advancements and the potential commercialization of these devices [30]. However, recently, a research team at the University of Ottawa developed a prototype motorized HKAF prosthesis, which underwent initial testing to validate its design integrity [31, 32]. Building on this foundation, the research in this thesis focused on developing user-friendly control strategies, conducting structured experiments with HD participants, and quantifying the performance of the motorized hip joint. This research seeks to assess the viability and potential of motorized HKAF prostheses as a

practical alternative to passive designs, paving the way for improved mobility solutions for HD amputees.

1.3 Objectives

The objectives of this thesis were to develop and assess motorized HKAF prosthesis control strategies to assist HD amputees walk, sit, and stand. These specific objectives are as follows:

1. Develop a motorized HKAF prosthesis control strategy for gait initiation, termination, and level walking.
2. Develop a motorized HKAF control strategy for sit-to-stand and stand-to-sit transitions.
3. Quantify prototype and control strategy performance by comparing walking with the prototype to walking with the participant's prescribed mechanical HKAF prosthesis.
4. Quantify chair sitting and standing performance by comparing prototype performance to the performance of the participant's prescribed mechanical HKAF prosthesis.

1.4 Contributions

1. **Identification of pelvic movement patterns as predictive factors for hip kinematics:** This research established that specific pelvic movement patterns significantly correlate with hip kinematics during gait. These patterns were validated as predictive factors for desired hip motion, offering a novel biomechanical framework to enhance predictive modeling in prosthetic control systems.
2. **Development of the first viable motorized HKAF control system for HD amputees:** The thesis presents the first series of functional control systems enabling individuals with hip disarticulation to achieve seamless ambulation, sitting, and standing transitions using a motorized HKAF prosthesis. Biomechanical analysis combined with qualitative participant feedback demonstrated reduced compensatory upper-body movements and improved locomotor efficiency.
3. **Creation of a clinician-focused software platform for Power Hip configuration:** A novel software interface was engineered to enable clinicians and rehabilitation engineers to visualize real-time prosthesis sensor data, streamline device setup, and personalize control parameters for powered hip users.

1.5 Thesis outline

The thesis is organized as follows:

- Chapter 2 presents a literature review of existing methods for gait biomechanics analysis and relevant research on control strategies for active lower extremity prostheses.
- Chapter 3 details the development of the Power Hip prototype, instrumentation, and back-end software architecture.
- Chapter 4 adapted from the published journal article "A pelvic kinematic approach for calculating hip angles for active hip disarticulation prosthesis control", introduces a model to estimate prosthetic hip rotation trajectories using pelvic movement data and ground reaction forces.
- Chapter 5 adapted from the submitted publication "Design and preliminary evaluation of a gait control strategy for hip-knee-ankle-foot prosthesis with motorized hip joint," describes the gait control strategy algorithm developed for the Power Hip prototype. This chapter evaluates the algorithm's ability to adapt to user-desired gait speeds by comparing kinematic outcomes to those of TF amputees.
- Chapter 6 adapted from the to-be submitted publication "Comparison of hip-disarticulation prosthesis gait between conventional and motorized hip joints," quantifies performance differences between the Power Hip and conventional hip-knee-ankle-foot (HKAF) prostheses using gait laboratory functional tests.
- Chapter 7 adapted from the to-be submitted publication "Design and evaluation of stand-to-sit and sit-to-stand control protocols for a hip-knee-ankle-foot prosthesis with a motorized hip joint," presents control strategies for sit-to-stand and stand-to-sit transitions. A comparative study evaluates performance differences between the Power Hip and a conventional HKAF prosthesis during these movements.
- Chapter 8 concluded the thesis by summarizing its contributions and discussing potential directions for future research.

Chapter 2: Literature review

2.1 Hip disarticulation prostheses

A hip disarticulation prosthesis is a type of lower extremity prosthesis used by people with amputation at the hip joint level and is comprised of a prosthetic hip, knee, ankle and foot. These prostheses are often referred to as HD or HKAF prostheses [33]. The history of modern HD prostheses can be traced back to the early 20th century. The saucer-type (Fig. 2.1A) and tilting table prostheses (Fig. 2.1B) were eventually replaced due to poor stability and functionality [34]. These designs consisted of a rigid socket that encased the pelvis and a single-axis hip joint that allowed only flexion and extension movements.

In 1954, McLaurin published his first report on the Canadian hip disarticulation prosthesis. This design featured a prosthetic hip joint mounted anteriorly on the socket and below the level of the anatomical hip joint (Fig. 2.1C) [34]. Compared to existing prostheses at the time, this design improved gait biomechanics by improving overall gait stability and functional reliability [35]. Since then, various modifications and improvements have been made, such as adding a shoulder strap for suspension, using different types of feet and knee systems, adjusting the length and alignment of the prosthesis, and incorporating a hydraulic damper for better control [5].

Despite these advances, hip disarticulation prostheses still face challenges and limitations regarding user comfort, mobility, appearance, cost, and acceptance [35]. Some common problems reported by HD users are skin irritation, exhaustion after short walking sessions, limited range of motion, and high cost [14]. These factors affect the quality of life and psychological well-being of HD users and may lead to low prosthesis use or abandonment [35]. Therefore, further research and development are needed to address these issues and provide better solutions for HD users.

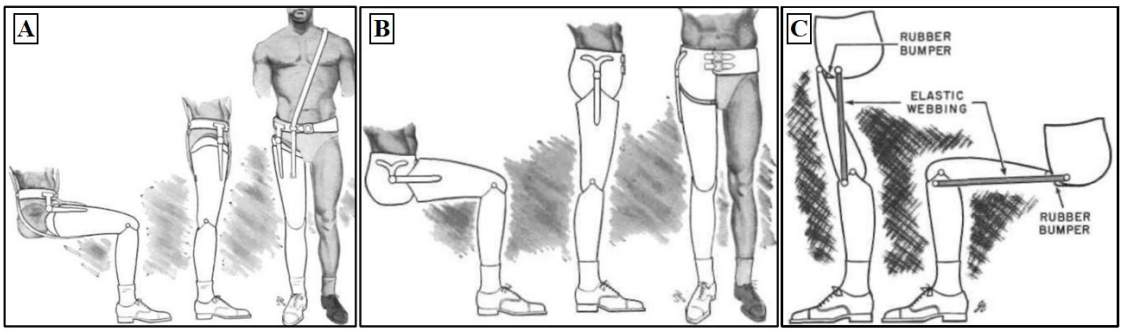

Fig. 2.1 Evolution of hip disarticulation prostheses, A: saucer-type prosthesis, B: Tilting-table prosthesis, C: Canadian-type hip prosthesis [34].

2.1.1 Canadian type hip prosthesis components

Canadian type hip prosthesis components are similar to other lower limb prostheses but may vary depending on the amputation level and user needs. Generally, they include a socket, hip joint pylon, knee joint, and foot system. In addition, other optional components such as offsets, adapters, liners, vacuum pumps, etc., may enhance prosthesis fit, function, or appearance (Fig. 2.2) [33].

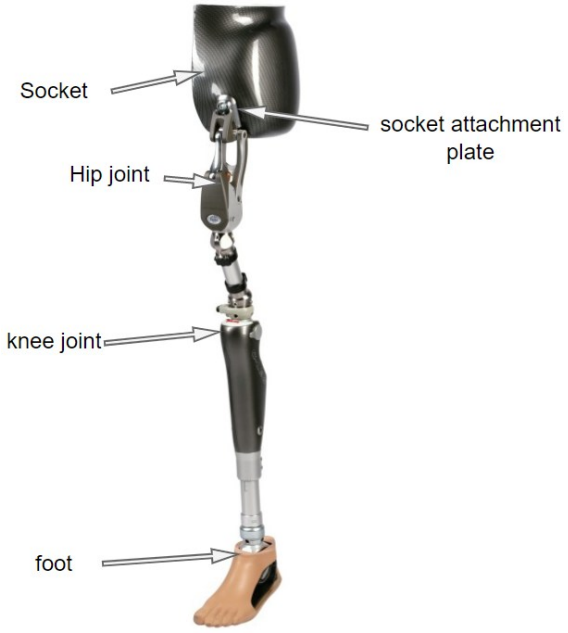

Fig. 2.2 An example of a complete HKAF prosthesis (www.ottobock.com).

The prosthetic socket is a plastic receptacle that fits over the residual limb and connects the body to the prosthetic components. The prosthetic hip joint is mounted anteriorly on the socket, allowing hip flexion and extension and level sitting. The pylon is a metal rod that connects the hip joint to the knee joint. The prosthetic knee joint allows knee flexion and extension. The prosthetic foot may be a solid ankle cushion heel, dynamic response foot, or other types, providing shock absorption, energy return, and stable standing.

Prosthetic knee systems use passive (Fig. 2.3A), semi-passive (Fig. 2.3B), or active (Fig. 2.3C) control methods to simulate normal biological knee function for individuals with transfemoral amputation [36]. Prosthetic knee systems include single-axis, multi-axis, hydraulic, pneumatic and microprocessor-controlled designs. Each type has advantages and disadvantages regarding stability, mobility, cost and maintenance. However, with advancements in prosthetic and sensor technologies, microprocessor-controlled knee prostheses have overtaken the market due to their effective gait control adaptability, and design flexibility [8].

Fig. 2.3 Prosthetic knee joints, A: polycentric passive knee, B: microprocessor controlled adaptive dampening single axis knee (semi-passive), C: microprocessor controlled active (motorized) single axis knee (www.ossur.com).

Unlike prosthetic knees, all commercially available hip joints are fully passive and have had slow technological advances compared to prostheses for lower levels of amputation. This is likely due to the combination of the following factors [33]:

- Since walking with an HKAF prosthesis is energy-demanding, the prosthesis must be lightweight. However, the benefits of a more complex passive hip joint may not compensate for the additional weight and increased energy demand.
- A very small number of people with lower limb amputations use HKAF prostheses, so there is minimal business incentive for expensive research and development.
- Engineering the whole limb control strategy can be challenging compared to transfemoral prostheses.

In the past, HD amputees were often fitted with simple single-axis hip joints to keep the overall prosthesis weight minimal (Fig. 2.4A). However, in 2008, Ottobock introduced a passive 4-bar linkage (polycentric) prosthetic hip joint equipped with passive hydraulics (Fig. 2.4B) [37]. Interestingly, despite the added weight, users felt more mobile and comfortable using the new hip joint than the Ottobock single axis 7E7 hip joint [10].

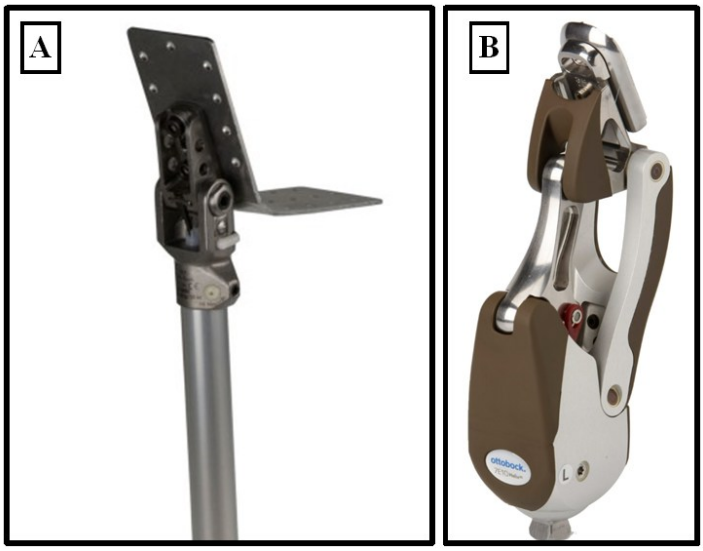

Fig. 2.4 Canadian type prosthetic hip joints, A: 7E7 single-axis hip joint, B: Helix 3D polycentric hip joint (shop.ottobock.ca).

2.1.2 Canadian-type hip prosthetic alignment

The Canadian-type Prosthesis Alignment System (CTPAS) is a commonly used approach for aligning HD prostheses. This system was first developed by Canadian prosthetist Robert LeBlanc in the early 1970s and has since become widely accepted for prosthetic alignment in Canada and elsewhere [5]. CTPAS provides amputees with a stable and functional prosthetic limb that closely mimics the motion and function of a natural hip joint. This is achieved by aligning the prosthetic components to distribute weight and provide a stable base of support for the amputee.

The CTPAS approach involves several key considerations, including the following [33]:

- Socket alignment: The prosthetist begins by aligning the prosthetic socket with the amputee's pelvis. This is done by ensuring the socket is level and aligned with the pelvis.
- Thigh alignment: The prosthetic thigh pylon is aligned with the socket by adjusting the pylon length to match the intact thigh length. The angle is adjusted such that the projected line from the thigh pylon passes 25 to 50 mm behind the prosthetic foot (Fig. 2.5).
- Knee alignment: After prosthetic thigh alignment, the prosthetic knee is aligned parallel to the intact knee and perpendicular to level ground.

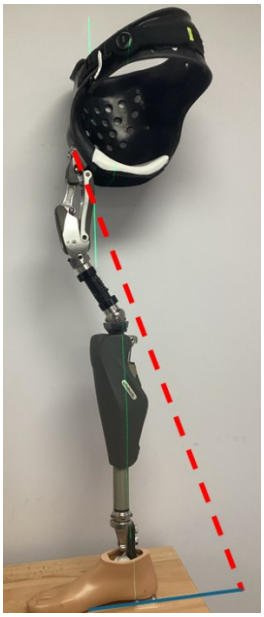

Fig. 2.5 Canadian-type hip prosthesis alignment.

2.2 Gait biomechanics

Human gait is a cyclical activity achieved through complex interactions between body segments [38]. Systematic gait analysis segments gait behaviour into periods, tasks, and phases [39]. This approach has consistently been used in research and medicine to characterize gait dynamics and diagnose pathologies [38]. Ideal gait is divided into the cyclical stance and swing phases (Fig. 2.6). "Stance" is the phase during which the ipsilateral (the side of interest or observed) foot has contact with the ground (0 to ~60% of the gait cycle) and "swing" is the phase where the ipsilateral foot is in the air (~60% to 100% of the gait cycle [38]).

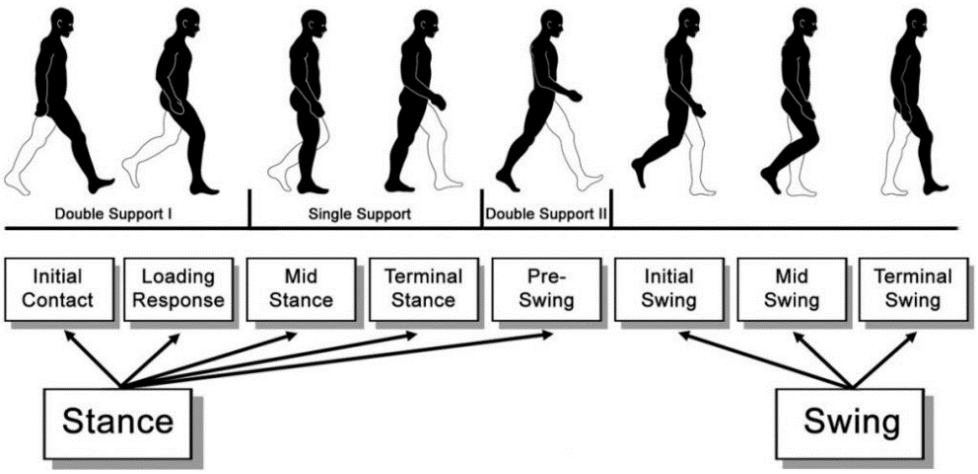

Fig. 2.6 Gait cycle division [40].

Stance phase is further divided into multiple sub-phases. Initial contact is the instance where the foot contacts the ground and initiates stance phase. Initial contact is followed by weight acceptance, when body weight transfers from the contralateral limb (opposite limb) to the ipsilateral limb (0 to ~8% of the gait cycle). Midstance is when the body progresses forward while only the ipsilateral limb has contact with the ground and the contralateral limb is swinging forward (~8% to ~50% of the gait cycle). Stance phase is concluded during terminal stance where body weight is transferred from the ipsilateral to the contralateral limb (~50% to ~60% of the gait cycle) [38, 41].

Swing phase has three sub-phases: initial swing, mid-swing, and terminal swing. Initial swing is forward movement of the limb to reach the desired step length. Mid-swing is elevation of the foot to avoid contact with the ground or uneven terrain. Terminal swing is adjustment of limb posture and orientation to prepare for foot strike and weight acceptance [38, 41].

2.2.1 Motion capture technologies and methods

Kinematic gait analysis is commonly performed using marker-based optical motion capture techniques [42]. However, in recent years, markerless motion capture technologies have become popular due to their convenience for participants and researchers since minimal preparations are needed prior to data collection and multiple people can be tracked simultaneously [43]. THEIA 3D is a markerless 3D motion capture system that provides high precision in tracking body segment movements, with robust applications in sports biomechanics, gait analysis, and clinical assessments [44]. Studies demonstrated its reliability in identifying key kinematic markers for postural pathology diagnosis and tracking complex and fast athletic movements [45, 46]. When compared with other markerless systems, such as OpenPose or DeepLabCut, THEIA 3D is gaining traction for its ease of use, adaptability, and provision of 3D data [47]. While open-source systems like OpenCap are also popular due to their accessibility, THEIA 3D's accuracy and specific use in clinical gait analysis and sports assessments make it a strong contender [48].

Regardless of the motion capture technology used, transforming motion capture data into joint kinematics involves a structured pipeline that integrates biomechanical modelling and computational analysis. Initially, motion data is acquired through either marker-based systems like Vicon or markerless systems such as THEIA 3D. Marker-based systems use reflective markers placed on anatomical landmarks, while markerless systems rely on advanced AI algorithms to detect key points directly from video or depth sensor data (Fig. 2.7).

After data acquisition, a biomechanical model is created, representing the human body as rigid segments connected by joints [49]. This model is scaled to match the person’s anthropometry using

calibration trials or anatomical measurements. Each marker or key point is assigned to a corresponding segment, laying the groundwork for trajectory reconstruction [50]. Smoothing filters, like Butterworth or Kalman filters, are applied to interpolate and clean any noisy data. Then inverse kinematics calculations are performed by optimizing the alignment between the observed marker or key point positions and the skeletal model [51]. A Joint Coordinate System (JCS) is defined for each joint, allowing for the calculation of relative joint orientations for degrees of freedom such as flexion/extension and rotation. The output includes joint angles, velocities, and accelerations, which are further validated against known benchmarks or gold-standard datasets.

Markerless systems like THEIA 3D provide advantages by reducing setup time and eliminating the need for markers. However, they face challenges such as skin artifacts and noise, which can be mitigated using AI-driven models [46].

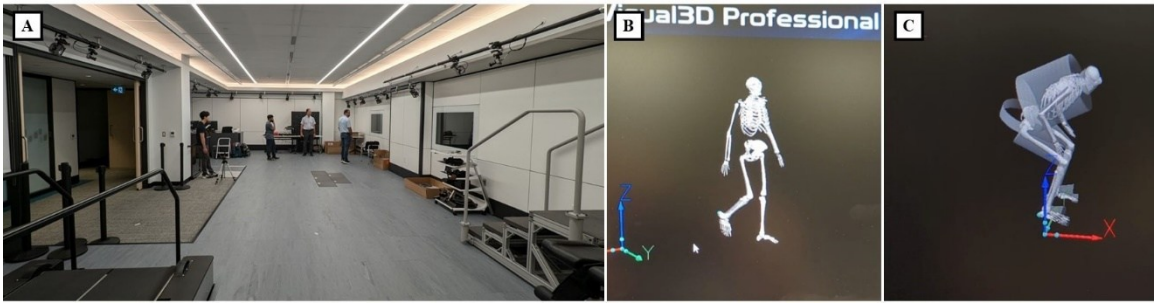

Fig. 2.7 THEIA 3D markerless system at Carleton University Abilities Living Lab. A: Motion capture room, B: Pose estimation of normal gait captured by THEIA 3D (2023.1.0.3161) and visualized by Visual3D (version 2024.11.2), C: Pose estimation of sit-stance-sit transition capture by THEIA 3D and processed by Visual3D.

2.2.2 Knee kinematics

In able-bodied individuals (Fig. 2.8A), the knee flexes approximately 25° as the foot contacts the ground (start of double support) to absorb impact and then extends as body weight is transferred to the contralateral side [52]. During swing phase, the knee flexes (60° maximum) to allow the foot to clear the ground and then extends again to prepare for the next stance phase. As a result, knee flexion-extension can have two distinct peaks for each gait cycle.

For TF and HD amputees, the prosthetic knee is designed to stay in extension during stance to provide stability and avoid knee collapse (Fig. 2.8B) [53]. As the prosthetic user approaches the end of stance phase, body weight is transferred from the prosthetic side to the intact side. Thus, the prosthetic knee flexion resistance is removed in preparation for the prosthetic foot to swing. Despite the difference in amputation level, knee angle curves of people with HD and TF amputations have

similar shapes (Fig. 2.8B and Fig. 2.8C). This similarity may be attributed to the use of similar prosthetic knee and foot components.

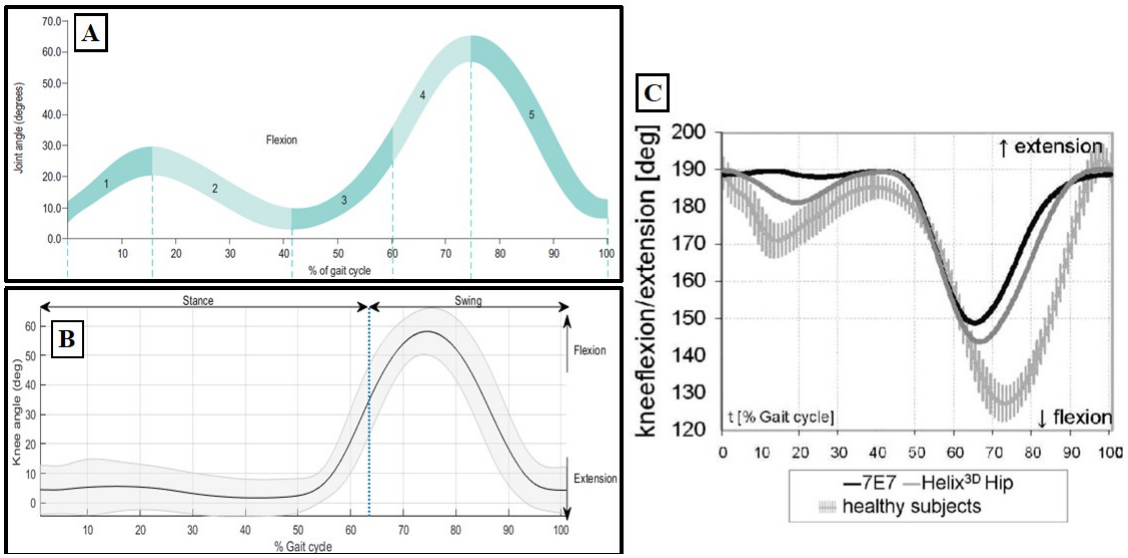

Fig. 2.8 Knee kinematics during gait, A: able-bodied persons [52], B: TF amputee with passive and semi-passive prostheses [54], C: comparison of able-bodied and HD amputees with 7E7 and Helix 3D passive hip prostheses [10] (Permission from Wolters Kluwer Health, Inc).

2.2.3 Hip kinematics

Similar to knee kinematic analysis, hip flexion/extension are typically analyzed since these are the primary hip movements during many functional activities such as walking [55]. However, hip kinematic analysis of activities that require active balancing, such as jumping, will also require analysis of abduction/adduction and internal/external rotation [56].

During stance, the hip joint extends, moving the body forward. Then, approaching 50 to 60% of the gait cycle, hip rotation direction changes from extension to flexion and continues flexing until the end of the gait cycle [55]. Comparing able-bodied (Fig. 2.9A) and TF (Fig. 2.9B) individuals, TF prosthetic users tended to have much faster hip flexion [57] as a compensatory effort to flex the prosthetic knee for proper prosthetic foot to ground clearance during swing. As a result, TF hip extension-to-flexion motion often coincides with prosthetic knee extension to flexion through chained kinematics (Fig. 2.8B and Fig. 2.9B) [57].

HD amputees exhibit reduced flexion and extension range of motion during gait compared to able-bodied and TF populations, partly due to prosthetic joint design considerations (Fig. 2.9C) [58, 59]. Since commercially available hip prosthesis systems are passive, hip extension is purposefully limited by design to keep the load line behind the hip joint centre of rotation

throughout the gait cycle. This restriction would enable the HKAF prosthesis user to swing the prosthesis forward during stance by performing a forward pelvic tilt (Fig. 2.9D) or circumduction.

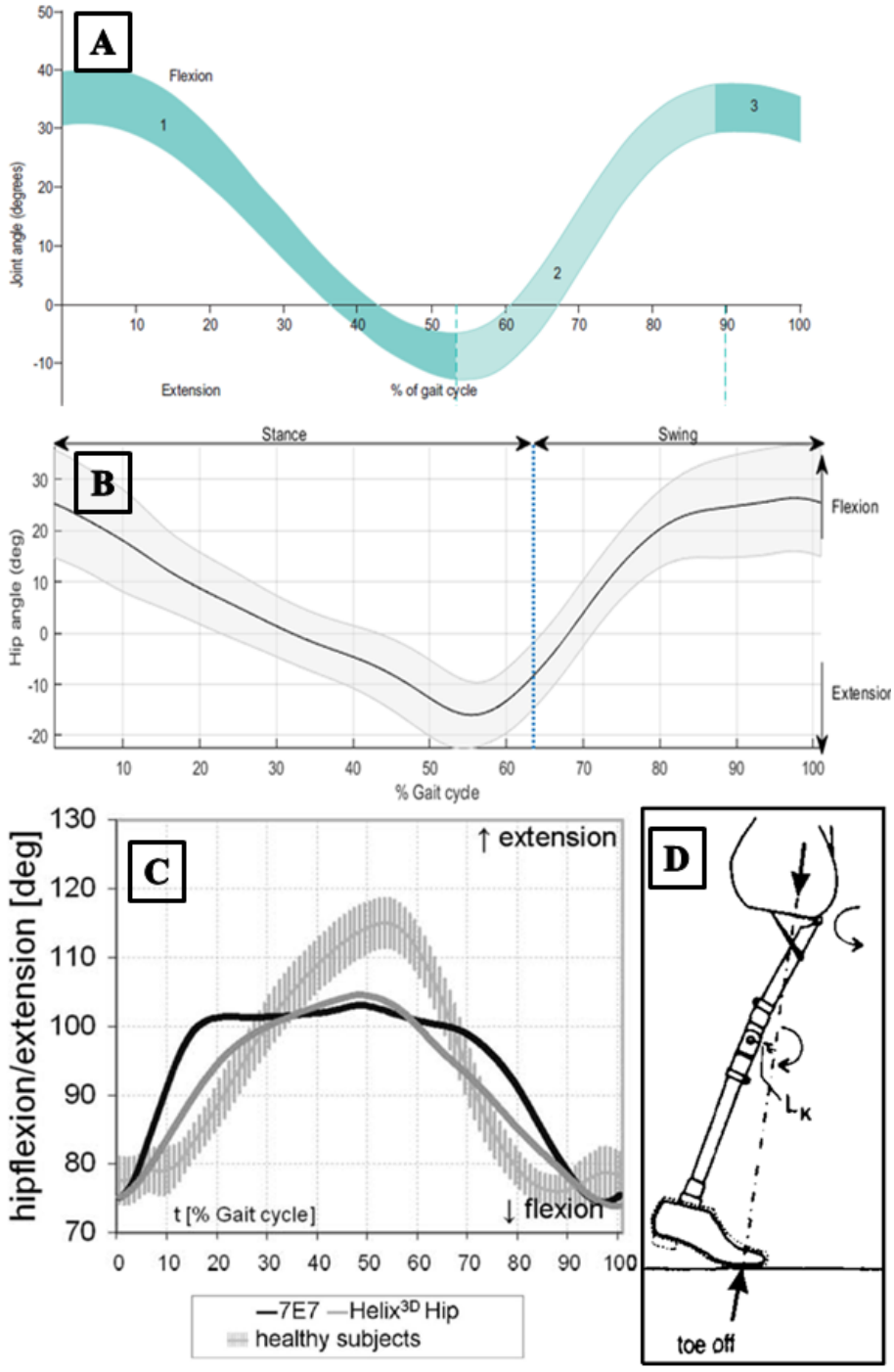

Fig. 2.9 Hip kinematics during gait, A: able-bodied persons [52], B: TF amputees with passive and semi-passive prostheses [54], C: comparison of able-bodied and HD people with 7E7 and Helix 3D passive hip prostheses [10] (Permission from Wolters Kluwer Health, Inc), D: Canadian-type hip prosthesis extension stop and knee lock at the end of the stance phase [60].

2.2.4 Pelvis kinematics

Pelvic kinematics analysis is commonly performed on HKAF prosthetic users since the loss of major lower extremity muscles can result in compensatory movements, leading to altered pelvic kinematics [61]. As shown in Fig. 2.10, HD prosthesis users typically exhibit exaggerated pelvic tilt (pelvic motion in the sagittal plane) during gait compared to TF prosthesis users. This is due to their reliance on pelvic tilt to move the prosthesis [56, 58]. Additionally, hip disarticulation prosthesis users may exhibit a wider base of support during stance, which can lead to increased pelvic obliquity angle (frontal plane pelvic motion in the) on the prosthetic side [58, 62].

In HKAF prosthetic users, the prosthetic knee remains at maximum extension (Fig. 2.8C) during stance. Therefore, hip extension and forward progression are achieved by tilting the prosthesis backward (anterior tilt) and allowing the body to fall forward due to forward momentum [63]. The prosthetic hip joint is designed to approach the extension stop at 10 to 15% of the gait cycle (approximately 10° of extension) [10]. Thus, further hip extension during stance phase is only achievable via anterior pelvic tilt (Fig. 2.11).

Early swing is controlled by a higher-velocity pelvic forward tilt (posterior tilt) that leads to prosthetic hip and knee flexion for foot clearance. Since flexion is controlled by pelvic tilt in passive hip prostheses, prosthetic hip flexion always occurs after posterior pelvic tilt (Fig. 2.9). During mid-swing, higher-velocity anterior pelvic tilt is performed to slow hip flexion, which leads to knee extension in preparation for the next foot strike [63]. Prosthetic knee full extension before foot-strike (initial contact) is essential to avoid knee collapse due to foot-ground impact.

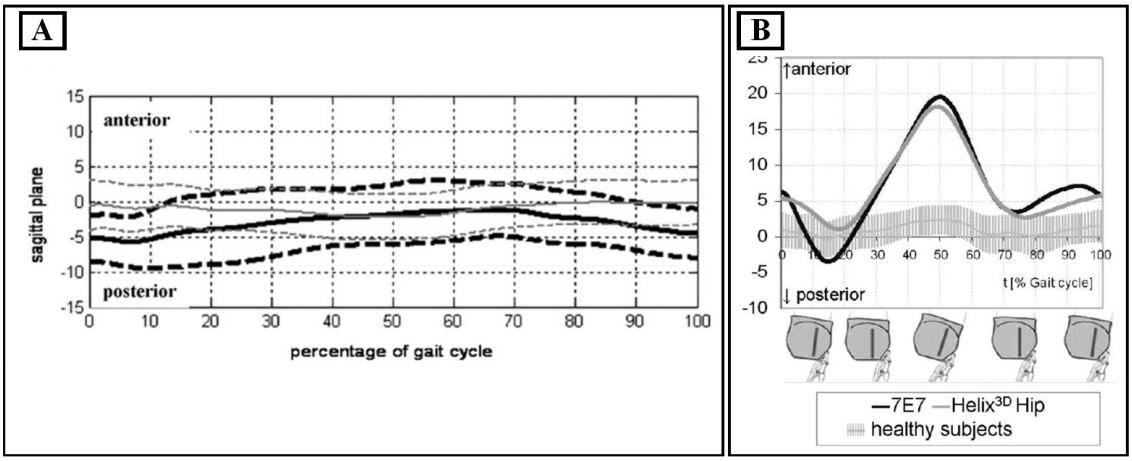

Fig. 2.10 Pelvic tilt kinematics, A: comparison of able-bodied persons (gray line) and TF prosthetic users (black line) [64] (Permission from Elsevier) , B: comparison of able-bodied and HD persons with 7E7 and Helix 3D passive hip prostheses [10] (Permission from Wolters Kluwer Health, Inc).

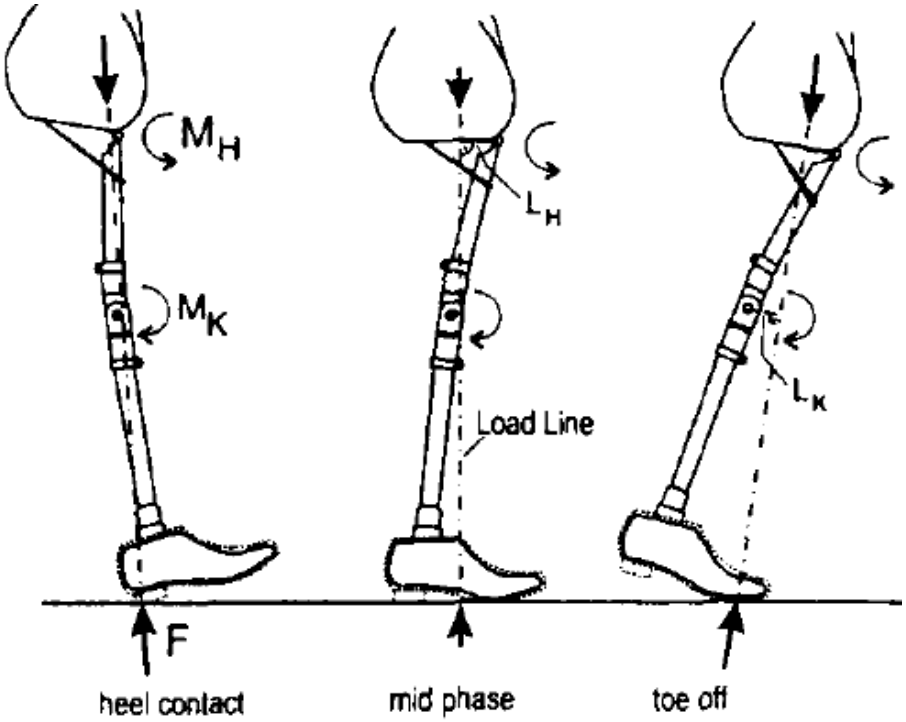

Fig. 2.11 Contribution of HD amputee's pelvic anterior tilt during stance. At heel contact, the prosthetic knee is in full extension while the hip joint is at maximum flexion. Since the body has forward momentum, the prosthetic hip joint extends until mid-stance. Approaching mid-stance, the hip reaches the physical extension stop and cannot extend further [60].

2.2.5 Gait symmetry

Gait symmetry is the degree of coordination and balance between movements of the left and right sides of the body during walking or running [55]. This is a key aspect of human locomotion and is essential in maintaining stability and reducing fall risk [65]. However, lower extremity amputees often have mild to moderate gait asymmetry. This results in further reliance on their intact side and remaining residual limb [66]. The overreliance on intact limbs often leads to shorter stance phase duration, smaller range of motion, and lower ground reaction force on the prosthetic side [65]. Since an active prosthesis can provide partial or full net-positive moments needed for actuation, in theory, a well-built active prosthesis should restore gait symmetry by reducing the prosthetic user's reliance on their intact limb [67].

Wolf et al. [20] conducted a study comparing walking biomechanics between the Ossur power knee (active) and semi-passive Ottobock C-leg. The study found that while ascending a ramp, people with the power knee tended to take smaller steps (0.52±0.09 m) compared to the C-leg group (0.61±0.08 m). The shorter step length with the power knee was likely a compensation effort to reduce loading on the intact limb, improving walking efficiency. Kinetic analysis showed that,

during ramp ascent, power knee users generated significantly lower peak hip power on their intact side (1.9±0.8 W/kg) compared to participants with the C-leg (2.3±0.8 W/kg).

People using HKAF prostheses have more gait asymmetry compared to able-bodied people or TF prosthesis users [59]. This is expected since HD amputees lack a hip joint and moment-generating capacity [10]. A case study with an Ottobock Helix 3D prosthetic user evaluated and compared gait dynamics between the prosthetic side and intact side [68]. The study found that the participant tended to have a much lower hip and knee range of motion on the prosthetic side relative to the intact side (approximately 10° less). This resulted in shorter steps on the prosthetic side compared to the intact side. Similarly, the person spent much longer in stance phase on the intact side (72% of the gait cycle) compared to the prosthetic side (57% of the gait cycle).

2.2.6 Gait variability

Gait variability is an individual's gait pattern variation over time. This variation can be affected by changes in walking speed, surface incline, and environmental conditions [69]. Gait variability can be further influenced by the type and fit of prosthetic devices [70]. The temporal and spatial aspects of gait variability refer to the fluctuations in time and distance parameters that occur from one stride to another. Temporal parameters include cadence, speed, stride frequency, single limb support duration and stride time. Spatial parameters include stride length, step width, and lower extremity joint angles [71]. Temporal and spatial gait variability are directly correlated with energy expenditure and walking efficiency [72, 73]. When adults walk at 1 Hz (1.25 m/s), the metabolic energy expenditure is kept at a minimum and the least amount of gait variability is observed [74]. However, due to external factors (such as terrain type) and internal factors (such as muscle fatigue), maintaining a 1 Hz stride frequency is not always possible [69].

Danion et al. [74] conducted a study on able-bodied individuals to determine how gait variability could be influenced by spatial and temporal parameters. Changes in gait speed were more significantly influenced by stride length rather than stride frequency, meaning that temporal aspects of gait had minor fluctuations during walking compared to spatial aspects such as hip range of motion. However, these results were inconsistent with those of TF amputees. Fakoorian et al. [75] found that as TF amputee walking speed increased from 0.75 m/s (slow walking) to 1.25 m/s (fast walking), the magnitude of gait variation in both temporal and spatial aspects also increased. The increase in spatial aspects of gait variability is likely a strategy to ensure adequate foot clearance during swing phase [76].

2.3 Biomechanics of sit-stand-sit transitions

Sit-to-stand and stand-to-sit transitions are among the most mechanically demanding functional tasks in daily life, requiring coordination of trunk and lower limb movements. These transitions are essential for maintaining independence and can be challenging for individuals with amputations and mobility impairments. Shojaei et al. [77] noted that these activities require complex muscle activation and spinal loading, particularly in individuals with unilateral TF amputations. The inability to perform these transitions can lead to considerable limitations, where many individuals remained chair-bound without appropriate interventions [78, 79].

According to the literature, two factors predominantly affect successful sitting and standing: task execution timing and center of mass (COM) dynamics. The timing of trunk and lower limb movements is critical for sit-to-stand and stand-to-sit transitions. Prolonged durations of these movements in individuals with amputations have been associated with an increased risk of falls due to a reduced base of support [80]. Furthermore, limited torque generation at the hip and knee exacerbates these difficulties [81].

Maintaining stability during sitting or standing also depends on COM movement. Pai et al. [82] described the COM trajectory during sit-to-stand as an initial horizontal phase of mass transfer followed by a vertical ascent (Fig. 2.12). Conversely, a similar but inverted trend was observed during stand-to-sit. This movement requires lower limb coordination to ensure stability within the base of support [81].

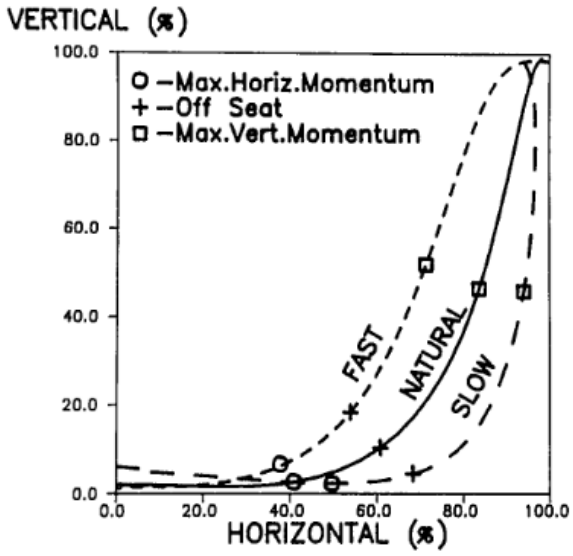

Fig. 2.12 COM trajectory of healthy participants during sit-to-stand at different speeds. The COM trajectory is divided into a horizontal movement phase and vertical movement phase [82] (permission from Wolters Kluwer Health, Inc.).

2.3.1 Hip joint dynamics

As illustrated in Fig. 2.13, the hip actively extends during sit-to-stand, contributing to the forward momentum necessary to elevate the body. This motion is characterized by a peak hip extension moment during the initial lift-off phase, which is critical for generating the vertical force required to counteract body weight. Conversely, during stand-to-sit, the hip performs controlled flexion to decelerate the descent. Eccentric activation of the hip flexors during this phase ensures a smooth and controlled lowering of the body, thereby mitigating abrupt impact on the seat [83].

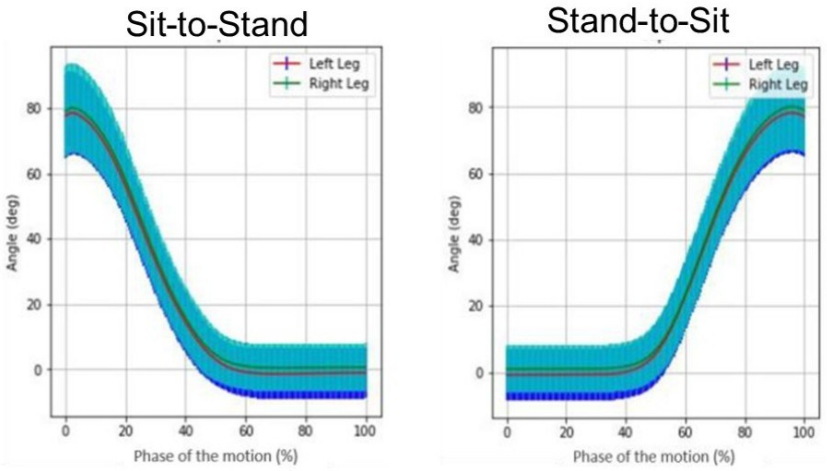

Fig. 2.13 Sagittal hip joint angle during sit-to-stand and stand-to-sit [84].

2.3.2 Knee joint dynamics

The knee joint experiences considerable mechanical load during both sit-to-stand and stand-to-sit. Acting as a fulcrum during the rising phase of sit-to-stand, the knee supports the body's progression from a forward lean to an upright position. As shown in Fig. 2.14, a noticeable knee extension moment is generated, particularly during the mid-phase of sit-to-stand as the body transitions to vertical alignment [85]. During this movement, the knee extension moment increases steadily, reaching its peak when the thighs lift off the seat. In stand-to-sit, the thigh muscles eccentric contraction moderate's descent, ensuring controlled lowering and reducing abrupt impact.

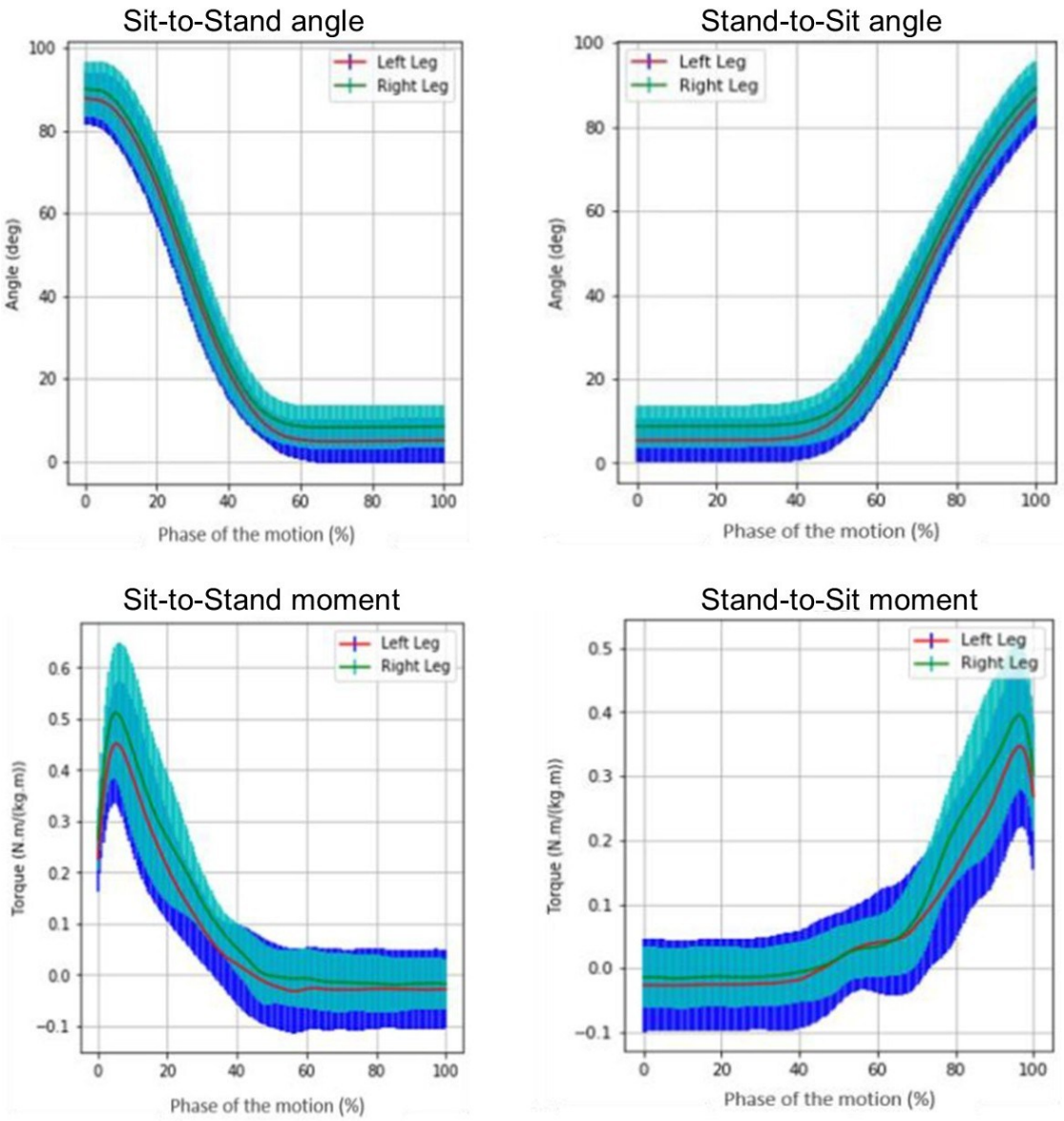

Fig. 2.14 Sagittal knee angle and moment during sit-to-stand and stand-to-sit [84].

2.3.3 Trunk dynamics

The trunk serves as a counterbalance to regulate COM location. During sit-to-stand, the trunk shifts forward to minimize the moment arm between the hip and the center of gravity, facilitating lift-off [86]. This forward leaning also directly influences COM horizontal movement, aiding in the transition from a seated to a standing position (Fig. 2.12). In contrast, during stand-to-sit, the trunk adopts a backward lean to help control the body's descent, with the backward lean similarly affecting the COM horizontal trajectory.

In early sit-to-stand, trunk flexion angles increase to generate the momentum required for the transition, reaching their maximum just before lift-off. This forward lean is essential for overcoming inertia and initiating movement. However, excessive or insufficient trunk flexion can compromise efficiency, placing additional demands on the lower limb joints for stability and propulsion. In older adults, compensatory strategies such as pronounced forward trunk lean are often observed due to the reduced strength in the hip and knee extensors [87].

2.3.4 Prosthetic user limitations

Prosthetic users face distinct challenges during sit-to-stand and stand-to-sit, largely due to the mechanical constraints of prostheses and joint asymmetry. TF amputees exhibit greater joint moment asymmetry than able-bodied individuals, relying heavily on momentum transfer by trunk forward leaning and stabilization strategies to compensate for the lack of knee functionality [88]. During sit-to-stand, the progressive resistance of prosthetic knee joints often hinders movement, requiring users to actively pull the knee into extension to complete the task. This reliance on compensatory mechanisms places increased demands on the hip joint, which has been identified as a primary contributor to increased COM horizontal movement [79].

Emerging technologies offer potential solutions for improving the biomechanics of sit-to-stand and stand-to-sit for prosthetic users. Ann et al. [89] compared powered knee-ankle prostheses with traditional passive prostheses, focusing on sit-to-stand and stand-to-sit. Powered prostheses demonstrated superior weight-bearing symmetry, allowing users to distribute weight more evenly between limbs and reducing reliance on the intact limb. The dynamic active control strategy in powered devices enabled precise moment generation at the knee and ankle, improving force production and balance during transitions. Stand-to-sit movements were smoother, with better deceleration control, reducing the risk of abrupt seating. Although powered prostheses showed no significant differences in movement duration compared to passive devices, their improved symmetry and control may mitigate secondary physical issues and improve daily functional mobility for amputees.

2.3.5 Phase-based standardization of sit-stand-sit

The concept of phase-based standardization has been utilized to understand the biomechanical intricacies of sit-to-stand and stand-to-sit. This approach divides the tasks into four discrete phases of trunk forward lean, knee angular displacement, vertical displacement, and recovery. Each phase represents distinct biomechanical challenges, enabling researchers to target specific issues [90].

Welker et al. [91] and Schultz et al. [92] demonstrated the application of phase-based strategies in powered prosthetics and exoskeletons. Welker et al. used a data-driven phase control system to enhance sit-to-stand and stand-to-sit efficiency, while Schultz et al. employed phase-based electrical stimulation to improve trunk control during transitions.

2.4 Active prosthesis control strategies

The generalized control framework introduced by Tucker et al. [23](Fig. 2.15) describes interactions between user, device, and environment with a multi-level hierarchical controller. This hierarchical framework aims to provide a common language for describing different control strategies and to facilitate comparisons and improvements of existing and future active prostheses.

The "device" provides actuation, sensing, and communication capabilities to replace the user's impaired limb function. Depending on its design and functionality, the device can have different degrees of freedom (DOF), power sources, actuators, sensors, and communication interfaces. The "user" is the biological system interacting with the device through physical contact points (e.g., sockets or cuffs). The user can provide voluntary inputs to control the device through residual muscles or gestures. The user can also receive sensory feedback from the device through tactile, auditory, or visual modalities. The "environment" is the external system that influences the user and the device through physical interactions (e.g., ground reaction forces or obstacles) and social interactions (e.g., norms or expectations). The environment can be static (e.g., terrain type or slope) or dynamic (e.g., traffic or pedestrians). The environment can also be known (such as maps or landmarks) or unknown (e.g., new places or situations).

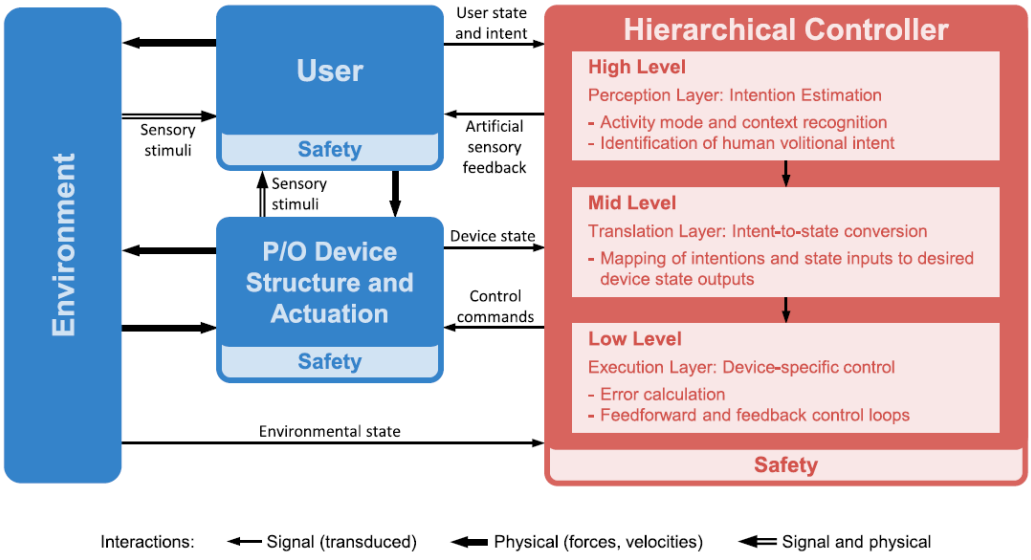

Fig. 2.15 Generalized controller framework [23]. P/O: prosthetics and orthotics

The hierarchical controller is a software-programmable three-level framework that evaluates the user and environment inputs to calculate prosthetic compensatory actuation. The three levels are [93]:

- **High-level controller framework**: A high-level controller determines the user's overall goals and intentions and provides appropriate commands to the mid-level controller. For example, a high-level controller may detect the user's current locomotion mode (walking, running, stair climbing, etc.) and then send corresponding signals to the mid-level controller for further processing. A high-level controller may also incorporate user feedback (e.g., voice commands, switches, etc.) and environmental information (e.g., terrain type, obstacles, etc.) to enhance performance.
- **Mid-level controller framework**: A mid-level controller generates reference trajectories or desired outputs for the low-level controller based on commands from the high-level controller. For example, a mid-level controller may calculate the optimal joint angles or torques for each gait cycle phase-based on biomechanical models (rule based) or data-driven methods (Artificial Intelligence based).
- **Low-level controller framework**: A low-level controller drives the prosthetic actuators to follow the reference trajectories or desired outputs from the mid-level controller. For example, a low-level controller may use feedback control methods (e.g., proportional-integral-derivative (PID) control) or feedforward control methods (e.g., model predictive control) to regulate the voltage or current applied to each prosthetic device motor. In addition, using fault detection and isolation methods, a low-level controller may also monitor and protect the hardware components from damage or malfunction.

Over the years, with advancements in active prosthetic controls and designs, the generalized control strategy framework has been improved and established as a reliable approach for active knee and ankle prosthesis studies [22-24, 94, 95]. However, this approach has never been considered for active hip prosthesis development. As discussed in Section 2.1.1, since TF and HD amputees use the same types of prosthetic knees, their knee kinematics are in principle very similar. In theory, active hip joints that closely mimic the hip kinematics of TF prosthetic users could enable HKAF prosthetic users to achieve gait symmetry and variabilities comparable to TF amputees [16].

Artificial intelligence (AI) methods are often used in new studies to explore various controller strategies and to optimize prosthetic device performance. However, these methods have several drawbacks that limit their applicability and scalability in real-world scenarios [96, 97]. These

limitations are safety and reliability issues (lack of calculation transparency), high computational power consumption, and large training datasets needed to train such devices. Considering these limitations, and that no adequate databases exist for kinetics and kinematics for active HKAF prostheses to train an AI-based control strategy, this literature review excludes AI-based studies since they will not provide information that could be utilized for the thesis objectives.

2.4.1 Sensors

Sensors are utilized by a prosthesis to recognize the person's activity and detect the corresponding gait cycles [98]. Typically, multiple sensors are incorporated in a prosthesis, depending on the type of actuator and control strategy [98]. The most common sensor types are:

- **Force sensors** measure ground reaction forces applied to the prosthesis during stance. These sensors are either embedded into the prosthesis or shoe insoles [99]. The control strategy utilizes force readings to determine gait phase transition instances and to estimate the relative center of mass location [100-102].
- **Position sensors** are used for prosthetic actuator kinematics measurements. Regardless of the prosthetic hardware design or control strategy, all semi-passive and active prostheses are equipped with position sensors [98]. These sensors are typically optical or magnetic.
- **Inertial sensors** measure limb absolute orientation to determine gait cycle subphases [103, 104]. Control strategies primarily rely on these measurements to assess the user's desired prosthetic state [23]. In recent years, solid-state inertial measurement unit (IMU) sensors have been used to determine 3D prosthesis orientation and limb segment angular velocity [98].
- **Electromyography (EMG) sensors** detect electrical activity of muscle neuron cells. They are often used to control upper limb prostheses since they can measure the residual muscle activation location and intensity [51]. However, EMG sensors have not been widely applied to lower limb prostheses, and only a few recent studies have explored their feasibility [105]. These studies have shown that EMG sensors have limitations for lower limb prosthetic control, such as low signal quality, high variability, and poor robustness. Therefore, EMG sensors are currently less reliable than other sensor technologies for use with lower extremity prosthesis controls.

2.4.2 High-level controller framework: intention estimation

Detection of semi-passive and active prosthetic user locomotion intent is often achieved through finite state machines (FSM) [106-109]. An FSM is a mathematical model consisting of a set of states, a set of input symbols, a set of output symbols, and state transition rules. For example, if a prosthetic user is seated, the initial state is sitting. Based on this initial state, the two possible state outputs are to remain seated or to stand up. Hence, the state transition rule will continuously measure the prosthetic sensor data and check if stand-up state transition conditions are met. Once sensor values exceed the state transition rule thresholds, the high-level controller will then assume that the person is ready to stand up and will request the mid-level controller to complete the state transition from sitting (initial state) to standing up (output state) [107].

Herr and Wilkenfeld [110] defined an FSM approach for a high-level prosthesis control strategy by dividing the gait cycle into 5 subphases (5 finite states), as shown in Fig. 2.16A. By analyzing biological knee kinematics during walking, they defined transition rules (pre-defined thresholds) to detect user intent to transition from one finite state to another. Later studies reduced the number of subphases to 4 finite states by combining states 4 and 5 (Fig. 2.16B) [111]. The parameters used to define finite state transition rules are dependent on the ground reaction force, residual limb angle, residual limb angular velocity relative to the prosthesis, and stride time [83].

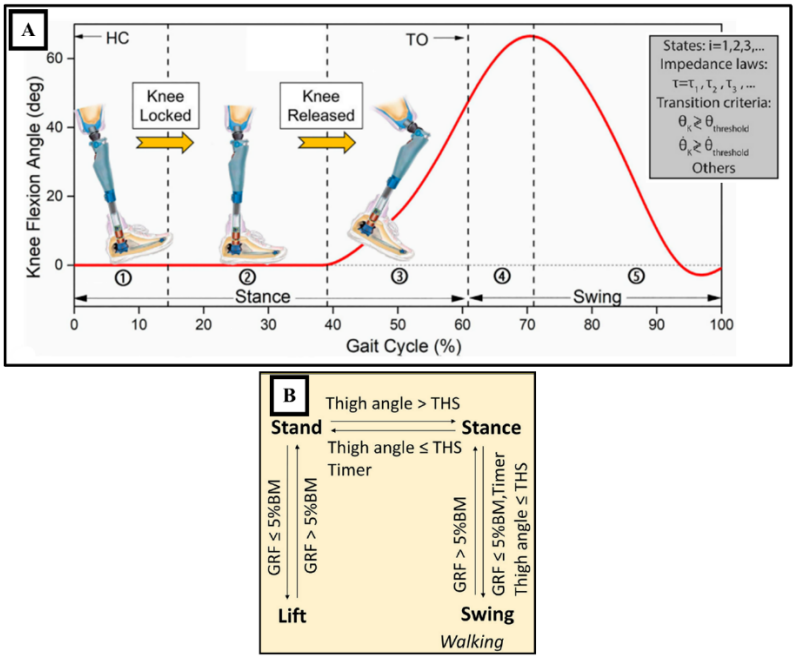

Fig. 2.16 Finite state transitions of prosthetic knee gait cycle. State 1: initial double support (IDS). State 2: single support (SS). State 3: terminal double support (TDS). State 4: swing flexion (SWF). State 5: swing extension (SWE). GRF = ground reaction force, θ = residual limb angle, and $\dot{\theta}$ = angular velocity relative to the prosthesis [36]. BM: body mass, THS: threshold

2.4.2.1 Gait initiation and termination finite state machine

Gait initiation (GI) and gait termination (GT) refer to the processes of starting and stopping the act of walking or running [38]. GI and GT transitions are achieved through anticipatory postural adjustments (APA) that can directly influence COM kinetics and kinematics and lower extremity joint motions [112, 113]. In TF prosthesis control strategy studies, GI and GT detections are achieved by measuring ground reaction forces, joint angles, muscle activity, center of pressure, and COM [114]. These parameters provide information about the timing and magnitude of APAs, which can help predict the transition events of GI and GT.

Miff et al. [115] examined the temporal aspects of GI and GT from ten able-bodied adults and ten TF amputees. Using kinematic data, body COM forward acceleration and the time needed to start and stop walking at different speeds were determined. Both groups performed trunk forward lean APA to accelerate during GI and backward lean APA to decelerate during GT. Furthermore, GI acceleration magnitude directly correlated with participant average steady-state gait speed during each trial session. This indicates that APA during GI could be used to predict desired gait velocity during the first step of the gait cycle.

Novak et al. [116] analyzed nondisabled participants' APAs to develop a GI and GT FSM for prosthesis and exoskeleton control strategies, and determined that GI detection would only require hip and knee kinematics thresholds (Fig. 2.17A). In contrast, GT event detection would require measurement of hip and knee kinematics, centre of pressure positioning relative to the sagittal plane, and ground reaction force magnitude (Fig. 2.17B).

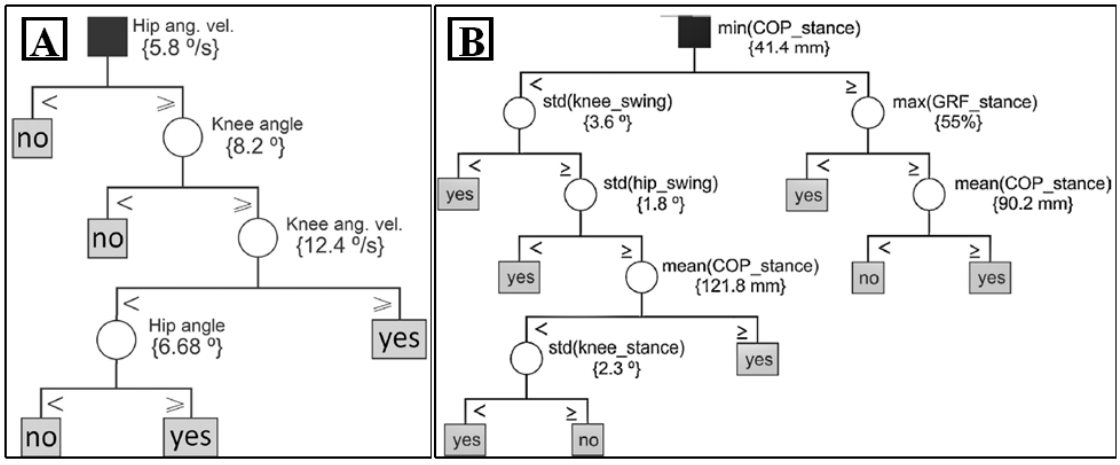

Fig. 2.17 Finite state machine transition detection rule for gait initiation (A) and gait termination (B) [116] (permission obtained from Elsevier).

When developing FSM and tuning transition rules for active prostheses, two important factors should be taken into consideration: imposed locomotion mode errors and critical time [23].

- Imposed locomotion mode errors occur due to active prosthesis back-drive torque when generating forward-drive torque. Since finite state transition rule thresholds depend on the residual limb angle and angular velocity, an imposed back-drive torque onto the residual limb can affect overall lower limb kinematics and reduce FSM detection accuracy [117].
- Critical time is the maximum time window by which the state or activity transition must be detected to ensure prosthetic user stability [26]. Critical time window variability depends on the prosthetic type and the control strategy approach. Therefore, a critical time for each state transition must be obtained through experimentation.

2.4.3 Mid-level controller framework: desired joint kinematic profile estimation

Mid-level controllers can be grouped into phase-based and non-phase-based categories [23]. Phase-based controllers use a predefined sequence of discrete phases (e.g., stance, swing) to coordinate device behaviour with the cycle. The controller relies on sensors to detect transitions between phases and trigger appropriate actions. Phase-based controllers are simple, robust, and widely used but have limited adaptability to different walking conditions and user preferences [23, 25, 118, 119].

Non-phase-based controllers do not use discrete phases, but use continuous variables such as intact joint angles, torques, or muscle activations to modulate device behaviour according to user state and intent [23, 120-122]. The controller can be based on biomechanical models, neural networks, fuzzy logic or other probability-based algorithms. Non-phase-based controllers are more flexible, adaptive and natural than phase-based controllers but rely on the prosthetic user's skills, muscle strength and residual limb flexibility to control the prosthesis. As previously explained in Section 2.2.4, due to major lower limb loss, HD amputees rely much more on their pelvis and intact limbs to provide the needed compensation during walking compared with lower-level amputees. This can lead to higher energy demands, significantly reducing their ability to influence the prosthesis directly. Therefore non-phase-based controllers are considered not ideal for active HKAF prostheses [16].

Phase-based controllers provide natural gait patterns by performing predefined actions specific to the detected state transition event [23]. In the case of TF amputees, the predefined actions are normalized knee angle trajectories of able-bodied individuals. As shown in Fig. 2.18, temporal and spatial aspects of the normalized gait trajectory must be scaled upon state transition detection to

match the prosthetic user's desired gait variability [94]. The temporal aspect of the normalized knee angle trajectory is adjusted through interpolation, and the spatial aspect is commonly adjusted using an impedance-based control equation [123], given by

$$\tau(t) = -k(\emptyset)\big(\theta(t) - \theta_d(t,\emptyset)\big) - b(\emptyset)\dot{\theta}(t)\,, t \geq 0 \qquad (2.1)$$

where τ is the desired motor torque, θ is the prosthetic joint angle, $\dot{\theta}$ is the prosthetic joint angular velocity, θ_d is the predefined normalized knee angle, b is the damping ratio, k is the linear impedance (stiffness ratio), and $\emptyset$ is the state transition number (refer to Fig. 2.16). The tunable parameters are the impedance ratios $k(\emptyset)$ and damping ratios $b(\emptyset)$. Since each person has unique gait characteristics, a tuning routine is always performed after prosthetic fitting to ensure user safety and efficiency [94].

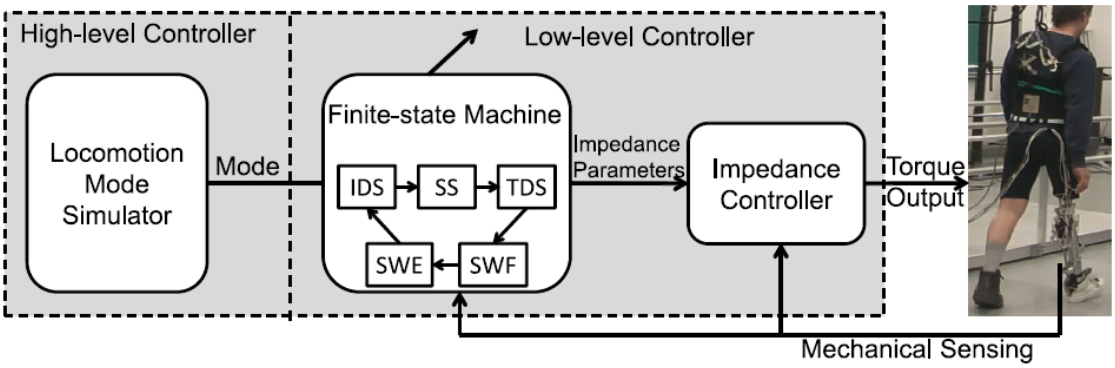

Fig. 2.18 Active knee prosthetic control strategy with impedance-base control [124].

The main limitation of phase-based controllers is achieving a balance between input-output responsiveness and adaptability to users' intent. A common method to achieve this balance is to use impedance-based control, which modulates the stiffness and damping of the prosthesis according to the gait phase and user intention. However, using a constant stiffness ratio as a function of state transition number ($\emptyset$) may limit the performance and versatility of the prosthesis for different tasks and environments [98]. Therefore, some researchers have proposed alternative methods such as cubic impedance ratio parameter for nonlinear impedance modulation [119] or a virtual constraint control approach using a time-varying stiffness ratio function [100] to improve the tunability and flexibility of impedance-based control. These methods demonstrated the potential of using more sophisticated impedance functions to improve the functionality and usability of the mid-level controller strategies. Furthermore, to control non-cyclic events such as GI and GT, a secondary mid-level controller called "echo control" is often used instead of impedance-based controllers [121]. Echo control is a phase-based controller approach that simultaneously records

the prosthetic joint trajectory while feeding it back to the low-level controller with some delay and adjusted gains, hence following the user's non-cyclic motion (Fig. 2.19) [23, 25, 98]. The echo controllers, however, require the user to wear additional sensors on the waist and/or contralateral limb.

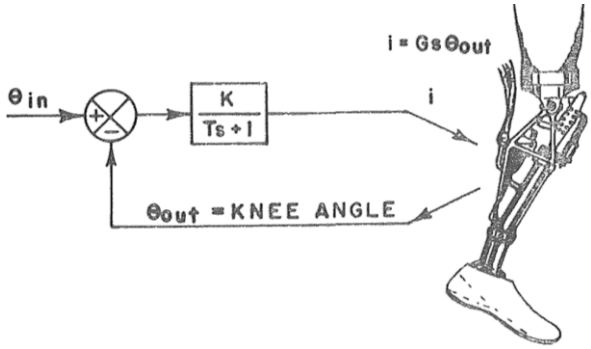

Fig. 2.19 Simple echo controller block diagram for active prosthetic knee control [25] (permission obtained from American Society of Mechanical Engineers ASME). θ_{in} represents the knee angle measured on the contralateral limb. The θ_{out} represents the prosthetic-side knee angle measured by an encoder. After calculating the knee angle error (θ_{in} - θ_{out}) the error is passed to a first-order transfer function to calculate the motor current. The input/output delay is introduced by the slow response time of first-order transfer function.

2.4.4 Low-level controller framework: control system

The low-level controller is the software-to-hardware translation layer in the form of a closed-loop control system (Fig. 2.20) that is responsible for monitoring hardware outputs and performing required error corrections based on desired parameters obtained from the mid-level controller [23]. Therefore, while designing the closed-loop control system, considerations must be made of the prosthetic hardware's mechanical characteristics (plant) and the signal conditioning performed to remove external disturbances (feedback controller) [22].

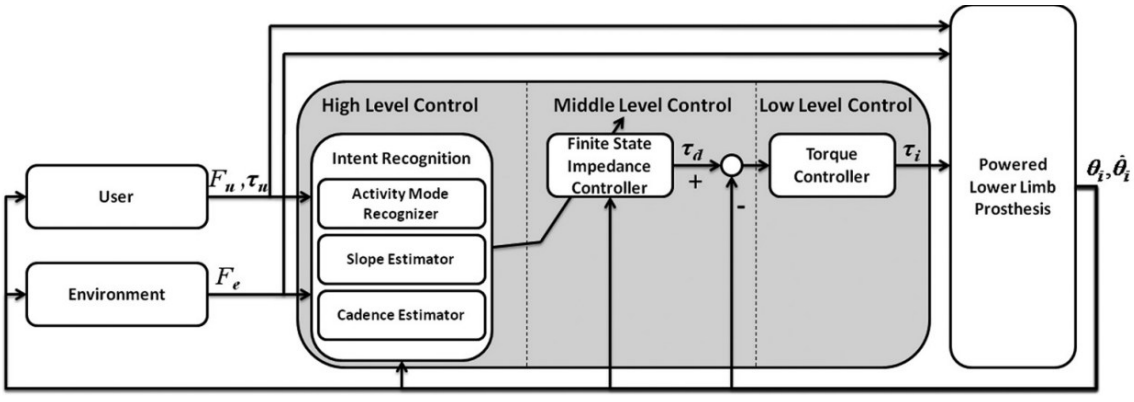

Fig. 2.20 Active prosthesis, hierarchical controller framework with closed-loop low-level control system [93].

2.4.4.1 Plant

Prosthetic joint designs in commercial products and prototypes are diverse. Researchers often develop complex polycentric joint systems to introduce motion non-linearities and mimic biological joint kinematics [122]. This is achieved by transferring motor actuation to the prosthetic joint centre of rotation through multiple interconnected components, such as springs or dampers (Fig. 2.21). Therefore, motor actuation and induced torque may not directly correlate with overall prosthesis actuation and torque.

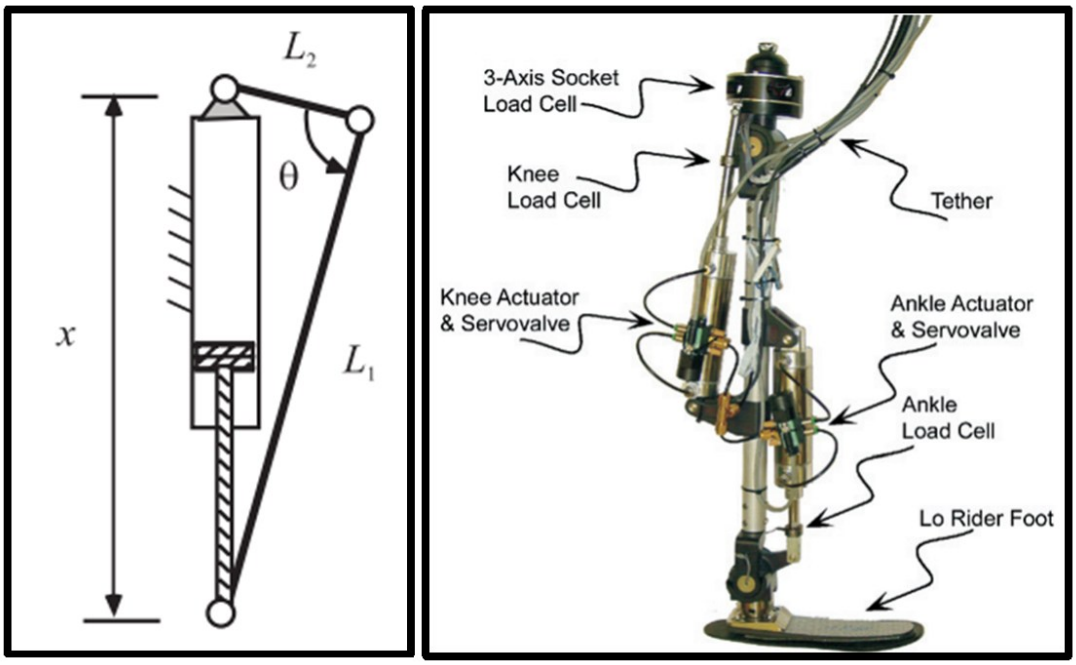

Fig. 2.21 Example of an active prosthetic knee prototype (right) and the equivalent mechanical model (left) [119] (permission obtained from Sage Publications).

Since most mid-level controllers are designed to be modular and hardware independent, their outputs represent the prosthetic system's overall desired dynamics and not the actuator dynamics. Therefore, further signal processing (torque controller) is often required at the low-level feedforward controller to ensure the desired torque is achieved at the joint centre of rotation, regardless of joint complexities and non-linearities [22].

Torque controllers are based on prosthesis theoretical models. As shown in Fig. 2.22, prosthetic models are designed to be simple, utilizing mass, linear spring, and linear damping elements to approximate overall system behaviour [122]. Then, using these theoretical models, the equation of motion and torque controller transfer function is obtained [16, 122, 125-128].

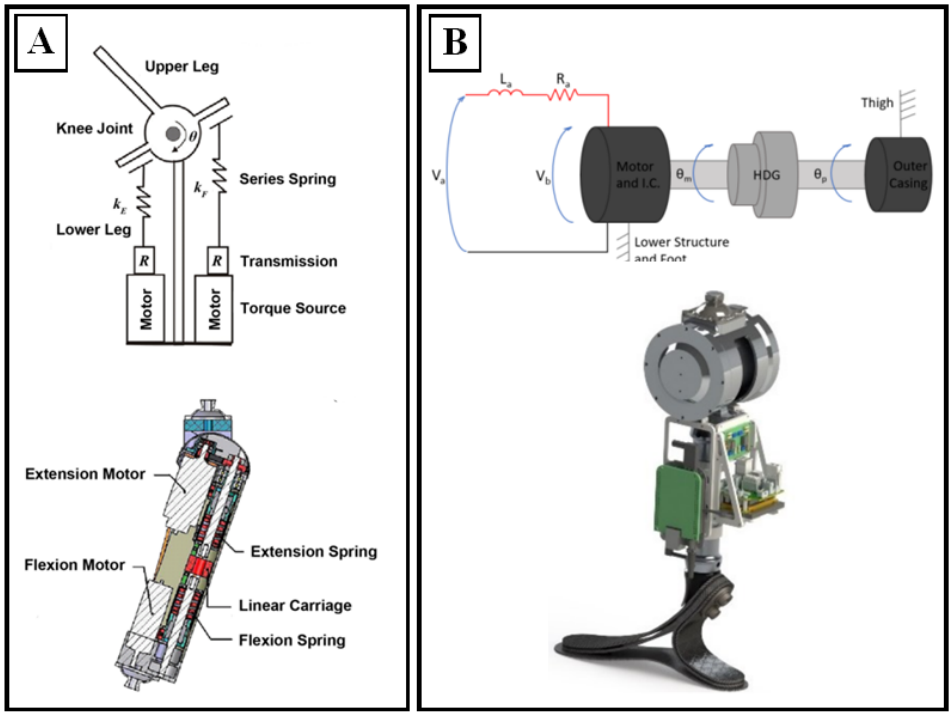

Fig. 2.22 Active prosthesis modelling, A: Overall system behaviour approximation [129], B: Actuator characteristics modelling [128].

2.4.4.2 Feedback controller

PIDs are the most common type of low-level feedback controllers used for active prostheses [22]. These controllers achieve disturbance immunity, which refers to the ability of the controller to maintain stable control in the face of external disturbances or unpredictable hardware behavioural changes (e.g., sudden body weight increase after donning a backpack) [130]. In addition, the robustness and ease of implementation make PIDs ideal for most prosthetic designs.

2.5 Discussion

Replacing passive and semi-passive knee joints with active joints has the potential to improve gait dynamics for prosthetic users, enabling them to engage in demanding locomotion activities that they previously avoided or found challenging [19-21]. Although extensive research has been conducted on active prosthesis actuators and control strategies, these advancements have yet to be integrated into HKAF prostheses. Given that individuals with HD amputations lack all leg muscles on the amputated side, active prosthetic technologies could potentially address net torque deficits and provide benefits to the user.

In active prosthesis research, designing a controller strategy that can adapt to different walking conditions and user preferences is essential [22, 23, 94, 122]. A common way to address this challenge is to use a hierarchical control strategy approach, which divides the controller into three layers: high-level, mid-level and low-level [23]. The high-level layer determines the gait phase and mode based on sensor inputs and user commands. The mid-level layer generates the desired joint trajectories and impedance parameters based on the high-level layer outputs and biomechanical models. The low-level layer implements the joint torque control based on the mid-level layer outputs and feedback signals. This hierarchical approach allows developers to simplify and modularize the controller design and evaluation process, as well as to compare different methods within each layer. Therefore, we adopted a similar hierarchical control strategy approach for our motorized HKAF prosthesis research.

Many biomechanical models of swing phase kinematics adopt a double pendulum model as a simplifying assumption for lower limb motion [131]. Considering this assumption, the passive or semi-passive knee movements in TF prostheses is achievable through compensatory hip joint extension and flexion. Therefore, knee and hip kinematics could be obtained by measuring hip joint kinematics [29]. For HKAF prostheses, coordinated prosthetic hip and knee joint motions during the swing phase can only be achieved by compensatory pelvic tilt movements [63]. As a result, HKAF prosthesis users exhibit exaggerated pelvic motions for prosthesis control [10]. When developing control strategies for a motorized HKAF prosthesis, inverse kinematics can be used to achieve appropriate prosthetic knee and foot control from hip movements [132]. Therefore, the important role of pelvic motion in prosthetic controls and gait variability must be taken into consideration.

Section 2.4 introduced a generalized multi-layered framework that could potentially be used to develop active HKAF prosthesis control strategies. As shown in Fig. 2.15, a controller framework should be able to adjust prosthesis hardware behaviour to adapt to the environment and user commands. Hence, the user, environment and prosthesis observabilities are vital parts of the control strategy [94].

Canadian type HKAF prosthesis alignment was designed to provide stability during stance phase and ensure adequate ground clearance during swing phase [5]. However, this alignment system requires the passive hip joint to be placed anterior to the pelvis and inferior to the biological hip joint, resulting in shorter overall prosthetic limb length and reduced hip rotation range of motion [58, 59]. These limitations contribute to reduced walking speed and 2-minute walk test scores relative to TF amputees and able-bodied individuals [59]. Recent studies on active TF prosthetic

users have shown that, by providing a positive net force on the prosthetic side, these prostheses can mimic natural joint movements, reducing dependence on the intact limbs and improving gait symmetry [20, 133]. Therefore, gait symmetry analysis is an important metric to quantify the success of these technologies and guide further improvements.

Apart from gait symmetry, another crucial factor related to gait pathologies is gait variability since walking efficiency is directly linked to gait variability [70, 134]. Individuals who use HKAF prostheses frequently exhibit greater gait variability due to the heightened energy required for walking when compared to able-bodied individuals and TF amputees [135]. Consequently, by monitoring gait variability, the effectiveness of therapeutic interventions and rehabilitation can be assessed [69]. Furthermore, since evaluating gait symmetry and variability can offer a comprehensive overview of a prosthetic user's performance, these approaches can also be utilized to compare the performance of the developed controller strategy to the gait symmetry and variability of passive prostheses.

2.5.1 Research gaps

Commercially available HKAF prostheses are equipped with mechanical hip joints to reduce the overall prosthesis weight. However, since the resultant net hip torque is negative, users must spend up to 80% more energy than able-bodied people for walking but also have slower walking speeds [14]. Prolonged prosthesis use can increase the risk of spinal injuries due to excessive pelvic utilization, and accelerate intact side arthritis [12].

Considering the advancement in motorized actuator technologies, HKAF prosthetic users could benefit from a prosthesis with motorized hip joint; however, only two studies have explored this possibility [16, 132] and performed efficacy assessments on either able-bodied participants using simple controls [16] or through mathematical simulations [132]. Thus, we identified two overarching research gaps:

- Development of user-centric control strategies for a self-contained prosthetic system (requiring no additional body-worn sensors beyond the prosthesis itself).
- Rigorous evaluation of motorized HKAF prostheses to quantify their effectiveness in mitigating the energy expenditure, reduced mobility, and excessive utilization of pelvic movements.

To address these gaps, the following research questions guided this thesis:

1. How should the hierarchical control strategy for active HKAF prosthesis be implemented?
    a. How to design a high-level controller that can detect the user's intent and switch between different modes of operation?
    b. How to design a mid-level controller that can generate reference torque trajectories for the desired mode of operation?
2. Is developing a control strategy that relies on HD amputee natural pelvic movement to control the active HKAF prosthesis feasible?
    a. What methods should be used to extract prosthetic user's control commands from the pelvic movements?
    b. Which pelvic movement features correlate with desired hip kinematics?
    c. Will a hierarchical control strategy approach reduce the HKAF prosthetic user's need to perform exaggerated pelvic tilt motion during walking?
3. Will utilizing an active HKAF prosthesis and control strategy improve HKAF prosthesis user gait and sitting/standing? If so, what improvements could be observed?
    a. Compared to passive HKAF prosthesis, will walking on an active HKAF prosthesis improve the prosthetic users gait?
    b. Can active HKAF prosthesis users achieve a gait symmetry and kinematics similar to TF prosthetic users?
    c. Compared to passive HKAF prosthesis, will active HKAF assist the user during sit-to-stand, and stand-to-sit by while ensuring consistent prosthetic side loading?

Chapter 3: Prototype development

3.1 Foreword

This chapter details the development of hardware and backend software required to establish a foundation for the prosthesis control strategies. This work lays the foundation towards addressing thesis objective 1: "*Develop a motorized HKAF prosthesis control strategy for gait initiation, termination, and level walking*" and objective 2: "*Develop a motorized HKAF control strategy for sit-to-stand and stand-to-sit transitions*". The prototype hip joint and chassis were designed by Kelly Brannen, Yousef Bader and Lucas Cho, each responsible for exploring the mechanics of different joint designs and prosthetic thigh chassis designs. The motor system and the electronics that powered the motor were provided by Össur. The author's hardware development contributions were electronics circuits board development and chassis instrumentation to ensure appropriate sensor input for the control system.

The motor controller software (low-level controller discussed in Section 2.4.4) was provided by Össur. Motor control system tuning, control strategy development, hardware abstraction layer programming, and software backend programming discussed in this Chapter were the author's contributions.

Initial validation tests of the prototype were conducted with a simple control system before implementing a full hierarchical controller. The author programmed the motorized hip joint to perform basic high impedance actuation cycles (follow the desired hip angle trajectory at high torque), replicating the kinematic patterns described in Section 2.2.3. To evaluate practical usability, three able-bodied participants walked with the prosthesis using an HD prosthesis simulator [136], following protocols and measurement criteria outlined in prior research [31, 32, 137]. These tests provided preliminary data on hardware performance and user interactions.

In preparation for control strategy development, force sensors and inertial measurement units (IMUs) were integrated into the mechanical design and calibrated. The author designed and assembled initial control electronics, including circuit boards and communication interfaces. A modular software framework was implemented by Farshad Golshan, featuring a hardware abstraction layer to simplify code updates. The electronics and code were intentionally designed for flexibility, allowing design adjustments as the control strategy evolved. The hardware and software underwent several iterations throughout this research and notable iterations are discussed in this chapter.

3.2 Prototype design

Fig. 3.1A illustrates the first prototype that was used for the control strategy development. The mechanical design and validation of this prototype was performed by Yousef Bader [31], Sarah Mroz [137], and Kelly Brannen [138]. The prototype was named "Power Hip" and consisted of an active hip joint, prosthetic chassis, semi-passive prosthetic knee (Össur Rheo knee), and energy storing prosthetic foot (Össur pro-flex ST). In a collaborative effort between Össur (prosthesis manufacturer) and the University of Ottawa, Össur's power knee actuator and control electronics were adapted for the hip joint system and thigh chassis module. In this thesis work, prototype development was progressed by instrumenting the prosthetic thigh chassis, programming the necessary software to perform initial gait tests, and adding electronics for prototype experimentation and data acquisition.

Power Hip consisted of a motorized hip joint and a prosthetic thigh chassis. The hip joint was designed to be front socket mountable and compatible with the Canadian-type alignment requirements (Fig. 3.1B). The prosthetic thigh chassis housed the hip joint battery, electronics, and sensors. The hip joint system used a single-axis pully mechanism to translate actuator torque to the centre of rotation. This meant that the actuation commands (motor angle and motor speed) were equivalent to the prosthetic hip states (hip angle and hip angular velocity), requiring no observer controller. This simplified the low-level controller design and reduced the computational load.

During the later stages of control strategy development and testing, the initial prototype's height limitations became apparent; therefore, further hardware modifications were necessary. The initial prototype length was 312 mm and only compatible with participants taller than 170 cm. This limited HD participant recruitment criteria. To reduce the overall height of the prosthesis, modifications were made to the thigh chassis design and some internal electronics. As shown in Fig. 3.2, in the final version of the prototype, the Power Hip component height was decreased by 86 mm, which permitted recruitment of participants with body heights of 150 cm and above.

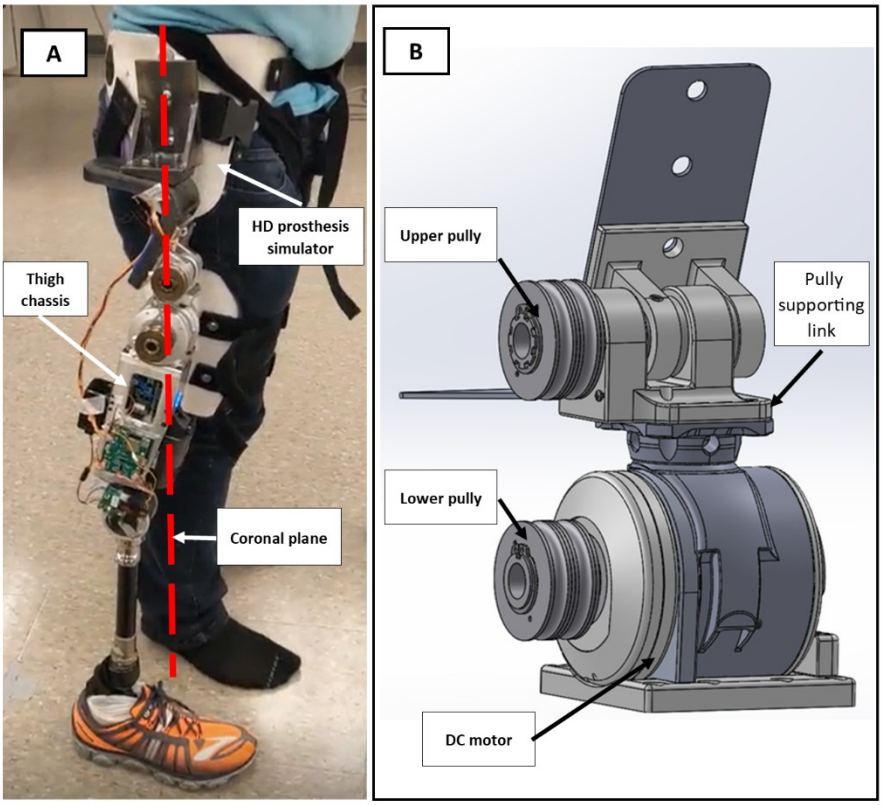

Fig. 3.1 A: Powered Hip joint anteriorly mounted to the simulator for testing, B: Isometric view of the hip joint system.

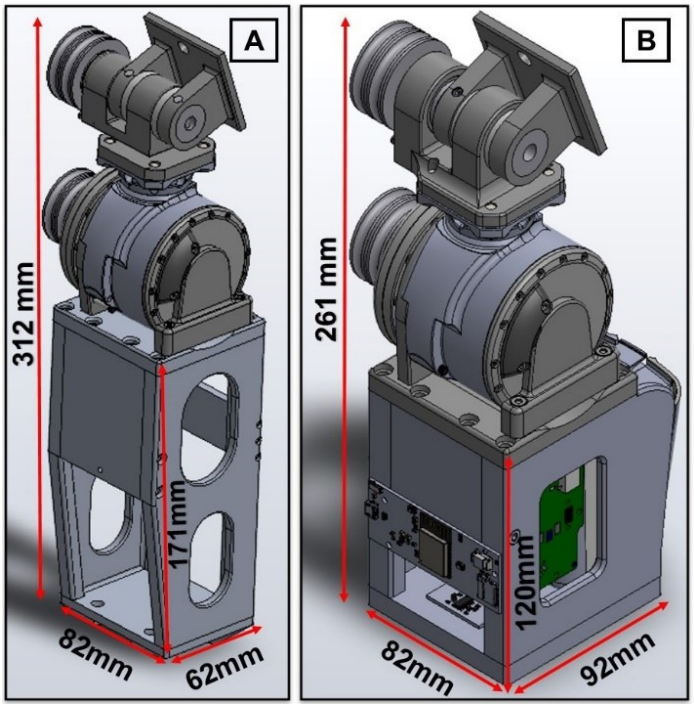

Fig. 3.2 CAD rendering and dimensional differences between first prototype (A) and the final prototype (B).

3.3 Embedded system hardware

In addition to the electronics provided by Össur, an external electronic circuit board was required to perform load cell signal conditioning, pelvic motion analysis, sensor data acquisition, and performance monitoring. The author developed this additional circuit board and named it data acquisition board since its primary purpose was to log all the raw sensor data and processed control outputs. From the start of this research work, five iterations were made to the design of this board each addressing limitations of previous versions (Fig. 3.3). The final version of the board was divided into a circuit board that separated the digital signal and analog signal processing units. This design choice was necessary since in the final prototype version, the motor was close to the sensitive loadcell. Hence, to reduce the motor's electromagnetic interference, the instrumentation amplifier and Analog-to-Digital converter (ADC) chip had to be placed near the loadcells. The datasheet of the final iteration of the data acquisition board has been provided in Appendix A.

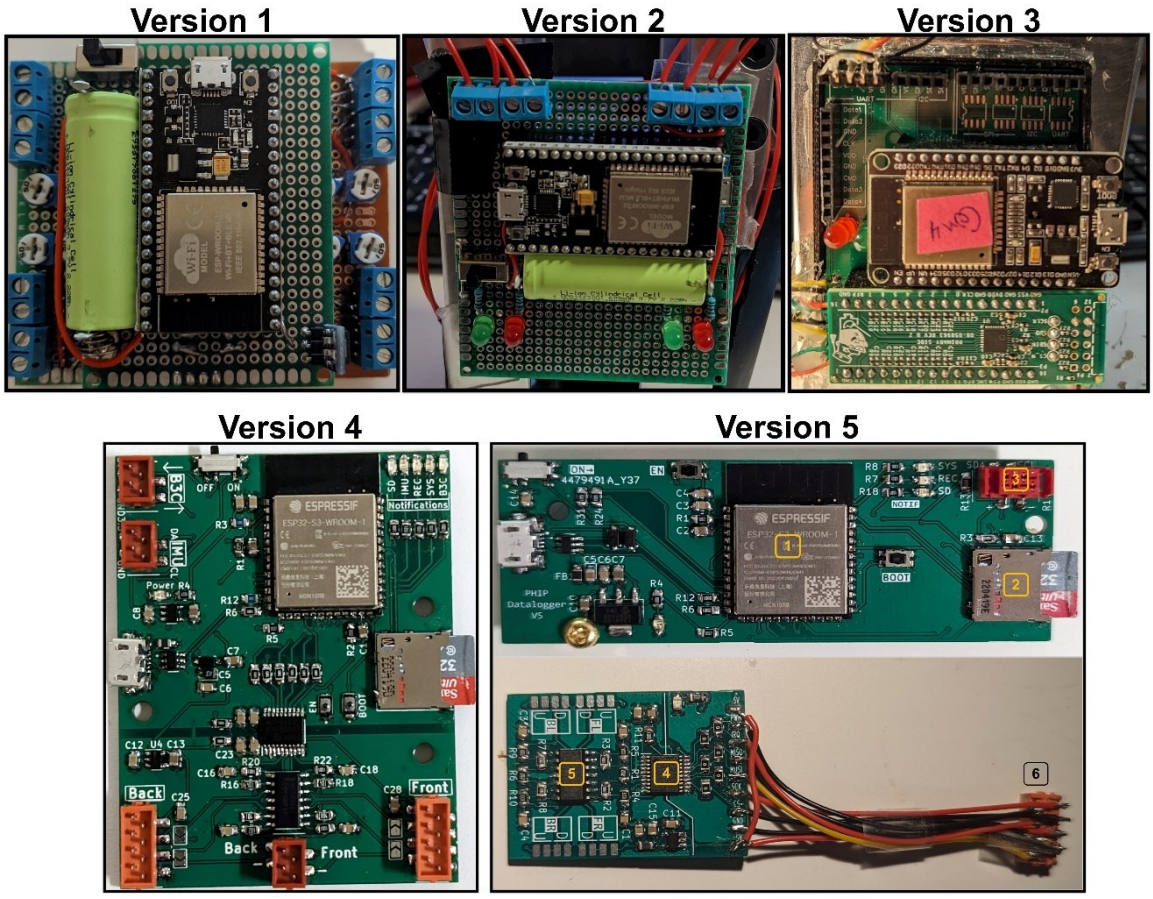

Fig. 3.3 All iterations of data acquisition circuit board. Main components of the version 5 iterations are the ESP32-S3 microcontroller and BLE communicator (1), Micro SD card slot (2), Pelvic IMU I2C port (3), MCP3562R ADC (4), NCS4325 instrumentation amplifier (5) and, SPI communication port connecting analog board to digital board (6).

The data acquisition circuit consisted of several components performing different functions:

- **Load cell signal conditioning Integrated Circuit (NCS4325):** The analog circuit was designed with NCS4325 to amplify and filter the signal from the strain gauges. Since the magnitude of strain gauge voltage fluctuation was small (microvolts), the load cell signals were susceptible to external noise (e.g., temperature fluctuations, electro-magnetic interference). Therefore, an instrumentation amplifier circuit was designed to filter high-frequency noise (100 Hz cutoff frequency) and amplify the signal (gain of 50) before analog to digital conversion.

- **Analog to digital conversion Integrated Circuit (MCP3562R):** A 2-channel, 24-bit ΔΣ ADC MCP3562R was utilized due to its high sampling rate and suitability for instrumentation applications. As illustrated in Fig. 3.3 (version 5), the design of the ADC printed circuit board (PCB) included a separation between the analog and digital sections of the MCP3562R chip by isolating their grounding paths. This approach helped to minimize digital noise interference [139]. The MCP3562R communicated with the microcontroller through a serial peripheral interface (SPI) port, attached to the back of digital data acquisition board (not shown in Fig. 3.3).

- **Pelvic IMU (BNO085):** BNO085 is a 9-axis IMU, consisting of a 3-axis accelerometer, a 3-axis gyroscope, and a 3-axis magnetometer. This IMU features a proprietary algorithm that combines data from all 9 axes to calculate high-accuracy, high-sampling-rate quaternion coordinates of three-dimensional orientation, thereby reducing the computational load on the main microcontroller. This IMU communicated with the microcontroller via an inter-integrated circuit (I2C) protocol.

- **Communication port to the Össur electronics board:** The Power Hip was specifically designed to work with the electronics and motor provided by Össur. To facilitate data transmission between the Össur electronics board and the data acquisition board, a communication method was necessary. The universal asynchronous receiver-transmitter (UART) protocol was selected since it required minimal modifications to the Össur electronics.

- **Sensor data storage into SD card:** During control strategy development and experimentation, it was necessary to log sensor data and control strategy outputs at a high sampling rate. To achieve this, an SD card (and card slot) was utilized to record the data in

real time while the Power Hip was untethered. The SD card communicated with the main microcontroller via MultiMedia Card (MMC) protocol.

- **Wireless data transmission between microcontroller and PC:** In addition to storing data on the SD card, during walking tests, the same sensor data were transmitted to a nearby PC using the low-energy Bluetooth (BLE) communication protocol. However, this transmission occurred at a much lower sampling rate of 10 Hz, compared to the faster data logging speed of the SD card. The computer operated a graphical user interface (GUI) that provided an overview of system performance, including sensor output plots and microcontroller diagnostic information. Using the same GUI and communication protocol, control strategy tuning parameters were transmitted from PC to the data acquisition circuit board.

In this study, the Össur electronics board was referred to as the motor controller board, as its main function was to regulate DC motor torque output. This motor controller board also contained two supplementary sensors utilized by the control strategy algorithm: a thigh orientation IMU (BNO055) and a hip rotation angle sensor.

3.3.1 Load cell instrumentation

The developed control strategy utilized ground reaction force measurements to identify transitions between gait cycle phases by measuring the axial force (single axis force passing through the prosthesis from bottom to top). To implement this approach, tests were conducted to determine the optimal locations for strain gauge placement within the thigh chassis, as well as the associated voltage-to-force calibration parameters. The placement locations were identified through SolidWorks simulations (Fig. 3.4A). These simulations revealed that the bottom corners of the chassis experienced the highest strain under a vertical load of 1000 N applied to the prosthesis [31]. Based on these findings, two BF350 strain gauges were installed at each bottom corner of the chassis, forming two full Wheatstone bridge load cells, one located at the front of the chassis and the other at the back (Fig. 3.4B).

The author performed load cell calibrations using an Instron 4482 universal testing machine at the University of Ottawa (Fig. 3.4C). The machine was configured to apply 2300 N at 125 N/s to the thigh chassis in five consecutive trials. During these tests, the data acquisition board recorded the corresponding load voltages, which were stored on an SD card. The voltage outputs were subsequently fitted to a first-order polynomial in MATLAB to determine the calibration

parameters. As illustrated in Fig. 3.5, the load cells measured forces up to 2300 N with a root mean square error (RMSE) of 29.8 N, corresponding to an error of 2.3%.

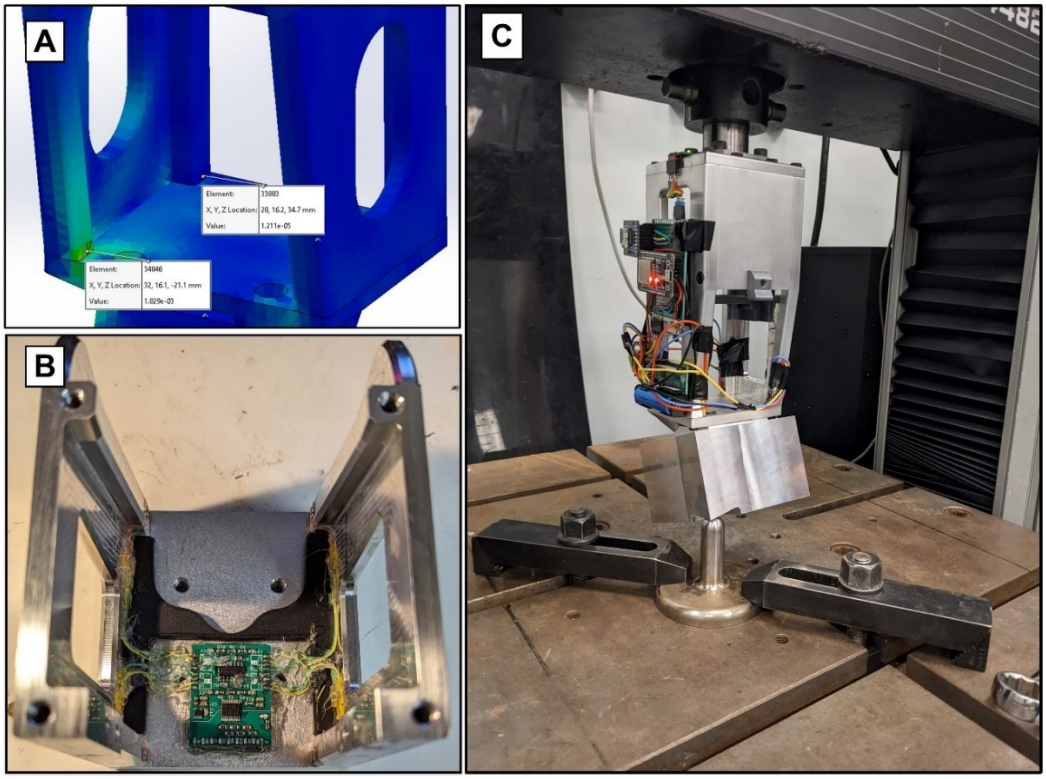

Fig. 3.4 A: Strain simulation of thigh chassis showing locations with greater strain. B: Strain gauge placement on the chassis columns near the base plate. C: Instron strain test.

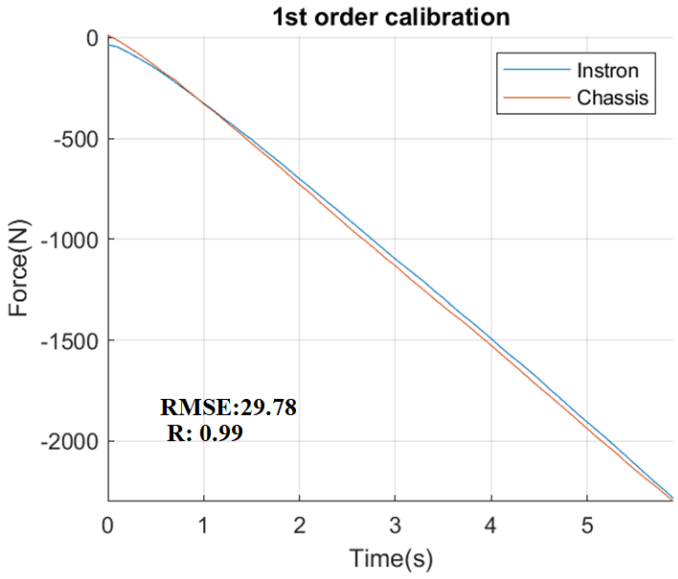

Fig. 3.5 Instron testing machine force and the measured force by the load cells (calibrated) during calibration tests.

3.3.2 Motor controller tuning

The Power Hip is equipped with a brushless, three-phase DC motor originally designed for the third-generation Ossur Power Knee. Paired with a harmonic drive gear (1:96 gear ratio), the motor can deliver a maximum torque of 96 N·m at speeds up to 300°/s. Since the Power Hip's mechanical characteristics differ from the Ossur Power Knee, the motor control parameters required retuning. The motor is controlled via a TMC4671 field-oriented controller (FOC) integrated chip. Fig. 3.6 shows a typical FOC block diagram employed by TMC4671.

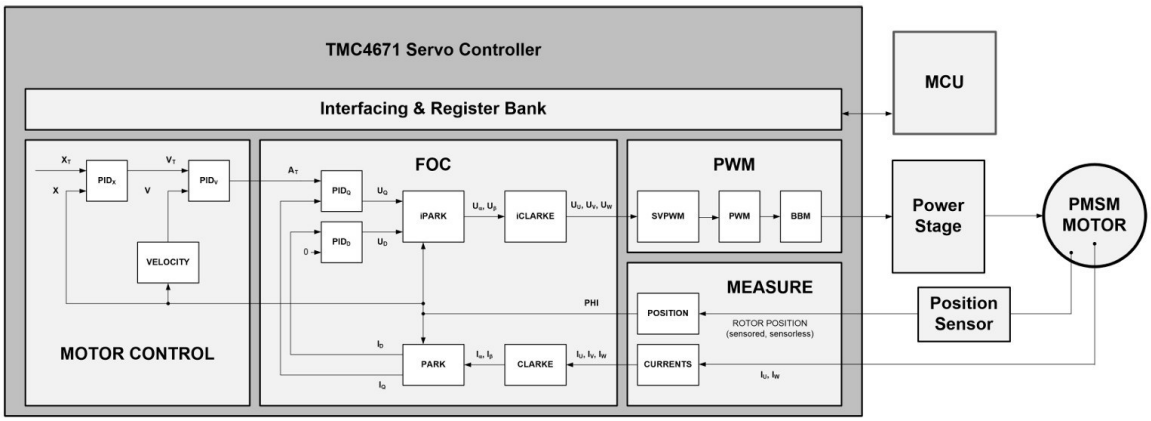

Fig. 3.6 TMC4671 FOC block diagram [140]. PWM: pulse width modulation, PMSM: permanent magnet synchronous motor, MCU: microcontroller

FOC is a well-established method for managing three-phase brushless DC motors [141]. By decoupling the torque and flux components of the motor current, FOC enables independent regulation for optimal performance. Initially, the three-phase stator currents (i_a, i_b, i_c) are transformed into a two-dimensional stationary reference frame using the Clarke transformation [142] given by

$$\begin{bmatrix} i_\alpha \\ i_\beta \end{bmatrix} = \frac{2}{3}\begin{bmatrix} 1 & -\frac{1}{2} & -\frac{1}{2} \\ 0 & \frac{\sqrt{3}}{2} & -\frac{\sqrt{3}}{2} \end{bmatrix}\begin{bmatrix} i_a \\ i_b \\ i_c \end{bmatrix} \qquad (3.1)$$

This transformation yields two orthogonal components, i_α and i_β, which are then rotated into the rotor's d–q reference frame (Fig. 3.7) via the Park transformation [143] using the rotor's electrical angle (θ) given by

$$\begin{bmatrix} i_d \\ i_q \end{bmatrix} = \begin{bmatrix} cos\theta & sin\theta \\ -sin\theta & cos\theta \end{bmatrix}\begin{bmatrix} i_\alpha \\ i_\beta \end{bmatrix} \qquad (3.2)$$

In this framework, the direct-axis current (i_d) aligns with the rotor's magnetic flux, while the quadrature-axis current (i_q) is directly linked to the produced torque. Many control strategies aim to minimize i_d so that nearly all coil current contributes to torque generation via i_q [141]. This approach permits output torque estimation from i_q readings in applications where incorporating a torque sensor is impractical, such as in the Power Hip prototype.

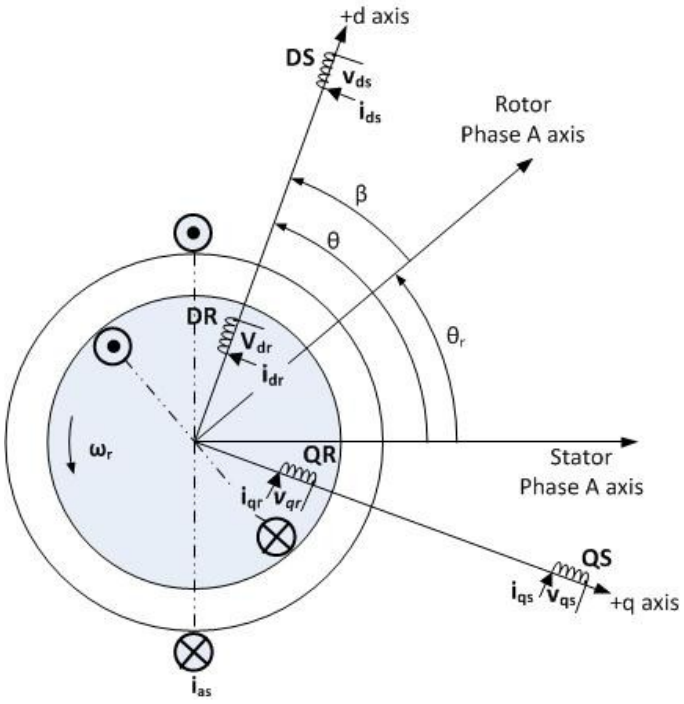

Fig. 3.7 d-q coordinate system of 3-phase FOC [144].

Rotor angle accuracy in the Park transformation is dependent on angle sensor (encoder) alignment relative to the rotor's magnetic poles. Tuning the encoder offset angle relative to the position of the rotor's magnetic poles is essential to minimize torque ripple and maintain a low i_d.

FOC proportional-integral (PI) controllers did not require further tuning beyond the values already established for the Ossur Power Knee, because these gains are typically selected based on the motor's electrical time constant and mechanical properties rather than on prosthesis-specific characteristics. Therefore, considering the FOC controller's core functionality, the encoder offset angle (Φ offset) and i_d-to-output torque ratio required tuning for our prototype.

In preparation for tuning these two parameters, the setup shown in Fig. 3.8 was prepared to apply known torque onto the joint. Using an electric chain hoist attached to a weighted lever arm, the speed at which the load was applied to the joint was safely controlled. This setup allowed us to

easily adjust the applied torque and perform cyclic loading and unloading to determine the repeatability of the tuned FOC.

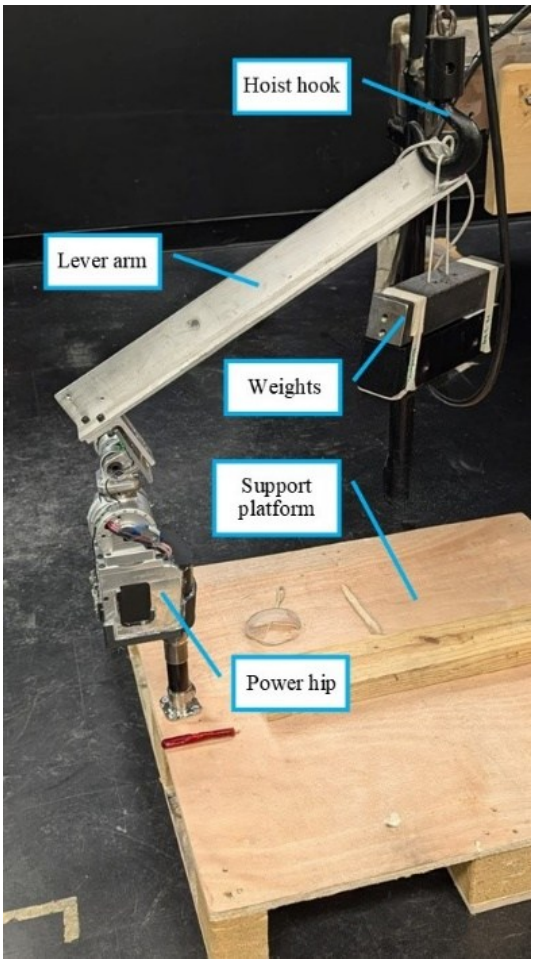

Fig. 3.8 Power Hip motor tuning setup.

3.3.2.1 Encoder offset tuning (Φ tuning)

The magnetic flux (Φ) linkage generated by the rotor's permanent magnets defines the magnitude of the magnetic field in the air gap between the rotor and stator, thereby directly influencing the motor's back-electromotive force (back-EMF) and the resultant torque production.

In practical systems, the nominal flux linkage, as provided in datasheets or obtained through theoretical calculations, does not always match the actual flux due to factors such as manufacturing tolerances, variations in magnet properties, and measurement errors in sensors. To compensate for these discrepancies, a Φ offset is introduced and tuned.

The author performed Power Hip Φ offset tuning by first setting the low-level controller to hold position in a very high impedance mode. Ideally, when a known external torque is applied and

the corresponding motor torque is measured, gradually adjusting the offset should cause the motor torque to change and get closer to the applied external torque. However, during initial Power Hip tuning, because the i_d-to-output torque was not yet configured, we instead monitored the relative changes in the motor torque as the offset was adjusted. The offset was continuously adjusted under the same constant external torque until only minimal deviation in the measured motor torque and actual applied torque were observed. Fig. 3.9 illustrates the changes in measured output torque after finalizing the Φ offset tuning.

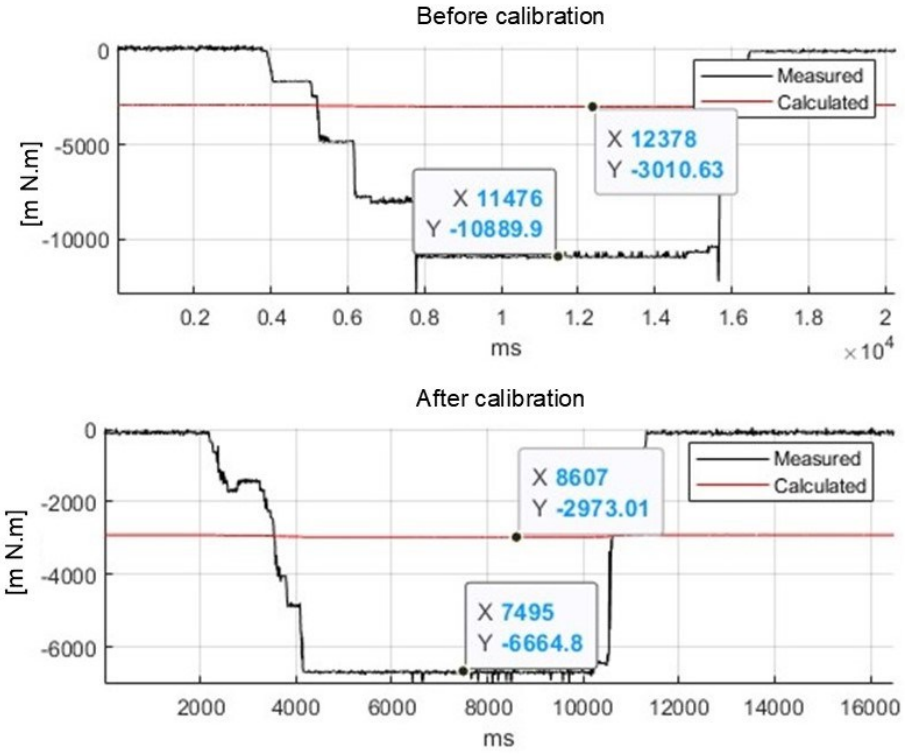

Fig. 3.9 Results before and after Φ offset. Calculated: known applied torque, Measured: Power Hip motor output torque estimate.

Since the load was gradually applied to the system, the measured torque gradually increased before reaching the maximum value. Then the measured and calculated torques were compared. Φ offset was adjusted after each trial to reduce the difference between the maximum measured torque and calculated torques. The calibration was deemed complete once the difference was the smallest.

3.3.2.2 Motor current to output torque ratio tuning

To determine the ratio, an initial value of 1 was assumed. Using the experimental setup described in Section 3.3.2, a progressively increasing known load was applied to the joint while the motor torque was measured, thereby establishing the relationship between the applied load and the

measured torque. From this relationship, a linear equation was derived to represent the load-to-torque behaviour. To verify that the ratio was accurately determined, the same test was repeated after tuning ratio and the root mean square error (RMSE) was calculated. After each trial, the linear equation was adjusted to reduce the RMSE. The tuning deemed complete when further reduction of RMSE was not achievable. As shown in Fig. 3.10, once the ratio was tuned, the RMSE was greatly reduced compared to its initial value.

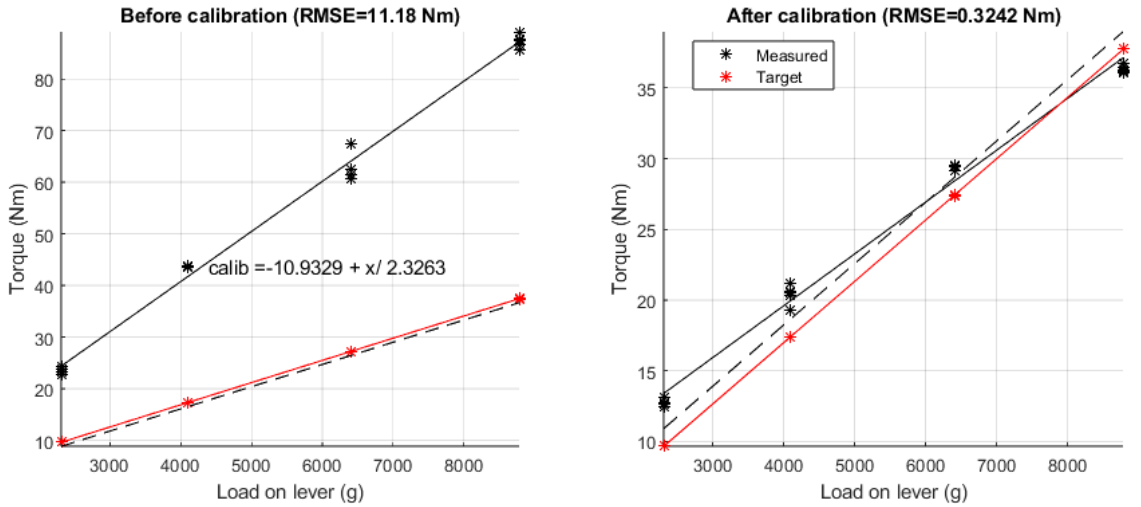

Fig. 3.10 Incremental loading of the Power Hip joint and the derived load to torque curve before and after calibration, Measured: obtained from Power Hip, Target: calculated torque based on applied load.

3.3.3 Initial prototype testing

Initial prototype testing was conducted to evaluate functionality and assess hip flexion and extension under load. These preliminary tests were carried out on able-bodied participants using an HD prosthesis simulator developed by Fanous et al. [136]. The HD prosthesis simulator is a specialized system that enables non-amputees to attach the prosthesis to the side of their body, allowing for functionality testing (Fig. 3.1A).

After obtaining ethics approval from the University of Ottawa's ethics committee (H-08-21-7062), able-bodied participants were recruited and trained to walk with the prosthesis. During walking tests, actuator functionality was evaluated using a simple high-impedance controller. This controller was designed to rotate the hip joint along a predetermined trajectory at a constant speed, ensuring consistent performance assessment across participants.

3.3.3.1 Hip angle trajectory generator

During initial prototype testing, the control strategy had not yet been fully developed. Instead, a MATLAB script was created to generate predefined hip angle trajectories based on user-defined preferences, such as gait timing, range of motion, and flexion/extension rotation speeds. These trajectories were designed to closely replicate the natural hip motion of TF amputees, using data from prior studies and biomechanical models (Fig. 3.11). This approach proved effective for quickly testing various hip joint designs. The results of the initial prototype testing with able-bodied participants have been documented in [31, 137, 138].

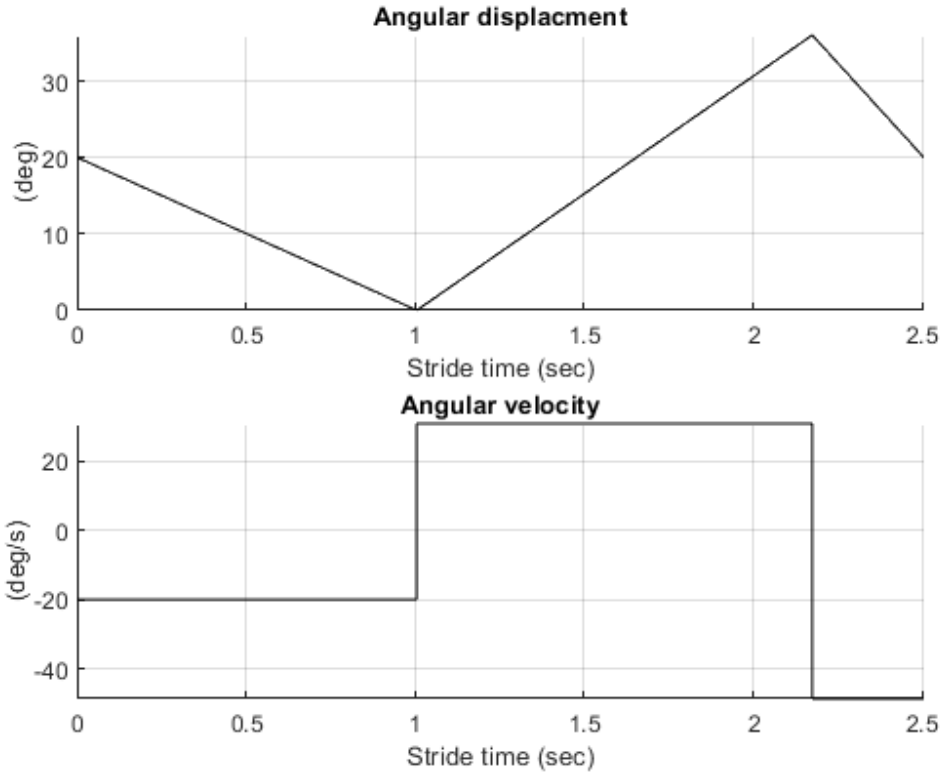

Fig. 3.11 An example of a generated hip trajectory profile.

3.4 Embedded system software abstraction layer

In this thesis, the term "abstraction layer" refers to the programming code that enables the main application (control strategy software) to function reliably on the microcontroller. In its final implementation, the abstraction layer managed BLE communication with the PC, data transfer to and from the motor controller board, real-time sensor data collection, and real-time data logging.

The simultaneous operation of all tasks was facilitated in part by the dual-core architecture of the ESP32-S3 microcontroller, which allowed two operations to run concurrently. However, since more than two tasks needed to be active simultaneously, an automated task scheduling system was

required to ensure that sensor data collection and processing occurred approximately in real-time. FreeRTOS task scheduling software was selected for this purpose due to its full compatibility with the ESP32-S3 software development toolchain.

FreeRTOS is an open-source real-time operating system designed for microcontrollers, specializing in managing multiple concurrent tasks (looping code blocks requiring indefinite execution). One key feature of FreeRTOS is its ability to assign priority levels to tasks, enabling critical operations such as sensor measurements to be executed at strict time intervals without interruptions. Priority levels are assigned using 8-bit integer numbers where 0 is the lowest priority and 255 is the highest priority.

Table 3.1 provides an overview of all tasks in the system, detailing the order of their initial activation, priority levels, and execution time intervals. In our software's final version, seven tasks were programmed to operate in tandem. The control strategy software itself was also implemented as a task and was activated last to enable sensor data to function effectively.

Table 3.1 Abstraction layer tasks, activation order, priority, and execution interval time.

Initial activation order	Task name	Task function description	Priority level	Execution interval	Executed on CPU core number (0 or 1)
1	SD_manager	Manage data written into the SD card	3	1 ms	0
2	IMU_read	Measure pelvic movement	3	2 ms	1
3	ADC_read	Measure reaction force	3	1 ms	1
4	UART_rx_event	Capture incoming data from motor controller board	2	When incoming data is detected	0
5	UART_tx_event	Send control strategy requests to the motor controller board	2	When data transmission is requested by CS_task	1
6	BLE_manager	Sending and receiving data via BLE peripheral	1	100 ms	0
7	CS_task	Control strategy high-level controller processing	3	2 ms	0

3.4.1 Communication between data acquisition board and motor control board

Efficient communication between the data acquisition board and the motor controller board was crucial for implementing the control strategy. While high-level controller calculations were initiated on the data acquisition board, a portion of these calculations and the complete execution of the mid and low-level controllers were carried out on the motor controller board. This division of computational tasks was necessary due to the control strategy's (discussed in Chapter 5) reliance on data from pelvic kinematics, hip rotation kinematics, thigh kinematics, and ground reaction forces.

The UART protocol, used for communication, imposed bandwidth limitations that made direct high-rate streaming of sensor data to either board impractical, leading to data loss. To address this issue, high-level controller calculations were distributed between the two boards. For instance, hip and thigh kinematics were measured on the motor controller board, necessitating efficient communication to synchronize the high-level controller tasks. Tuning mid-level controller parameters, such as stiffness and damping ratios, required communication between the two boards since the updated parameters were stored on the data acquisition board's SD card by default.

A tailored communication strategy was developed to mitigate data loss and optimize performance by transmitting only essential information in small, manageable batches. As depicted in Fig. 3.12, the system startup involves transferring tuning parameters from the data acquisition board to the motor controller board. Once these parameters are fully transferred, the control strategy application is activated. During runtime, instead of streaming raw sensor data, the data acquisition board processes the data locally and transmits event flags to the motor controller board. These flags signal critical events, such as transitions in gait phases or detections of pelvic tilt features, that directly influence high-level controller operations. By limiting data transmission to these essential updates, the communication strategy ensures efficient and reliable coordination between the boards.

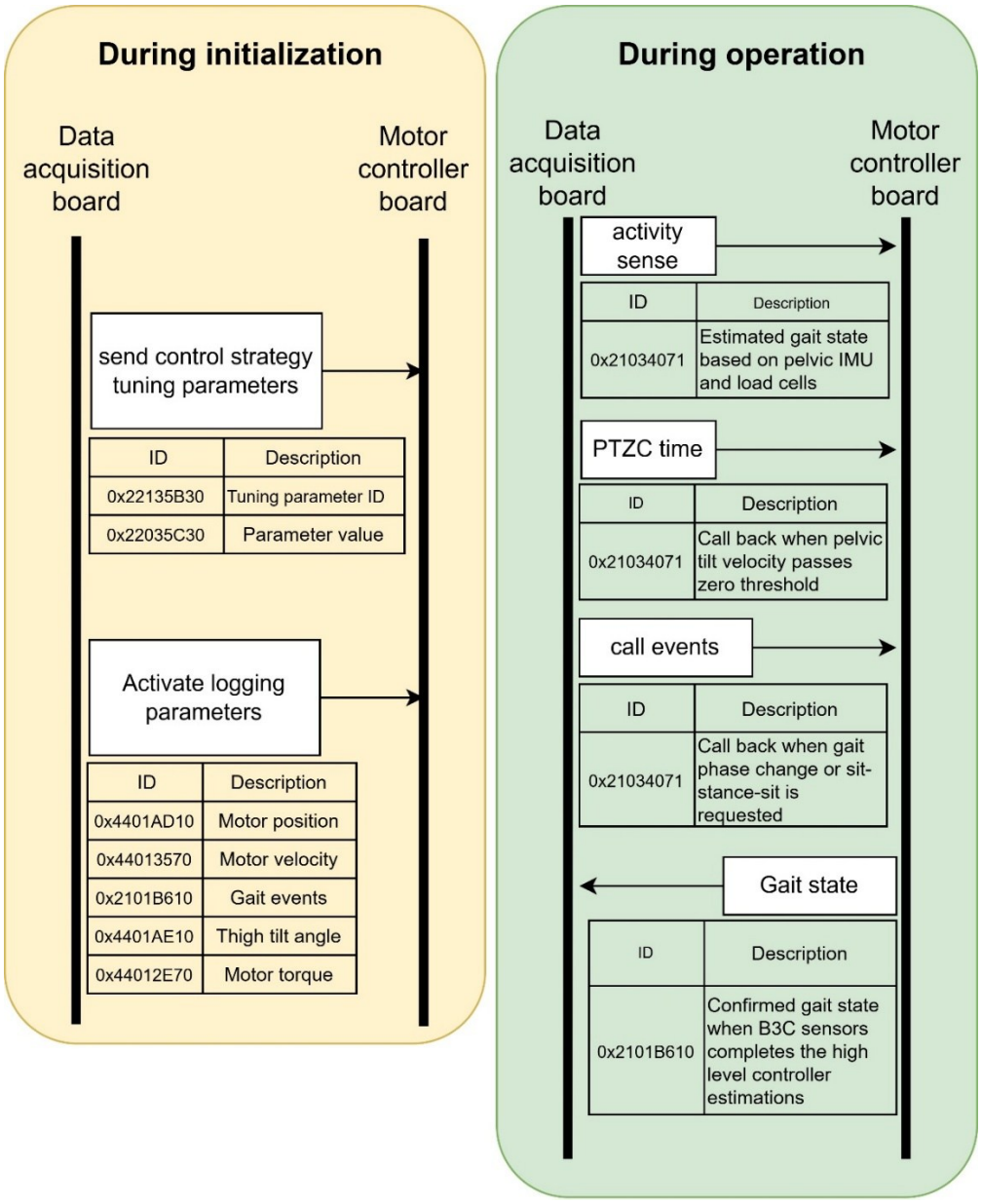

Fig. 3.12 Communication events between data acquisition board and motor controller board during startup initialization and during operation.

3.4.2 Pelvic motion IMU

IMUs typically output three-dimensional rotation data in either Euler angles or quaternions [145]. While Euler angles are commonly used, they are prone to gimbal lock, where the alignment of two rotational axes results in the loss of one degree of freedom. In contrast, quaternions do not suffer from this limitation and provide smooth and continuous representations of rotation. Furthermore,

quaternions are computationally more efficient, requiring fewer mathematical operations to combine rotations, which is particularly advantageous for real-time applications.

The IMU employed for pelvic measurements in this study (BNO085) was capable of outputting rotation data in quaternions. However, since pelvic measurements are often expressed in Euler angles, each quaternion output had to be converted to Euler angles in real time to align with conventional reporting formats. This conversion was performed for every data sample to ensure compatibility with the analysis framework.

Equation 3.3 was used for the conversion [146] and is given by

$$\begin{bmatrix}\phi\\ \theta\\ \psi\end{bmatrix} = \begin{bmatrix} \tan^{-1}\left(\frac{2(q_\omega q_x + q_y q_z)}{1-2(q_x^2+q_y^2)}\right) \\ -\frac{\pi}{2} + 2\tan^{-1}\left(\frac{\sqrt{1+2(q_\omega q_y - q_x q_z}}{\sqrt{1-2(q_\omega q_y - q_x q_z)}}\right) \\ \tan^{-1}\left(\frac{2(q_\omega q_x + q_x q_y)}{1-2(q_y^2+q_z^2)}\right) \end{bmatrix} \quad (3.3)$$

where ϕ is the rotation angle about the x-axis (pelvic tilt movement), θ is the rotation about the y-axis (pelvic obliquity movement), ψ is the rotation angle about z-axis (pelvic rotation), $[q_x\ q_y\ q_z]$ are the three imaginary parts of quaternions, and q_ω is the real part of quaternions. The pelvic movement terminologies with respect to each anatomical planes are illustrated in Fig. 3.13.

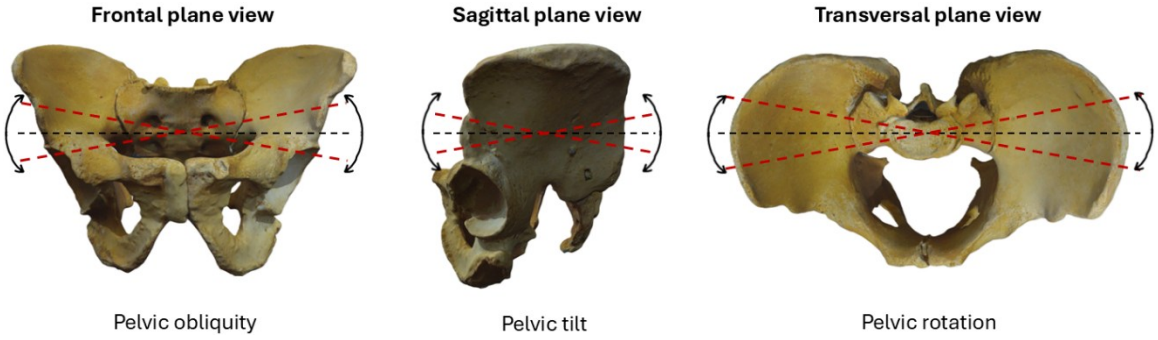

Fig. 3.13 3-dimensional movement of pelvis (3D model created by Andreas Kontny [147])

3.4.3 BLE communication with PC

The author, with assistance from an undergraduate engineering student (Lucas Cho), developed a PC application to interface with the Power Hip system. Although the Power Hip and its control strategy were designed for untethered operation, a wireless communication application was essential for technical diagnostics during control strategy development and for parameter tuning during participant training.

The application was implemented using Python (version 3.10) with the PyQt5 library to create a simple graphical user interface (GUI). The GUI was designed with two tabs (Fig. 3.14). The first tab facilitated software diagnostics by providing real-time plotting of various sensor data values. The second tab was dedicated to parameter tuning (Fig. 3.15). During participant training, tuned parameters could be adjusted and saved for reuse in subsequent training or trial sessions.

To establish communication with the PC application, a BLE service was implemented on the data acquisition board. The BLE service was configured as a server driver and assigned a random universally unique identifier (UUID). All data transmissions and receptions were conducted through a single Generic Attribute (GATT) service.

Typically, separate services are created for data transmission and reception to optimize performance. However, since a high data streaming rate was not a priority for this application, a single service was used to simplify the programming process.

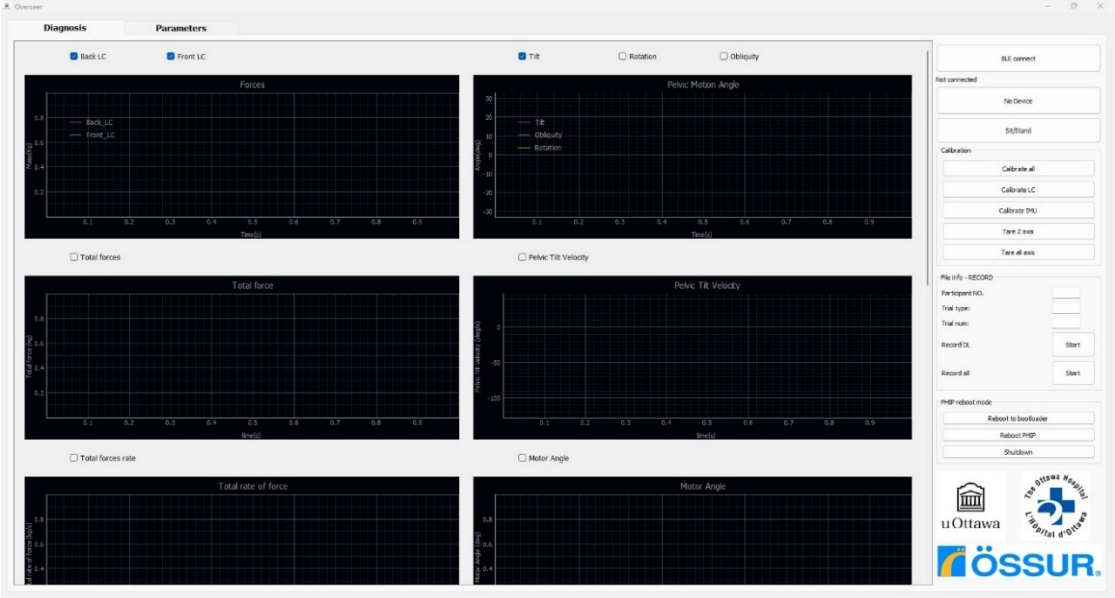

Fig. 3.14 PC application GUI of Power Hip diagnosis tab.

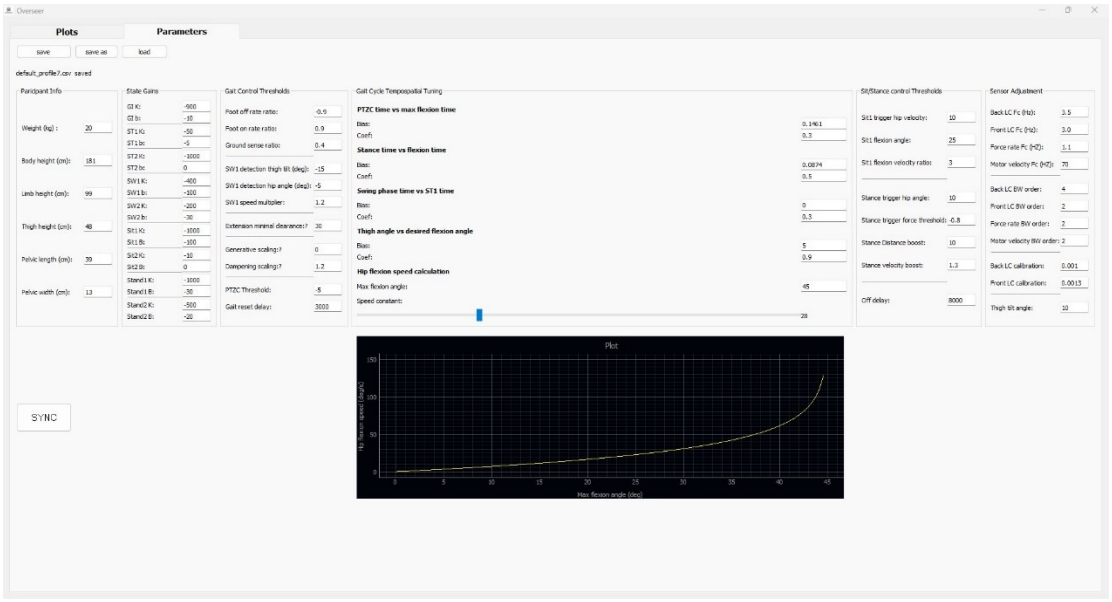

Fig. 3.15 PC application GUI of Power Hip parameter tuning tab.

Chapter 4: A pelvic kinematic approach for calculating hip angles for active hip disarticulation prosthesis control

4.1 Foreword

As discussed in Section 2.4.3, the phase-based mid-level controller performs spatial and temporal modulation on the normalized hip trajectory to generate the hip angle trajectory. Therefore, a novel algorithm was required to calculate the hip angle of HD amputees from pelvic motions.

The development of this algorithm was based on TF amputee gait data utilizing the pelvic motions and ground reaction forces. Specifically, 3D pelvic motion and stance time data from 10 TF prosthesis users were used to extract unique features to design a hip angle calculation algorithm. This algorithm was tested on a different set of TF gait data to evaluate accuracy. The algorithm estimated hip angle and angular velocity with high precision and low error, using only pelvic rotation, pelvic tilt, and stance time as inputs. These findings suggested that small pelvic movements can be a reliable user input method to control gait of an active hip prosthesis, reducing the need for excessive pelvic motion while increasing the hip joint's range of motion. Outcomes of this study directly contributed to partial fulfilment of thesis objective 1: "Develop a motorized HKAF prosthesis control strategy for gait initiation, termination, and level walking".

This chapter was published in the Journal of NeuroEngineering and Rehabilitation:

F. Golshan, N. Baddour, H. Gholizadeh, and E. D. Lemaire, "A pelvic kinematic approach for calculating hip angles for active hip disarticulation prosthesis control," *J Neuroeng Rehabil,* vol. 20, no. 1, p. 152, Nov 9 2023, doi: 10.1186/s12984-023-01273-x.

4.2 Introduction

People with an amputation at the hip level have the most difficulty returning to walking [35]. Operating a passive hip disarticulation (HD) prosthesis can be physically demanding, especially for elderly users, and requires sufficient physical fitness [14], [148]. Furthermore, in cases where people continued to use their prostheses, excessive pelvic tilt and rotation during ambulation could eventually lead to spinal injuries [10]. The lack of muscle power at the hip, knee, and ankle/foot can also result in a fixed and slow cadence. A possible solution to reduce physical demand and improve mobility in people with HD amputation is to utilize active actuators to operate the hip joint intelligently. User input is required for hip control; however, identifying viable user input that could

be used for prosthetic control is a challenge since hip disarticulation amputees lack the entire hip and leg.

In conjunction with knowledge of 3D gait biomechanics, advancements in actuator and sensor technologies have produced effective control systems for lower extremity prostheses [149]. Powered knee joints that actively aid the prosthetic user in challenging terrains can be beneficial by reducing strain on the body [18], [129]. However, microprocessor-controlled and powered hip joints are only now being investigated in the research domain [16].

Ueyama et al. [16] substituted conventional prosthetic hip and knee joints with robotic motorized joints to actuate the knee and hip. Their prototype used a simple gait control strategy to mirror intact limb motion. A feedback controller allowed the hip to extend while compressing a virtual spring as the participant moved the intact limb forward. The compressed virtual spring's potential energy was released during swing phase, allowing the actuators to swing the prosthesis forward. While this gait control method produced natural gait patterns, the control method was not viable for day-to-day activities due to limited user control. User control becomes especially crucial while operating a powerful joint capable of propelling the user forward. Mirroring the intact limb is also problematic for stumbles or other asymmetric gait activities (e.g., working in a kitchen, etc.). With the evolution of hip prosthetic actuation, the need for a robust and reliable control mechanism has become essential [23].

Similar to people with transfemoral (TF) and transtibial amputations, some people with an HD amputation are fitted with a prosthesis and receive rehabilitation to use the new prosthesis appropriately [1]. Unlike TF and transtibial amputees that utilize thigh or shank skeletomuscular segments to help control their prosthesis, HD patients typically rely on their pelvis and torso to operate and control their passive hip-knee-ankle-foot (HKAF) prosthesis [66, 150, 151]. Since motorized HD prosthesis kinetics and kinematics differ from gait with passive devices [16], applied torque through the motorized hip joint will require a specific gait control strategy [23]. That is, conventional mechanical HD prosthesis biomechanics cannot be directly used for optimal motorized hip joint performance. A more appropriate comparator for walking with a powered hip joint would be TF amputee gait since both powered-hip-HKAF, and TF prostheses can have similar prosthetic knee joints and feet; therefore, a well controlled hip joint could allow an HD amputee to walk as well as a TF amputee [103]. The sole body segment an HD amputee can directly control is the pelvis. Thus, understanding how TF amputees' pelvic motion relates to hip angle during the gait cycle can be the basis of a powered hip joint control approach.

In this research, we identified common pelvic motion features during the gait cycle among TF prosthesis users and determined how these features influence hip flexion and extension. These pelvic features and their relationship with hip rotation were then used to develop an algorithm to estimate the hip angle at each instant of gait cycle. Thus, this algorithm enables hip angle to be calculated from pelvic motion measurements. Successful evaluation of this algorithm with a separate TF amputee gait dataset demonstrates the viability of this new approach. This pelvis-based approach enables progression to the next phase of powered hip joint control system development, leading to better mobility for people with hip-level amputations.

4.3 Methods

We investigated TF amputee pelvic motions (pelvic tilt, pelvic obliquity, pelvic rotation) and their relationship with hip rotation. These data were used to develop an algorithm to calculate hip angles throughout the gait cycle, from pelvis motion while walking on level ground. Hip angles calculated by the algorithm were compared with measured (motion-captured) hip angles to quantify algorithm performance. This model focused on level steady-state walking.

4.3.1 Databases

Two databases of transfemoral amputee gait were used in this study, for algorithm development and validation. Dataset selection requirements were: all participants must be TF amputees, participants must ambulate without relying on walking assistive devices such as canes, walkers, or treadmill assistive bars; gait data must be from steady-state sequences of level walking tests.

A database from a group of 10 people with unilateral transfemoral amputation with K3 and K4 activity levels [152] was used for algorithm development. Data were collected in the CAREN Extended virtual reality laboratory at The Ottawa Hospital Rehabilitation Centre and processed with C-motion Visual 3D (version 6) and MATLAB software version 2021a [76], [153]. People walked on a treadmill (level walking) at self-selected walking speeds, and ten strides per person were extracted (a total of 100 strides). The development group's mean age was 47 ± 9.4 years, mass was 85 ± 8.6 kg, and height was 176 ± 9 cm. The Ottawa Health Science Network Research Ethics Board approved the secondary use of this dataset.

Testing group data were obtained from a recently published database ([154], [155]) that used 10 VICON 3D motion capture cameras and a dual-belt instrumented Bertec treadmill. Ten people with unilateral transfemoral amputation with K2 and K3 activity levels met our inclusion criteria. Participants walked at different fixed speeds based on their activity level. People with K2 activity

levels completed separate walking trials at 0.4, 0.5, 0.6, 0.7, and 0.8 m/s. Those with K3 activity levels walked at 0.6, 0.8, 1.0, 1.2, and 1.4 m/s. MATLAB™ R2021a was used to extract C3D files, apply a CODA pelvic model [156], and calculate 3D pelvis angles. The testing group's mean age was 47 ± 15 years, weight was 84.5 ± 17.6 kg, and height was 177 ±11 cm.

Differences between the development and testing groups for activity level, walking speed, or prosthetic components are desirable when evaluating model performance on different groups of participants. This helps to determine model generalizability and avoid cases where better results are due to training and testing on the same group. Prosthesis details for both groups are presented in Table 4.1 and Table 4.2 below.

Table 4.1 Testing group details

PNO.	Mobility Class	Prosthetic knee	Knee control method	Number of strides
1	K3	Plié[1]	MPU	166
2	K2	C-leg[2]	MPU	263
3	K3	C-leg[2]	MPU	232
4	K3	Rheo[3]	MPU	210
5	K2	C-leg[2]	MPU	249
6	K3	C-leg[2]	MPU	243
7	K2	C-leg[2]	MPU	235
8	K3	C-leg[2]	MPU	310
9	K3	Plié[1]	MPU	285
10	K3	C-leg[2]	MPU	210

Manufacturers: 1=Freedom innovations, 2=Ottobock, 3=Össur

Table 4.2 Development group details

PNO.	Mobility Class	Prosthetic knee	Knee control method	Number of strides
1	K4	C-leg[1]	MPU	10
2	K4	C-leg[1]	MPU	10
3	K3	C-leg[1]	MPU	10
4	K3	C-leg[1]	MPU	10
5	K4	Endolite	Mechanical	10
6	K4	Mauch[2]	Mechanical	10
7	K3	C-leg[1]	MPU	10
8	K4	Trulife	Mechanical	10
9	K3	X3[1]	MPU	10
10	K4	X3[1]	MPU	10

Manufacturers: 1=Ottobock, 2=Össur

4.3.2 Algorithm development

Pelvic movement in sagittal (anterior/posterior tilt), frontal (lateral tilt or obliquity), and transverse (pelvic rotation) planes were investigated, and gait phase transition timing was assessed to determine their correlation with hip angle throughout the gait cycle. The hip angle calculation algorithm development required:

A. **Hip angle features**: Temporal and spatial hip angle features to calculate hip angular velocity.

B. **Correlations**: Analyze pelvic motion and stance time data to determine common features and correlations with hip angle features.

C. **Hip angle feature calculation equations**: Develop regression equations to calculate the hip angle features using the identified pelvic features in step B.

D. **Identification of per-person constants**: Determine constant parameters unique to each person's gait characteristics that could be used for algorithm development.

E. **Sequential hip angle calculation**: Develop an algorithm for real-time hip angle calculation using parameters obtained in steps C and D.

F. **Algorithm performance**: Evaluate the model with a new data set (testing group).

Each of these will be considered in turn.

A. Hip angle features

A typical gait cycle for people with transfemoral amputation includes ([157], [103]): foot contacts the ground (foot strike) with the hip flexed to ~30°; hip moves to ~5° of extension at the end of stance; hip starts to flex ~35° until 80%-90% of stride; and hip flexion decreases ~5° in terminal swing to ensure that the prosthetic knee is fully extended before the next foot-strike [53, 57, 119, 127].

Hip angle kinematics can be divided into three periods (Fig. 4.1), with each period having a linear progression of hip angle by time (i.e., constant slope or constant angular velocity).

- **Period 1 (hip extension):** Initiates at foot-strike and ends at 50%-60% of the gait cycle. The angular velocity vector is always negative.
- **Period 2 (hip flexion):** Initiates at hip max extension and continues through the stance-to-swing transition with minor angular velocity change. The velocity vector is always positive.

- **Period 3 (knee control):** Knee joint behaviour directly affects hip rotation in this period, with hip rotation acting to keep the prosthetic knee fully extended. For this study, hip angle throughout period 3 was assumed to be constant (angular velocity is zero) until the next foot strike.

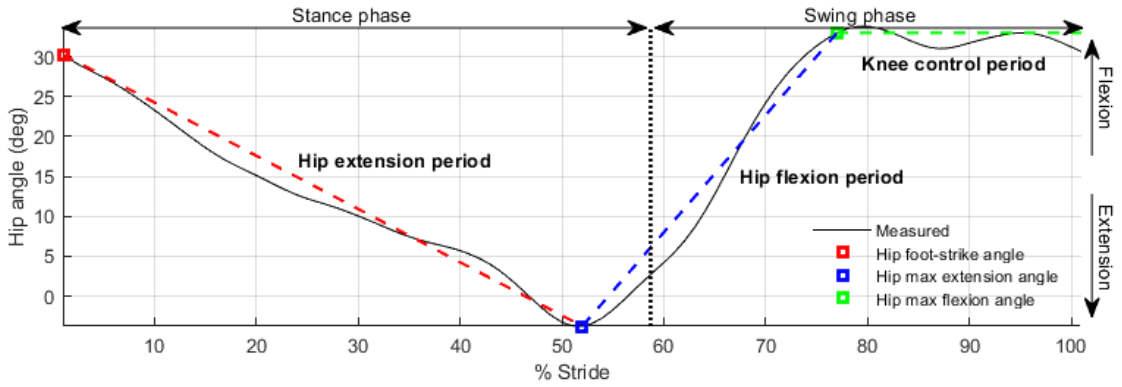

Fig. 4.1 Three hip angle periods during gait cycle: hip rotation toward negative angle (extension), hip rotation toward positive angle (flexion), constant angle. Measured curve is the average of 100 strides in the development group.

Hip angular velocity was assumed to remain mostly constant throughout each period, simplifying the hip angle calculation. Five features were present for all participants; therefore, these features were used to calculate the constant angular velocity during each period. Spatial features were hip angle at foot strike ($H\theta_{FS}$), maximum hip extension angle ($H\theta_{ME}$), and maximum hip flexion angle ($H\theta_{MF}$). Temporal features were maximum hip extension time ($H\tau_{ME}$) and maximum hip flexion time ($H\tau_{MF}$).

For period 1 (hip extension), the constant angular velocity was calculated using $H\theta_{FS}$, $H\theta_{ME}$, and the difference in time between the two features. For period 2 (hip flexion), the constant angular velocity was calculated using $H\theta_{ME}$, $H\theta_{MF}$, and the difference in time between the two features. In period 3 (knee control), hip angle was assumed to be constant at $H\theta_{MF}$ (i.e., zero angular velocity).

The algorithm uses these angular velocity values to calculate hip angle at each time point. Therefore, equations that define the relationships between pelvic kinematics and hip features are required.

B. Correlations

Pelvic angular velocity, pelvic tilt, pelvic obliquity, pelvic rotation, and stance time per stride in the development group were analyzed to determine common features that could be used to calculate the constant hip angular displacement and velocities. Twenty-two magnitudes of three-axis pelvic

angle and angular velocities and, three-axis pelvic velocity zero threshold crossing (ZC) timing features were identified as potential candidates.

Next, Pearson correlation analyses were applied to each feature candidate to determine which features were most related to the hip angle features. The strongest correlations were (Fig. 4.2):

- Pelvic tilt angle at foot strike ($PT\theta_{FS}$) and hip angle at foot-strike ($H\theta_{FS}$): r=0.95
- Timing of pelvic rotation angular velocity zero-crossing in early stance ($PR\tau_{ZC}$) and the hip rotation angle range of motion during that period ($\Delta H\theta$): r =-0.75
- Timing of pelvic tilt angular velocity first zero crossing in midstance ($PT\tau_{ZC1}$) and hip max extension time ($H\tau_{ME}$): r=0.90
- $PT\tau_{ZC1}$ and hip max flexion time ($H\tau_{MF}$): r=0.82
- Stance time (τs) and hip max flexion time ($H\tau_{MF}$): r=0.93

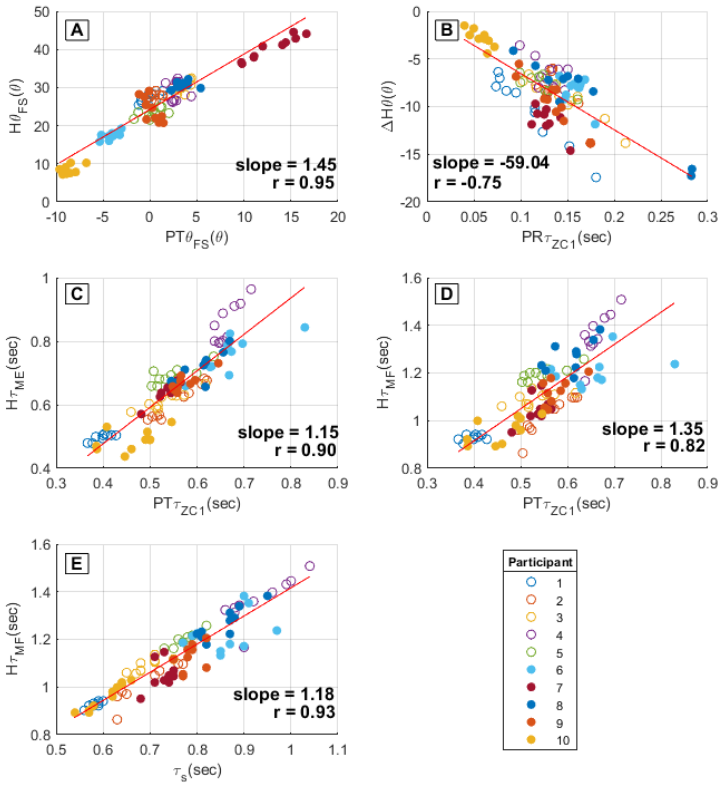

Fig. 4.2 Pelvic feature and stance time correlation with hip angle features. A: pelvic tilt angle at foot strike ($PT\theta_{FS}$) and hip angle at foot-strike ($H\theta_{FS}$), B: Timing of pelvic angular velocity zero-crossing in early stance ($PR\tau_{ZC1}$) and hip angle range of motion during that period ($\Delta H\theta$), C: Timing of pelvic tilt angular velocity first zero crossing in midstance ($PT\tau_{ZC1}$) and hip max extension time ($H\tau_{ME}$), D: Timing of pelvic tilt angular velocity first zero crossing in mid-swing ($PT\tau_{ZC1}$) and hip max flexion time ($H\tau_{MF}$), E: stance time (τs) and hip max flexion time ($H\tau_{MF}$).

$PT\tau_{ZC}$ (Timing of pelvic rotation angular velocity zero-crossing in early stance) can be detected in real-time by continuously monitoring the 10 most recent pelvic tilt angular velocity data samples. If the most recent sample is positive while the prior 10 samples are negative, positive zero-crossing is detected (Fig. 4.3).

$PR\tau_{ZC1}$ (Timing of pelvic tilt angular velocity first zero crossing in mid-swing) is detectable by measuring the pelvic rotation angular velocity zero-crossing (Fig. 4.4). Initially, angular velocity should be in the positive region. The crossing instance is marked if the angular velocity vector crosses the zero value into the negative angular velocity region.

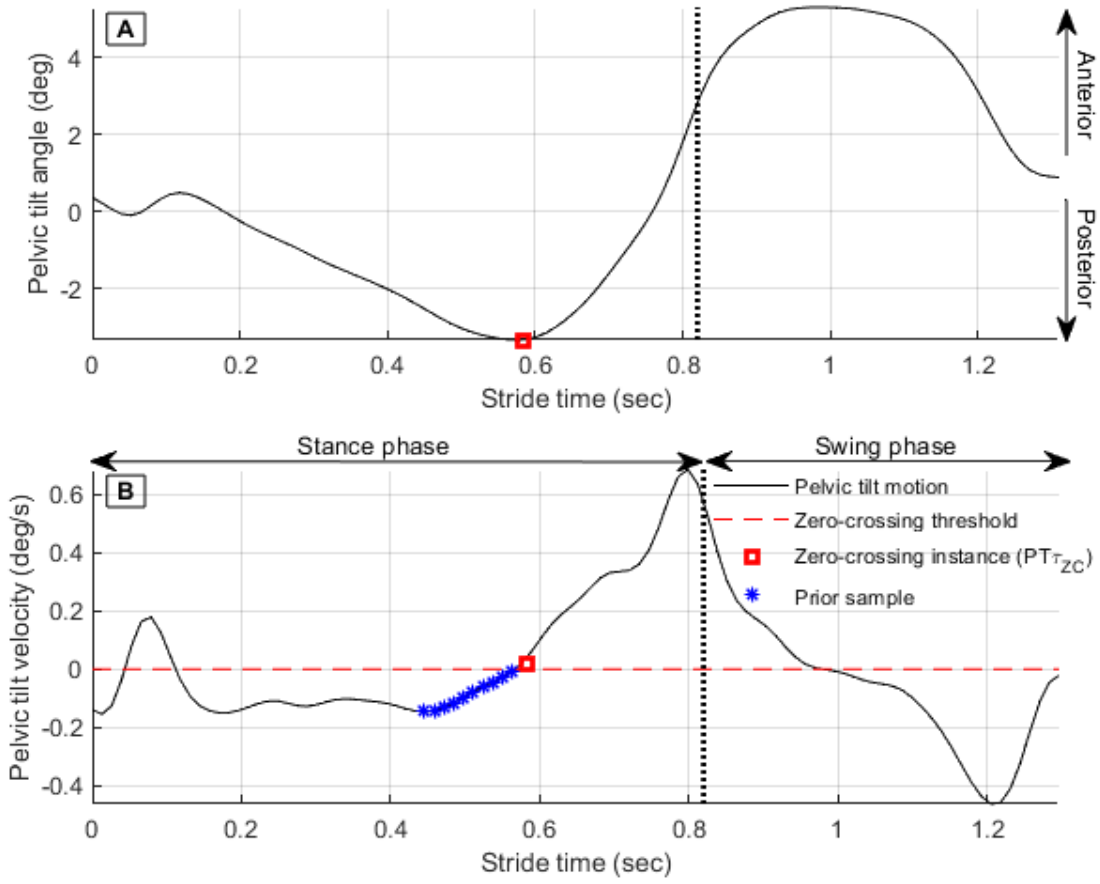

Fig. 4.3 Pelvic tilt angular displacement (A) and corresponding pelvic tilt angular velocity (B). The red square represents the most recent sample, while the blue stars represent the 10 data samples prior to the most recent sample.

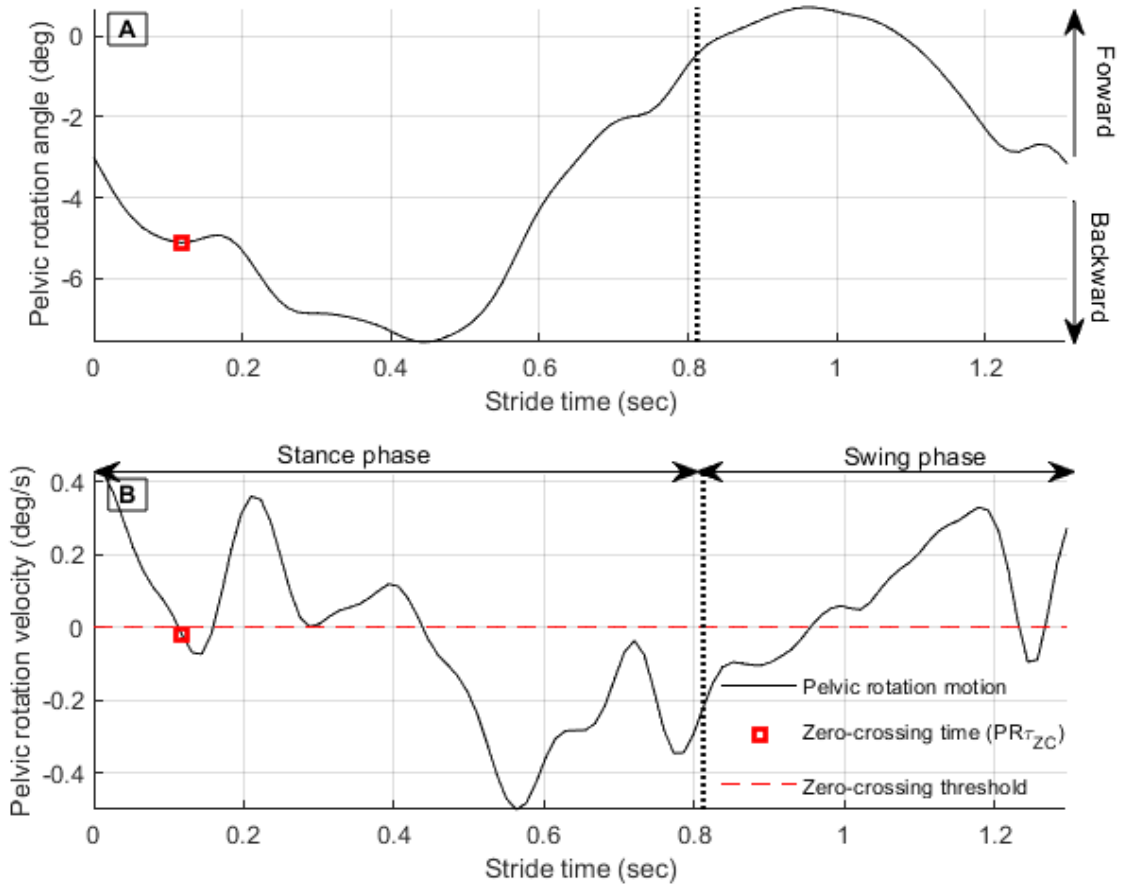

Fig. 4.4 Pelvic rotation angular displacement (A) and corresponding pelvic rotation angular velocity (B).

C. Hip angle feature calculation equations

A series of linear regression equations were determined to calculate the hip angle features based on the linear relationships and correlations between pelvic motion features, stance time, and hip rotation features (Fig. 4.2).

Regression equation 4.1 calculates hip angle at foot strike.

$$H\theta_{FS} = 24.27 + (1.45 \times PT\theta_{FS}) \quad (4.1)$$

where $H\theta_{FS}$ is hip angle at foot strike and $PT\theta_{FS}$ is pelvic tilt angle at foot strike.

Regression equation 4.2 determines $\Delta H\theta$ using $PR\tau_{ZC}$ (Fig. 4.2).

$$\Delta H\theta = -0.6261 - (59.04 \times PR\tau_{ZC}) \quad (4.2)$$

where $PR\tau_{ZC}$ is the difference between the time of pelvic rotation angular velocity first zero crossing and foot-strike time. $\Delta H\theta$ is the difference between hip angle at foot-strike and hip angle at $PR\tau_{ZC}$ time (Fig. 4.3).

Regression equation 4.3 calculates hip max extension time using $PT\tau_{ZC}$.

$$H\tau_{ME} = 0.0462 + (1.15 \times PT\tau_{ZC}) \quad (4.3)$$

where $PT\tau_{ZC}$ is the time of pelvic tilt angular velocity zero crossing and $H\tau_{ME}$ is the hip max extension time.

During stance phase, when pelvic tilt zero crossing ($PT\tau_{ZC}$) occurs, equation 4.4 is used to calculate the hip max flexion time ($H\tau_{MF}$). $H\tau_{MF}$ correlation with $PT\tau_{ZC}$ was 0.82. At the end of stance phase, $H\tau_{MF}$ is updated by using equation 4.5, since the correlation between the end of stance phase time (τ_s) and $H\tau_{MF}$ is much higher (R = 0.94) than the correlation between $PT\tau_{ZC}$ and $H\tau_{MF}$. Therefore, algorithm accuracy is improved for the remainder of the gait cycle.

$$H\tau_{MF\alpha} = 0.3461 + (1.35 \times PT\tau_{ZC}) \quad (4.4)$$

where $PT\tau_{ZC}$ is the timing of pelvic tilt zero crossing (Fig. 4.2), and $H\tau_{MF\alpha}$ is the hip max flexion time at the $PT\tau_{ZC}$ instant.

$$H\tau_{MF\beta} = 0.0874 + (1.18 \times \tau_S) \quad (4.5)$$

where τ_S is the gait stance time, and $H\tau_{MF\beta}$ is max hip flexion time at foot-off.

D. Per person, unique constants

For hip angle calculation using the developed algorithm, two unique input constants were defined for each person after analyzing the development dataset: mean hip max extension and mean hip max flexion angles. In practice, during the fitting process, a prosthetist would increase or decrease these constants through trial and error for each patient until results are satisfactory [158]. That is, iterative changes are made to the values during the prosthetic fitting process until gait is acceptable to the end-user and clinician, similar to the process for tuning other microprocessor controlled prosthetic joints.

Hip max extension and max flexion angles tended to be in a unique but limited range for each TF amputee in the development group. Studies suggested that this unique hip ROM is due to prosthesis user control strategies to maintain balance during walking [159], [160]. The per-person-specific hip max extension and max flexion angle constants for both development and testing groups are provided in Table 4.3 below.

Table 4.3 Per-person unique constants of development and testing group datasets

PNO.	Development group		Testing group	
	$\overline{H\theta}_{ME}$	$\overline{H\theta}_{MF}$	$\overline{H\theta}_{ME}$	$\overline{H\theta}_{MF}$
1	-23.22	27.86	-4.69	37.14
2	-17.55	24.06	-5.1	27.93
3	-3.85	34.74	-10.26	28.02
4	-10.24	24.29	-9.25	37.33
5	-22.56	28.52	-10.88	32.82
6	-25.02	16.05	-7.61	41.01
7	-12.74	33.50	-4.64	27.35
8	-1.55	36.81	-9.52	32.64
9	-17.80	26.15	-7.16	32.03
10	-20.22	7.54	-15.94	38.64

Note: $\overline{H\theta}_{ME}$=Hip max extension angle constant, $\overline{H\theta}_{MF}$=Hip max flexion angle constant

E. Hip angle calculation

Fig. 4.5 shows the general block diagram of the hip angle calculation algorithm for steady state gait. Initially, pelvic features are extracted from pelvic motion data. Then, using the hip-angle feature calculation equations and foot-off time, the hip parameters necessary for constant hip angular velocity calculations are obtained. In the algorithm's last two stages, the calculated hip features are used to calculate hip angular velocity and hip angle.

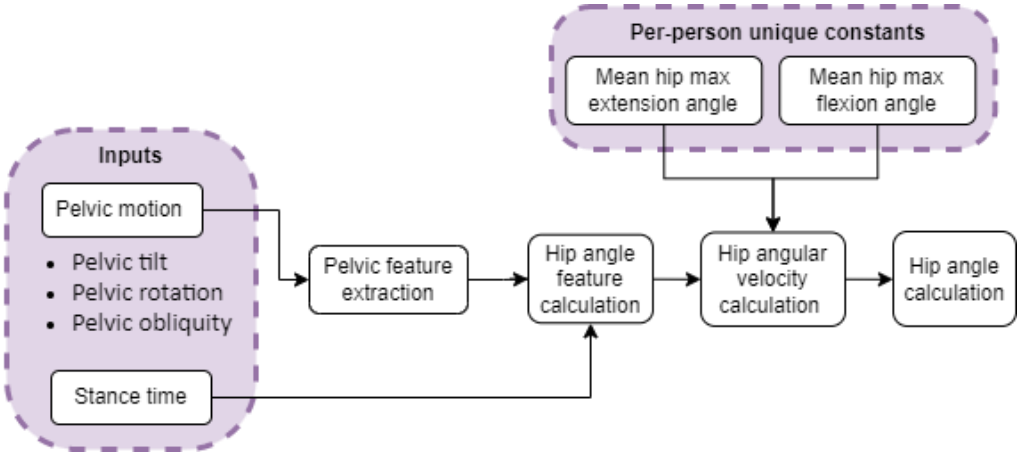

Fig. 4.5 Gait cycle hip angle calculation block diagram.

The six sequences shown in Fig. 4.6 represent six different hip angle equations used in the algorithm. Since the algorithm was developed to run in real time, pelvic features are detected by the algorithm at different times during the gait cycle (since people walk at different speeds).

Therefore, different hip calculation equations are used depending on the timing of each pelvic feature detected. The hip extension angle (period 1) is calculated during the first three sequences. During sequences 4 and 5, the hip angle during hip flexion (period 2) is calculated, and during sequence 6 the hip angle during period 3 is calculated. For detailed mathematics of hip calculations for each sequence, see Appendix B.

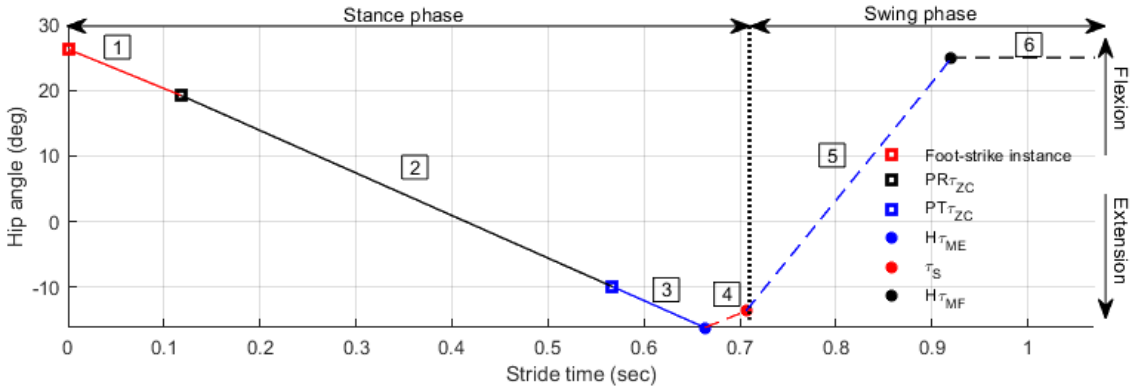

Fig. 4.6 Calculated hip angle throughout the gait cycle. $PR\tau_{ZC}$: pelvic rotation zero-crossing time, $PT\tau_{ZC}$: pelvic tilt zero-crossing time, $H\tau_{ME}$: hip max extension time, τ_s: Stance time, $H\tau_{MF}$: hip max flexion time. Sequences are foot-strike to $PR\tau_{ZC1}$ (sequence 1, solid red line), $PR\tau_{ZC1}$ to $PT\tau_{ZC1}$ (sequence 2, solid black line), $PT\tau_{ZC1}$ to $H\tau_{ME}$ (sequence 3, solid blue line), $H\tau_{ME}$ to τ_{FO} (sequence 4, red dashed line), τ_{FO} to $H\tau_{MF}$ (sequence 5, blue dashed line), and $H\tau_{MF}$ to the end of the gait cycle (sequence 6, black dashed line).

F. Algorithm evaluation

The developed algorithm was applied to both testing and development groups. Algorithm performance was assessed by calculating hip angle feature differences between calculated (algorithm) and motion capture system data (ground truth). To provide a reference for whether the differences were appropriate or beyond typical participant variability, the calculated differences were compared with participant-averaged hip feature standard deviations in the testing and development set.

4.4 Results

4.4.1 Development group

The average differences between motion-captured features and algorithm-calculated data for the development group are shown in Table 4.4. Hip max extension angle had the largest difference compared to other features, with the per-participant averaged difference ranging from 1.5° to 3.5°. The greatest overall mean difference was for hip max extension angle (2.4 ± 1.8°). Hip temporal features had the lowest difference, indicating that pelvic motion temporal features were in sync

with hip temporal features during the gait cycles. Hip angle had close agreement between measured and calculated data, with correlation values varying from 0.94 to 0.99.

The mean and standard deviation of hip feature angles for each participant in the development group are provided in Table 4.5 Motion-captured hip angle (average and standard deviation) of development group walking at a self-paced speed. On average, standard deviations were 1.7° at foot-strike, 1.4° at max extension, and 2.0° at max flexion. The mean differences in Table 4.4 were compared with the average standard deviation for each participant in Table 4.5. The algorithm-calculated features were at most 1° greater than the average standard deviations for development group participants walking at self-paced speed.

Table 4.4 Difference and correlation between motion-captured hip angle features and algorithm results in the development group

PNO.	$H\theta_{FS}$	$H\theta_{ME}$	$H\tau_{ME}$	$H\theta_{MF}$	$H\tau_{MF}$	Corr
1	3.0 ± 1.0	1.9 ± 1.6	0.0 ± 0.0	1.1 ± 1.2	0.2 ± 0.0	0.98 ± 0.01
2	2.5 ± 0.9	1.7 ± 1.1	0.0 ± 0.0	2.8 ± 1.5	0.1 ± 0.0	0.99 ± 0.00
3	1.1 ± 1.0	2.6 ± 1.8	0.0 ± 0.0	1.0 ± 1.4	0.2 ± 0.0	0.94 ± 0.03
4	2.6 ± 2.8	3.3 ± 1.9	0.1 ± 0.0	1.8 ± 1.9	0.2 ± 0.1	0.96 ± 0.02
5	1.6 ± 1.4	3.5 ± 3.5	0.0 ± 0.0	2.8 ± 0.8	0.2 ± 0.0	0.98 ± 0.01
6	1.0 ± 0.8	3.2 ± 2.8	0.0 ± 0.0	1.9 ± 2.2	0.1 ± 0.1	0.97 ± 0.01
7	2.6 ± 1.1	2.5 ± 2.5	0.0 ± 0.0	3.3 ± 4.8	0.1 ± 0.1	0.95 ± 0.03
8	1.7 ± 1.4	1.8 ± 2.1	0.0 ± 0.0	3.1 ± 2.0	0.2 ± 0.0	0.99 ± 0.01
9	3.6 ± 4.2	2.3 ± 2.6	0.0 ± 0.0	1.7 ± 2.1	0.1 ± 0.0	0.96 ± 0.02
10	3.2 ± 1.2	1.5 ± 1.1	0.1 ± 0.1	1.6 ± 1.1	0.2 ± 0.0	0.97 ± 0.01
Mean	2.3 ± 1.3	2.4 ± 1.8	0.0 ± 0.0	2.1 ± 1.7	0.2 ± 0.1	0.99 ± 0.01

Note: PNO. = Participant number, $H\theta_{FS}$ = Hip angle at Foot-strike(°), $H\theta_{ME}$ = Hip max extension angle(°), $H\tau_{ME}$ = Hip max extension time(sec), $H\theta_{MF}$ = Hip max flexion angle(°), $H\tau_{MF}$ = Hip max flexion time(sec), Corr = Pearson correlation.

Table 4.5 Motion-captured hip angle (average and standard deviation) of development group walking at a self-paced speed

PNO	$H\theta_{FS}$	$H\theta_{ME}$	$H\theta_{MF}$
1	27.4 ± 1.2	23.2 ± 0.6	28.7 ± 1.2
2	27.9 ± 1.1	17.6 ± 0.5	27.8 ± 1.5
3	30.2 ± 1.4	3.9 ± 0.5	34.2 ± 1.4
4	29.2 ± 2.6	12.3 ± 1.9	29.5 ± 2.4
5	23.2 ± 1.2	22.6 ± 1.3	26.1 ± 0.8
6	17.5 ± 1.0	25.0 ± 2.3	16.6 ± 2.2
7	40.4 ± 3.0	12.7 ± 3.3	34.9 ± 4.8
8	30.7 ± 0.9	1.6 ± 1.0	33.7 ± 2.0
9	24.3 ± 3.2	17.8 ± 1.5	26.7 ± 2.1
10	8.4 ± 1.1	20.2 ± 1.3	8.8 ± 1.1
Mean	25.9 ± 1.7	15.7 ± 1.4	26.7 ± 2.0

Note: PNO = Participant number, $H\theta_{FS}$ = Hip angle at foot-strike (°), $H\theta_{ME}$ = Hip max extension angle (°), $H\theta_{MF}$ = Hip max flexion angle (°).

4.4.2 Testing group

The algorithm was applied to 2403 strides from the testing group. The outcomes (Table 4.6) showed small differences between motion capture and algorithm measured data, similar to the development group results (Table 4.4). Mean hip max extension angle had the largest difference (3.4 ± 2.8°). Per-participant analysis showed that participant 7 had the largest overall difference compared to other participants in the testing group. Participant 7 also had the lowest correlation; however, most correlations were greater than 0.95.

Measured hip features for the testing group are provided in Table 4.7. Although testing group participants walked at a fixed speed, the hip feature standard deviations were approximately 0.3° more than the development group results. On average, hip feature standard deviations for the testing group were 2.6° at foot-strike, 3.0° at max extension, and 1.8° at max flexion. The measured and calculated hip feature differences in Table 4.6 were compared with the mean hip feature standard deviations in Table 4.7. Algorithm-calculated hip angle at foot-strike (2.0°) and hip max flexion angle (1.9°) were within the standard deviations for each feature. However, hip max extension angle difference was overestimated by 1.2°.

Table 4.6 Difference and correlation between the motion-captured hip angle features and the algorithm results in the testing group

PNO.	$H\theta_{FS}$	$H\theta_{ME}$	$H\tau_{ME}$	$H\theta_{MF}$	$H\tau_{MF}$	Corr
1	2.2 ± 1.7	3.1 ± 2.2	0.1 ± 0.0	2.4 ± 1.6	0.1 ± 0.0	0.97 ± 0.01
2	2.3 ± 1.4	2.8 ± 1.8	0.0 ± 0.0	2.2 ± 1.5	0.0 ± 0.1	0.96 ± 0.01
3	2.2 ± 1.4	2.3 ± 1.5	0.0 ± 0.0	2.0 ± 1.1	0.2 ± 0.0	0.95 ± 0.01
4	1.7 ± 1.3	3.1 ± 2.3	0.1 ± 0.0	1.9 ± 1.1	0.0 ± 0.0	0.97 ± 0.01
5	1.8 ± 1.4	3.5 ± 2.4	0.1 ± 0.0	1.5 ± 1.1	0.2 ± 0.1	0.97 ± 0.02
6	2.3 ± 1.7	2.9 ± 1.8	0.0 ± 0.0	2.5 ± 2.0	0.0 ± 0.1	0.94 ± 0.03
7	2.8 ± 1.8	4.5 ± 4.3	0.1 ± 0.1	1.8 ± 1.4	0.3 ± 0.4	0.90 ± 0.09
8	1.4 ± 1.3	2.8 ± 1.8	0.0 ± 0.0	1.4 ± 1.3	0.0 ± 0.0	0.95 ± 0.02
9	1.6 ± 1.0	3.4 ± 2.6	0.0 ± 0.0	1.5 ± 1.1	0.1 ± 0.0	0.92 ± 0.02
10	2.1 ± 2.1	3.1 ± 3.9	0.1 ± 0.0	2.0 ± 1.3	0.1 ± 0.0	0.98 ± 0.01
Mean	2.0 ± 1.6	3.4 ± 2.8	0.1 ± 0.1	1.9 ± 1.4	0.1 ± 0.2	0.95 ± 0.04

Note: PNO. = Participant number, $H\theta_{FS}$ = Hip angle at foot-strike(°), $H\theta_{ME}$ = Hip max extension angle(°), $H\tau_{ME}$ = Hip max extension time(sec), $H\theta_{MF}$ = Hip max flexion angle(°), $H\tau_{MF}$ = Hip max flexion time(sec), Corr = Pearson correlation.

Table 4.7 Motion captured hip angle (average and standard deviation) of testing group

PNO.	$H\theta_{FS}$	$H\theta_{ME}$	$H\theta_{MF}$
1	34.5 ± 3.3	4.7 ± 1.8	37.1 ± 2.9
2	23.4 ± 1.7	5.1 ± 1.9	27.9 ± 2.7
3	26.1 ± 3.1	10.3 ± 1.8	28.0 ± 2.2
4	31.3 ± 1.8	9.3 ± 2.6	37.3 ± 2.2
5	24.8 ± 2.0	10.9 ± 1.8	32.8 ± 1.9
6	29.9 ± 2.9	7.6 ± 2.2	41.0 ± 3.2
7	24.3 ± 1.8	4.6 ± 1.6	27.4 ± 2.3
8	26.7 ± 1.9	9.5 ± 2.2	32.6 ± 1.9
9	30.4 ± 2.0	7.2 ± 3.4	32.0 ± 1.8
10	34.7 ± 2.6	15.9 ± 3.0	38.6 ± 2.4
Mean	28.6 ± 2.3	8.5 ± 2.2	33.5 ± 2.3

Note: PNO. = Participant number, $H\theta_{FS}$ = Hip angle at foot-strike (°), $H\theta_{ME}$ = Hip max extension angle (°), $H\theta_{MF}$ = Hip max flexion angle (°).

4.5 Discussion

In this research, we investigated pelvic movements of people with transfemoral amputation and developed a viable algorithm for calculating hip angles based on pelvic motion and stance time. With the introduction of powered prosthetic joints, the limitations of existing prostheses are mitigated by transferring a large amount of the mechanical work to the actuator, reducing the reliance on the user's physical capabilities to operate the prosthesis [16], [37]. Since only the pelvis segment is available for user control of a motorized hip joint, a new approach is required to convert pelvic motion (system input) into a hip angular map for a gait controller to follow. The approach proposed in this research addresses this need.

The newly developed algorithm requires only three features (pelvic tilt angle at foot strike, timing of pelvic rotation angular velocity zero-crossing in early stance, and timing of pelvic tilt angular velocity first zero crossing in midstance) and stance time data for hip angle calculation. After pelvic angle analysis, pelvic tilt and rotation exhibited common behaviours among most people in the development and testing groups and hence could be used for hip angle calculation. Pelvic angle features that correlated well with the hip angle features were then extracted for algorithm development.

Pelvic obliquity varied greatly between strides in both groups and although some common features were found, none were viable features for a motorized hip prosthetic control system. Although the pelvic tilt zero-crossing feature ($PT_{\tau ZC}$) was common among all persons in both groups, pelvic tilt of participant 7 in the testing group tended to be irregular relative to other people, even though there was no gait pathology observed during data acquisition. This irregularity resulted in many pelvic feature detection errors. Adequate gait training is required to avoid pelvic motions leading to pelvic feature or hip angle errors.

Model output from both development and testing datasets had very high correlations between motion capture and algorithm calculated data (R= 0.99 for development group and R= 0.95 for testing group). The high correlations indicated that the assumed three-period hip angle model (Fig. 4.1) closely matched typical hip angles for transfemoral amputees.

Motion capture and algorithm-measured hip angle features had small differences for all testing and development group participants. The largest difference was hip max extension angle for the development group (2.4 ± 1.8°) and hip max extension angle for the testing group (3.4 ± 2.8°). Furthermore, the temporal hip feature differences (hip max extension time, max flexion time) were close to zero, indicating that the algorithm can accurately calculate temporal hip features.

Comparing the differences with standard deviations of both datasets showed that only the calculated hip max extension angle exceeded the participant's typical standard deviation (by 1° for development group and by 1.2° for testing group). All other hip feature differences between calculated and measured values were within the measured standard deviations. We hypothesize that, in practice, exceeding the typical hip angles by 1.2° should not substantially affect an active hip prosthesis user's stability or comfort. However, further testing with a prototype prosthesis is necessary to assess the effect of the hip angle algorithm on mobility.

Analysis of development and testing group data showed that hip max extension and hip max flexion angles during the gait cycle tended to vary slightly in a unique range for each person. Thus, each participant's hip max extension and flexion angles averaged over all strides were used as input constants for each participant in this study (Fig. 4.5). As a person walks, hip max extension and flexion angles remain consistent or vary slightly within a limited range, even with changes in walking speed. It is important to note that per-person unique constants were determined because people in both groups walked at speeds between 0.4 m/s to 1.5 m/s; therefore, an additional analysis could be required for people with preferred walking speeds outside this range. When the algorithm is used in practice for a powered hip control system, the clinician responsible for prosthetic fitting should adjust the hip max extension angle and hip max flexion angle constants to accommodate the user. These parameters would then be entered into the system as unique per-person constants.

While we utilized correlation analysis to identify the relationship between pelvic motions and sagittal hip angles, additional biomechanical signal analysis tools, such as wavelet analysis [161], and biomechanical pattern recognition approaches, such as machine learning and state estimation [162], could be investigated in future research.

This research used gold-standard 3D motion capture data for pelvic kinematics measurements [163]. However, wearable systems such as lower limb prosthetics need integrated measurement technology to provide real-time input for prosthesis control. Recent studies have investigated the feasibility of using inertial measurement units (IMUs) to measure lower extremity kinematics [164, 165]. In a study by Berner et al. [164], multiple IMUs were used to measure the kinematics of different body segments with high accuracy. In another study, researchers accurately measured pelvic kinematics of an able-bodied participant by utilizing a single IMU mounted to the lower back [165].

In theory, the required pelvic motion input data for the developed algorithm could be provided by an IMU integrated into the socket connection component (i.e., IMU moves with the socket,

which is attached to the pelvis, to provide pelvis kinematics) and a loadcell in the joint to measure applied forces such as at foot strike. Considering the greater reliance of HD amputees on pelvic and trunk motions, future algorithm tuning of the pelvis feature detection and hip angle calculation algorithm are anticipated to optimize the prosthesis gait controller. By utilizing powered and intelligent hip joints, gait in people with an HD amputation could be improved to a level similar to people with transfemoral amputation. As powered hip prostheses become more widely available, new gait data could be collected with HD participants and used to improve the algorithm.

Ultimately, the algorithm proposed in this research is an important step towards creating a powered hip prosthesis controller that enables more efficient movement in the person's chosen environment, potentially with less strain on the lower back and less effort as a result of reduced pelvic movements.

4.5.1 Limitations

The testing group people walked on a treadmill at fixed speeds that were different than the development group. Furthermore, all gait cycle data used in this study were at a steady state. Therefore, it is possible that fixed-speed steady-state walking reduced the natural gait variation and thus contributed to the high accuracy of our algorithm.

4.6 Conclusion

A viable algorithm was developed and evaluated to calculate hip angles throughout the gait cycle using only pelvis angles and stance time data. This new hip angle calculation method lays the groundwork for the future development of an intelligent powered hip prosthesis control system since it permits the use of measurable pelvic data to generate hip data as user input for a person's HKAF prosthesis. Based on our gait kinematics and kinetics analysis, hip angle calculations would require sensors in the prosthesis capable of detecting pelvic kinematics and stance phase.

Chapter 5: Design and preliminary evaluation of a gait control strategy for hip-knee-ankle-foot prosthesis with motorized hip joint

5.1 Foreword

This chapter describes the implementation and evaluation of the gait control strategy developed for the motorized hip prosthesis prototype, thus continuing to contribute towards addressing thesis objective 1: *Develop a motorized HKAF prosthesis control strategy for gait initiation, termination, and level walking.* The framework for the control strategy was adapted from the hierarchical approach proposed by Tucker et al. [23], with modifications to address the unique challenges of powered hip joint control. Unlike motorized knee prostheses, which rely on hip kinematic and ground reaction force, hip control requires predictive inputs derived from pelvic tilt movements (discussed in Chapter 4), prosthetic thigh tilting angle, prosthetic hip sagittal angle, and ground reaction force to determine gait subphase, target hip angle and angular velocity. A novel algorithm was introduced to estimate this state at high-level controller framework (described in Section 2.4.2).

Initial testing involved able-bodied participants walking with the prosthesis via an HD prosthesis simulator [136], allowing iterative refinement of the algorithm. Feedback from subsequent trials with HD participants further guided adjustments to improve responsiveness and user comfort. The final control strategy enabled users to initiate, terminate, and adjust walking speed for each trial by automatically adjusting the tempo-spatial hip biomechanics. A three-speed walk test was conducted with one participant to quantify performance, evaluating the controller's ability to dynamically adjust temporal and spatial parameters across slow, self-paced, and fast speeds.

Contents of this chapter have been submitted to the IEEE Transactions on Neural Systems and Rehabilitation Engineering journal for review and eventual publication. The design process detailed in this chapter, from simulation-based validation discussed in Chapter 4 to real-world testing, lays the foundation for future work to explore engineering methods for developing motorized HKAF control strategies.

5.2 Introduction

Hip disarticulation (HD) or hemipelvectomy (HP) amputation is a life-altering surgery that can severely restrict the mobility of the affected individual. Removal of ankle, knee, and hip joints impedes mobility and drastically changes a person's lifestyle [12]. While a hip-knee-ankle-foot

(HKAF) prosthesis can be prescribed, end-user acceptance of the prosthesis is never guaranteed. Case studies have shown that walking with an HKAF prosthesis can be a difficult experience with a steep learning curve, which not all people are willing to undertake [12, 35]. Moreover, to operate the prosthesis, prosthetic users must perform energy-demanding complementary maneuvers such as sound-side vaulting (heel hike) and excessive pelvic tilting that can induce muscle fatigue during short walks [14]. Over the long term, compensation by the residual limb during walking, sitting down, standing up, and climbing stairs can lead to other complications, such as back pain [166].

Over the years, many advancements have been made to improve reliability and reduce the physical demand for operating HKAF prostheses. However, prosthetic hip joints available on the market are primarily passive mechanical joints. In contrast, knee and foot prostheses have continued to evolve by utilizing the latest sensors and actuator technologies [98, 122]. Although passive prosthetic joints are much lighter than microprocessor-controlled joints, studies and surveys have proven that the added weight can be an acceptable compromise [167]. A notable benefit of powered knee and ankle prostheses is reduced residual limb compensations during strenuous tasks, which can help the prosthetic user walk longer and faster [168].

Research on motorized HKAF prostheses, particularly for HD and HP amputees, is still in its infancy. Currently, studies have only been conducted with able-bodied participants or through simulations using alignment setups unsuitable for daily use by HD or HP amputees [16, 30]. This lack of comprehensive research leaves the viability of the motorized HKAF approach for HD and HP amputees untested. We believe that HD and HP amputees could greatly benefit from a motorized HKAF prosthesis. However, a feasibility study would be impossible without a motorized HKAF prosthesis prototype compatible with existing prosthetic standards and an intuitive control strategy that prosthetic users can easily adapt.

Recent systematic reviews of motorized knee and ankle prostheses have demonstrated significant advancements in design and software approaches [23, 94, 98, 122]. Building upon our previous research on single-axis motorized hip joint design [31], we integrated the mechanical design using a similar hierarchical control strategy as used in motorized prosthetic knees [23]. This enabled us to create and evaluate a new HKAF prosthesis prototype with a motorized hip joint, which we named the "Power Hip".

The primary objective of this study is to develop and validate a gait speed-adaptive control strategy that emulates the hip kinematics of TF amputees. To evaluate the prototype, an HD participant who had previously used a passive HKAF prosthesis was trained to walk with the Power

Hip. In the Carleton University Abilities Living Lab, markerless motion capture was used to compare hip joint kinematics and spatiotemporal gait parameters at different walking speed between Power Hip and data from TF prosthesis users. The rationale for benchmarking against TF amputees stems from the shared use of knee prostheses in both TF and HKAF prostheses. This study has the potential to pave the way for a new category of HKAF prostheses, expanding options for HD amputees whose needs may not have been met with the currently available choices.

5.3 Prototype design

The prototype configuration consisted of an HD socket, the Power Hip module, Össur Rheo knee XC, and Össur Proflex foot (Fig. 5.1). In comparison to the original design detailed in [31], the Power Hip module's height was reduced to better accommodate individuals with shorter thigh lengths. The final prototype could be worn by HD participants with a minimum lower limb length of 77 cm (measured from the ischium to the foot sole) and body mass up to 100 kg. To customize the prototype for the participant, their original socket was replicated, and the connecting pylons were adjusted to match their overall lower limb height.

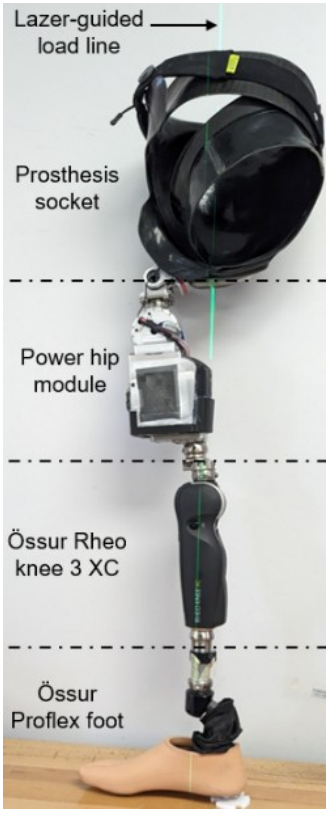

Fig. 5.1 Final prototype for Power Hip testing.

5.3.1 Power Hip module

Fig. 5.1 shows a detailed view of the Power Hip module, which comprises the thigh section and the joint section. The thigh section houses the motor driver board, main microcontroller, 95.04 Wh (3.3 Ah) battery, and a data logging board. The data logging board can record sensor data and communicate over Bluetooth with a computer for gait control parameter adjustments. The overall dimensions of the power module were 261x82x92 mm.

The Power Hip joint is driven by a 3-phase, brushless DC motor (80 W), initially designed for Össur Power Knee, which was modified to be attached to the thigh section. This motor can generate a peak torque of 96 N·m and a maximum rotational speed of 300°/sec. The motor is connected to the socket via a single-axis joint system to overcome the space limitations near the socket. The hip joint system uses a cross-belt drive mechanism initially proposed in [32]. This cross-belt design maintains consistent belt tension during clockwise and counterclockwise rotations, thereby mitigating the need for additional components such as belt tensioner arms.

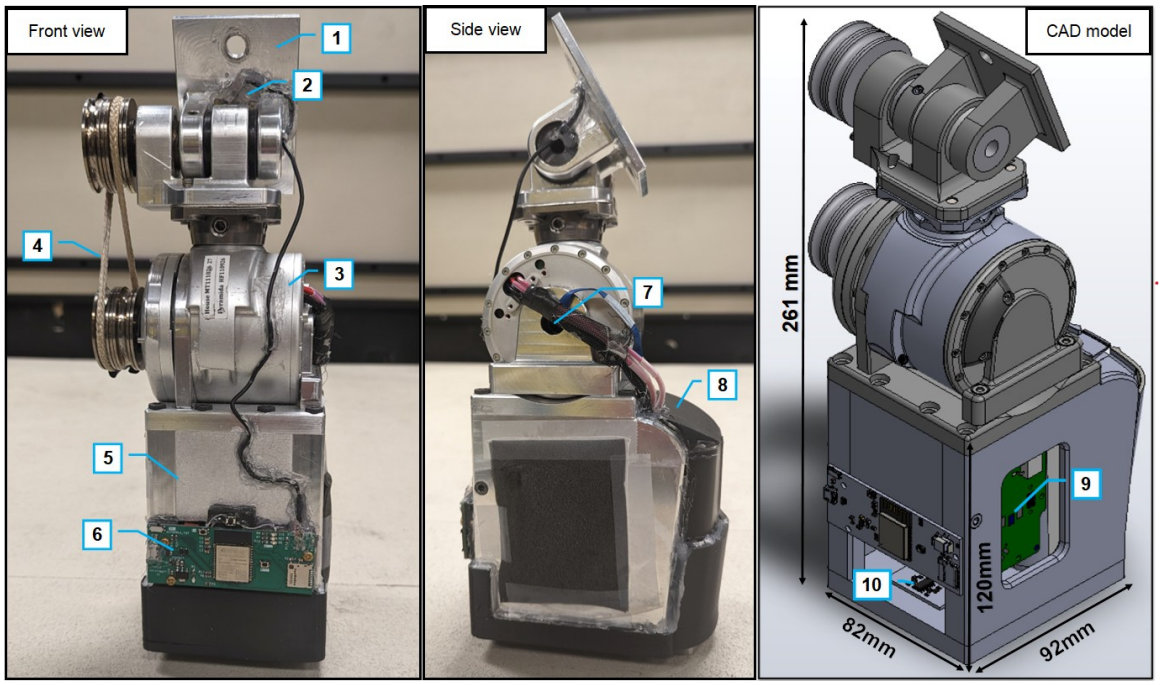

Fig. 5.2 Front view, side view, and CAD model of Power Hip module. 1: joint to socket attachment plate, 2: pelvic IMU, 3: DC motor, 4: single axis cross-belt drive hip joint, 5: thigh chassis, 6: gait controller and data logger, 7: hip joint angle sensor and motor encoder, 8: battery, 9: motor driver and thigh IMU, 10: loadcell and ADC board.

The Power Hip module is equipped with four sensors to collect essential feedback data needed for the gait control algorithm. These sensors include the pelvic inertial measurement unit (IMU), thigh IMU, hip angle sensor, and load cells (Fig. 5.2). The pelvic IMU is positioned on the joint-

to-socket attachment plate to measure pelvis angle and angular velocity. The thigh IMU is within the chassis and measures the prosthetic thigh angle. The hip angle sensor is integrated into the DC motor casing to measure the angle and velocity of the hip joint relative to the pelvis. Load cell strain gauges are installed at the base of the chassis to measure axial force.

Gait control, sensor data processing, and data logging functions are managed by an ESP32-WROOM-S3 microcontroller situated on the primary electronic board. This microcontroller also interfaces with the motor driver board within the chassis to execute actuation commands. Furthermore, the microcontroller facilitates wireless communication with a PC, enabling real-time adjustment of gait control parameters during prosthetic fitting and participant training sessions.

5.4 Gait control strategy architecture

The gait control strategy was structured according to the hierarchical control framework established by Tucker et al. [23]. As illustrated in Fig. 5.3, at the highest level, the prosthetic user's intended activity is determined and the target hip states (hip angle θ_{Target}, hip angular velocity ω_{Target}) are calculated and passed to the mid-level controller. The mid-level controller applies a control law to derive the target actuator torque (τ_{Target}). At the lowest level, τ_{Target} is converted into motor actuation signals through a field-oriented control (FOC) system.

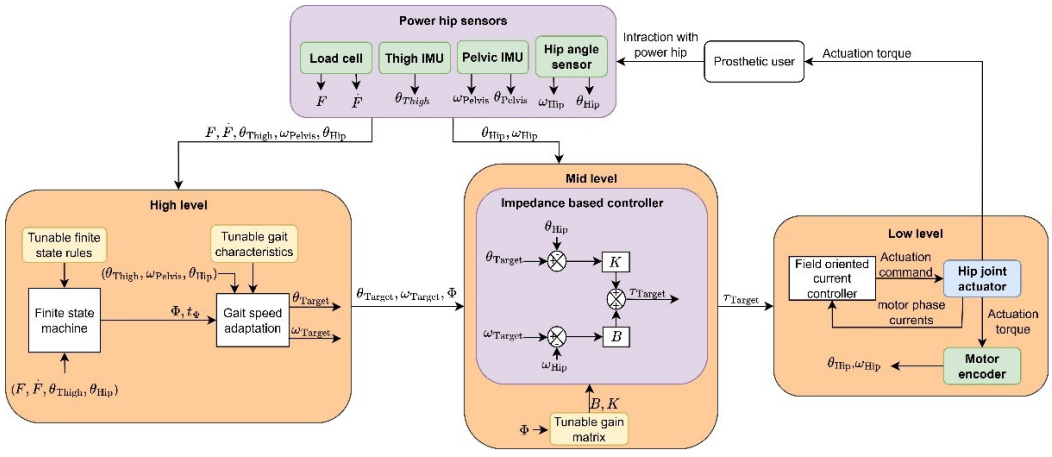

Fig. 5.3 Power Hip control strategy framework. $\theta_{Hip}, \omega_{Hip}$: Hip joint angle and angular velocity relative to the socket. $\theta_{Target}, \omega_{Target}$: Target hip angle and angular velocity relative to the socket. $\theta_{Pelvis}, \omega_{Pelvis}$: Pelvic tilt absolute angle and angular velocity. θ_{Thigh}: Prosthetic tight absolute angle. τ_{Target}: Target motor output torque. Φ: Gait sub-phase number.

During ambulation, hip joint kinetics and kinematics vary depending on the gait state and walking speed. Therefore, it is essential for the high-level controller to accurately determine the desired gait state and speed to compute the target hip states. This process involves segmenting the

gait cycle into discrete sub-phases (Φ) and detecting sub-phase transitions using a finite-state machine. For each identified activity mode, specific algorithms are used to estimate the desired gait speed and compute the target hip states relative to the estimated gait speed. The high-level controller algorithms in this study were developed based on the kinetic and kinematic characteristics of TF amputee gait with a microprocessor-controlled knee. Utilizing chained kinematics, the moment induced at the prosthetic knee joint is projected from the hip joint torque. Thus, by closely replicating the hip kinematics of TF amputees, it is theoretically possible for Power Hip users to achieve gait characteristics similar to those of TF amputees.

The mid-level controller regulates prosthetic joint impedance. Excessive joint impedance is undesirable since it may overpower the prosthetic user or interfere with fine adjustments required for altering gait characteristics during ambulation. Power Hip joint impedance can be dynamically adjusted for each activity mode using an impedance-based controller, given by

$$\tau_{target} = K\left(\theta_{Target} - \theta_{Hip}\right) + B(\omega_{Target} - \omega_{Hip}) \qquad (5.1)$$

where K is the stiffness coefficient, B is the dampening coefficient, θ_{Hip} is the measured prosthetic hip angle, and ω_{Hip} is the measured prosthetic hip angular velocity [122].

Each prosthesis user has unique gait kinematic variations and joint impedance preferences. We incorporated tunable parameters in our control strategy to account for these variations. Tunable finite state condition parameters can adjust the state machine's sensitivity during each activity mode transition. Tunable gait characteristics parameters can adjust the magnitude of temporal and spatial parameters (range of motion, swing time, stance time, etc.). The tunable gain matrix at the mid-level controller can adjust the joint stiffness and dampening for each activity mode. The algorithms and tuning process for the high- and mid-level controllers are discussed in the following subsections.

5.4.1 Gait events and finite state machine

The high-level controller utilizes a finite state machine to determine the transition between sequential sub-phases of gait cycle and calculates the new activity sub-phase target hip angles (θ_{Target}) and angular velocities (ω_{Target}). These activity sub-phases are defined as gait cycle sub-divisions, based on changes in kinetics and kinematics throughout the cycle [169, 170]. For the Power Hip control strategy, these sub-phases are based on TF amputee hip kinetics and kinematics during gait phase transitions, hip extension-flexion rotation vectors, and hip joint power vectors [171]. As illustrated in Fig. 5.4, six gait sub-phases were defined for the finite state machine: gait

initiation (GI), loading response (ST1), mid stance (ST2), pre-swing (ST3), early to mid swing (SW1), and terminal swing (SW2). The transition between the gait sub-phases follows a pre-defined cyclic path (Fig. 5.5). The rules for executing each transition are unique and use single to several sensor inputs. Through tests and trials with HD participants, we determined that an optional transition between SW1 and ST1 events was necessary to ensure uninterrupted walking.

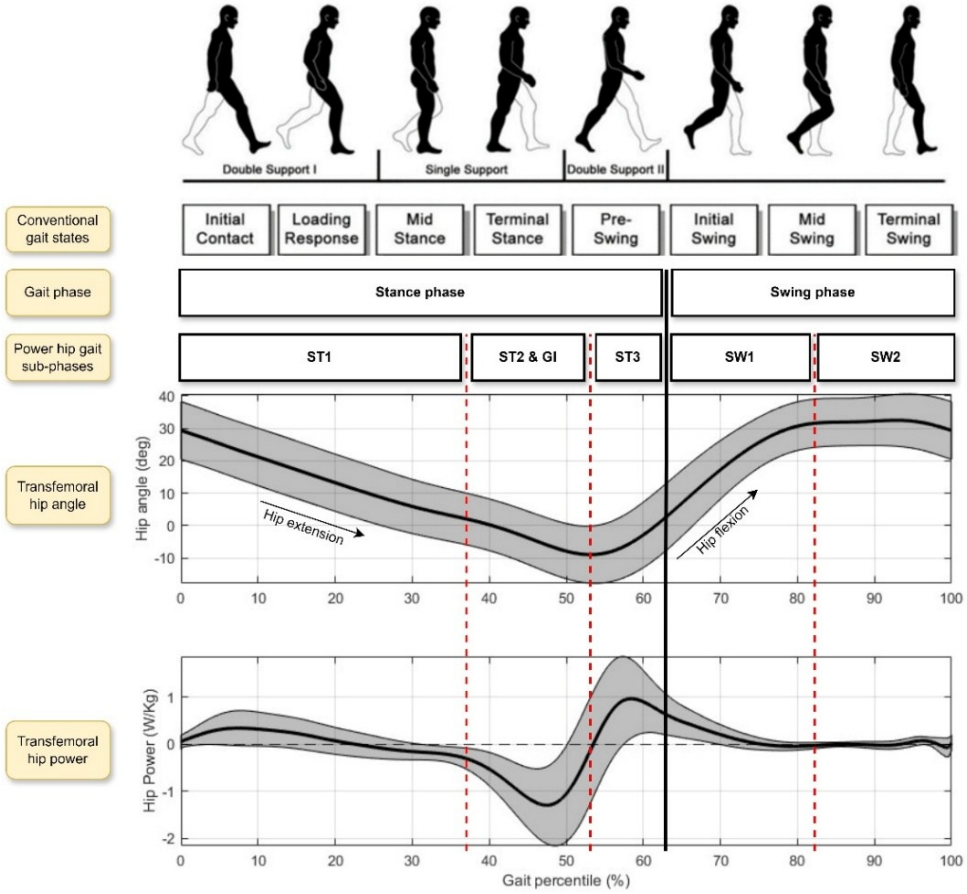

Fig. 5.4 Power Hip gait cycle compared to conventional gait states according to Perry and Burnfield [38], and relative to transfemoral amputee hip kinematics and kinetics [155].

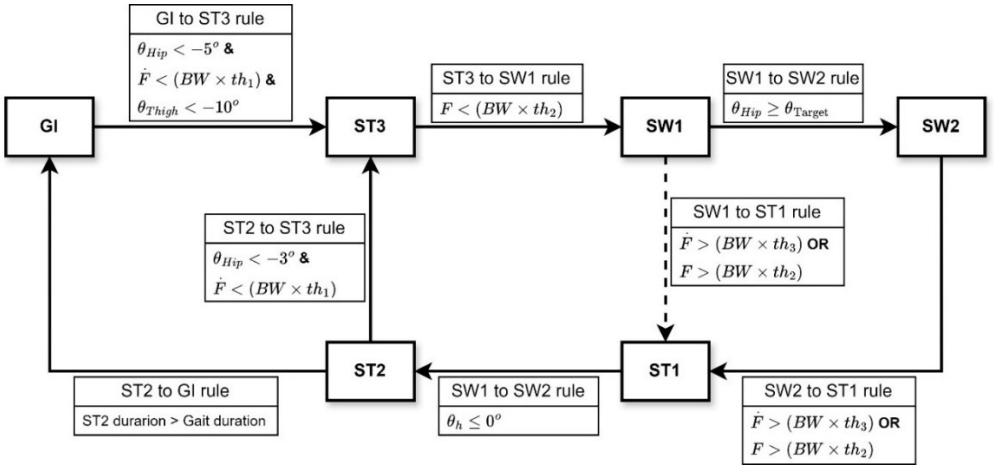

Fig. 5.5 Power Hip finite state machine with gait event transition paths and transition rules. θ_{Hip}: measured prosthetic hip angle, θ_{Thigh}: prosthetic thigh absolute tilt angle,θ_{Target}: target prosthetic hip angle, F: prosthetic chassis axial force, $\dot{F}$: prosthetic chassis axial rate of force, BW: prosthetic user's body weight, th_1: rate of force threshold to detect ipsilateral to contralateral load transfer, th_2: force threshold to detect foot-off, th_3: rate of force threshold to detect contralateral to ipsilateral load transfer.

GI is a non-cyclic subphase representing the starting point of walking from an idle standing posture. During GI and before transition to ST3, the Power Hip continuously applies low-impedance negative power (dampening torque) to dampen hip flexion and hip extension motions, helping the prosthetic user maintain an upright posture when standing. Exiting from GI to ST3 requires the user to swing the contralateral limb forward, causing the center of mass (COM) to fall while the dampening torque at the prosthetic hip controls COM descent speed [172]. During the GI to ST3 transition, the prosthetic hip joint is extended (ST2 & GI in Fig. 5.4), the prosthetic thigh is tilted back, and at the end of ST2 & GI, when entering double limb support, a sudden load transfer from the prosthetic side to the intact side occurs ($\dot{F} < threshold < 0$ N/s, F > 0 N) [172, 173]. Therefore, a transition rule was defined using sensor measurements of prosthetic hip angle (θ_{Hip}), prosthetic thigh angle (θ_{Thigh}), and rate of axial force ($\dot{F}$). The transition from GI to ST3 shares similarities with the transition from ST2 to ST3 in terms of kinetics and kinematics characteristics [173]. However, stricter rules were established for the GI to ST3 transition to prevent false detections when the prosthetic user sways side to side or back and forth while idly standing.

ST3 is the shortest gait subphase and occurs during pre-swing. As shown in Fig. 5.4, to prepare for swing phase, a large positive hip power (assistive torque) is needed before foot-off to perform knee flexion and achieve adequate toe clearance from the ground [174]. Therefore, the Power Hip must continuously produce hip flexion assistive torque until the transition from stance to swing is complete (F ≤ Threshold > 0 N), ending the transition to SW1 and starting swing phase.

SW1 occurs during early to mid-swing. During this period, a constant hip flexion velocity is applied to maintain the knee flexion moment through chained kinematics and sustain toe-to-ground clearance as the foot moves forward underneath the body [175]. The transition from SW1 to SW2 is achieved when the hip angle reaches the target hip flexion angle calculated ($\theta_{Hip} \geq \theta_{Target}$). Alternatively, for safety, if load transfer to the prosthetic side or ground reaction force is sensed during SW1 ($\dot{F}$ > Threshold > 0 N/s or $F > 0$ N), the state machine will promptly enforce transition to ST1 and end the swing phase.

SW2 is a simple buffer gait event where the Power Hip maintains the target hip flexion angle until foot strike is achieved. Hence, the Power Hip must produce assistive torques in flexion and extension at high impedance (resisting external moment). Similar to SW1, SW2 transitions to stance phase, and ST1 occurs when load transfer from the intact side to the prosthetic side is sensed ($\dot{F}$ > Threshold > 0 N/s or $F > 0$ N).

ST1 represents the gait cycle's early- to mid stance stages where the prosthetic limb is anterior to the body. At this stage, an assistive hip extension torque must be induced to push the COM upward [176]. Once max COM height is reached ($\theta_{Hip} \leq 0°$), transition to ST2 is achieved.

ST2 mirrors the GI, where the Power Hip must apply continuous braking torque to resist hip flexion and control COM descent. However, the ST2 to ST3 transition rules are more lenient than the GI to ST3 transition rules since the prosthetic user is already in steady-state walking motion and load transfer to the prosthetic side is inevitable once max hip extension is achieved. Moreover, ST2 can act as a gait terminator. Suppose the transition to ST3 is not accomplished within a specified time limit (less than or equal to the past stride duration). In this case, the finite state machine will infer that the prosthetic user intends to interrupt the gait cycle and cease walking, ultimately reverting to the GI sub-phase.

As shown in Fig. 5.6, three thresholds (th_1, th_2, th_3) are used to fine-tune transition rule sensitivity in response to loading and unloading the prosthesis. Given that the force and rate of force applied onto the prosthesis are relative to the prosthetic user's body weight (BW), the process of tuning these thresholds can be streamlined by enabling the microcontroller to automatically scale these force parameters relative to the participant's BW, thereby normalizing the threshold values.

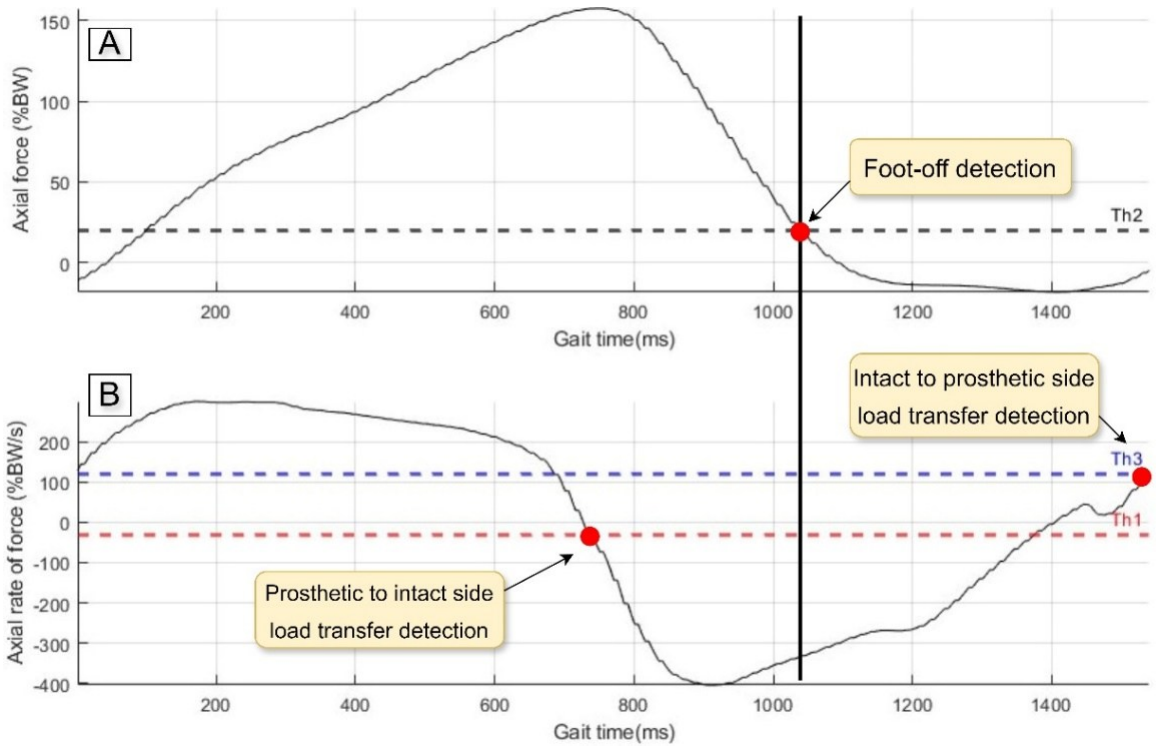

Fig. 5.6 Sample participant's Power Hip axial force and rate of force normalized for body weight relative to the thresholds.

5.4.2 Gait speed adaptation

Changes in gait speed depend on stride length and cadence [177]. During assistive torque gait sub-phases (ST1, ST3, SW1), through chained kinematics, the Power Hip is able to adjust stride length and cadence by calculating target hip states (θ_{Target}, ω_{Target}). Conversely, calculating target hip states for gait sub-phases that require dampening torque (GI, ST2, SW2) are unnecessary since the contralateral limb controls prosthesis actuation through COM movement. In the scope of this research, we developed a gait speed adaptation algorithm capable of assessing the prosthetic user's stride length and cadence-dependent biomechanical attributes and subsequently calculating the target hip states before entering each generative torque gait sub-phase.

5.4.2.1 Hip flexion target states

Target hip flexion angle (θ_{Target}) calculation is performed at the end of either GI to ST3 or ST2 to ST3 transitions. The method for calculating θ_{Target} is based on previous studies that established the correlation between the trailing limb angle and stride length [178, 179]. Garcia et al.'s mathematical model first proposed this correlation [178], and later was validated by McGrath et al. [179]. Given that the trailing limb angle can be used to determine stride length [178], and since

through chained kinematics hip range of motion defines stride length, the per-stride target hip flexion angle can be calculated using the equation

$$\theta_{Target} = \left|\theta_{Thigh}\right| \times r_{\theta flexion} \qquad (5.2)$$

where θ_{Thigh} is the prosthetic thigh tilting angle (trailing limb's angle) and $r_{\theta flexion}$ is a ratio between θ_{Thigh} and θ_{Target} that can be adjusted (from the initial value of 1) by the clinician during Power Hip gait training.

The target hip flexion angular velocity (ω_{Target}) can be calculated during stance phase in three consecutive instances ($\omega_{Instance\,1}, \omega_{Instance\,2}, \omega_{Instance\,3}$) since gait kinetic and kinematics data are continuously obtained by the sensors throughout the gait cycle. By averaging the calculated instances, ω_{Target} can be dynamically adjusted for more accurate estimations before ST3 and foot-off [180].

The first instance occurs during either GI or ST2, where the logarithmic relationship between stride length (hip range of motion) and cadence (hip flexion velocity) can be used to calculate ω_{Target}. From very slow walking speeds (≤ 0.5m/s), as the prosthetic user gradually increases their gait speed, the stride length increase tends to be favoured more than cadence increase [181, 182]. However, due to biomechanical limitations, an indefinite increase in stride length to achieve faster walking speeds is not sustainable [183]. Thus, prosthetic users will gradually favour increased cadence to achieve faster walking speeds. In the Power Hip control strategy, this relationship can be expressed as

$$\omega_{Instance\,1} = \ln\left(1 - \frac{\theta_{Target\,ROM}}{\theta_{Max\,ROM}}\right) \times S_C \qquad (5.3)$$

where $\omega_{Instance\,1}$ is the first instance of target hip flexion angular velocity,

$$\theta_{Target\,ROM} = \theta_{Hip} - \theta_{Target} \qquad (5.4)$$

$\theta_{\text{Max ROM}}$ is tunable maximum hip flexion range of motion and S_C is a speed constant that can be adjusted to change the logarithmic rate (Fig. 5.7). Adjustment of $\theta_{\text{Max ROM}}$ can influence the maximum achievable stride length on the prosthetic side while S_C adjustments will determine how early the cadence is favoured over the stride length as walking speed increases.

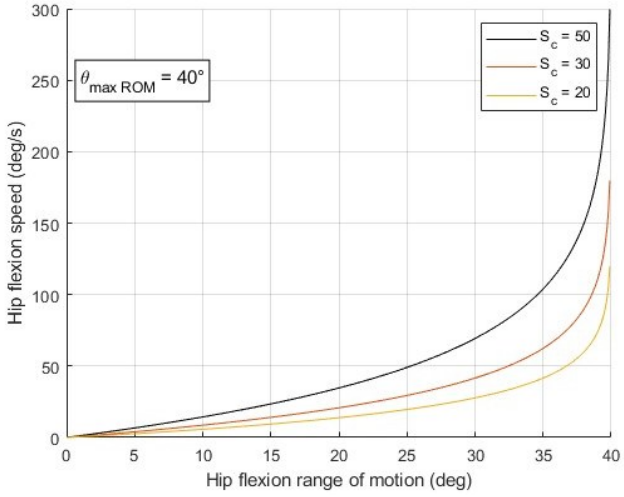

Fig. 5.7 Logarithmic relationship example between hip flexion range of motion ($\theta_{Target\ ROM}$) and hip flexion speed (ω_{Target}) as speed constant S_C is adjusted. Increasing S_C will increase the rate at which hip flexion speed (cadence) contribution to the gait speed is favoured over the hip flexion range of motion (stride length).

The second target hip flexion angular velocity calculation instance occurs when pelvic tilt rotation changes from posterior pelvic tilt to anterior pelvic tilt, during stance phase. In our past study on TF amputee pelvic kinematics [180], hip flexion duration was highly correlated and had a linear relationship with the timing of pelvic tilt posterior-to-anterior rotation direction change event. This pelvic tilt event can be detected when pelvic tilt angular velocity (ω_{Pelvis}), measured by a pelvis IMU, crosses the zero deg/s threshold from negative to positive. This linear relationship can be used to calculate hip flexion time and the second instance of target hip flexion angular velocity using equation (5.5)

$$\omega_{Instance\ 2} = \frac{\theta_{Target\ ROM}}{r_{ZC} \times t_{Pelvic\ ZC} + b_{ZC}} \qquad (5.5)$$

where $\omega_{Instance\ 2}$ is the calculated hip flexion velocity at pelvic tilt velocity zero-crossing, $t_{Pelvic\ ZC}$ is the time at which the ω_{Pelvis} zero-crossing is detected, r_{ZC} is a tunable linear coefficient, and b_{ZC} is a tunable bias coefficient (between $t_{Pelvic\ ZC}$ and hip flexion duration). Initial values of $r_{ZC} = 1.35$ and $b_{ZC} = 0.3461$ were based on our analysis of TF amputee's gait kinematics in [180]. Reducing either of these parameters results in faster hip flexion speed.

The third target hip flexion angular velocity calculation occurs during stance to swing phase transition. The linear relationship between stance duration and swing duration was used to calculate hip flexion time and $\omega_{instance\ 3}$. The linear relation between swing phase and stance phase duration in able-bodied individuals is well understood [184]. This linear relationship is maintained between

stance phase duration and SW1 [180]. Thus, the target hip flexion angular velocity during the third instance can be calculated using equation (5.6)

$$\omega_{Instance\ 3} = \frac{\theta_{Target\ ROM}}{r_{Stance} \times t_{Stance} + b_{Stance}} \qquad (5.6)$$

where $\omega_{Instance\ 3}$ is the calculated hip flexion velocity at foot-off, t_{Stance} is the measured stance phase duration, r_{Stance} is a tunable linear ratio, and b_{Stance} is a tunable bias factor (between stance duration and hip flexion duration). The initial values of $r_{Stance} = 1.18$ and $b_{Stance} = 0.0874$ were based on our prior study [180].

Once all instances of target hip flexion angular velocity are calculated, they are averaged to obtain hip flexion ω_{Target}. However, as mentioned in Section 5.4.1, to achieve knee flexion during ST3, the Power Hip should produce hip flexion generative torque before transitioning to swing phase, hence $\omega_{Instance\ 3}$ cannot be used at ST3 since the $\omega_{Instance\ 3}$ equation is dependent on t_{Stance}. Therefore, while all three instances are averaged to calculate ω_{Target} for SW1, only $\omega_{Instance\ 1}$ and $\omega_{Instance\ 2}$ are averaged for ST3.

5.4.2.2 Hip extension target states

During ST1, the Power Hip produces a hip extension generative torque to push the centre of mass upward until the hip equilibrium angle (hip angle at idle stand) is reached; hence, $\theta_{target} = \theta_{Equ}$. The target hip extension velocity can be calculated by assuming that changes in gait speed occur gradually. Since a person typically completes at least one to three strides to reach a steady-state gait speed, between each stride, the temporal changes due to gait speed adjustments are small [185]. Considering this assumption and the fact that stride duration and stance duration have a strong linear correlation [186], the target angular velocity during ST1 can be expressed as

$$\omega_{Target} = \frac{\theta_{Equ-}\theta_{Hip}}{t_{Last\ stride} \times r_{ST1\ time}} \qquad (5.7)$$

where θ_{Hip} is hip flexion at foot strike, $t_{Last\ stride}$ is the previous stride's total duration, and $r_{ST1\ time}$ is a tunable ratio that determines the ST1 duration relative to the last stride's total duration.

5.5 Experiment protocol

Prosthesis testing and data presentation received ethical approval from the University of Ottawa Ethics Board (H-08-21-7062) and Carleton University Ethics Board (122696). One participant, who met all inclusion criteria, took part in the Power Hip prototype assessment. The inclusion

criteria required that the participant have a unilateral HD amputation of the right limb, body weight between 40 kg and 100 kg, functional classification level of K2–K4, ability to ambulate without assistance or walking aids, be over 18 years of age, have at least three months experience using an HD prosthesis, and be proficient in English.

The participant provided informed consent for training with the Power Hip and subsequent gait evaluation. This individual, who sustained a right traumatic HD amputation, was prescribed an Ottobock Helix3D hip joint, an Ottobock C-Leg knee joint, and Otto Bock Terion K2 foot. At the time of data collection, the participant had six years of experience using their HKAF prosthesis. The participant was an active prosthetic user, 25 years old, 1.80 m tall, weighing 64 kg, and used their prosthesis almost daily.

After fitting with the Power Hip prosthesis by a certified prosthetist, ten training sessions were completed that involved gait initiation, gait termination, and self-paced walking (progressing from walking between parallel bars to unassisted walking). Throughout training, the general gait control algorithm and participant-specific tunable parameters were adjusted based on observations, participant feedback, and Power Hip kinetic and kinematic data obtained from sensors. The training was considered successful when the participant was able to walk outside of the parallel bars without assistance.

To evaluate the Power Hip prosthesis's ability to replicate TF amputee kinematics, an experimental test protocol was developed. This protocol assessed biomechanical changes across multiple walking speeds using markerless motion capture (Mocap) technology. The participant performed three walking trials per speed condition (self-paced, fast, slow), walking back and forth within a motion capture area five times for each trial, totaling 15 straight walkways. All trials were performed in the Ability Living Lab at Carleton University. The use of Mocap ensured compatibility with existing biomechanical datasets, which predominantly rely on motion capture methodologies, enabling direct comparison and minimizing methodological discrepancies to TF amputee gait patterns [154].

During the data collection session, the participant wore the Power Hip prosthesis and warmed up by walking for one minute. Once the participant was ready, they walked within the motion capture area while sensor data from the Power Hip (motor torque, angular velocity, control strategy subphase transitions) were recorded at 500 Hz via an onboard microcontroller and stored on a microSD card and Theia3D markerless motion capture technology (Theia Markerless Inc.) was used to collect total body 3D movement data at 100 Hz.

5.5.1 Data analysis

Raw motion data were processed using the Theia3D software (version 2024-1-0-4409), which automatically mapped anatomical key points to a 13-segment, six-degree-of-freedom biomechanical model (feet, shanks, thighs, pelvis, trunk, head, upper arms, forearms). The resultant skeletal position coordinates were imported into Visual3D (v2024.07.2), where a customized processing pipeline estimated lower-extremity joint angles and angular velocities. Processed kinematic data were exported to MATLAB (R2024a) for outcome measure calculations, including peak hip flexion/extension kinematics, peak knee flexion kinematics and gait phase durations.

Power Hip algorithm calculations and sensor data were extracted from the SD card and segmented into individual strides using MATLAB, with stride events synchronized to motion capture derived foot-strike and foot-off timings. Generated motor torque was normalized to 100% of stride and time series were averaged across all strides. Algorithm outputs (sub-phase durations, target hip flexion angle and angular velocity) for each stride were averaged across strides for each trial.

To assess speed adaptability, motion-captured hip and knee kinematics (e.g., peak flexion/extension angles, angular velocity profiles) were compared to a reference dataset of TF amputee gait kinematics [154].

5.6 Results

A total of 60 strides were recorded during walking trials (10 strides for each walk speed) involving the Power Hip prosthesis. The participant successfully completed all three walking speed trials on the first attempt, demonstrating consistent balance maintenance and independence from spotter assistance throughout the protocol.

5.6.1 Control strategy calculations

When walking back and forth within the capture area, the participant would perform a controlled turn and then pause for 3 seconds to allow the gait controller to reset to the default gait initiation (GI) subphase before starting the next round. Throughout the trials, the Power Hip microcontroller continuously logged sensor measurements, while the microcontroller performed real-time algorithmic processing. A summary of the sensor data, control outputs, and Power Hip motor kinetics are provided in Fig. 5.8 and Table 5.1.

All gait subphases (ST1, ST2, ST3, SW1, SW2) were identified for each trial, as shown with different color shading in Fig. 5.8. The ST1, ST2, and ST3 subphases were completed before the

transitions from stance to swing phase, while the hip joint continually extended during ST1 and ST2, followed by flexion initiation in ST3. This biomechanical transition coincides with the polarity change of motor power output. During ST2, the Power Hip predominantly generated negative power (-0.21 ± 0.09 W/kg), reflecting energy dissipation to stiffen the joint and prevent hyperextension. During ST3, power polarity changes to positive assistive power (0.36 ± 0.14 W/kg), facilitating the change in hip rotation direction from extension to flexion.

As shown in Table 5.1, ST2, SW1, and SW2 durations decreased with increasing walking speed, while ST3 duration remained unchanged between slow (0.19 ± 0.01 s) and self-paced walking (0.19 ± 0.02 s). Conversely, ST1 duration increased at fast walking speeds (0.48 ± 0.03 s for fast, 0.43 ± 0.07 s for self-paced), diverging from trends observed in other subphases. The target hip flexion angle (θ_{Target}) calculated using Equation (5.2) increased linearly with speed. However, calculated hip extension velocities were consistently lower than measured motor velocities (mean difference: 12.3 ± 3.1%), indicative of over-restricted dampening controls. Target hip flexion velocity was slower during self-paced walking (31.34 ± 7.52 deg/s) than during slow walking (34.30 ± 9.72 deg/s), while extension velocity increased predictably with speed. Despite the discrepancies in target velocity calculation trends, peak assistive (positive) / dampening (negative) motor output powers and measured trailing angles scaled with walking speed.

Table 5.1 Power Hip control strategy calculations at different walking speeds

Parameters	**Slow**	**Self-paced**	**Fast**
ST1 time (s)	0.45 ± 0.06	0.43 ± 0.07	0.48 ± 0.03
ST2 time (s)	0.39 ± 0.05	0.31 ± 0.06	0.24 ± 0.04
ST3 time (s)	0.19 ± 0.01	0.19 ± 0.02	0.15 ± 0.01
SW1 time (s)	0.36 ± 0.16	0.24 ± 0.07	0.20 ± 0.03
SW2 time (s)	0.25 ± 0.12	0.23 ± 0.06	0.20 ± 0.03
Target hip flexion angle (θ_{Target})	17.30 ± 1.57	17.33 ± 2.81	18.71 ± 1.68
Flexion ω_{Target} (deg/s)	34.30 ± 9.72	31.34 ± 7.52	52.01 ± 6.90
Extension ω_{Target} (deg/s)	-16.80 ± 9.60	-18.12 ± 8.04	-28.92 ± 9.60
Max motor dampening power (W/kg)	0.60 ± 0.07	0.70 ± 0.08	0.79 ± 0.10
Max motor assistive power (W/kg)	0.24 ± 0.07	0.37 ± 0.16	0.43 ± 0.07
Trailing limb angle (θ_{Thigh})	33.58 ± 2.60	34.10 ± 4.49	35.93 ± 2.58

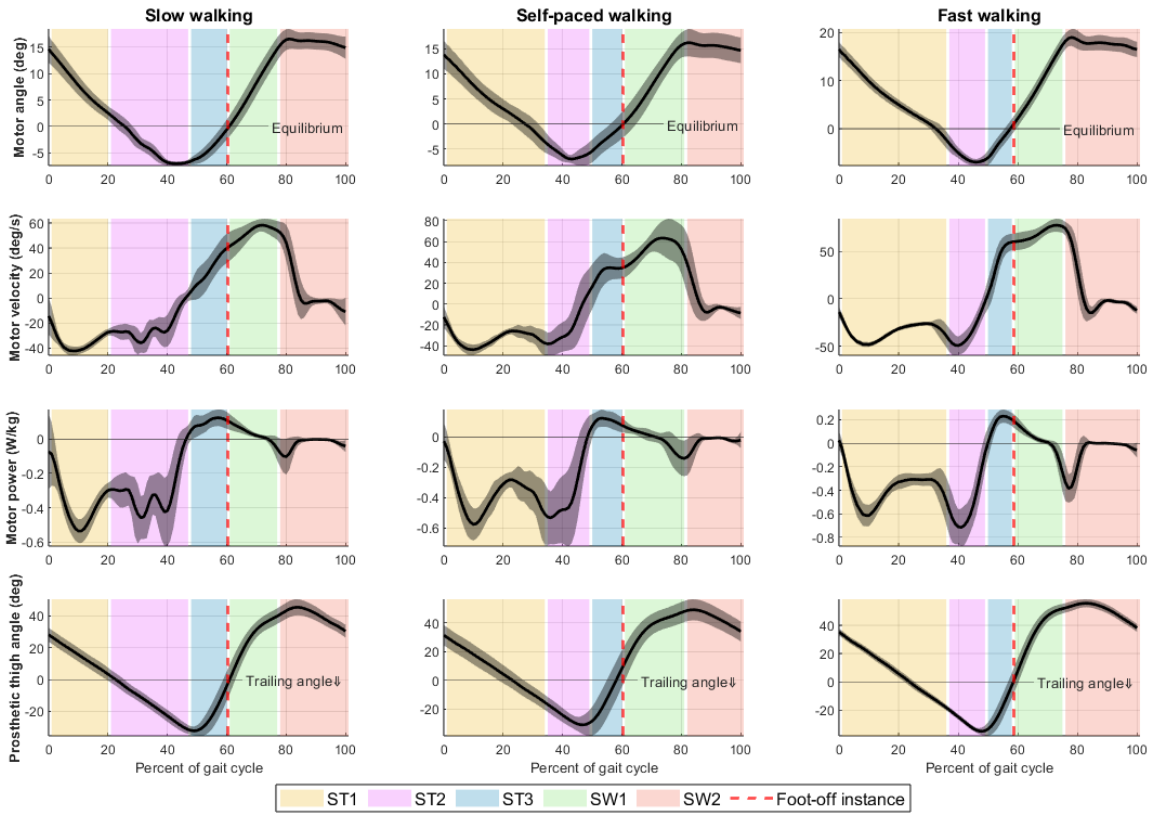

Fig. 5.8 Power Hip sensor measurements and the control strategy calculated gait subphases for each walking speed.

5.6.2 Motion capture measurements and comparison to TF dataset

The participant on average walked at 0.69 m/s for slow, 0.90 m/s for self-paced, and 1.01 m/s for fast walking speeds. Motion captured kinematic outcomes were compared to a reference dataset of five TF amputees walking at closest matched speeds of 0.7 m/s, 0.8 m/s, and 1.0 m/s (total strides: 520) [154]. Results are summarized in Fig. 5.9 and Table 5.2.

Both TF and Power Hip groups initiated hip flexion before stance-to-swing phase transitions (Fig. 5.9). Maximum hip extension velocities were comparable between Power Hip (60.15 to 104.88 deg/s), and TF (61.42 to 128.29 deg/s). At slow speeds, the Power Hip group had higher maximum hip flexion velocities than the TF group (Power Hip: 153.87 ± 18.31 deg/s; TF: 132.99 ± 10.72 deg/s). However, at faster speeds, TF amputees had greater hip flexion velocity (Power Hip: 149.06 to 234.70 deg/s; TF: 201.87 to 253.71 deg/s).

Notable differences emerged in knee kinematics. TF amputees exhibited 2.1° to 5.0° greater swing-phase knee flexion magnitude and consistently greater knee flexion velocities across all speeds (Power Hip: 171.74 to 303.51 deg/s; TF: 223.66 to 460.56 deg/s).

As quantified in Table 5.2, TF amputees exhibited consistent speed-related adaptations: hip and knee ROM and angular velocities increased with walking speed while stride duration, stance phase, and swing phase durations decreased. The Power Hip results mirrored these trends for ROM, angular velocities, and stride/stance phase reductions. However, unlike TF amputees, the Power Hip results maintained similar swing phase durations between self-paced and fast walking conditions, diverging from the expected inverse relationship between speed and swing time observed in the TF group.

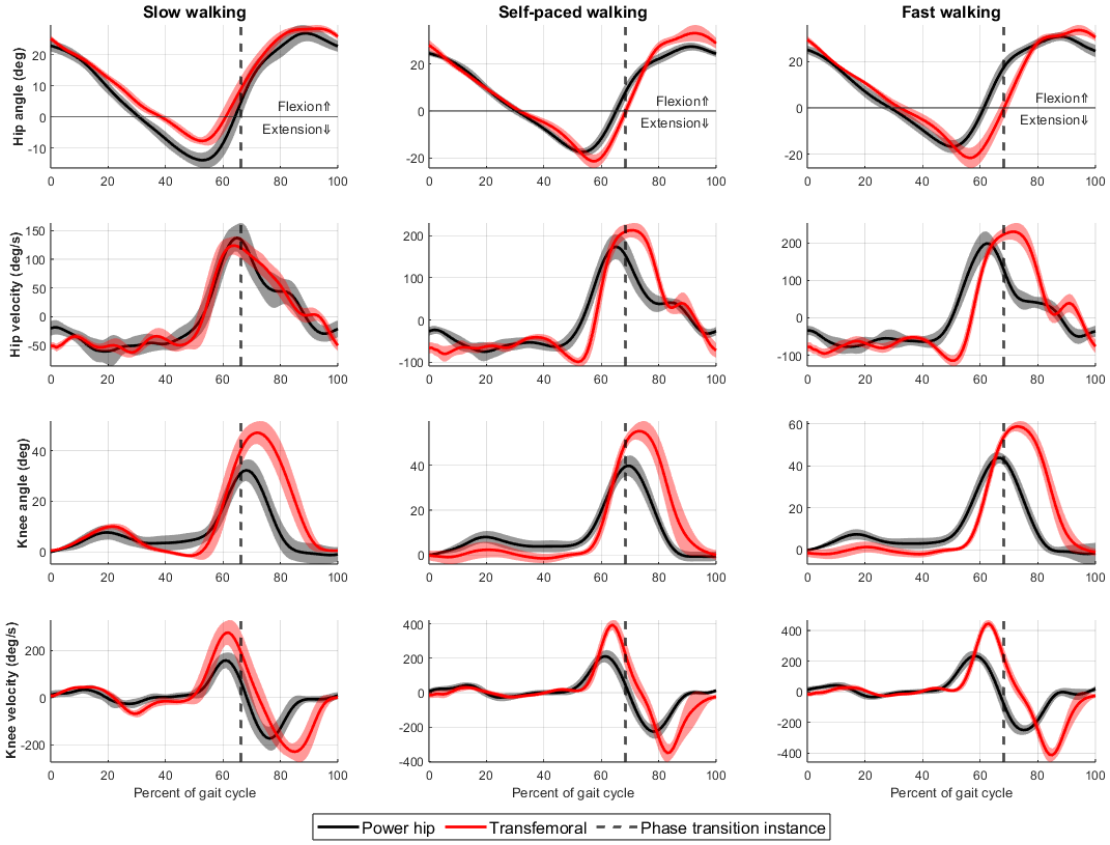

Fig. 5.9 Average hip and knee kinematics of Power Hip and TF amputees [154].

Table 5.2 Average and standard deviation for motion capture results for Power Hip and transfemoral gait [154]. Transfemoral walking speed was fixed for each condition.

Parameters	Prosthesis type	Slow	Self-paced	Fast
Walking speed (m/s)	Power Hip	0.69 ± 0.04	0.90 ± 0.04	1.01 ± 0.05
	Transfemoral	0.70	0.80	1.00
Stride time (s)	Power Hip	1.68 ± 0.06	1.48 ± 0.08	1.41 ± 0.05
	Transfemoral	1.39 ± 0.05	1.33 ± 0.05	1.20 ± 0.03
Stance time (s)	Power Hip	0.99 ± 0.06	0.85 ± 0.05	0.80 ± 0.05
	Transfemoral	0.91 ± 0.04	0.90 ± 0.03	0.81 ± 0.02
Swing time (s)	Power Hip	0.69 ± 0.04	0.62 ± 0.03	0.62 ± 0.03
	Transfemoral	0.48 ± 0.04	0.43 ± 0.02	0.39 ± 0.01
Max hip extension (deg)	Power Hip	-14.90 ± 2.20	-16.55 ± 1.80	-16.44 ± 2.05
	Transfemoral	-10.61 ± 0.85	-21.73 ± 2.86	-21.84 ± 4.08
Max hip flexion (deg)	Power Hip	27.93 ± 2.51	28.43 ± 2.18	32.03 ± 1.46
	Transfemoral	38.77 ± 1.09	33.45 ± 2.94	33.88 ± 1.76
Max hip extension velocity (deg/s)	Power Hip	-69.84 ± 9.69	-88.52 ± 14.07	-92.17 ± 12.71
	Transfemoral	-68.43 ± 7.01	-105.65 ± 9.67	-119.17 ± 9.12
Max hip flexion velocity (deg/s)	Power Hip	153.87 ± 18.31	175.52 ± 26.46	210.71 ± 24.07
	Transfemoral	132.99 ± 10.72	217.07 ± 15.20	234.35 ± 16.36
Max knee flexion (deg)	Power Hip	44.56 ± 3.34	50.33 ± 3.80	55.05 ± 2.78
	Transfemoral	48.73 ± 3.14	56.05 ± 4.83	58.99 ± 3.02
Max knee flexion velocity (deg/s)	Power Hip	204.62 ± 32.88	247.01 ± 32.05	275.18 ± 28.33
	Transfemoral	248.41 ± 24.34	382.44 ± 23.45	431.86 ± 28.70

5.7 Discussion

In this study, we introduced a new Power Hip prosthesis with a gait-speed adaptable control strategy framework specifically designed for unilateral HD amputees, laying the foundation for motorized HKAF prosthesis locomotion. The results demonstrated that this viable prototype prosthesis, which is self contained (i.e., no external batteries or control boards) and fits underneath clothing, can enable walking at a range of speeds expected in the community and provide performance similar to TF amputees. Comparison to TF amputee prosthesis users is relevant since both groups walk with a prosthetic knee and foot.

The prototype prosthesis was designed to be compatible with conventional HD prosthesis sockets and rely solely on internal sensors for decision-making and activity control, eliminating the need for prosthetic users to wear additional sensors. The Power Hip and control strategy evaluation involved a HD participant, in contrast to lower extremity HKAF prosthesis development research in recent years which only tested their powered prosthesis on able-bodied participants [122].

5.7.1 Parameter tuning considerations

The final iteration of the tuned parameters is summarized in Appendix C. During training with the Power Hip, adjustments to some tunable parameters were required as the participant grew more

confident with the prototype. The changes made to tunable parameters followed a consistent trend as the participant gained proficiency:

- Finite state machine transition rule sensitivity was reduced due to quicker load transfer between intact and prosthetic limbs, resulting in improved load symmetry as the person decreased their reliance on parallel bars.
- The calculated minimum target angular velocity and cadence had to be increased by reducing the r_{ZC}, r_{Stance} and $r_{ST1\ time}$ tunable values, which allowed the person to walk at a faster pace and spend less time in each gait event.
- The mid-level controller stiffness (K) gain was reduced for braking torque gait events (GI and ST2) to achieve fast Power Hip extension angular velocity during COM descent. This gave the participant more control over the stance phase duration.

The mid-level controller's dampening gain (B) was intentionally constrained to values below half the proportional gain (K) across all gait subphases to mitigate motor vibrations induced due to the noise in the joint angle sensor measurements. While the lower gain stabilized the motor against oscillations, the reduced B gain inherently limited velocity control bandwidth. Consequently, the motor consistently exceeded target velocities during actuation. To resolve this, we propose integrating low-noise, high-resolution Hall effect angle sensors (e.g., 14-bit resolution) in future iterations. This upgrade would improve velocity control accuracy, ensuring closer alignment between target and achieved motor velocities, while reducing high frequency oscillations at higher gains.

5.7.2 Hip kinetics and kinematics

The Power Hip prosthesis demonstrated adaptive temporal characteristics observed in TF gait, including reductions in stride duration and stance phase time as walking speed increased. The prosthesis also achieved hip extension velocities akin to those of TF amputees during stance phase. However, during swing phase, the Power Hip maintained consistent swing durations across speed conditions, diverging from the expected inverse-relationship between walking speed and swing time observed in TF amputees.

At slower walking speeds, the Power Hip exhibited higher hip flexion velocities than those of TF amputees. However, performance lagged at higher walking speeds, suggesting potential constraints in actuator responsiveness or suboptimal tuning of control parameters. These limitations

might be addressed through iterative adjustments to the target hip target flexion calculation tuning parameters in Equations (5.3), (5.5), and (5.6).

Discrepancies in knee flexion magnitude and velocity between the Power Hip and TF groups may reflect hardware variability, since TF participants used diverse prosthetic knee models. None of the TF amputees used the Össur Rheo Knee. Future studies incorporating different prosthetic knee types could clarify the influence of knee hardware and knee settings on coordinated hip-knee kinematics with the Power Hip.

Compared to existing HKAF prostheses described in the literature, the participant achieved a hip range of motion (ROM) of up to 52°, which exceeds the 30° ROM reported for prostheses such as the Helix3D hip joint [10]. Therefore, Power Hip achieved partial biomimicry of TF amputee gait, and greater biomechanical advantage over existing HKAF prosthesis, but it requires targeted improvements in swing-phase dynamics and high-speed actuation to fully replicate natural gait kinematics.

5.7.3 Gait speed adaptability

The control strategy exhibited mixed responsiveness to increased gait speed. While stride, stance, and swing times decreased as expected, certain subphase parameters remained unchanged or increased inversely. For instance, ST3 duration remained consistent between slow and self-paced walking speeds (Table 5.1), a result attributed to the restrictive foot-off detection threshold. Transition from ST3 to SW1 during the foot-off instance is reliant on prosthetic load measurements falling below a predefined threshold; therefore, lowering this threshold could improve phase transition sensitivity and reduce the ST3 duration during self-paced walking.

During ST1, the prosthesis consistently underestimated hip extension velocity, leading to unintended dampening power generation instead of the intended assistive torque. This hip extension target velocity miscalculation prolonged ST1 duration at faster speeds. Adjusting the $r_{ST1\ time}$ tuning parameter in Equation (5.7), could mitigate this issue. Alternatively, an auto-tuning algorithm could be implemented to gradually reduce the $r_{ST1\ time}$ in each step until the motor produces assistive power during ST1.

During self-paced walking, target hip flexion velocity ω_{Target} was unexpectedly lower than during slow walking. As shown in Fig. 5.10 this anomaly stemmed from inconsistent detection of the pelvic tilt zero-crossing (PTZC) event that is required for calculating the second instance of target flexion velocity in Equation (5.5). PTZC is detected by the control strategy when the pelvis

is first tilted posteriorly by more than -10°, followed by a posterior pelvic tilting with speeds that pass through a -15 deg/s threshold. However, limited pelvic tilt during self-paced walking resulted in PTZC detection in only 56% of strides, compared to 85% and 98% detection rate in slow and fast walking, respectively. If the strides that did not detect PTZC were excluded from data, the self-paced ω_{Target} could have been improved to 43.13 ± 10.75 deg/s, higher than ω_{Target} during slow walking speeds.

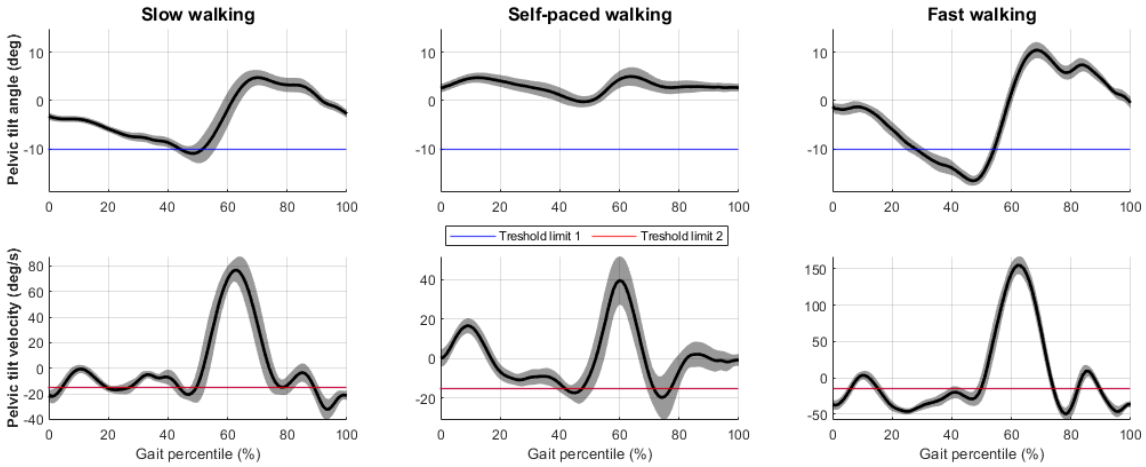

Fig. 5.10 IMU measured pelvic tilt kinematics of participants walking at different speeds.

While the Power Hip minimizes the need for exaggerated pelvic movements, moderate user-specific kinematic adjustments remain essential for reliable PTZC detection. Improved detection rates may require targeted user training to familiarize wearers with subtle pelvic coordination. Since a preliminary prototype prosthesis was used in this study, the participant was not able to take the device home and acclimate to the new powered prosthesis. Weeks of experience are typically needed for a person to adjust and make better use of new microprocessor-controlled features of their prosthesis. Therefore, next-phase research should provide better guidance as to ideal prosthesis settings, since the person will likely have different pelvis and contralateral limb kinematics as they adapt to efficient gait with the new intelligent technology.

5.7.4 Limitations

This study has several limitations that should be considered when interpreting its findings. Although 3 participants were recruited to develop the control strategy, due to scheduling issues, this study reported on one participant, which limits generalizability of the results to broader HD amputee populations. This participant has an active lifestyle; thus, the findings may not accurately represent the effectiveness of the system for less active users or those new to HKAF prosthetics.

The training period was only 10 sessions; therefore, the results may not fully reflect how users adapt to the Power Hip over time or how their movement patterns might improve with practice.

Considering these limitations, future work should involve a larger and more diverse group of participants, including those with different activity levels and prosthetic experience. Extending training periods and observing users in everyday settings could also provide deeper insights into long-term usability and benefits. Addressing these gaps will help ensure motorized HKAF prostheses meet the needs of most people with HD amputation.

5.8 Conclusion

The results of this study showcase the potential of motorized HKAF prostheses. By using a powered hip prosthesis with a gait speed adaptable control strategy, the HD participant was able to effectively and comfortably walk at their desired speed. Further research in this area is necessary, including a next phase prototype that improves on sensor integration and can be used in the community. Microprocessor controlled powered hip technology has great potential to meet the requirements of people who have lost their entire leg, thereby improving quality of life and mobility in the person's chosen environment.

Chapter 6: Comparison of hip-disarticulation prosthesis gait between conventional and motorized hip joints

6.1 Foreword

This chapter compares gait characteristics between the Powered Hip prototype and a participant's prescribed passive prosthesis, addressing the third thesis objective: "*Quantify chair sitting and standing performance by comparing prototype performance to a participant's prescribed mechanical HKAF prosthesis*".

While prior studies have explored motorized HKAF systems, these investigations were primarily conducted with able-bodied participants or robotic simulators [16, 30]. As a result, the biomechanical influence of motorized HKAF prostheses on HD amputee gait remains unexplored, leaving a gap in understanding their potential to restore mobility. To bridge this gap, a HKAF prosthesis user was recruited to perform the two-minute walk test and three-speed walk test using both their prescribed passive prosthesis and the Powered Hip prototype. Additionally, the participant provided subjective feedback through satisfaction questionnaires, offering insights into usability and comfort.

The contents of this chapter are a manuscript in preparation for submission to the ISPO journal.

6.2 Introduction

Hip disarticulation (HD) amputees face considerable challenges in returning to an active lifestyle. This is primarily due to the physical demand required to operate a Hip-Knee-Ankle-Foot (HKAF) prosthesis [14, 35, 148]. Consequently, HKAF prosthesis users exhibit asymmetrical gait patterns, marked by increased pelvic rotation, compensatory trunk motions, and overreliance on the contralateral limb for both propulsion and stability [68]. Furthermore, prolonged prosthesis use is often correlated with chronic spinal injuries [10].

The excessive reliance on pelvic movement and the contralateral limb is due to the limitations of conventional HKAF prostheses that have fully mechanical hip joints. During early stance phase, the user loads the prosthesis to rotate the hip joint until maximum extension angle is reached (socket contacts the physical extension stop of the hip joint). Max hip extension angle is then maintained until the end of stance phase [10]. Thus, adjustments to stride length during stance must be achieved through compensatory pelvic posterior tilting and users must perform pelvic anterior tilting to

initiate hip flexion at the start of the swing phase [187]. As a result of these mechanical constraints, user control of the prosthesis is limited; hence, walking tends to be slower and leads to early muscle fatigue [59]. Moreover, due to the limited torque-generating capacity of pelvic muscles, increased loading and vaulting on the sound limb are required at higher walking speeds to compensate for the absence of active propulsion from the prosthetic limb and reduced ground clearance. The resultant asymmetrical loading raises concerns regarding long-term musculoskeletal health, including potential joint degeneration and overuse injuries on the intact side [60].

Motorized prosthetic knees offer distinct advantages for transfemoral (TF) amputees in terms of walking speed and gait symmetry. These types of prostheses actively generate power for propulsion, enabling faster walking speeds and better adaptability to varied terrains, making them ideal for high-activity users [168]. Additionally, prostheses with powered knee joints reduce metabolic cost during gait [111]. Comparative studies demonstrated that motorized prosthetic knees could outperform active dampening and mechanical prostheses during dynamic tasks, such as navigating inclines or walk speed transitions, and offer better temporal and spatial symmetry in controlled environments [20].

Based on trends observed in motorized knee research, we hypothesize that substituting HKAF mechanical hip joints with microprocessor-controlled actuators may similarly improve gait symmetry, increase walking speeds and reduce complementary movements of HKAF prosthesis users. However, research on motorized hip joints remains relatively limited. Notable developments include the passive Helix3D prosthesis by Ottobock, which mimics natural hip motion and reduces energy expenditure over previous passive hip joints [10]. Ueyama et al. [16] introduced a robotic motorized joint system with a feedback controller, enabling the hip to extend and compress a virtual spring for energy-efficient swing-phase transitions. Despite producing natural gait patterns, this system lacked robust user control for everyday activities. Luo et al. designed a motorized HD prosthesis with double-parallelogram for the hip and four-link structure for the knee [30]. Their prototype was tested with a 6-axis robotic arm and demonstrated promising results in simulating biological joint kinematics under varying walking speeds. Despite these advancements, no motorized HD prosthesis has been tested by HD amputees to date, and the feasibility of such devices in enhancing walking speed and gait symmetry for this population remains largely unexamined.

To address this research gap, a prototype motorized HKAF prostheses (Power Hip) was evaluated as an alternative to conventional mechanical prostheses. Using motion analysis and qualitative assessments, a comprehensive analysis of the effects of a motorized hip joint on HD

amputee gait was completed, thereby contributing to the advancement of effective motorized prosthetic hip solutions.

6.3 Methods

6.3.1 Power Hip prosthesis

The prototype HKAF employed in this research was comprised of the HD socket, power hip joint (motorized prosthetic hip joint), Össur Rheo Knee 3 XC, and Össur ProFlex foot. The power hip module shown in Fig. 6.1 is a modified version of the design initially presented in [31, 138], optimized for compactness by reducing its overall height. This modification facilitates fitting the prosthesis to participants with shorter legs. The device accommodates body mass up to 100 kg and is front mounted, consistent with prescribed prosthetic practice. The Power Hip thigh section houses a three-phase DC motor, motor driver electronics, gait controller electronics, 95.04 Wh (3.3 Ah) battery, and all gait control sensors.

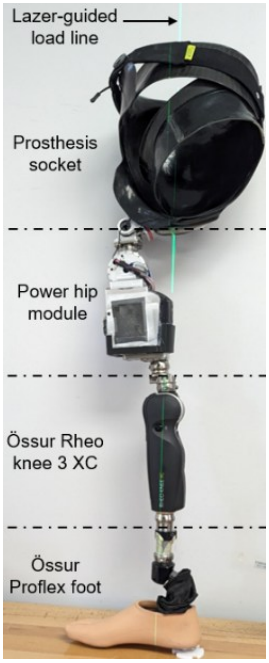

Fig. 6.1 Power Hip prototype.

The Power Hip provides a greater range of hip motion compared to fully mechanical (passive) hip joints, allowing prosthetic users to achieve up to 25° of hip flexion and 90° of hip extension. This increased range of motion enables users to take longer strides without excessive posterior pelvic tilting, thereby reducing compensatory pelvic movements.

In addition to the extended range of motion, the Power Hip dynamically adjusts hip angular velocity during each gait cycle to match the desired walking speed. Using input from sensors that measure ground reaction forces, pelvic tilt patterns, hip angle, and thigh tilt angle, the Power Hip microcontroller calculates the target torque required and determines whether assistive (increase angular velocity) or dampening (decrease angular velocity) torque should be applied, depending on the sub-phase of the gait cycle. These adaptive responses throughout the gait cycle aid the prosthesis user in maintaining steady forward momentum. Additional details on the Power Hip control strategy algorithm can be found in Chapter 5.

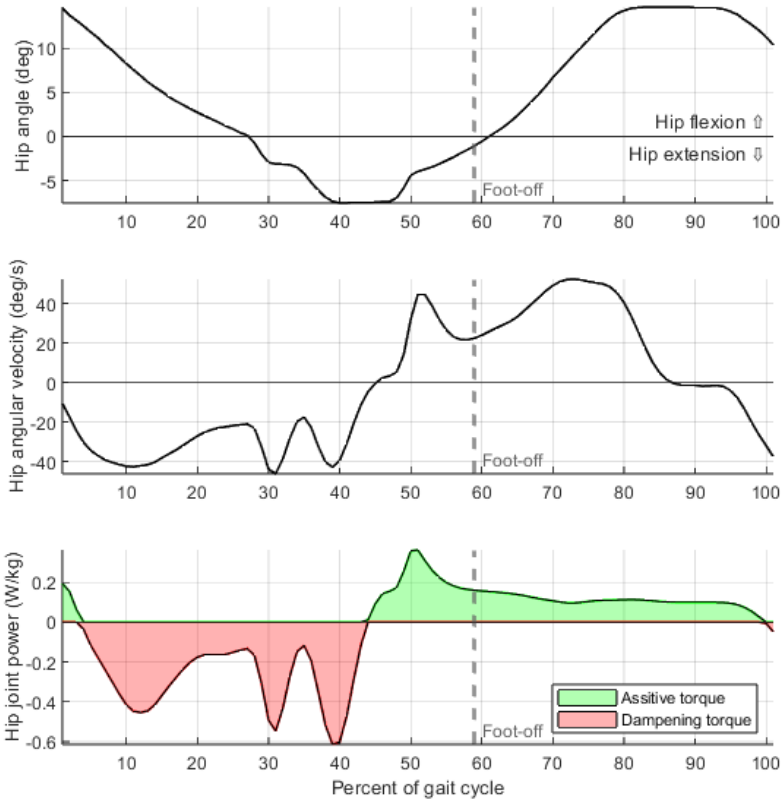

Fig. 6.2 Hip kinetics and kinematics of a stride measured by Power Hip sensors during walking.

As illustrated in Fig. 6.2, during initial double limb support, the Power Hip generates assistive torque upon foot-strike to propel the user forward and elevate the center of mass (COM). As gait progresses into mid-stance, the Power Hip transitions into hip extension, applying dampening torque to control COM descent after reaching its peak height. Approaching the end of the stance phase, the Power Hip generates assistive torque to initiate hip flexion. This movement causes the prosthetic knee to flex, thereby improving ground clearance during the swing phase through chained dynamics. In contrast, users of passive hip joints often compensate for the limited joint motion by relying on posterior pelvic tilting at the start of the swing phase, leading to delayed

transitions from hip and knee extension to flexion [10]. This delay results in slower walking speeds and necessitates vaulting on the intact side to ensure adequate ground clearance [5]. Throughout swing phase, the Power Hip maintains hip flexion while gradually reducing angular velocity. This controlled deceleration uses inertia of the prosthetic knee and foot to facilitate knee extension, ensuring the knee reaches full extension just before the subsequent foot-strike.

6.3.2 Participant preparation

Following approval from the University of Ottawa (H-08-21-7062) and Carleton University (122696) ethics boards, an experienced HKAF prosthesis user was recruited for this study (Table 6.1). The inclusion criteria were unilateral HD amputation of the right limb, body mass ranging from 40 kg to 125 kg, activity level between K2 and K4, ambulate independently without assistive walking devices, over 18 years of age, at least three months of experience with HD prostheses, and proficiency in English. The participant was briefed on the research objectives and potential risks and provided informed consent.

Table 6.1 Participants details

Body height (cm)	HKAF height (cm)	Age (yr)	Body mass (kg)	HKAF prosthesis use years	Prescribed prosthesis	
					Hip joint	Knee joint
1.80	89	25	64	6	Ottobock Helix3D	Ottobock C-Leg

Before beginning training with the new prosthesis, the participant's original socket was replicated at Nielen Orthotics and Prosthetics (Ottawa, Canada) to ensure compatibility with the Power Hip system. Over a 12-month period, which included iterative refinement of the Power Hip prototype, the participant underwent ten training sessions, each lasting 2 hours. During the initial visit, the participant was fitted with the Power Hip prosthesis. The fitting process involved replicating the shank and thigh lengths based on the dimensions of the previous prosthesis (Fig. 6.3). Additionally, static and dynamic alignment adjustments were performed to optimize the prosthesis configuration. The dynamic alignment was fine-tuned by observing and analyzing gait behaviour during training sessions [188, 189].

Each training session was conducted under the supervision of a certified prosthetist, with exercises performed between parallel bars to ensure safety. During these sessions, the gait control algorithm was tuned to meet the participant's specific needs. The participant was trained in essential gait techniques using the Power Hip, including gait initiation, gait termination, walking speed

adjustment, and turns. The training was deemed complete when the participant walked independently with the Power Hip without relying on parallel bars or other external support.

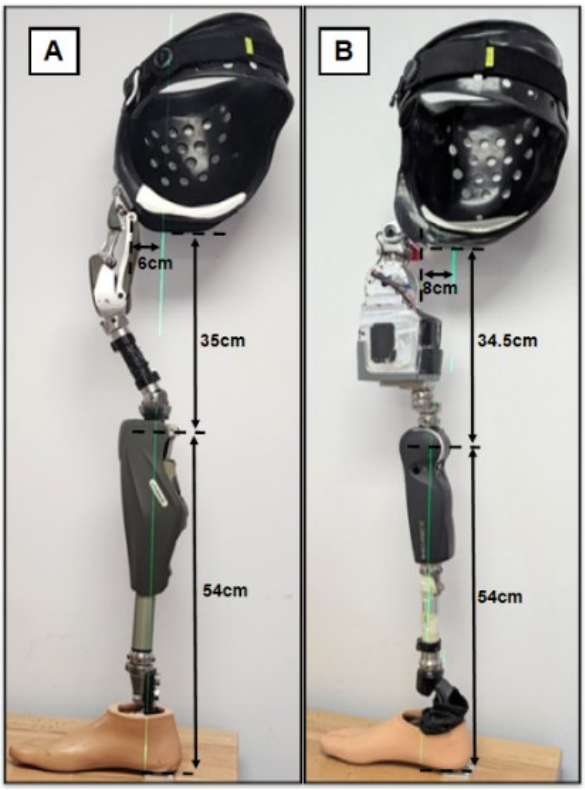

Fig. 6.3 A Participant's personal prosthesis with Ottobock Helix3D hip joint, C-leg knee module, and Taleo foot, B: Power Hip HKAF prototype.

6.3.3 Test protocol

The participant completed a satisfaction questionnaire, a Two-Minute Walk test (2MWT), and a three-speed walk test (3SWT) with their prescribed HKAF prosthesis and Power Hip prosthesis (Table 6.2). The outcomes were participant satisfaction ratings, 2MWT time and cadence, gait kinematics, and stride parameters.

The Two-Minute Walk Test (2MWT) assesses an individual's functional capacity by measuring the total distance covered in a set time. For this test, the participant walked back and forth along a 15-meter hallway, covering as much ground as possible within two minutes. A spotter walked near the participant to ensure safety, and another person video recorded the person. After completing the test, the participant completed a satisfaction questionnaire comprising seven items rated on a scale of 1 to 5. The 2MWT protocol was completed for both their prescribed prosthesis and the Power Hip.

Table 6.2 Summary of measured parameters and evaluation methods

Test type	Data acquisition method	Measured parameters	Test outcomes for each prosthesis
Satisfaction grading	Questionnaire	5-point scale	Per question score Summed score
Two-Minute Walk Test	Video recording	Cadence, number of steps, walking speed	Cadence mean and standard deviation Total number of steps.
Three-speed Walk Tests	THEIA motion capture	Walking speed	Mean and standard deviation differences for each speed
		Stride time, stride length	Mean and standard deviation for each speed Averaged symmetry index for each speed
		Stance and swing duration	Mean and standard deviation of "stance/swing percentile ratio" for each speed Averaged symmetry index for each speed
		Pelvic tilt angle	Mean and standard deviation of pelvic range of motion for each speed
		Sagittal hip angle	Mean and standard deviation of hip extension and flexion range of motion for each speed

The Three-Speed Walk Test (3SWT) evaluates changes in gait kinematics due to temporal and spatial variations in walking patterns [190]. This test was conducted using the participant's prescribed prosthesis and the Power Hip. Walking was recorded using 11 cameras and processed using THEIA 3D motion analysis technology (version 2024.07.2) at the Abilities Living Lab, Carleton University, Ottawa, Canada. Before the test, the participant rested in a seated position for 5 minutes. Then the participant walked 5 times through a 10 m long motion capture area at three speeds: self-paced, faster than self-paced, and slower than self-paced. For each walking speed, ten steady state-strides were analyzed, resulting in a total of 30 strides.

6.3.4 Data analysis

Outcome measures of walking with the prescribed prosthesis were compared to results from the Power Hip. TF prosthetic gait was used as a benchmark since TF prostheses use the same knees

and feet as HD prostheses. Subjective opinions of walking with the prescribed prosthesis and Power Hip were assessed and compared via a questionnaire.

During the 2MWT, the participant walked back and forth multiple rounds along the predefined 15 m hallway path. Total distance walked, cadence (steps per minute), and gait speed were calculated and compared between the Power Hip and prescribed prostheses. Cadence was determined by reviewing video recording. Foot strikes were manually counted post-hoc, excluding steps taken during turns or pauses at the hallway ends. The duration of each round was measured from the initiation of forward walking to the completion of the final step before turning. Cadence was computed as

$$Round\ Cadence\ (steps/min) = \frac{Number\ of\ foot\ strikes \times 60\ sec}{Round\ duration\ (s)} \qquad (6.1)$$

where a round is one walkway length and walking speed for each round was derived by dividing the fixed trial distance (15 m) by the measured round duration

$$Speed\ (m/s)\ = \frac{15.24\ m}{Round\ duration\ (s)} \qquad (6.2)$$

THEIA 3D markerless motion capture software was used to generate 4×4 pose matrices for each segment of a 13-segment body model, capturing the local coordinates of anatomical landmarks on the feet, shank, thigh, pelvis, trunk, head, upper arms, and forearms [44]. These pose matrices were processed using a 10 Hz Butterworth low-pass filter and exported in .c3d format into Visual3D software.

In Visual3D, pelvis segment angles were calculated relative to the laboratory coordinate system, while hip joint angles were derived from the relative orientation of the thigh and pelvis segments. Gait events, including foot-off and foot-strike, were initially identified using the automated method proposed by Zeni et al. [191] and subsequently verified manually. The automated method determines gait events by analyzing the z-axis and x-axis velocities of the toe marker coordinates relative to the pelvis segment. These gait events were then used to calculate stride parameters, such as walking speed and stride time.

The symmetry differences in hip range of motion, gait phase durations, and stride length were assessed using the symmetry index equation:

$$SI = \frac{X_P - X_I}{0.5(X_P + X_I)} \times 100\% \qquad (6.3)$$

where X_P represents prosthetic-side metrics, and X_I represents intact-side metrics. The SI is appropriate for this study since it reduces bias from changes in gait speed or prosthesis-specific characteristics [192].

The mean and standard deviation of symmetry index values, along with other research outcomes, were calculated for each walk speed trial of each prosthesis type to evaluate gait characteristics differences between the prescribed prosthesis and the Power Hip prosthesis.

6.4 Results

6.4.1 Two-minute Walk test

The participant successfully completed the 2MWT with both prostheses without losing balance or requiring assistance from the spotter. Results are summarized in Table 6.3. With the prescribed prosthesis, the participant walked 131 steps, covering 106.68 m, whereas with the Power Hip prosthesis, they completed 118 steps over 85.97 m.

Table 6.3 2MWT per round and overall average and standard deviation for cadence, total distance covered, and walking speed for the Power Hip and prescribed HKAF

	Power Hip		Prescribed HKAF	
Rounds	**Cadence (steps/min)**	**Speed (m/s)**	**Cadence (steps/min)**	**Speed (m/s)**
1	85.05	0.98	83.08	1.17
2	78.33	0.99	82.70	1.17
3	81.93	0.94	82.13	1.16
4	81.54	1.09	84.64	1.13
5	78.60	0.95	81.02	1.08
6	84.00	0.98	82.02	1.04
7	---	---	81.08	1.08
Average	81.73 ± 2.87	0.99 ± 0.05	83.26 ± 1.94	1.12 ± 0.05

The challenge observed with the Power Hip prosthesis was a delay in performing a spin turn at the end of the walkway (i.e., rotate body around a fixed prosthetic limb). This was attributed to lack of training for this task (i.e., the participant made longer turns during the training trials) and Power Hip controls restrictions requiring the participant to stop and wait for 3 seconds to terminate walking before performing gait initiation for the next walkway length. As a result, the total distance covered with the Power Hip was 20.71 m shorter than with the prescribed prosthesis. However, when excluding the stop-and-turn instances, the difference in cadence between the two conditions

was small (1.3 steps/min difference). Walking speeds were also comparable, with the prescribed prosthesis providing a slight advantage of 0.13 m/s.

6.4.2 Three-speed Walk test

A summary of the motion capture-derived gait kinematics is presented in Fig. 6.4 and Table 6.4. The participant completed 74 strides with the Power Hip prosthesis at walking speeds ranging from 0.67 to 1.12 m/s, and 56 strides with the prescribed prosthesis at speeds between 0.54 and 1.21 m/s.

To contextualize gait differences between the two prosthesis types, a TF prosthetic user database was selected as a reference [154]. This dataset includes walking at fixed speeds of 0.7, 0.8, and 1.0 m/s, aligning with the participant's slow, self-paced, and fast walking speeds during the trial. As illustrated in Fig. 6.4, the participant exhibited restricted hip kinematics when using the prescribed prosthesis, and their pelvic tilt range deviated from both the TF dataset and the Power Hip condition. In the TF dataset, maximum hip extension angle increased proportionally with walking speed. However, due to the limited hip extension capability of the Helix3D hip joint, the participant achieved a minimum hip extension across all walking speeds with their prescribed prosthesis (averaging -0.37° ± 1.12°). In contrast, the Power Hip prosthesis allowed for greater hip extension (averaging -6.29° ± 2.70°), following a trend similar to the TF dataset, where maximum hip extension increased from slow to self-paced speeds but did not increase further at the fast-walking speed.

Maximum hip flexion velocity also increased with walking speed for both prosthesis types, consistent with the TF dataset. However, the Power Hip prosthesis exhibited a notable advantage, with an average hip flexion velocity of 179.39 ± 33.62 deg/s, which was closer to the TF dataset (227.08 ± 16.20 deg/s) compared to the prescribed prosthesis (147.77 ± 23.58 deg/s).

Pelvic tilt range of motion (ROM) varied considerably between the two HKAF prostheses. When using the prescribed prosthesis, the participant exhibited greater posterior pelvic tilt (averaging 19.48° ± 5.22°). Additionally, pelvic ROM increased with walking speed when using the prescribed prosthesis. In contrast, pelvic tilt ROM with the Power Hip prosthesis averaged 6.67° ± 1.63° and closely matched the TF dataset (7.00° ± 0.94°), with minimal change in ROM magnitude relative to walking speed.

Stride time and stride length were shorter with the Power Hip prosthesis compared to the prescribed prosthesis across all walking speeds, aligning more closely with the TF dataset. Additionally, the participant spent more time in the stance phase with the Power Hip prosthesis (58.22% ± 2.39% of the gait cycle) compared to the prescribed prosthesis (56.51% ± 2.51%).

However, with both prostheses, the stance phase duration remained substantially shorter than the TF dataset across all walking speeds (67.74% ± 1.13% of the gait cycle).

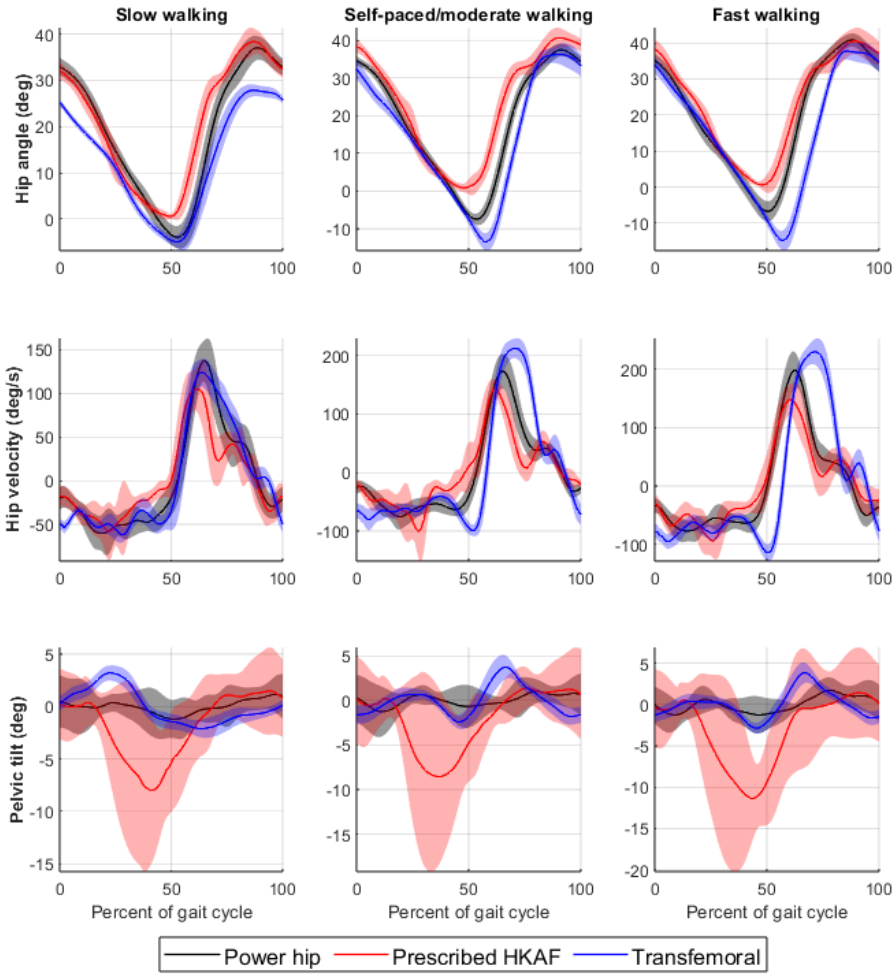

Fig. 6.4 Hip and pelvic tilt kinematics of participant walking with Power Hip and prescribed HKAF compared to transfemoral gait.

Symmetry index (SI) analysis (Table 6.5) revealed differences in gait symmetry between the Power Hip and prescribed prosthesis. A smaller absolute SI value indicates improved inter-limb symmetry, with negative values denoting intact-side bias and positive values reflecting prosthetic-side bias.

The Power Hip prosthesis demonstrated better symmetry across most metrics compared to the prescribed HKAF prosthesis, with the exception of maximum hip flexion velocity. Interestingly, the prescribed HKAF prosthesis achieved better hip flexion velocity symmetry than TF amputee benchmarks. Both HKAF prostheses had small SI results for stride time and stride length, though the Power Hip yielded better overall symmetry and was closer to the TF group at all walking speeds.

However, the prescribed prosthesis exhibited a prosthetic-side time bias (positive SI), whereas the Power Hip shifted bias toward the intact side (negative SI).

Table 6.4 Gait kinematics for Power Hip and prescribed HKAF prosthesis during three-speed walk test relative to TF amputee benchmark [154]

	Prosthesis types	Slow	Self-paced	Fast
Walking speed (m/s)	Power Hip	0.69 ± 0.04	0.90 ± 0.04	1.02 ± 0.05
	Prescribed	0.60 ± 0.04	0.89 ± 0.04	1.12 ± 0.05
	Transfemoral	0.70	0.80	1.00
Stride time (s)	Power Hip	0.97 ± 0.06	0.87 ± 0.04	0.79 ± 0.05
	Prescribed	1.14 ± 0.08	0.94 ± 0.05	0.80 ± 0.04
	Transfemoral	1.39 ± 0.05	1.33 ± 0.05	1.20 ± 0.03
Stride length (m)	Power Hip	1.16 ± 0.07	1.33 ± 0.05	1.44 ± 0.05
	Prescribed	1.19 ± 0.06	1.47 ± 0.04	1.64 ± 0.04
	Transfemoral	0.97 ± 0.04	1.07 ± 0.04	1.20 ± 0.03
Stance phase percentile (%)	Power Hip	58.67 ± 2.31	59.45 ± 1.61	56.19 ± 1.97
	Prescribed	57.20 ± 2.44	56.98 ± 2.24	55.01 ± 2.36
	Transfemoral	65.55 ± 2.48	67.83 ± 1.16	67.53 ± 0.91
Pelvic tilt range of motion (deg)	Power Hip	6.62 ± 1.65	6.69 ± 1.77	6.72 ± 1.49
	Prescribed	17.18 ± 3.88	19.65 ± 4.87	22.77 ± 5.76
	Transfemoral	5.66 ± 1.38	6.96 ± 0.86	7.11 ± 0.96
Max hip extension (deg)	Power Hip	-4.53 ± 2.41	-7.76 ± 1.50	-7.04 ± 2.85
	Prescribed	-0.76 ± 0.80	-0.47 ± 1.09	-0.22 ± 0.77
	Transfemoral	-5.44 ± 1.14	-13.71 ± 2.32	-15.03 ± 2.48
Max hip extension velocity (deg/s)	Power Hip	-81.13 ± 14.81	-92.23 ± 14.52	-95.29 ± 16.12
	Prescribed	-91.82 ± 22.95	-132.64 ± 35.37	-120.48 ± 24.08
	Transfemoral	-68.43 ± 7.01	-105.65 ± 9.67	-119.17 ± 9.12
Max hip flexion (deg)	Power Hip	37.50 ± 2.53	37.60 ± 1.64	41.13 ± 1.83
	Prescribed	39.00 ± 2.31	41.18 ± 2.27	41.23 ± 3.33
	Transfemoral	28.13 ± 1.31	36.61 ± 2.14	38.14 ± 2.03
Max hip flexion velocity (deg/s)	Power Hip	152.99 ± 18.72	186.59 ± 27.36	207.60 ± 29.41
	Prescribed	134.24 ± 22.68	150.92 ± 17.58	164.90 ± 18.00
	Transfemoral	132.99 ± 10.72	217.07 ± 15.20	234.35 ± 16.36

Maximum hip flexion angle SI was low for both HKAF prostheses and the TF amputee group, with a slight intact-side bias across all walking speeds. As walking speed increased, symmetry improved for all groups, though the Power Hip prosthesis more closely aligned with TF amputee benchmarks at faster speeds. The most pronounced disparity between the Power Hip and the prescribed HKAF emerged in maximum hip extension, where the Power Hip had lower SI (-57.67 ± 66.27) compared to the prescribed HKAF prosthesis (170.49 ± 34.03), with a strong prosthetic-side bias. This aligns with the biomechanical constraints of the passive HKAF prosthesis, which limited active hip extension, whereas the Power Hip enabled near-physiological extension through controlled actuation.

Table 6.5 Symmetry index averages and standard deviations for Power Hip and prescribed HKAF [154] during three-speed walk test

SI parameter	**Prosthesis type**	**Slow**	**Self-paced**	**Fast**
Stride time	Power Hip	-0.41 ± 5.25	-0.30 ± 5.43	-0.32 ± 3.00
	Prescribed	1.05 ± 3.96	1.22 ± 3.66	0.71 ± 4.14
	Transfemoral	0.09 ± 4.16	0.03 ± 1.91	-0.07 ± 1.64
Stride length	Power Hip	0.07 ± 6.52	1.05 ± 4.83	1.42 ± 3.24
	Prescribed	1.06 ± 5.90	1.49 ± 3.26	0.59 ± 2.60
	Transfemoral	0.09 ± 4.16	0.03 ± 1.91	-0.07 ± 1.64
Stance phase ratio	Power Hip	-12.23 ± 6.70	-7.26 ± 4.25	-9.40 ± 5.72
	Prescribed	-14.76 ± 6.71	-5.48 ± 4.54	-8.21 ± 4.63
	Transfemoral	-17.90 ± 5.17	-8.51 ± 3.12	-5.73 ± 2.79
Max hip flexion	Power Hip	19.05 ± 9.53	12.80 ± 6.55	14.85 ± 7.28
	Prescribed	37.73 ± 10.38	24.87 ± 9.19	19.19 ± 10.95
	Transfemoral	10.88 ± 3.65	12.56 ± 5.32	8.24 ± 5.57
Max hip flexion velocity	Power Hip	34.17 ± 14.76	35.02 ± 17.44	28.67 ± 20.01
	Prescribed	25.56 ± 21.88	11.65 ± 20.13	7.73 ± 15.51
	Transfemoral	-10.50 ± 10.08	29.41 ± 6.88	23.69 ± 7.32
Max hip extension	Power Hip	-64.92 ± 94.03	-73.20 ± 28.46	-29.92 ± 39.32
	Prescribed	-163.73 ± 30.96	-170.83 ± 34.44	-146.18 ± 31.99
	Transfemoral	-96.28 ± 28.06	-71.86 ± 19.20	-54.66 ± 22.93
Max hip extension velocity	Power Hip	-18.37 ± 22.03	-6.80 ± 26.64	5.13 ± 25.86
	Prescribed	-23.71 ± 34.18	-35.25 ± 24.30	-11.44 ± 24.92
	Transfemoral	-2.31 ± 21.16	-6.43 ± 15.85	-12.18 ± 12.67

6.4.3 Questionnaire

The results of the questionnaire are presented in Table 6.6. The participant reported higher overall satisfaction with the Power Hip prosthesis (22) compared to their prescribed prosthesis (20), out of a maximum total score of 25. The improvement was driven primarily by comfort while walking, where the Power Hip scored 5/5 versus the prescribed prosthesis's 3/5. Other metrics remained identical between devices (weight: 4/5; balance: 4/5; sounds: 5/5). Notably, the overall satisfaction scores were equal (4/5).

Table 6.6 Satisfaction questionnaire results from participant walking with Power Hip and prescribed prosthesis

Satisfaction enquiry	Prescribed prosthesis score	Power Hip score
Weight of the prosthesis while walking	4	4
Comfort while walking	3	5
Balance while walking	4	4
Prosthesis sounds during use	5	5
Overall prosthesis satisfaction	4	4
Sum	20	22

6.5 Discussion

This study demonstrated that a motorized hip prostheses (Power Hip) can improve walking performance and satisfaction as compared to a conventional HKAF prosthesis with a passive mechanical hip joint. By comparing kinematic performance, gait symmetry, and user satisfaction between the Power Hip prosthesis and the prescribed passive prosthesis, we aimed to quantify functional trade-offs and advantages inherent to motorized hip actuation.

6.5.1 Gait kinematics

The Power Hip improved gait kinematics compared to the prescribed prosthesis, achieving movement patterns closer to TF amputees (Table 6.4). During the 3SWT, the Power Hip had a lower walking speed standard deviation and better stride time symmetry. The participant corroborated these findings subjectively, reporting greater satisfaction with the Power Hip's speed adaptability during the 2MWT. Furthermore, when benchmarked against the reference TF dataset, the Power Hip outperformed the prescribed prosthesis across multiple metrics, including stride time, stride length, pelvic tilt ROM, hip ROM, and maximum hip flexion velocity.

6.5.2 Two-minutes Walk test

During the 2MWT, while the participant achieved higher initial speeds with the prescribed prosthesis, the Power Hip enabled more consistent speed retention across walkways. The average walking speed decline from the first to last round was small with the Power Hip (0.01 m/s) compared to the prescribed prosthesis (0.1 m/s), which could be because of improved biomechanical efficiency and reduced fatigue. This aligns with observed reductions in compensatory movements, such as diminished reliance on pelvic tilting. The participant also reported feeling less physically burdened during testing, likely due to the Power Hip's active

control and prolonged prosthetic-side stance time, since increased stance phase duration is inversely associated with energy-intensive postural adjustments [193]. The slower overall walking speed with Power Hip during 2MWT could have been attributed to the participants unfamiliarity with Power Hip compared to their prescribed prosthesis, However, we were not able to confirm this with these tests. A long-term study and more refined control software may improve the walking speeds.

6.5.3 Gait symmetry

The Power Hip had better overall gait symmetry compared to the prescribed prosthesis, as evidenced by reductions in SI across most temporal and kinematic parameters. However, an exception was observed in maximum hip flexion velocity SI, where the Power Hip was less symmetrical between limbs than the prescribed prosthesis. This suggests a compensatory strategy wherein the participant favored faster hip flexion on the intact side when using the Power Hip. We hypothesize that the Power Hip's active motor actuation enabled faster hip extension and COM rise during early stance phase that prompted the participant to adopt quicker intact-side hip flexion to synchronize with the prosthesis's assistive power output. This pelvis movement pattern may change with more experience walking with the Power Hip prosthesis as users become more familiar with the feel and control behaviour of the prosthesis.

Within the Power Hip prosthesis SI results, the highest values were for maximum hip flexion/extension angle and flexion velocity. These asymmetries are likely mitigatable through iterative software adjustments and structured user training. Given that the prosthesis control logic fundamentally differs from conventional HKAF prostheses, users may require extended acclimatization. Experienced HKAF prostheses users often develop compensatory habits, such as vaulting, to walk with their prostheses [59]. Despite the Power Hip's design to reduce reliance on such strategies, the participant struggled to unlearn these ingrained behaviors during the limited training period. These residual compensatory movements may have contributed to the measured asymmetries.

6.5.4 Participant's overall satisfaction

The Power Hip's greater comfort aligns with its improved biomechanical performance, particularly in hip extension symmetry and stance-phase control, which likely reduced compensatory movements and physical strain. Despite being 2 kg heavier than the prescribed prosthesis, the participant reported equal satisfaction with the Power Hip weight (4/5 for both devices). This suggests that the biomechanical advantages of the Power Hip lifting and rotating the entire leg,

such as improved symmetry, active hip flexion, and extension controls offset the added mass, potentially by reducing metabolic or kinematic strain associated with complementary movements.

6.5.5 Limitations

Several limitations for this study must be acknowledged. First, the findings are derived from one participant who has an active lifestyle and extensive daily prosthetic use. This may limit generalizability to individuals with lower activity levels or limited experience with HKAF prostheses. Second, the training period with the Power Hip was brief. The short adaptation window likely influenced observed gait patterns, since users require time to acclimate to prosthesis active control logic. Extended training and time using the Power Hip in the community could reveal evolving strategies for optimizing coordination, further reducing compensatory movements.

6.6 Conclusion

The Power Hip prosthesis demonstrated meaningful advancements in gait biomechanics compared to conventional passive prostheses, achieving movement patterns closer to TF prosthetic user ambulation while reducing compensatory movements. Furthermore, participants reported greater satisfaction with balance and movement fluidity. Power Hip's ability to improve user comfort despite increased weight and prototype-specific design constraints illustrates the potential of the future research in this field.

Future work should focus on expanding accessibility and refining usability. This includes evaluating the prosthesis across diverse user populations, such as individuals with varying physical fitness or limited prior experience with HKAF prostheses. Longitudinal studies are needed to assess long-term adaptations in endurance, joint health, and real-world performance outside controlled environments. Experimentation with a more efficient training protocol would as well be beneficial to help reduce the overall rehabilitation time.

By addressing these priorities, iterative improvements to the prosthesis's design, control algorithms, and training frameworks could bridge remaining gaps between compensatory and natural gait. This study represents a critical step toward redefining mobility for individuals with hip disarticulation, offering a foundation for HKAF prostheses that prioritize both biomechanical fidelity and quality of life. Ultimately, integrating motorized hip actuation into HKAF prosthetics marks a transformative shift in rehabilitation, reimagining possibilities for improved independence.

Chapter 7: Design and evaluation of stand-to-sit and sit-to-stand control protocols for a hip-knee-ankle-foot prosthesis with a motorized hip joint

7.1 Foreword

This chapter focuses on the development of a control strategy for stand-to-sit and sit-to-stand using the Power Hip prosthesis, alongside a biomechanical analysis with HD amputees. In able-bodied individuals and TF amputees, hip torque is the main contributor in facilitating these movement tasks. Since conventional HKAF prostheses do not provide hip torque, prosthesis users typically use their intact limb and arm rests when sitting and standing. This study investigated whether generating torque at the prosthetic hip joint could improve biomechanical symmetry and functional outcomes during these daily activities, addressing thesis objective 2: "*Develop a motorized HKAF control strategy for sit-to-stand and stand-to-sit transitions*" and objective 4: "*Quantify chair sitting and standing performance by comparing prototype performance to a participant's prescribed mechanical HKAF prosthesis".*

To accommodate the non-cyclic nature of sitting and standing, the hierarchical control framework introduced in Chapter 5 was adapted while retaining its core structure. When developing the control strategy, emphasis was placed on achieving kinetic symmetry, ensuring that executing these transitions did not require the user to shift load to the intact side. By prioritizing kinetic symmetry, the control system aimed reducing physical demand on the intact limb.

A HKAF prosthesis user was evaluated in a motion capture laboratory to quantify kinetic and kinematic symmetry between the intact and prosthetic limbs during sit-to-stand and stand-to-sit tasks. Results indicated that torque generation at the prosthetic hip during sit-to-stand reduced loading asymmetry by lessening reliance on the intact limb. During stand-to-sit, improved load distribution enabled a wider base of support, potentially enhancing balance control.

This research provides the first control system specifically for HKAF prosthesis sitting and standing and advances the broader aim of restoring autonomy in daily life for HD amputees. The contents of this chapter are a paper in preparation for submission to Journal of Bionic Engineering.

7.2 Introduction

Amputees who use lower extremity prostheses, particularly those with hip disarticulation (HD) or hemipelvectomy (HP) amputations, face considerable challenges in common daily activities, including walking, sitting, and rising from a chair [12]. Typical hip-knee-ankle-foot (HKAF) prostheses require significant effort, especially for individuals who may lack the needed physical fitness to walk with a full leg prosthesis [13, 194].

In individuals with transfemoral (TF), HD, or HP amputations, the prosthetic joints contribute very little to sit-to-stand and stand-to-sit activities [195]. Most of the effort involves the intact limb and/or upper body, thereby requiring chair armrests or other aids to stand up or sit down [195]. Achieving the joint moments required for critical actions, such as push-off during the initial sit-to-stand transition or knee flexion during stand-to-sit, often necessitates compensatory movements that can affect balance [196]. Adequate intact limb muscle strength is crucial for sitting and standing, yet even after rehabilitation many prosthesis users struggle to maintain balance while sitting or standing [196, 197].

For TF prosthesis users, poor balance during sitting and standing is attributed to a centre of mass (COM) medial-lateral translation and longer task duration. The COM typically translates to the intact side during sitting or standing, as the intact limb provides propulsion or descent control [198]. This strategy is also employed by frequent fallers [199]. Due to the greater COM translation, the base of support boundaries are passed much earlier, and more time is spent outside of the base where the person is vulnerable to balance disturbances [78]. Furthermore, sitting and standing are performed much slower than able-bodied people since moment generation is limited on the prosthetic side and built-in stance control features of most microprocessor-controlled prosthetic knees slow descent. Prolonging the ascent or descent time can increase the likelihood of failed push-off attempts during sit-to-stand and sudden falls during stand-to-sit [196, 200].

Sit-to-stand and stand-to-sit are physically demanding tasks for HKAF prosthesis users. The lack of assistance by the HKAF prostheses likely contributes to the challenges for sitting and standing; however, to date, no published research has investigated methods to reduce the physical effort required for these activities, and no biomechanical studies for sitting or standing are available in the literature. Further research is needed to explore potential strategies to reduce the physical demand and failed transition attempts in these critical daily tasks [5]. A Powered Hip joint could be a solution for enabling more effective standing and sitting.

Recent advancements in motorized prosthetic knee joints demonstrate the potential benefits of active components in prosthetic devices. Motorized knee joints provide better kinetic symmetry and enhanced control during demanding activities compared to microprocessor-controlled and passive knee joints [89, 201, 202]. During sit-to-stand and stand-to-sit, motorized knee joints generate net-positive torque, increasing internal joint moments and reducing necessary compensation by the intact limb. Improved kinetic symmetry can alleviate physical strain and improve balance control during these tasks [203]. Furthermore, motorized prostheses may reduce the physical demands required to operate the device, thereby increasing independence for less active users [204].

Considering current HKAF prosthesis limitations and current prosthetic knee actuation technology trends, a motorized HKAF prosthesis control method was developed and evaluated to increase prosthetic side assistance, reduce intact side loading and shorten task execution duration during sit-to-stand and stand-to-sit transitions compared to conventional passive prostheses. The findings from this study will contribute to our understanding of the effectiveness of motorized hip joints in HKAF prostheses for these activities. Moreover, this research may stimulate further innovations aimed at improving the quality of life for individuals with HD or HP amputations.

7.3 HKAF prosthesis prototype (Power Hip)

The HKAF prosthetic prototype shown in Fig. 7.1 was developed to enable walking, sitting, and standing for HD amputees. The prototype consists of a HD socket, prototype front mountable Power Hip, Össur Rheo knee 3 joint, and Össur Pro-Flex foot. Building upon previous research [31, 137, 138], the Power Hip module design was further optimized for this study by reducing the overall length to accommodate people with a shorter legs while ensuring compatibility with the existing HD socket designs and conventional prosthesis alignment methods [33].

The Power Hip module comprises two segments: prosthetic hip joint and thigh. The hip joint segment features a single-axis joint that can transmit motor-induced torque to the anterior mounted prosthetic hip centre of rotation. The thigh segment houses the electronics, sensors, and a 95.04 Wh (3.3 Ah) battery. Due to space constraints near the mounting point, the DC motor was positioned further below the socket, and torque transfer to the joint center of rotation was achieved using a cross-belt pulley system [32]. The DC motor is a three-phase brushless motor equipped with a harmonic drive gear system, capable of delivering up to 96 N·m of torque to support hip moment generation for users weighing up to 100 kg. The Power Hip was developed as a self-contained and untethered system, with all sensing, data processing, and power delivery operations performed in

real time by the integrated microcontroller and motor driver electronics inside the prosthesis, eliminating the need for external wiring to a computer or external power source.

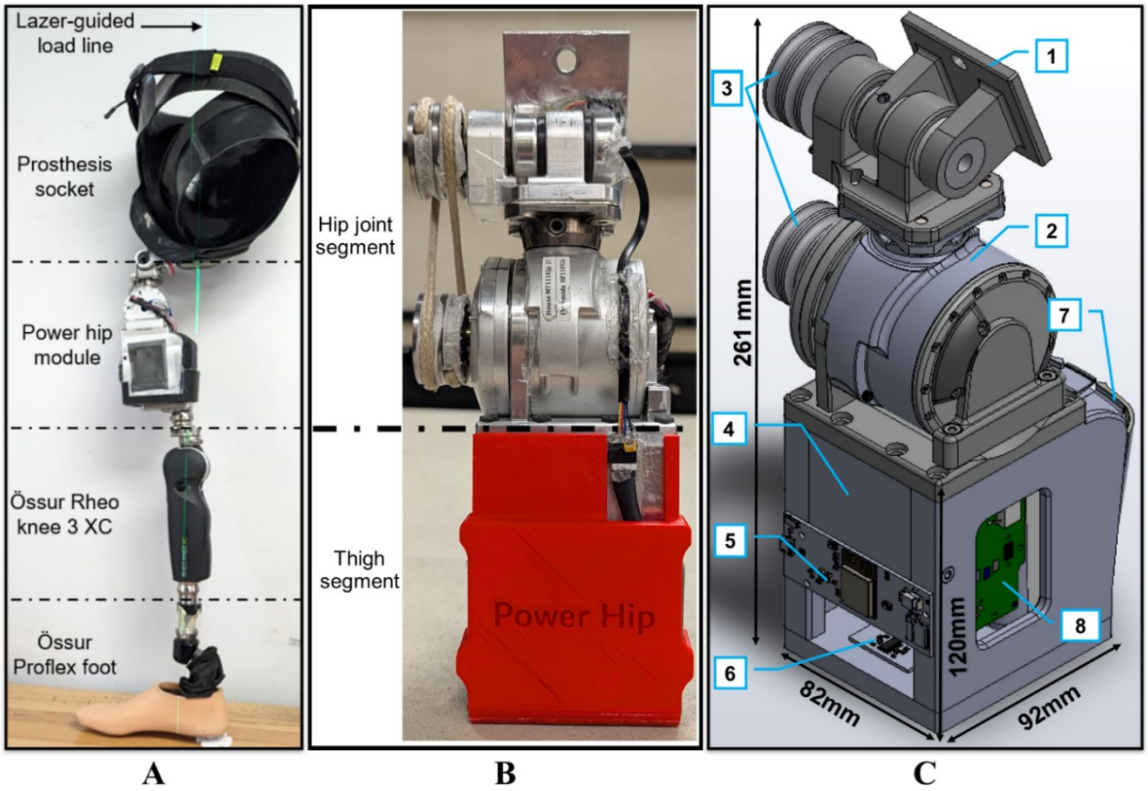

Fig. 7.1 Fully assembled Power Hip HKAF prototype (A), closeup frontal view of Power Hip module (B), and computer-aided design (CAD) of the Power Hip module (C). 1: Interface plate between Power Hip and prosthetic socket lamination plate, 2: DC motor, 3: Motor torque transfer pulleys, 4: Thigh chassis frame, 5: Sensor signal processing and active control electronics, 6: Load cells, 7: Battery, 8: Motor driver electronics.

7.4 Power Hip control strategy

A hierarchical control framework, initially developed for Power Hip gait control (Chapter 5), was adapted to incorporate sit-to-stand and stand-to-sit transitions. The main distinction between this study's control strategy and the control strategy discussed in Chapter 5 is the integration of Bluetooth communication to enable real-time activation of activity sequences and the development of two sets of finite state machines to decompose each activity into a series of shorter phases.

Custom software, running on a separate PC, transmitted specific commands to the prosthetic control system. Upon receiving these commands, the Power Hip module emitted an audible beep, signalling to the user that it was ready to perform the requested activity. This signalling mechanism was implemented to minimize the risk of unintentional activation in the prototype system. Although Bluetooth was used for this purpose, other methods, such as double

tapping the prosthetic socket or using a remote-control dongle similar to stand control knee orthoses could also be considered for future applications.

As shown in Fig. 7.2, when a sit or stand execution request is submitted to the Power Hip, the control software first evaluates the user's initial posture (idle sitting or standing) using hip angle sensors, a thigh inertial measurement unit (IMU) sensor, and the strain-gauged chassis (axial force sensor). If the user is in idle sitting, the sit-to-stand control protocol is executed to assist the user in standing. Conversely, if the user is in idle standing, the stand-to-sit protocol is activated to facilitate sitting. Idle sitting is determined when the hip flexion/extension angle (θ_{Hip}) and the prosthetic thigh sagittal tilt angle (θ_{Thigh}) remain greater than or equal to 60° for more than five seconds. Quiet standing is determined when the hip is at an approximate equilibrium angle ($-1° \leq \theta_{Hip} \leq 1°$, $-1° \leq \theta_{Thigh} \leq 1°$) and ground reaction force (GRF) exceeds 12% of the prosthetic user's body weight at the time the request signal is received.

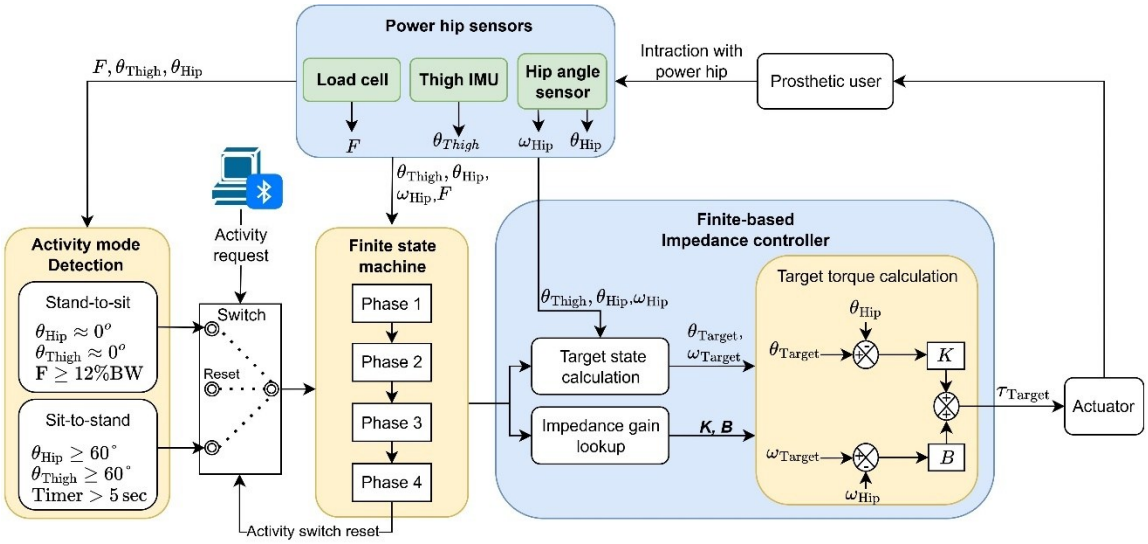

Fig. 7.2 Overview of Power Hip control strategy for sit-to-stand and stand-to-sit. BW: Body weight, F: ground reaction force

Regulation of Power Hip assistive and dampening torques for both activities was performed by a finite-based impedance controller. This type of controller has been widely implemented in motorized transfemoral prostheses due to its simplicity and adaptability [23, 122]. Finite-based impedance controllers operate by decomposing activities into smaller, sequential phases. Specific algorithms and gain values are applied for each phase to adjust the prosthesis angle and velocity impedance (magnitude of joint stiffness) [169].

In this study, the phase-based decomposition approach introduced by Kerr et al. [90] was adopted for the Power Hip impedance controller. Sit-to-stand and stand-to-sit activities were divided into four distinct chronological phases. Progression between phases occurs only when predefined conditions for transition are met. At the start of each phase, the target hip angle (θ_{Target}), target hip angular velocity (ω_{Target}), velocity gain (B), and displacement gain (K) are computed and then integrated into the motor torque equation as

$$\tau_{Target} = (\theta_{Hip} - \theta_{Target})K + (\omega_{Hip} - \omega_{Target})B \qquad (7.1)$$

where θ_{Hip} is the hip angle relative to the socket, ω_{Hip} is the measured hip angular velocity, and τ_{Target} is the calculated target torque to be outputted by the Power Hip motor. Depending on the vector direction of τ_{Target} and ω_{Hip}, the Power Hip torque may dampen or assist movement. When $\frac{\tau_{Target}}{\omega_{Hip}} < 0$, the Power Hip produces dampening torque to slow down or halt actuation. When $\frac{\tau_{Target}}{\omega_{Hip}} > 0$, the Power Hip produces assistive torque to accelerate or maintain hip joint actuation velocity.

θ_{Target} and ω_{Target} are dynamically calculated for each phase-based on real-time and past states of ω_{Hip}, θ_{Hip}, and θ_{Thigh}, while the B and K gains are manually tuned during participant training sessions to adjust for velocity and displacement impedance, respectively. The algorithms for computing the target states and procedures for tuning B and K gains, for each phase, are detailed in the subsequent subsections.

7.4.1 Sit-to-stand control phases

Observations of HD participant kinematics showed that their sit-to-stand transitions with mechanical hip joints were performed in a comparable manner to transfemoral amputees [90, 196]. Since active hip torque generation is required throughout sit-to-stand, passive hip joints are unable to assist the user, resulting in a minimum loading on the prosthetic side. As shown in Fig. 7.3, sit-to-stand can be decomposed into four main phases: trunk forward lean, chair push-off, vertical displacement, and recovery [196].

7.4.1.1 Phase 1: Trunk forward lean

Sit-to-stand initiation involves trunk forward leaning. This motion reduces the distance between the COM and the base of support, thereby decreasing hip and knee extension moments during the subsequent chair push-off (Phase 2) [205].

During Phase 1, the Power Hip does not assist the user. Instead, a small damping torque is applied to enable the force sensors to sense COM movement as soon as trunk forward leaning occurs. This dampening torque is achieved by setting the target hip angle (θ_{Target}) to 90° and maintaining the displacement gain (K) at $0 < K \leq 1$. The velocity gain (B) is set to zero since controlling the velocity during this phase would not provide any benefit.

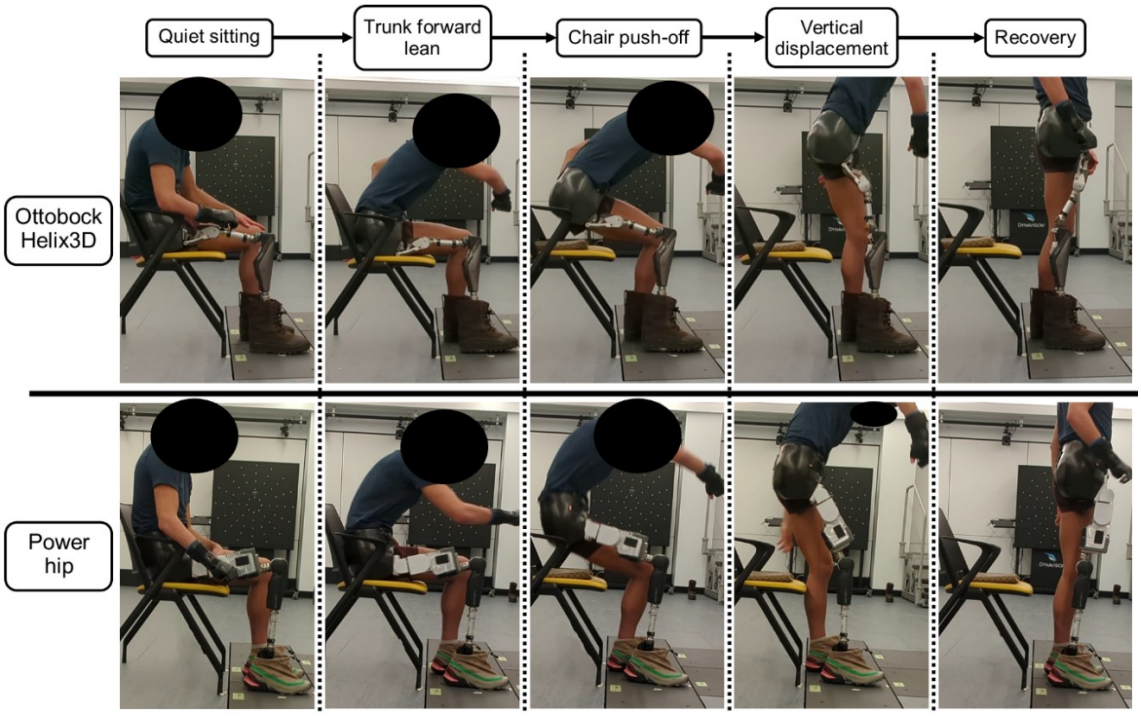

Fig. 7.3 Decomposition of the sit-to-stand activity for an HD participant using a HKAF prosthesis with a mechanical hip joint (top row) and Power Hip joint (bottom row).

The transition from Phase 1 to Phase 2 is detected by the Power Hip when the COM is sufficiently close to the base of support to allow for assisted push-off [206]. Hence, the ground reaction force (F), measured by Power Hip, must exceed 2% of the body weight (BW), and the hip angle (θ_{Hip}) must meet or exceed the hip extension threshold angle θ_{ST_Phase1}. The threshold θ_{ST_Phase1} is an adjustable parameter that is tuned during prosthesis fitting and training.

7.4.1.2 Phase 2: Chair push-off

Chair push-off transfers body weight from the chair to the feet by moving the COM toward the base of support area over the feet as fast as possible. Immediately following the transition to Phase 2, a substantial hip extension moment is applied while both knees are loaded within a short period. This generates a downward force on the ground (action), facilitating COM ascent (reaction) [206]. During this phase, the Power Hip assists the user by producing a high assistive hip extension torque.

This is achieved by setting stiffness $K \geq 50$ and $B \geq 20$ at a controlled target angle $\theta_{Target} = 0°$ and a target angular speed (ω_{Target}) defined as

$$\omega_{Target} = -\left|\omega_{ST\_Phase1}\right| \times C_{ST\_Phase2} \quad (7.2)$$

where ω_{ST_Phase1} represents the peak hip flexion speed measured during Phase 1 and C_{ST_Phase2} is a participant-specific tunable linear scaling factor. Since the Power Hip joint extends during Phase 2, the ω_{Target} must always be negative.

The transition from Phase 2 to Phase 3 occurs when sufficient propulsion height is achieved. This height can be calculated using the thigh angle (θ_{Thigh}) measured by the Power Hip IMU. Hence, completion of the transition can be determined when

$$(L_{Thigh} \times \sin(\theta_{\text{ST\_Thigh}} - \theta_{Thigh})) \geq (h_{\text{ST\_Phase2}} + h_{\text{ST\_Phase1}}) \quad (7.3)$$

Where, as illustrated in Fig. 7.4, L_{Thigh} is the length of the Power Hip module, $\theta_{\text{ST\_Thigh}}$ is the thigh angle during quiet sitting, $h_{\text{ST\_Phase1}}$ is the calculated hip joint height during Phase 1 of sit-to-stand, and $h_{\text{ST\_Phase2}}$ is the tunable target propulsion height.

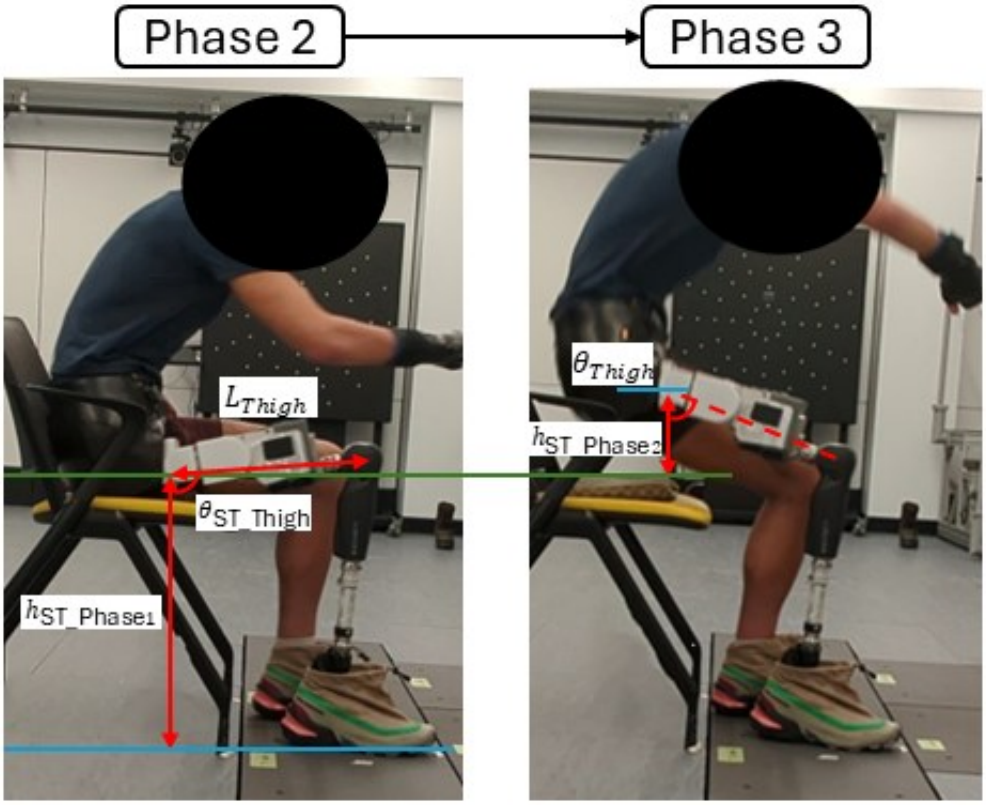

Fig. 7.4 Visualization of chair push-off calculation parameters.

7.4.1.3 Phase 3: Vertical displacement

During Phase 3, the trunk begins to lean anteriorly while the hip continues to extend. At this stage, the high assistive torque used during push-off propulsion is no longer required since the COM is already in motion and remains within the base of support after completing the preceding phase. Instead, the Power Hip generates a small assistive torque to support continued hip extension and upward COM movement. This is achieved by setting torque parameters to $1 < K < 10$, $B = 0$, and $\theta_{Target} = 0°$.

For a successful sit-to-stand completion, the hip joint must continue extending ($\omega_{Hip} \leq 0$), since any hip flexion during this phase results in COM descent, potentially causing the user to fall back into a seated position [78]. To prevent this, the Power Hip control locks in position when a downward COM displacement is detected (when $\omega_{Hip} > 0°/s$). COM displacement direction dependant torque control was implemented by alternating between high damping torque and low assistive torque based on the ω_{Hip} direction. High damping torque is applied by setting $K > 100$, $B = 0$, and $\theta_{Target} = \theta_{ST\_Phase3}$, where θ_{ST_Phase3} is the last measured hip angle while $\omega_{Hip} < 0$.

Phase 3 is concluded when the prosthetic thigh absolute tilt angle reaches zero while $\theta_{Hip} > 0$, indicating that the maximum COM height is achieved while prosthetic knee and hip joints are in flexion.

7.4.1.4 Phase 4: Recovery

At the start of Phase 4, both prosthetic hip and knee joints are in flexion, and therefore hip extension must be performed toward the equilibrium angle to ensure COM stability [78] (i.e., prosthetic knee positioned directly beneath the prosthetic socket at its maximum extension angle to lock the knee in stance mode and prevent accidental knee buckling [189]). To facilitate this motion, the Power Hip generates a high assistive hip extension torque, achieved by setting $K > 100$, $B = 0$, and $\theta_{Target} = 0°$. This high assistive torque drives the θ_{Hip} toward the equilibrium position. Through the coupled kinematics of Power Hip and prosthetic knee, this action simultaneously rotates the knee joint into full extension, ensuring stability and readiness for subsequent activities.

Once the θ_{Hip} reaches equilibrium, a high dampening torque is continuously applied to maintain standing position.

7.4.2 Stand-to-sit control phases

The progressive stance-controlled resistance of prosthetic knees can pose challenges for transfemoral and HKAF prosthetic users during the stand-to-sit transition [201]. Users often rely on complementary maneuvers to generate sufficient hip and knee flexion moments for the full duration of the activity [88]. The Power Hip joint provides an advantage in this context by producing assistive and dampening torque to minimize the need for prosthetic side unloading or compensatory maneuvers.

Kerr et al. [90] previously decomposed the stand-to-sit activity of non-amputees into four distinct phases: trunk forward lean, knee flexion, vertical descent, and recovery. For the Power Hip, the decomposition was slightly modified to better represent the observed kinematic characteristics (Fig. 7.5). In preparation for knee flexion, instead of performing trunk forward leaning, the participant moved their prescribed prosthesis anterior to reduce the prosthetic knee extension moment. Therefore, trunk forward leaning during Phase 1 was replaced with "Knee extension moment reduction" to account for the differences in strategy.

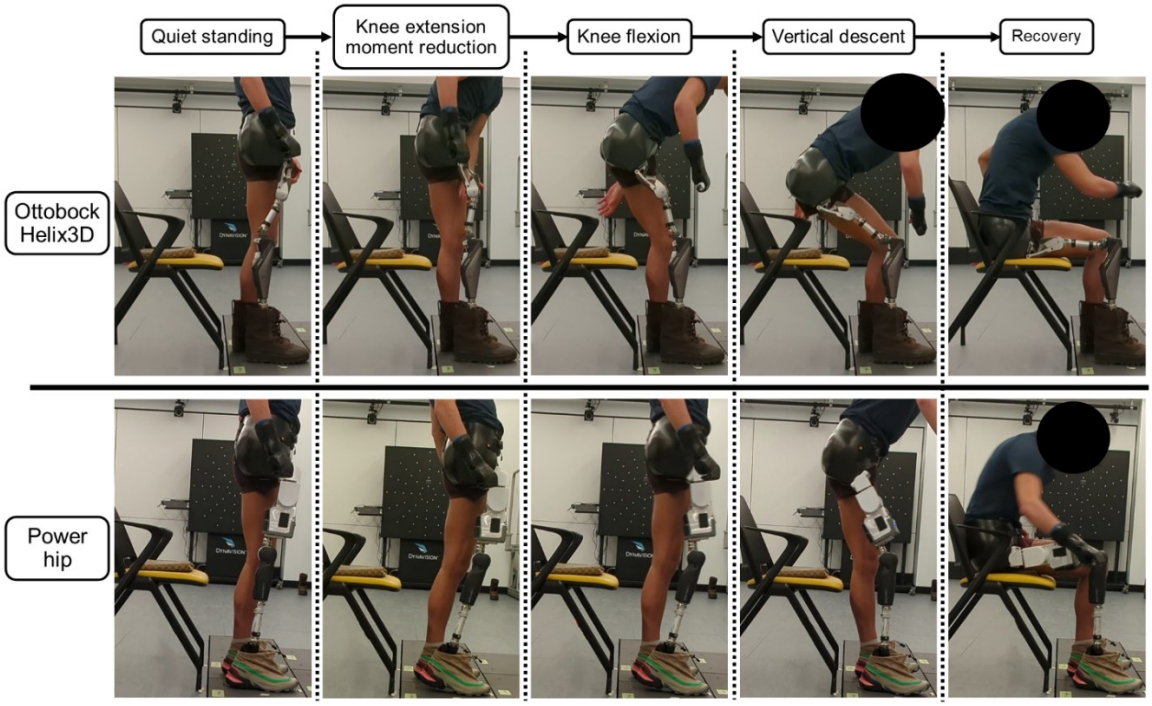

Fig. 7.5 Stand-to-sit activity phase-based decomposition for HKAF prostheses with mechanical hip joints (top row) and Power Hip joint (bottom row).

7.4.2.1 Phase 1: Knee extension moment reduction

During quiet standing, microprocessor-controlled knee joints are designed to generate high extension damping torque to prevent accidental buckling. However, this safety feature becomes a

limitation during the stand-to-sit transition since this approach increases the minimum torque required to initiate knee flexion [201]. Testing with participants in this study revealed that the torque required at the hip to counter the knee extension moment exceeded the maximum torque capability of the motor used in the prototype (96 N·m). This necessitated the development of a new strategy for prosthetic users to reduce the knee extension moment.

Since knee extension moment magnitude depends on the load applied to the prosthetic side and the load's horizontal distance from the knee's center of rotation, two possible strategies could be used by the prosthetic user to reduce this moment: reducing prosthetic-side loading or shifting the COM posterior. While unloading the prosthetic side can reduce the knee extension moment, this alters the base of support and decreases kinetic symmetry during the transition. Therefore, an alternative strategy was devised through participant experimentation to only use posterior COM movement. As depicted in Fig. 7.5, during Phase 1, the Power Hip maintains a steady damping torque near equilibrium (K > 100, B = 0, and $\theta_{Target} = 0°$) while the participant uses their pelvis to perform a rapid hip extension movement resembling a kicking motion. This maneuver momentarily (<1 second) shifts the COM posterior to the knee, increasing the moment arm length and thereby reducing the knee extension moment. The Phase 1 to Phase 2 transition is completed when rapid hip extension is detected. Hence $\omega_{Hip} < \omega_{SI\_Phase1} < 0°/s$, where ω_{SI_Phase1} is a tunable hip extension velocity threshold.

7.4.2.2 Phase 2: Knee flexion

By leveraging the reduced knee extension moment achieved during Phase 1 through chained kinematics, assistive flexion torque generation at the hip joint is sufficient to initiate knee flexion. Using the Power Hip, this is achieved by configuring the parameters as K > 100, B = 0, $\theta_{Target} = \theta_{SI\_Phase2} \geq 10°$, where θ_{SI_Phase2} is the tunable hip max flexion angle to be achieved during Phase 2.

To prevent balance loss caused by the kicking motion in Phase 1, hip flexion is performed immediately after transitioning to Phase 2. This motion is delivered as a brief hip flexion torque burst to initiate COM descent required for Phase 3. The transition from Phase 2 to Phase 3 is completed once $\theta_{Hip} \geq \theta_{SI\_Phase2}$.

7.4.2.3 Phase 3: Vertical descent

During Phase 3, hip and knee flexion are initiated, followed by forward trunk leaning during the vertical descent, which prepares the user for body weight transfer onto the seat. At this stage, the

Power Hip assists the user by providing assistive hip flexion. Assistive hip flexion is applied to the prosthetic knees that continually apply extension moments during sitting and thus, the assistive hip flexion torque is required to bend the knee during sitting [203]. This assistive torque is achieved by setting K > 100, B > 10, $\theta_{Target} = 90°$, and $\omega_{Target} = \omega_{SI\_Phase3}$, where ω_{SI_Phase3} is the hip flexion speed during stand-to-sit Phase 3 and is calculated using equation 7.4:

$$\omega_{SI\_Phase3} = \omega_{SI\_Phase1} \times C_{SI\_Phase3} \quad (7.4)$$

where C_{SI_Phase3} is a tunable ratio.

The transition from Phase 3 to Phase 4 is completed when the COM is a few centimetres above the seat. The distance can be estimated by measuring thigh absolute tilting angle and with the assumption that the seat is at knee height. Hence, the transition condition is met when

$$\theta_{Thigh} \leq \sin^{-1}\left(\frac{h_{\text{SI\_Phase3}}}{L_{Thigh}}\right) \quad (7.5)$$

where $h_{\text{SI\_Phase3}}$ is an adjustable threshold for the minimum height of the prosthetic user socket relative to the seat.

7.4.2.4 Phase 4: Recovery

During this phase, the prosthetic user transitions into quiet sitting by allowing their body to settle onto the seat. Power Hip does not assist during this phase, since neither displacement nor velocity control provides any functional benefit. Consequently, no torque is produced by the Power Hip, with the parameters set to K = 0 and B = 0.

7.5 Power Hip performance evaluation

Power Hip prosthesis performance was evaluated by comparing task execution times and kinetic symmetry between trials where a HD amputee used the prototype Power Hip or their prescribed prosthesis. This study was approved by the University of Ottawa (H-08-21-7062) and Carleton University (122696) ethics boards. Inclusion criteria required participants to have a unilateral hip disarticulation (right side), a minimum of three months of experience using a HKAF prosthesis, at least 18 years old, body mass under 100 kg (without the prosthesis), lead an active lifestyle, use their prosthesis daily, and ambulate independently without assistive devices such as a cane. As detailed in Table 7.1, a participant who met these criteria was recruited for the study. He was fitted with a new hip disarticulation socket at Nielen Prosthetic and Orthotic Clinic and trained by a certified prosthetist to use the Power Hip.

Table 7.1 Participant's details

Body height (cm)	HKAF height (cm)	Age (years)	Body mass (kg)	HKAF prosthesis use (years)	Prescribed prosthesis	
					Hip joint	Knee joint
1.80	89	25	64	6	Ottobock Helix3D	Ottobock C-Leg

Training consisted of ten sessions, each lasting two hours. During the training period, the control strategies for sit-to-stand and stand-to-sit activities were refined, and parameter adjustments were made to suit the participant's individual needs. The training was deemed complete once the participant successfully executed five consecutive sit-stand-sit transitions.

7.5.1 Test protocol

After training was completed, motion capture technology was employed to calculate joint kinematics and kinetics. Evaluation trials were conducted at the Abilities Living Laboratory (Carleton University, Ottawa, Canada). Full-body 3D movements were captured using a Theia3D markerless motion capture system (version 2024-1-0-4409, Theia Markerless Inc., Kingston, ON, Canada) with 11 high-definition cameras operating at 100 Hz. This motion capture system employs computer vision and artificial intelligence algorithms to track 3D human movement without requiring physical markers. Force platforms were used to capture ground reaction forces at 1000 Hz and were synchronized with the camera data.

Prior to testing, system calibration was completed following Theia3D documentation [207]. After calibration, a chair with armrests was positioned in front of the force platforms. Then, the participant was asked to sit on the chair with one foot on each force plate. Ten sit-stand-sit trials were completed, five using their prescribed prosthesis and five using the Power Hip. With the Power Hip, sit-to-stand and stand-to-sit modes were activated sequentially using Bluetooth commands sent via a custom-built personal computer application. A minimum of 10 s was provided between trials to allow the participant to adjust their posture and reestablish idle standing or sitting. For each trial, the Theia3D software was used to create a 13-segment, six-degrees-of-freedom skeletal model. The synchronized ground reaction force data were also labelled and prepared for further processing.

7.5.2 Data analysis

The 3D model generated by Theia3D was imported into Visual3D (version 2024.07.2) to compute and extract lower extremity joint kinetics and kinematics. Hip and knee joint angles were calculated using a Cardan sequence [208]. Trunk COM movements were calculated from the body model, in reference to the lab coordinate system. Joint moments were determined through inverse dynamics.

Each trial's data were segmented according to the activity type (sit-to-stand or stand-to-sit) using the method described by Highsmith et al. [203]:

- **Sit-to-stand**: Initiation occurs when the trunk COM moves forward by 10 mm and is completed when both the hip and knee are fully extended and remain extended for more than 0.25 seconds (±2° margin of error).
- **Stand-to-sit**: Initiation occurs when either the hip or knee (prosthetic side) flexes by more than 5° relative to the quiet standing equilibrium angle and is completed when the trunk COM ceases posterior movement for more than 0.25 seconds (±5 mm margin of error) and both the hip and knee are flexed beyond 60°.

The segmented kinetic and kinematic data were exported to MATLAB (R2024a) for further analysis and outcome measure calculation. Primary outcome measures included maximum vertical GRF, vertical GRF impulse, maximum knee moment, maximum hip moment, sit-to-stand duration, and stand-to-sit duration. GRF was normalized by body mass. Knee and hip moments were divided by the product of participant body mass and height.

The control strategy was designed to ensure that the prosthetic user maintained consistent prosthetic-side loading during sitting and standing. Additionally, assistive hip torque was intended to counteract the prosthetic knee’s progressive resistance, thereby facilitating faster movements. Considering these capabilities, the Power Hip performance metrics should indicate shorter task execution times and reduced maximum kinetic differences between the intact side and the prosthetic side when compared to prescribed prosthesis results, as is the case for the TF amputees using microprocessor-controlled knees verses motorized knees [196, 203].

7.6 Results

The participant successfully completed all trials with both prostheses without losing balance or requiring external assistance. He used the chair armrests during push-off phases for both prostheses. The tunable parameters outlined in Section 7.4 were initially configured to default values that were deemed theoretically non-taxing for prosthesis users. As the participant gained proficiency with the

Power Hip during training, both finite state machine parameters and impedance controller gains were iteratively adjusted to optimize performance. The finalized parameter configurations are documented in Appendix D.

Sensor measurements from the Power Hip prosthesis are presented in Fig. 7.6, while maximum kinetic values (hip joint moments, knee joint moments, GRF) are summarized in Table 7.2. Kinetic profiles and COM trajectories are illustrated in Fig. 7.7. The positive knee and hip moments indicate external moments applied in the flexion direction, and negative moments indicate external extension moment generation.

7.6.1 Power Hip motor output

The Power Hip prosthesis executed all sit-to-stand and stand-to-sit transition phases as defined in Section 7.4. During sit-to-stand transitions, the prosthesis generated short, high-magnitude bursts of assistive power, peaking at 3.73 ± 0.35 W/kg during Phase 2 (chair push-off). In contrast, stand-to-sit transitions produced lower peak assistive power (1.77 ± 0.15 W/kg), which occurred during Phase 3 (vertical descent).

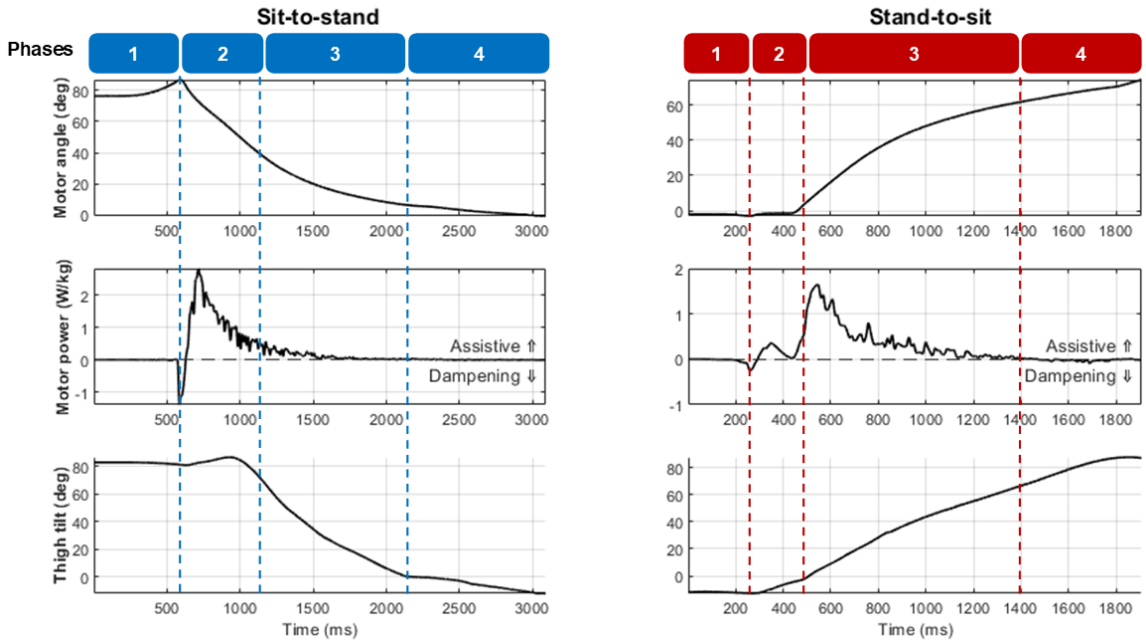

Fig. 7.6 Power Hip sensor measured motor angle, motor power, and sagittal thigh segment tilt angle of one sitting and standing trial.

As theorized, prosthesis actuation dynamics are reflected in kinetic outcomes. Fig. 7.7A illustrates the effect of the Power Hip's extension moment during Phase 2 of sit-to-stand transition (chair push-off), corresponding to the power that assisted in initiating COM upward movement.

Fig. 7.7B shows the hip and knee flexion external moments during Phase 2 of stand-to-sit transition, reflecting the prosthesis' ability to reduce knee extension moments through active hip flexion.

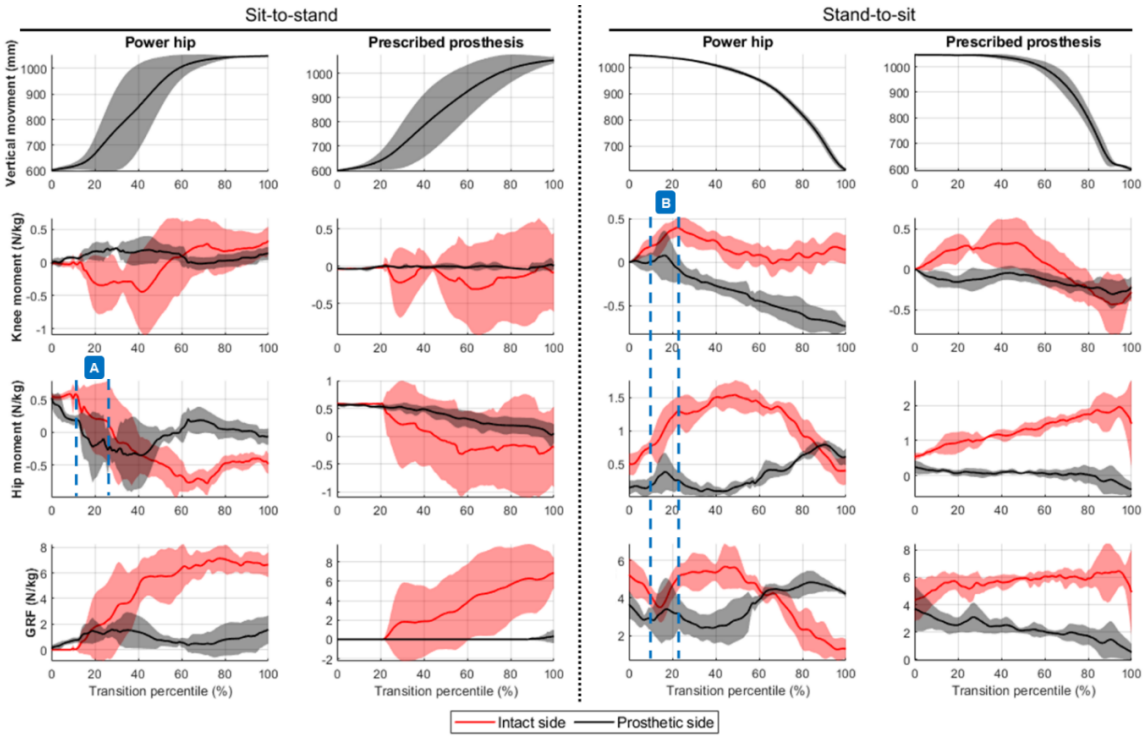

Fig. 7.7 Kinetics for sit-to-stand and stand-to-sit with Power Hip and participant's prescribed prosthesis (average and standard deviation). Knee and hip joint positive values represent external moments in flexion direction, negative values represent external moments in extension direction. Vertical movement represents the Z-axis movement of the pelvis COM. A: the period representing Power Hip extension to assist during chair push-off (sit-to-stand Phase 2), B: the period representing knee extension moment reduction (stand-to-sit Phase 1).

7.6.2 Ground reaction force

During both sit-to-stand and stand-to-sit transitions, the participant exhibited a preference for loading the intact limb, consistent with patterns observed in TF amputees [203]. However, the Power Hip prosthesis reduced the maximum force disparity between the prosthetic and intact sides during transitions, with differences of 5.34 ± 0.68 N/kg (sit-to-stand) and 1.00 ± 0.64 N/kg (stand-to-sit). These improvements were attributed to peak kinetic outputs facilitated by the Power Hip's actuation bursts during early transition phases (Fig. 7.7A and Fig. 7.7B). In contrast, the prescribed prosthesis resulted in larger force differences (7.34 ± 1.87 N/kg during sit-to-stand; 3.70 ± 1.95 N/kg during stand-to-sit).

Table 7.2 External joint moments, GRF, and execution duration differences between Power Hip and prescribed passive HKAF prosthesis during sit-to-stand and stand-to-sit transition

	Sit-to-stand		Stand-to-sit	
	Power Hip	**Prescribed**	**Power Hip**	**Prescribed**
Intact side GRF (N/kg)	8.03 ± 0.56	7.64 ± 2.04	6.37 ± 1.01	7.98 ± 1.03
Prosthetic side GRF (N/kg)	2.69 ± 0.34	0.30 ± 0.67	5.37 ± 0.52	4.28 ± 1.00
Intact side GRF impulse (N·s/kg)	7.91 ± 3.58	4.16 ± 4.02	4.97 ± 0.78	15.06 ± 2.90
Prosthetic side GRF impulse (N·s/kg)	1.66 ± 1.10	0.03 ± 0.07	4.36 ± 0.17	5.69 ± 0.66
Intact side knee moment (N/kg)	-0.90 ± 0.19	-0.84 ± 0.32	0.69 ± 0.06	0.60 ± 0.26
Prosthetic side knee moment (N/kg)	0.35 ± 0.02	0.09 ± 0.06	-0.48 ± 0.06	-0.10 ± 0.05
Intact side hip moment (N/kg)	-0.97 ± 0.06	-0.68 ± 0.62	1.61 ± 0.18	2.35 ± 0.48
Prosthetic side hip moment (N/kg)	-0.79 ± 0.06	0.01 ± 0.21	0.84 ± 0.06	0.32 ± 0.13
Transition Duration (s)	1.69 ± 0.49	1.22 ± 0.40	1.22 ± 0.08	2.62 ± 0.41

GRF impulse analysis further highlighted these differences. With the prescribed prosthesis, sit-to-stand transitions showed intact-side dominance, with impulses of 4.16 ± 4.02 N·s/kg (intact) versus 0.03 ± 0.07 N·s/kg (prosthetic). The Power Hip promoted more balanced loading, yielding 7.91 ± 3.58 N·s/kg (intact) and 1.66 ± 1.10 N·s/kg (prosthetic). Similarly, during stand-to-sit transitions, the Power Hip reduced GRF impulse differences (0.61 ± 0.83 N·s/kg) compared to the prescribed prosthesis (9.37 ± 2.69 N·s/kg).

Maximum summed GRF magnitudes during sit-to-stand transitions were lower than the participant's body mass (64 kg) for both prostheses (Power Hip: 55.94 ± 3.62 kg; prescribed: 49.88 ± 13.30 kg). This discrepancy likely arose from the participant's reliance on chair armrests for assistance, which reduced lower limb loading demands.

7.6.3 Hip moment

Hip joint moment differences between the intact and prosthetic sides were greatly reduced with the Power Hip prosthesis compared to the prescribed HKAF prosthesis during both sit-to-stand (Power Hip: -0.18 ± 0.09 N/kg, prescribed: -0.69 ± 0.67 N/kg) and stand-to-sit (Power Hip: 0.77 ± 0.20 N/kg, prescribed: 2.03 ± 0.58 N/kg).

During sit-to-stand, the Power Hip generated a maximum hip extension moment of -0.79 ± 0.06 N/kg, whereas the prescribed joint dampened hip movement by generating a small flexion torque (0.01 ± 0.21 N/kg). However, during stand-to-sit transitions, the prescribed HKAF appeared to contribute flexion moments, which was achieved through externally generated forces (e.g., using

his hand to manually reposition the prosthetic limb and flex the knee) rather than intrinsic joint actuation (Fig. 7.5). This contrasts with the Power Hip, which generated flexion moments via motor actuations.

7.6.4 Knee moment

During sit-to-stand transitions, the Power Hip prosthesis generated a prosthetic-side knee flexion moment of 0.35 ± 0.02 N·m/kg, actively damping joint movement, which was greater than that of the prescribed HKAF prosthesis (0.09 ± 0.06 N·m/kg). Similarly, during stand-to-sit transitions, the Power Hip's prosthetic knee produced a flexion moment of -0.48 ± 0.06 N·m/kg to dampen knee extension, compared to the small damping observed with the prescribed prosthesis (-0.10 ± 0.05 N·m/kg).

The high prosthetic knee damping during Power Hip sitting stemmed from the Rheo Knee 3 progressive stance control feature that resisted knee movement. The limited moment generation of the prescribed prosthetic knee could have been due to the limited prosthetic-side loading since prosthetic knees are designed to dampen only when they are loaded beyond a certain threshold [97].

7.6.5 Duration

The participant completed both sit-to-stand and stand-to-sit transitions more rapidly with both prostheses, compared to average durations reported in prior literature on TF amputees (Highsmith et al. [203]). However, distinct temporal patterns emerged between HKAF prosthesis types. During sit-to-stand transitions, the Power Hip prolonged the transition (1.69 ± 0.49 s) relative to the prescribed HKAF (1.22 ± 0.40 s), though both remained faster than reported TF amputees (2.0 ± 0.8 s). In contrast, during stand-to-sit transitions, the Power Hip enabled faster transitions (1.22 ± 0.08 s) compared to both the prescribed HKAF (2.62 ± 0.41 s) and the TF group (2.8 ± 0.6 s). This improvement during stand-to-sit may be attributed to the Power Hip's hip flexion assistance, which stabilized the descent phase and reduced the effect of progressive prosthetic knee dampening.

7.7 Discussion

This study demonstrated that a novel Power Hip prosthesis can enable more symmetric lower limb loading during sit-to-stand and stand-to-sit by providing appropriate hip moments at the right time. The participant used the Power hip for consecutive sitting and standing without losing balance while maintaining loading on both limbs during transitions. Furthermore, the stand-to-sit transition time was reduced. However, the sit-to-stand transition time was longer than conventional joints.

This hip joint advancement has the potential to improve functional outcomes during sit-to-stand and stand-to-sit transitions in individuals with HD amputations.

7.7.1 Kinetic differences

Analysis of kinematic data (Fig. 7.7) and peak kinetic values (Table 7.2) demonstrated two principal advancements of the Power Hip over the prescribed prosthesis: (1) improved weight-bearing on the prosthetic limb during transitions, and (2) reduced reliance on upper-body compensation.

7.7.1.1 Increased prosthetic-side loading

The Power Hip demonstrated improvements in redistributing kinetic demands between limbs during sit-to-stand and stand-to-sit transitions. The prosthesis reduced asymmetry in GRF and hip joint moments compared to the prescribed HKAF prosthesis. The Power Hip's assistive hip extension moments during sit-to-stand and controlled flexion resistance during stand-to-sit replicated biomechanical patterns observed in TF amputees [33], thereby reducing overloading of the intact limb.

However, the Össur Rheo Knee 3 XC (Knee module of the prototype) introduced challenges during stand-to-sit transitions. Unlike prosthetic knees with dedicated damping profiles for stand-to-sit transitions, the Rheo Knee 3 XC lacks such functionality, necessitating active hip flexion from the Power Hip to counter the progressive damping and regulate vertical descent. This constraint contrasts with prosthetic knees that produce limited damping during sitting. Therefore, if the Power Hip was equipped with such a prosthetic knee, an alternative control method might be required for Phase 3 of stand-to-sit.

7.7.1.2 Reduced upper-body reliance

The kinetic profiles in this study diverged from reported TF amputees and able-bodied results in the literature [79, 86, 199]. HD amputees inherently adopt distinct COM transitional strategies due to the absence of a femoral segment, which alters weight-shifting mechanics and increases reliance on upper-body support. However, in the context of HD amputees, the Power Hip reduced this reliance compared to the prescribed HKAF prosthesis.

During sit-to-stand, while direct upper-limb loading was not quantified, the Power Hip's redistribution of kinetic demands reflected in higher intact and prosthetic-side GRF values (from the beginning of Phase 1) suggests reduced compensatory reliance on the upper body (Fig. 7.7). This contrasts with the prescribed HKAF, where the participant initiated vertical COM movement

before loading either limb (no GRF reading on either side during 20–40% of the transition), resulting in total dependence on upper-body effort.

During stand-to-sit transition, with the prescribed prosthesis, upper-body engagement was necessary during Phases 1 and 2 to perform the hip and knee flexion. In contrast, the Power Hip eliminated upper-body involvement during these early phases, due to its active hip flexion control. However, as Phase 3 commenced, regardless of the prosthesis type, the participant consistently reached out to the chair arm rests for stabilization.

7.7.2 Transition execution time

The Power Hip demonstrated contrasting performance profiles during sit-to-stand and stand-to-sit transitions compared to the prescribed HKAF and TF amputee results from literature [203]. During sit-to-stand, the participant achieved faster transitions with the prescribed HKAF (1.22 ± 0.40 s) than with the Power Hip (1.69 ± 0.49 s). However, the prescribed HKAF reduced timing came at the cost of near-complete reliance on upper-body force generation, since the participant failed to load the prosthetic limb during chair push-off (Fig. 7.7). In contrast, the Power Hip promoted bilateral limb loading, reducing upper-body dependence and offering potential advantages for users with limited upper-limb strength.

While the Power Hip's motorized hip extension could theoretically further accelerate chair push-off, participant feedback during training indicated discomfort due to abrupt torque transmission through the socket and onto the participant's pelvis. In the future iterations of the sit-to-stand control strategy, this limitation could be addressed through torque-profile smoothing or control algorithms that can more accurately estimate the user's desired push-off acceleration.

The participant's faster overall transition times relative to the TF amputees may stem from methodological differences, particularly the permitted use of chair armrests for support in this study. Such external assistance likely reduced biomechanical demands, masking the full impact of prosthetic design on transition timing. With more time to accommodate to the powered sit-stand movements, the participant may evolve to a more balanced approach, with efficient bilateral limb loading but also effective use of armrests to aid in the movement tasks.

7.7.3 Limitations

A limitation of this study is the relatively brief training period, which may have influenced the outcomes. Extended training with the prosthesis could conceivably improve sitting and standing symmetry as well as activity completion duration [68]. Another factor potentially affecting the

results is the knee component utilized in this study. Because only the Össur Rheo XC 3 knee was evaluated, the findings may not directly translate to other knee designs that incorporate alternative sitting control strategies. Future research should encompass a broader array of prosthetic knee designs to assess their effect on kinetic symmetry and the duration of transitional movements.

Furthermore, the study sample was limited to one experienced prosthesis user with an active lifestyle. Consequently, the results may not be readily generalizable to the wider population of prosthesis users, particularly those with lower activity levels or less experience. Subsequent investigations should incorporate a larger and more diverse cohort to enhance the reliability of the findings.

7.8 Conclusion

This study demonstrated how a HKAF prosthesis with a motorized hip joint can improve sit-to-stand and stand-to-sit execution for HD amputees. The untethered Power Hip prototype successfully achieved more symmetric loading between limbs and enabled faster stand-to-sit transitions compared to a conventional HKAF prosthesis, potentially reducing the physical demand and improving the balance during transitions. The participant's adaptation to the device within a short training period further supports its viability for real-world applications. By mimicking TF amputees' hip kinematics through active moment generation, the Power Hip addresses some limitations of passive prostheses, which often necessitate excessive upper-body and intact-limb reliance.

However, challenges remain. The influence of external factors such as chair height and upper-body assistance on prosthetic performance warrants further investigation to improve the control strategies. Future studies should explore how the Power Hip prosthesis can facilitate transitions without upper-limb support from armrests (a common requirement in real-world environments) and evaluate its efficacy across varied seating configurations. Such research would clarify the Power Hip's adaptability to diverse user needs and environments. Ultimately, this research advances the design and evaluation of motorized prosthetic systems for HD amputees, offering a pathway to improved functional independence and quality of life.

Chapter 8: Conclusion

8.1 Summary of thesis work

This thesis advances the development and evaluation of motorized HKAF prostheses for individuals with HD amputations through novel control strategies, sensor integration, and comparative performance analyses. Collectively, this research demonstrated that motorized HKAF prostheses, driven by adaptive control algorithms, address many limitations of conventional prostheses such as: improving symmetry, increasing hip range of motion, reducing the magnitude of complementary movements, eliminating the need for external sensors, ensuring compatibility with existing sockets, and prioritizing HD user-centric controls, the developed system advances toward commercialization of Powered HKAF prostheses. Future research should focus on long-term usability studies where participants use the Power Hip in the community, refinement of pelvic kinematic feature extraction algorithms, and scalability to diverse user populations. These innovations mark a shift in prosthetic options for people with HD or HP amputations, offering renewed opportunities for functional independence and improved quality of life.

When assessing the testing outcomes, it should be noted that the participants were learning to use the prototype Power Hip while the hardware (rope system, electronics, etc.) and software were iteratively improved between training sessions. Therefore, the final evaluations were performed before the prosthesis user had fully learned to use the Power Hip advantages. Examples include large improvements in walking over the final training session outside of parallel bars (i.e., larger space for unconstrained walking) and lack of practice on sharp turns increasing their time to complete the 2MWT. More time using the Power Hip should enable HKAF prosthesis users to retrain their ingrained gait patterns to avoid unnecessary compensatory movements, find novel ways to efficiently turn and move in smaller spaces, sit and stand more efficiently, gain confidence in relying on the prosthesis to assist them, and unconsciously make better use of the motor to reduce energy expenditure.

The summarized contributions of Chapters 3 to 7 toward achieving the thesis objectives are detailed in following sub-sections.

8.1.1 Objective 1: Develop a motorized HKAF prosthesis control strategy for gait initiation, termination, and level walking

An algorithm was developed to calculate hip kinematics throughout the gait cycle for active prosthesis control using pelvic tilt, rotation kinematics, and stance time of TF amputees (Chapter 4). This method enabled real-time hip trajectory generation for a gait controller that only relied on pelvis and ipsilateral limb kinetics and kinematics. The algorithm was validated using TF prosthetic user kinetics and kinematics [154]. Small angular RMSE were found between the algorithm results and motion capture data. The greatest difference was for hip maximum extension angle ($2.5 \pm 2.0°$). Since differences between algorithm output and motion data were within averaged standard deviations (by 1° for development group and by 1.2° for validation group), the developed algorithm was deemed viable to be used in developing a gait control strategy for the Power Hip HKAF prototype.

Chapter 5 introduced a speed-adaptive gait control strategy for a motorized HKAF prosthesis, leveraging the algorithm presented in Chapter 4 and the framework proposed by Tucker et al. [23]. The Power Hip prototype demonstrated successful user speed adaptation, with the participant achieving hip kinematics comparable to TF amputees in all walking speeds (0.69 m/s for slow, 0.90 m/s for self-paced, and 1.01 m/s for fast walking speeds). Specifically, maximum prosthetic-side hip extension velocities and prosthetic-side hip ROM closely matched the TF amputee data. This proved that the Power Hip prototype and control strategy were viable tools that could be used for further studies on walking capabilities with motorized HKAF prostheses.

8.1.2 Objective 2: Develop a motorized HKAF control strategy for sit-to-stand and stand-to-sit transitions

Chapter 7 of this thesis reported on a successful control strategy for sit-to-stand and stand-to-sit using the Power Hip prosthesis. Research on prosthetic design or control methods aimed at improving chair sitting and standing remains limited, making the findings presented in this thesis work pioneering in the field. Due to the scarcity of kinetic and kinematic data on passive HKAF prostheses during these tasks, control strategy development relied on participant feedback and observational data.

Building on the gait control strategy framework discussed in Chapter 5, the control frameworks for sit-to-stand and stand-to-sit activities were developed to rely solely on internal sensors (pelvic IMU, axial force sensor, thigh IMU, hip joint angle sensor). As a result, the same Power Hip prototype was used during evaluations without requiring any hardware modifications.

The control strategy was verified during participant training with the prosthesis. After 10 training sessions during which the hardware and software were refined, the participant was able to stand up from and sit down onto a chair without losing balance or relying on parallel bars for support. Although the participant could perform these tasks without relying on the chair's armrests, additional training was required to provide sufficient experience and confidence to execute the movements independently. Consequently, the final evaluation study was conducted using a chair equipped with armrests that could provide support if needed.

The results of the evaluation demonstrated that the Power Hip provided sufficient torque to assist the user through the transitions without hindering their movements. The Power Hip's motor sensors measured maximum torque outputs of 63.90 N·m during sit-to-stand and 52.04 N·m during stand-to-sit. These values are well within the maximum capability of the Power Hip motor (96 N·m), further validating its effectiveness in aiding users during these transitions.

8.1.3 Objective 3: Quantify the gait control strategy and prototype performance by comparing the prototype performance to prescribed mechanical HKAFs used by HD amputees

Using the Power Hip prototype hardware and the control strategy developed in Chapter 5, a comparative study was conducted and detailed in Chapter 6 to quantify performance differences between the Power Hip and conventional HKAF prostheses. Two-minute and three-speed walk test outcomes revealed improved gait biomechanics with the motorized hip, including improved spatial and temporal gait symmetry and reduced complementary movements such as pelvic tilt, compared to same participant's prescribed prosthesis. This demonstrated the potential of motorized HKAF in improving mobility.

Although the participant walked slightly slower during the tests with the Power Hip (Power hip: 0.69 to 1.02 m/s, prescribed: 0.60 to 1.12 m/s), they reported greater satisfaction with speed adaptability and overall comfort. Additionally, despite the increased weight of the Power Hip, the participant did not perceive device weight as a hindrance. In fact, the Power Hip helped maintain forward momentum, contributing to a smoother walking experience.

8.1.4 Objective 4: Quantify the chair sitting and standing control strategy and prototype performance by comparing the prototype performance to prescribed mechanical HKAFs used by HD amputees

In Chapter 7, in addition to discussing the methods used to develop the control strategy, comparative tests were conducted to evaluate whether the motorized hip joint could provide quantifiable benefits to users compared to conventional HKAF prostheses. The findings demonstrated both advantages and trade-offs when comparing the Power Hip to the participant's prescribed HKAF prosthesis. During sit-to-stand, more body weight was applied to both lower limbs when using the Power Hip compared to the conventional prosthesis. Thus, reliance on upper-body forces during chair push-off was reduced, addressing a limitation of passive devices. However, this benefit came at the cost of increased transition duration (Power Hip: 1.69 ± 0.49 s; Prescribed: 1.22 ± 0.40 s). In contrast, during stand-to-sit, the participant was able to distribute weight more evenly between both legs while completing the movement faster with the Power Hip compared to the prescribed prosthesis. These results align with trends observed in past studies involving different prosthetic designs [89, 203], suggesting that the Power Hip reduces the physical demands of these tasks while enhancing balance stability. Overall, the motorized hip joint offered functional improvements, though further refinements and participant training time may be necessary to optimize task execution speed.

8.2 Future research directions

This thesis establishes foundational insights into the capabilities of the Power Hip prosthesis, yet numerous avenues for further investigation remain. The following short- and long-term research pathways are proposed to advance the Power Hip functionality, accessibility, and clinical integration:

8.2.1 Short-term research directions

1. **Expanded clinical validation**: Conduct multi-participant trials to evaluate Power Hip's performance across diverse anatomical and functional profiles. Data collection during walking and sit-stand-sit activities will assess reproducibility and refine control strategies for real-world variability.
2. **Adaptive control for complex terrains**: Extend the current control framework to accommodate sloped surfaces and uneven terrain. This development would enhance device adaptability to environmental challenges.

3. **Stair navigation capabilities**: Integrate stair ascent and descent functionalities into the control architecture. This advancement would address a mobility limitation for HD amputees, who may avoid stairs entirely with passive prostheses.
4. **Automated parameter tuning**: Implement self-learning algorithms (e.g., Recursive Least Squares, Simulated Annealing, or Simple Genetic Algorithms) to reduce manual control parameter tuning efforts. Automating parameter optimization would minimize training time and enable personalized adjustments for new users.
5. **Alternative joint design evaluations**: Adapt the control strategy for a side-mounted hip joint configuration, comparing its performance with the current front-mounted Power Hip and passive prostheses.
6. **Durability and field testing**: Develop a next-generation prototype for long-term loan to participants, enabling in-home and community-based evaluations. This step is critical for assessing reliability under prolonged use and refining maintenance protocols.

8.2.2 Long-term research directions

1. **Diverse population studies**: Evaluate the Power Hip's efficacy across broader user demographics, including individuals with varying physical fitness levels, or limited prior experience with HKAF prostheses. Such studies would ensure equitable accessibility and identify user-specific adaptation patterns.
2. **Longitudinal health outcomes**: Investigate the Power Hip's effect on musculoskeletal health, metabolic efficiency, and quality of life over long-term use. Metrics such as joint loading symmetry, muscle atrophy prevention, and user-reported satisfaction would clarify its clinical benefits.
3. **Standardized rehabilitation protocols**: Design evidence-based guidelines for parameter tuning and user training, streamlining the onboarding process for prosthetists and end-users. This would facilitate widespread clinical adoption and reduce barriers to implementation.
4. **Integration with emerging technologies**: Explore synergies with neural interfaces, wearable sensors, or predictive AI models to enable intuitive, anticipatory control. Such advancements could further reduce cognitive load and improve user-prosthesis symbiosis.

The Power Hip represents a transformative step toward restoring functional independence for HD amputees, but its full potential hinges on iterative refinement and scalability. By addressing these short- and long-term objectives, future research can bridge the gap between laboratory innovation and real-world impact, ultimately redefining mobility solutions for individuals with high-level amputations.

References

[1] J. E. Edelstein, "Amputations," in *A Comprehensive Guide to Geriatric Rehabilitation*, L. K. Timothy, S. Ron, O. B. John, and L. M. Michael Eds., Third Edition ed. Oxford: Churchill Livingstone, 2014, pp. 337-340.

[2] B. Aulivola *et al.*, "Major lower extremity amputation: outcome of a modern series," *Arch Surg,* vol. 139, no. 4, pp. 395-9; discussion 399, Apr 2004, doi: 10.1001/archsurg.139.4.395.

[3] J. Ebnezar, *Textbook of Orthopaedics*, 3rd ed. (Orthopaedics). Tunbridge Wells: Anshan, 2006.

[4] J. Griffet, "Amputation and prosthesis fitting in paediatric patients," *Orthop Traumatol Surg Res,* vol. 102, no. 1 Suppl, pp. S161-75, Feb 2016, doi: 10.1016/j.otsr.2015.03.020.

[5] H. Gholizadeh, N. Baddour, M. Botros, K. Brannen, F. Golshan, and E. D. Lemaire, "Hip disarticulation and hemipelvectomy prostheses: A review of the literature," (in eng), *Prosthet Orthot Int,* vol. 45, no. 5, pp. 434-439, Oct 1 2021, doi: 10.1097/PXR.0000000000000029.

[6] T. Chin, S. Sawamura, R. Shiba, H. Oyabu, Y. Nagakura, and A. Nakagawa, "Energy expenditure during walking in amputees after disarticulation of the hip. A microprocessor-controlled swing-phase control knee versus a mechanical-controlled stance-phase control knee," *J Bone Joint Surg Br,* vol. 87, no. 1, pp. 117-9, Jan 2005, doi: 10.1302/0301-620X.87B1.14617.

[7] R. E. Pecoraro, G. E. Reiber, and E. M. Burgess, "Pathways to diabetic limb amputation. Basis for prevention," *Diabetes Care,* vol. 13, no. 5, pp. 513-21, May 1990, doi: 10.2337/diacare.13.5.513.

[8] J. W. Micheal, "Lower limb prosthetic components: Updated classification and passive, body-powered components," in *Atlas of Amputations and Limb Deficiencies: Volume 2 Lower Limb Management Issues*, 4 ed: American Academy of Orthopadic Surgeons, 2016, pp. 429-443.

[9] E. Gailledrat *et al.*, "Does the new Helix 3D hip joint improve walking of hip disarticulated amputees?," *Annals of Physical and Rehabilitation Medicine,* vol. 56, no. 5, pp. 411-418, 2013/07/01/ 2013, doi: https://doi.org/10.1016/j.rehab.2013.05.001.

[10] E. Ludwigs, M. Bellmann, T. Schmalz, and S. Blumentritt, "Biomechanical differences between two exoprosthetic hip joint systems during level walking," *Prosthet Orthot Int,* vol. 34, no. 4, pp. 449-60, Dec 2010, doi: 10.3109/03093646.2010.499551.

[11] M. T. Houdek *et al.*, "Functional outcome measures of patients following hemipelvectomy," *Prosthet Orthot Int,* vol. 40, no. 5, pp. 566-72, Oct 2016, doi: 10.1177/0309364615574164.

[12] P. Yari, P. U. Dijkstra, and J. H. Geertzen, "Functional outcome of hip disarticulation and hemipelvectomy: a cross-sectional national descriptive study in the Netherlands," *Clin Rehabil,* vol. 22, no. 12, pp. 1127-33, Dec 2008, doi: 10.1177/0269215508095088.

[13] M. E. Kralovec, M. T. Houdek, K. L. Andrews, T. C. Shives, P. S. Rose, and F. H. Sim, "Prosthetic rehabilitation after hip disarticulation or hemipelvectomy," *Am J Phys Med Rehabil,* vol. 94, no. 12, pp. 1035-40, Dec 2015, doi: 10.1097/PHM.0000000000000292.

[14] T. Chin, H. Oyabu, Y. Maeda, I. Takase, and K. Machida, "Energy consumption during prosthetic walking and wheelchair locomotion by elderly hip disarticulation amputees," *Am J Phys Med Rehabil,* vol. 88, no. 5, pp. 399-403, May 2009, doi: 10.1097/PHM.0b013e3181a0dbe2.

[15] K. Lechler, B. Frossard, L. Whelan, D. Langlois, R. Muller, and K. Kristjansson, "Motorized biomechatronic upper and lower limb prostheses-clinically relevant outcomes," *PM R,* vol. 10, no. 9 Suppl 2, pp. S207-S219, Sep 2018, doi: 10.1016/j.pmrj.2018.06.015.

[16] Y. Ueyama, T. Kubo, and M. Shibata, "Robotic hip-disarticulation prosthesis: evaluation of prosthetic gaits in a non-amputee individual," *Advanced Robotics,* vol. 34, no. 1, pp. 37-44, 2019, doi: 10.1080/01691864.2019.1705908.

[17] M. P. Aragon, G. A. V. Orozco, and A. A. Altamirano, "Bionic hip prosthesis based on polycentric mechanisms," *Pan American Health Care Exchanges, PAHCE,* 2013, doi: 10.1109/PAHCE.2013.6568260.

[18] A. Brandt, Y. Wen, M. Liu, J. Stallings, and H. H. Huang, "Interactions between transfemoral amputees and a powered knee prosthesis during load carriage," *Sci Rep,* vol. 7, no. 1, p. 14480, Nov 3 2017, doi: 10.1038/s41598-017-14834-7.

[19] C. Shirota, A. M. Simon, and T. A. Kuiken, "Recovery strategy identification throughout swing phase using kinematic data from the tripped leg," 2014. [Online]. Available: https://dx.doi.org/10.1109/embc.2014.6945045.

[20] E. J. Wolf, V. Q. Everding, A. L. Linberg, B. L. Schnall, J. M. Czerniecki, and J. M. Gambel, "Assessment of transfemoral amputees using C-Leg and Power Knee for ascending and descending inclines and steps," *The Journal of Rehabilitation Research and Development,* vol. 49, no. 6, p. 831, 2012, doi: 10.1682/jrrd.2010.12.0234.

[21] B. E. Lawson, A. Huff, and M. Goldfarb, "A preliminary investigation of powered prostheses for improved walking biomechanics in bilateral transfemoral amputees," 2012. [Online]. Available: https://dx.doi.org/10.1109/embc.2012.6346884.

[22] I. Hernandez and W. Yu, "Recent advances on control of active lower limb prostheses," *IETE Technical Review,* vol. 39, no. 6, pp. 1225-1244, 2021, doi: 10.1080/02564602.2021.1994477.

[23] M. R. Tucker *et al.*, "Control strategies for active lower extremity prosthetics and orthotics: a review," *J Neuroeng Rehabil,* vol. 12, no. 1, p. 1, Jan 5 2015, doi: 10.1186/1743-0003-12-1.

[24] R. D. Gregg, T. Lenzi, L. J. Hargrove, and J. W. Sensinger, "Virtual constraint control of a powered prosthetic leg: from simulation to experiments with transfemoral amputees," *IEEE Trans Robot,* vol. 30, no. 6, pp. 1455-1471, Dec 2014, doi: 10.1109/TRO.2014.2361937.

[25] D. L. Grimes, W. C. Flowers, and M. Donath, "Feasibility of an active control scheme for above knee prostheses," *Journal of Biomechanical Engineering,* vol. 99, no. 4, pp. 215-221, 1977, doi: 10.1115/1.3426293.

[26] H. Huang, F. Zhang, L. J. Hargrove, Z. Dou, D. R. Rogers, and K. B. Englehart, "Continuous locomotion-mode identification for prosthetic legs based on neuromuscular-mechanical fusion," *IEEE Trans Biomed Eng,* vol. 58, no. 10, pp. 2867-75, Oct 2011, doi: 10.1109/TBME.2011.2161671.

[27] A. Nasr, A. Hashemi, and J. McPhee, "Model-based mid-level regulation for assist-as-needed hierarchical control of wearable robots: A computational study of human-robot adaptation," *Robotics (Basel),* vol. 11, no. 1, p. 20, Feb 2022, doi: 10.3390/robotics11010020.

[28] H. Warner, P. Khalaf, H. Richter, D. Simon, E. Hardin, and A. J. van den Bogert, "Early evaluation of a powered transfemoral prosthesis with force-modulated impedance control and energy regeneration," *Med Eng Phys,* vol. 100, p. 103744, Feb 2022, doi: 10.1016/j.medengphy.2021.103744.

[29] H. Vallery, R. Burgkart, C. Hartmann, J. Mitternacht, R. Riener, and M. Buss, "Complementary limb motion estimation for the control of active knee prostheses," *Biomed Tech (Berl),* vol. 56, no. 1, pp. 45-51, Feb 2011, doi: 10.1515/BMT.2010.057.

[30] S. Luo, Y. Chen, M. Fan, and H. Yu, "Design and control system of a new hip-knee integrated intelligent prostheses," *i-CREATe,* pp. 20-24, 2023, doi: 10.1145/3628228.3628487.

[31] Y. Bader, D. Langlois, N. Baddour, and E. D. Lemaire, "Development of an Integrated Powered Hip and Microprocessor-Controlled Knee for a Hip-Knee-Ankle-Foot Prosthesis," *Bioengineering (Basel),* vol. 10, no. 5, p. 614, May 19 2023, doi: 10.3390/bioengineering10050614.

[32] K. Brannen, "Design and evaluation of a microprocessor-controlled powered hip prosthesis," Biomedical engineering, Mechanical engineering, Université d'Ottawa / University of Ottawa, 2023.

[33] G. Stark, "Overview of Hip Disarticulation Prostheses," *JPO Journal of Prosthetics and Orthotics,* vol. 13, no. 2, pp. 50-53, 2001, doi: 10.1097/00008526-200106000-00014.

[34] A. C. McLaurin, "The evolution of the Canadian-type hip-disarticulation prosthesis," *Artif Limbs,* vol. 4, no. 2, pp. 22-8, 1957. [Online]. Available: https://www.ncbi.nlm.nih.gov/pubmed/13510139.

[35] A. Fernandez and J. Formigo, "Are Canadian prostheses used? A long-term experience," *Prosthet Orthot Int,* vol. 29, no. 2, pp. 177-81, Aug 2005, doi: 10.1080/03093640500217208.

[36] W. Liang *et al.*, "Mechanisms and component design of prosthetic knees: A review from a biomechanical function perspective," (in English), *Front Bioeng Biotechnol,* Review vol. 10, p. 950110, 2022-September-15 2022, doi: 10.3389/fbioe.2022.950110.

[37] S. Blumentritt, E. Ludwigs, M. Bellmann, and H. Boiten. (2008, 2008) The new Helix 3D hip joint. *Orthopädie Technik*. 1-4.

[38] J. Perry and J. M. Burnfield, *Gait analysis: normal and pathological function*. SLACK, 1992, p. 551.

[39] Los Amigos National Rehabilitation Center, *Observational gait analysis*, 4 ed. Los Amigos Research and Education Institute, 2001, p. 72.

[40] T. Stockel, R. Jacksteit, M. Behrens, R. Skripitz, R. Bader, and A. Mau-Moeller, "The mental representation of the human gait in young and older adults," (in eng), *Front Psychol,* vol. 6, p. 943, 2015, doi: 10.3389/fpsyg.2015.00943.

[41] B. Kaymak and A. R. Soylu, "Fundamentals of quantitative gait analysis," in *Musculoskeletal Research and Basic Science*, F. Korkusuz Ed. Springer: Springer International Publishing, 2016, ch. 6, pp. 93-106.

[42] C. D. Metcalf *et al.*, "Markerless motion capture and measurement of hand kinematics: validation and application to home-based upper limb rehabilitation," *IEEE Trans Biomed Eng,* vol. 60, no. 8, pp. 2184-92, Aug 2013, doi: 10.1109/TBME.2013.2250286.

[43] L. Wade, L. Needham, P. McGuigan, and J. Bilzon, "Applications and limitations of current markerless motion capture methods for clinical gait biomechanics," *PeerJ,* vol. 10, p. e12995, 2022, doi: 10.7717/peerj.12995.

[44] T. A. L. Wren, P. Isakov, and S. A. Rethlefsen, "Comparison of kinematics between Theia markerless and conventional marker-based gait analysis in clinical patients," *Gait Posture,* vol. 104, pp. 9-14, Jul 2023, doi: 10.1016/j.gaitpost.2023.05.029.

[45] P. Torvinen, K. S. Ruotsalainen, S. Zhao, N. Cronin, O. Ohtonen, and V. Linnamo, "Evaluation of 3D markerless motion capture system accuracy during skate skiing on a treadmill," *Bioengineering,* vol. 11, no. 2, p. 136, 2024, doi: 10.3390/bioengineering11020136.

[46] N. A. Edwards, J. B. Caccese, R. E. Tracy, J. Hagen, C. C. Quatman-Yates, and A. J. On, "The validity and usability of markerless motion capture and inertial measurement units for quantifying dynamic movements," *Med Sci Sports Exerc,* vol. 57, no. 3, pp. 641-655, Mar 1 2025, doi: 10.1249/MSS.0000000000003579.

[47] W. W. T. Lam, Y. M. Tang, and K. N. K. Fong, "A systematic review of the applications of markerless motion capture (MMC) technology for clinical measurement in rehabilitation," *J Neuroeng Rehabil,* vol. 20, no. 1, p. 57, May 2 2023, doi: 10.1186/s12984-023-01186-9.

[48] F. Gafoor, M. Ruder, V. E. Di Bacco, D. Kobsar, M. Malek, and K. Madden, "Concurrent analysis of knee kinematics between Theia 3d markerless and Opencap, an Open-Source markerless motion capture system," *Osteoarthritis and Cartilage,* vol. 32, pp. S240-S241, 2024, doi: 10.1016/j.joca.2024.02.350.

[49] N. Goldfarb, A. Lewis, A. Tacescu, and G. S. Fischer, "Open source Vicon toolkit for motion capture and gait analysis," *Comput Methods Programs Biomed,* vol. 212, p. 106414, Nov 2021, doi: 10.1016/j.cmpb.2021.106414.

[50] HAS-Motion Software, "Segment overview [HAS-Motion Software Documentation]." [Online]. Available: https://wiki.has-motion.com/doku.php?id=visual3d:documentation:modeling:segments:segment_overview

[51] D. G. E. Robertson, G. E. Caldwell, J. Hamill, G. Kamen, and S. N. Whittlesey, *Research methods in biomechanics*. Human Kinetics, 2014.

[52] J. Richards, A. Chohan, and R. Erande, "Biomechanics," in *Tidy's Physiotherapy*: Elsevier, 2013, pp. 331-368.

[53] S. M. Jaegers, J. H. Arendzen, and H. J. de Jongh, "Prosthetic gait of unilateral transfemoral amputees: a kinematic study," *Arch Phys Med Rehabil,* vol. 76, no. 8, pp. 736-43, Aug 1995, doi: 10.1016/s0003-9993(95)80528-1.

[54] C. Kendell, E. D. Lemaire, J. Kofman, and N. Dudek, "Gait adaptations of transfemoral prosthesis users across multiple walking tasks," (in eng), *Prosthet Orthot Int,* vol. 40, no. 1, pp. 89-95, Feb 2016, doi: 10.1177/0309364614568410.

[55] A. Bonnefoy-Mazure and S. Armand, *Normal gait* (Orthopedic Management of Children with Cerebral Palsy). Nova Science Publishers Inc, 2015, p. 567.

[56] D. S. Catelli, E. Kowalski, P. E. Beaule, and M. Lamontagne, "Increased pelvic mobility and altered hip muscles contraction patterns: two-year follow-up cam-FAIS corrective surgery," *J Hip Preserv Surg,* vol. 6, no. 2, pp. 140-148, Jul 2019, doi: 10.1093/jhps/hnz019.

[57] A. D. Segal *et al.*, "Kinematic and kinetic comparisons of transfemoral amputee gait using C-Leg and Mauch SNS prosthetic knees," *J Rehabil Res Dev,* vol. 43, no. 7, pp. 857-70, Nov-Dec 2006, doi: 10.1682/jrrd.2005.09.0147.

[58] R. D. McAnelly, M. Refaeian, D. G. O'Connell, G. D. Powell, and N. E. Walsh, "Successful prosthetic fitting of a 73-year-old hip disarticulation amputee patient with cardiopulmonary disease," *Arch Phys Med Rehabil,* vol. 79, no. 5, pp. 585-8, May 1998, doi: 10.1016/s0003-9993(98)90078-8.

[59] L. M. Nelson and N. T. Carbone, "Functional outcome measurements of a veteran with a hip disarticulation using a Helix 3D hip joint: A case report," *JPO Journal of Prosthetics and Orthotics,* vol. 23, no. 1, pp. 21-26, 2011, doi: 10.1097/JPO.0b013e318209777c.

[60] M. Nietert, N. Englisch, P. Kreil, and G. Alba-Lopez, "Loads in hip disarticulation prostheses during normal daily use," *Prosthet Orthot Int,* vol. 22, no. 3, pp. 199-215, Dec 1998, doi: 10.3109/03093649809164485.

[61] R. Y. Lee and A. Turner-Smith, "The influence of the length of lower-limb prosthesis on spinal kinematics," *Arch Phys Med Rehabil,* vol. 84, no. 9, pp. 1357-62, Sep 2003, doi: 10.1016/s0003-9993(03)00259-4.

[62] S. B. Michaud, S. A. Gard, and D. S. Childress, "A preliminary investigation of pelvic obliquity patterns during gait in persons with transtibial and transfemoral amputation," *J Rehabil Res Dev,* vol. 37, no. 1, pp. 1-10, Jan-Feb 2000. [Online]. Available: https://www.ncbi.nlm.nih.gov/pubmed/10847567.

[63] C. W. Radcliffe, "The biomechanics of the Canadian-type hip-disarticulation prosthesis," *Artif Limbs,* vol. 4, no. 2, pp. 29-38, 1957. [Online]. Available: https://www.ncbi.nlm.nih.gov/pubmed/13510140.

[64] H. Goujon-Pillet, E. Sapin, P. Fode, and F. Lavaste, "Three-dimensional motions of trunk and pelvis during transfemoral amputee gait," *Arch Phys Med Rehabil,* vol. 89, no. 1, pp. 87-94, Jan 2008, doi: 10.1016/j.apmr.2007.08.136.

[65] S. Cabral, "Gait symmetry measures and their relevance to gait retraining," in *Handbook of Human Motion*: Springer International Publishing, 2018, ch. Chapter 201, pp. 429-447.

[66] B. S. Baum, B. L. Schnall, J. E. Tis, and J. S. Lipton, "Correlation of residual limb length and gait parameters in amputees," *Injury,* vol. 39, no. 7, pp. 728-33, Jul 2008, doi: 10.1016/j.injury.2007.11.021.

[67] D. S. Pieringer, M. Grimmer, M. F. Russold, and R. Riener, "Review of the actuators of active knee prostheses and their target design outputs for activities of daily living," 2017: IEEE, doi: 10.1109/icorr.2017.8009420. [Online]. Available: https://dx.doi.org/10.1109/icorr.2017.8009420

[68] B. L. Schnall, B. S. Baum, and A. M. Andrews, "Gait characteristics of a soldier with a traumatic hip disarticulation," *Phys Ther,* vol. 88, no. 12, pp. 1568-77, Dec 2008, doi: 10.2522/ptj.20070337.

[69] J. M. Hausdorff, "Gait variability: methods, modeling and meaning," *J Neuroeng Rehabil,* vol. 2, no. 1, p. 19, Jul 20 2005, doi: 10.1186/1743-0003-2-19.

[70] O. Blin, A. M. Ferrandez, and G. Serratrice, "Quantitative analysis of gait in Parkinson patients: increased variability of stride length," *J Neurol Sci,* vol. 98, no. 1, pp. 91-7, Aug 1990, doi: 10.1016/0022-510x(90)90184-o.

[71] E. B. Lohman, 3rd, K. S. Balan Sackiriyas, and R. W. Swen, "A comparison of the spatiotemporal parameters, kinematics, and biomechanics between shod, unshod, and minimally supported running as compared to walking," *Phys Ther Sport,* vol. 12, no. 4, pp. 151-63, Nov 2011, doi: 10.1016/j.ptsp.2011.09.004.

[72] J. Brisswalter and D. Mottet, "Energy cost and stride duration variability at preferred transition gait speed between walking and running," *Can J Appl Physiol,* vol. 21, no. 6, pp. 471-80, Dec 1996, doi: 10.1139/h96-041.

[73] N. Sekiya, H. Nagasaki, H. Ito, and T. Furuna, "Optimal walking in terms of variability in step length," *J Orthop Sports Phys Ther,* vol. 26, no. 5, pp. 266-72, Nov 1997, doi: 10.2519/jospt.1997.26.5.266.

[74] F. Danion, E. Varraine, M. Bonnard, and J. Pailhous, "Stride variability in human gait: the effect of stride frequency and stride length," *Gait Posture,* vol. 18, no. 1, pp. 69-77, Aug 2003, doi: 10.1016/s0966-6362(03)00030-4.

[75] S. Fakoorian, A. Roshanineshat, P. Khalaf, V. Azimi, D. Simon, and E. Hardin, "An extensive set of kinematic and kinetic data for individuals with intact limbs and transfemoral prosthesis users," *Appl Bionics Biomech,* vol. 2020, p. 8864854, 2020, doi: 10.1155/2020/8864854.

[76] J. A. Sturk *et al.*, "Maintaining stable transfemoral amputee gait on level, sloped and simulated uneven conditions in a virtual environment," *Disabil Rehabil Assist Technol,* vol. 14, no. 3, pp. 226-235, Apr 2019, doi: 10.1080/17483107.2017.1420250.

[77] I. Shojaei, B. D. Hendershot, J. C. Acasio, C. L. Dearth, M. Ballard, and B. Bazrgari, "Trunk muscle forces and spinal loads in persons with unilateral transfemoral amputation during sit-to-stand and stand-to-sit activities," *Clin Biomech (Bristol),* vol. 63, pp. 95-103, Mar 2019, doi: 10.1016/j.clinbiomech.2019.02.021.

[78] S. B. Akram and W. E. McIlroy, "Challenging horizontal movement of the body during sit-to-stand: impact on stability in the young and elderly," *J Mot Behav,* vol. 43, no. 2, pp. 147-53, 2011, doi: 10.1080/00222895.2011.552077.

[79] L. Miramand, G. Moisan, V. Richard, B. J. McFadyen, and K. Turcot, "Whole body movement strategies during sit-to-stand and stair ascent in individuals with a lower limb amputation: A systematic review," (in eng), *Clin Biomech (Bristol),* vol. 100, p. 105811, Dec 2022, doi: 10.1016/j.clinbiomech.2022.105811.

[80] S. Ozyurek, I. Demirbuken, and S. Angin, "Altered movement strategies in sit-to-stand task in persons with transtibial amputation," (in eng), *Prosthet Orthot Int,* vol. 38, no. 4, pp. 303-9, Aug 2014, doi: 10.1177/0309364613497742.

[81] L. A. Nolasco, D. C. Morgenroth, A. K. Silverman, and D. H. Gates, "Effects of anterior-posterior shifts in prosthetic alignment on the sit-to-stand movement in people with a unilateral transtibial amputation," *J Biomech,* vol. 109, p. 109926, Aug 26 2020, doi: 10.1016/j.jbiomech.2020.109926.

[82] Y. C. Pai and M. W. Rogers, "Control of body mass transfer as a function of speed of ascent in sit-to-stand," (in eng), *Med Sci Sports Exerc,* vol. 22, no. 3, pp. 378-84, Jun 1990. [Online]. Available: https://www.ncbi.nlm.nih.gov/pubmed/2381306.

[83] G. Roy, S. Nadeau, D. Gravel, F. Piotte, F. Malouin, and B. J. McFadyen, "Side difference in the hip and knee joint moments during sit-to-stand and stand-to-sit tasks in individuals with hemiparesis," *Clin Biomech (Bristol),* vol. 22, no. 7, pp. 795-804, Aug 2007, doi: 10.1016/j.clinbiomech.2007.03.007.

[84] C. Pinheiro *et al.*, "Kinematic and kinetic study of sit-to-stand and stand-to-sit movements towards a human-like skeletal model," in *2019 IEEE 6th Portuguese Meeting on Bioengineering (ENBENG)*, 22-23 Feb. 2019 2019, pp. 1-4, doi: 10.1109/ENBENG.2019.8692569.

[85] C. D. C. d. M. Faria, V. A. Saliba, and L. F. Teixeira-Salmela, "Musculoskeletal biomechanics in sit-to-stand and stand-to-sit activities with stroke subjects: a systematic review," *Fisioterapia em Movimento,* vol. 23, no. 1, pp. 35-52, 2010, doi: 10.1590/s0103-51502010000100004.

[86] S. Sadeh, D. Gobert, K. H. Shen, F. Foroughi, and H. Y. Hsiao, "Biomechanical and neuromuscular control characteristics of sit-to-stand transfer in young and older adults: A systematic review with implications for balance regulation mechanisms," *Clin Biomech (Bristol),* vol. 109, p. 106068, Oct 2023, doi: 10.1016/j.clinbiomech.2023.106068.

[87] M. Blazkiewicz, I. Wiszomirska, and A. Wit, "A new method of determination of phases and symmetry in stand-to-sit-to-stand movement," *Int J Occup Med Environ Health,* vol. 27, no. 4, pp. 660-71, Aug 2014, doi: 10.2478/s13382-014-0280-x.

[88] B. D. Hendershot and E. J. Wolf, "Persons with unilateral transfemoral amputation have altered lumbosacral kinetics during sitting and standing movements," *Gait Posture,* vol. 42, no. 2, pp. 204-9, Jul 2015, doi: 10.1016/j.gaitpost.2015.05.011.

[89] A. M. Simon, N. P. Fey, K. A. Ingraham, S. B. Finucane, E. G. Halsne, and L. J. Hargrove, "Improved weight-bearing symmetry for transfemoral amputees during standing up and sitting Down with a powered knee-ankle prosthesis," *Arch Phys Med Rehabil,* vol. 97, no. 7, pp. 1100-6, Jul 2016, doi: 10.1016/j.apmr.2015.11.006.

[90] K. M. Kerr, J. A. White, D. A. Barr, and R. A. B. Mollan, "Standardization and definitions of the sit-stand-sit movement cycle," *Gait & Posture,* vol. 2, no. 3, pp. 182-190, 1994/09/01/ 1994, doi: 10.1016/0966-6362(94)90006-x.

[91] C. G. Welker, T. K. Best, and R. D. Gregg, "Data-driven variable impedance control of a powered knee-ankle prosthesis for sit, stand, and walk with minimal tuning," (in eng), *Rep U S,* vol. 2022, pp. 9660-9667, Oct 2022, doi: 10.1109/iros47612.2022.9982037.

[92] R. Schultz *et al.*, "Assisting sit-to-stand through event-based electrical stimulation of trunk control: A preliminary study," in *46th Annual International Conference of the IEEE Engineering in Medicine and Biology Society (EMBC)*, 15-19 July 2024 2024, pp. 1-5, doi: 10.1109/EMBC53108.2024.10781806.

[93] H. A. Varol, F. Sup, and M. Goldfarb, "Multiclass real-time intent recognition of a powered lower limb prosthesis," *IEEE Trans Biomed Eng,* vol. 57, no. 3, pp. 542-51, Mar 2010, doi: 10.1109/TBME.2009.2034734.

[94] M. Tschiedel, M. F. Russold, and E. Kaniusas, "Relying on more sense for enhancing lower limb prostheses control: a review," *J Neuroeng Rehabil,* vol. 17, no. 1, p. 99, Jul 17 2020, doi: 10.1186/s12984-020-00726-x.

[95] A. M. Simon, N. P. Fey, K. A. Ingraham, A. J. Young, and L. J. Hargrove, "Powered prosthesis control during walking, sitting, standing, and non-weight bearing activities using neural and mechanical inputs," presented at the 2013 6th International IEEE/EMBS Conference on Neural Engineering (NER), 2013, 2013. [Online]. Available: https://dx.doi.org/10.1109/ner.2013.6696148.

[96] R. K. Mohanty, R. C. Mohanty, and S. K. Sabut, "Application of control strategies and machine learning techniques in prosthetic knee: a systematic review," *Advances in Computational Intelligence,* vol. 2, no. 1, 2022, doi: 10.1007/s43674-021-00031-7.

[97] L. Li, X. Wang, Q. Meng, C. Chen, J. Sun, and H. Yu, "Intelligent knee prostheses: A systematic review of control strategies," *Journal of Bionic Engineering,* vol. 19, no. 5, pp. 1242-1260, 2022, doi: 10.1007/s42235-022-00169-1.

[98] R. R. Torrealba and E. D. Fonseca-Rojas, "Toward the development of knee prostheses: Review of current active devices," *Applied Mechanics Reviews,* vol. 71, no. 3, 2019, doi: 10.1115/1.4043323.

[99] Y. Dabiri, S. Najarian, M. R. Eslami, S. Zahedi, and D. Moser, "A powered prosthetic knee joint inspired from musculoskeletal system," *Biocybernetics and Biomedical Engineering,* vol. 33, no. 2, pp. 118-124, 2013/01/01/ 2013, doi: 10.1016/j.bbe.2013.03.004.

[100] R. D. Gregg, T. Lenzi, N. P. Fey, L. J. Hargrove, and J. W. Sensinger, "Experimental effective shape control of a powered transfemoral prosthesis," presented at the IEEE International Conference on Rehabilitation Robotics, 2013. [Online]. Available: https://ieeexplore.ieee.org/document/6650413/.

[101] H. T. T. Vu, F. Gomez, P. Cherelle, D. Lefeber, A. Nowe, and B. Vanderborght, "ED-FNN: A new deep learning algorithm to detect percentage of the gait cycle for powered prostheses," *Sensors (Basel),* vol. 18, no. 7, p. 2389, Jul 23 2018, doi: 10.3390/s18072389.

[102] S. Mo and D. H. K. Chow, "Accuracy of three methods in gait event detection during overground running," *Gait Posture,* vol. 59, pp. 93-98, Jan 2018, doi: 10.1016/j.gaitpost.2017.10.009.

[103] M. Eslamy, F. Oswald, and A. F. Schilling, "Estimation of knee angles based on thigh motion: A functional approach and Iimplications for high-level controlling of active prosthetic knees," presented at the IEEE Control Systems, 2020.

[104] B. E. Lawson, H. A. Varol, and M. Goldfarb, "Standing stability enhancement with an intelligent powered transfemoral prosthesis," *IEEE Trans Biomed Eng,* vol. 58, no. 9, pp. 2617-24, Sep 2011, doi: 10.1109/TBME.2011.2160173.

[105] A. Mathew and P. Rajalakshmy, "Surface electromyogram based techniques for upper and lower extremity rehabilitation therapy - A comprehensive review," presented at the 2021 3rd International Conference on Signal Processing and Communication (ICPSC), 2021, 2021. [Online]. Available: https://dx.doi.org/10.1109/icspc51351.2021.9451814.

[106] F.-Y. Leu, C.-Y. Ko, Y.-C. Lin, H. Susanto, and H.-C. Yu, "Fall detection and motion classification by using decision tree on mobile phone," in *Smart Sensors Networks*, X. Fatos, L. Fang-Yie, and H. Li-Ling Eds., no. Intelligent Data-Centric Systems): Academic Press, 2017, pp. 205-237.

[107] J. D. Farah, N. Baddour, and E. D. Lemaire, "Design, development, and evaluation of a local sensor-based gait phase recognition system using a logistic model decision tree for orthosis-control," *J Neuroeng Rehabil,* vol. 16, no. 1, p. 22, Feb 1 2019, doi: 10.1186/s12984-019-0486-z.

[108] A. V. Clausen, "Control systems and methods for prosthetic or orthotic devices," Iceland Patent US9017418B2 Patent Appl. 12/773,788, 2015.

[109] M. T. Redfield, J. C. Cagle, B. J. Hafner, and J. E. Sanders, "Classifying prosthetic use via accelerometry in persons with transtibial amputations," (in English), *J Rehabil Res Dev,* Report vol. 50, no. 9, pp. 1201-12, 2013/09 2013, doi: 10.1682/JRRD.2012.12.0233.

[110] H. Herr and A. Wilkenfeld, "User-adaptive control of a magnetorheological prosthetic knee," *Industrial Robot: An International Journal,* vol. 30, no. 1, pp. 42-55, 2003, doi: 10.1108/01439910310457706.

[111] M. Tran, L. Gabert, M. Cempini, and T. Lenzi, "A lightweight, efficient fully powered knee prosthesis with actively variable transmission," *IEEE Robotics and Automation Letters,* vol. 4, no. 2, pp. 1186-1193, 2019, doi: 10.1109/lra.2019.2892204.

[112] J. Mickelborough, M. L. van der Linden, R. C. Tallis, and A. R. Ennos, "Muscle activity during gait initiation in normal elderly people," *Gait Posture,* vol. 19, no. 1, pp. 50-7, Feb 2004, doi: 10.1016/s0966-6362(03)00016-x.

[113] M. Bishop, D. Brunt, N. Pathare, and B. Patel, "The effect of velocity on the strategies used during gait termination," *Gait Posture,* vol. 20, no. 2, pp. 134-9, Oct 2004, doi: 10.1016/j.gaitpost.2003.07.004.

[114] V. Cimolin, N. Cau, M. Galli, C. Santovito, G. Grugni, and P. Capodaglio, "Gait initiation and termination strategies in patients with Prader-Willi syndrome," *J Neuroeng Rehabil,* vol. 14, no. 1, p. 44, May 23 2017, doi: 10.1186/s12984-017-0257-7.

[115] S. C. Miff, D. S. Childress, S. A. Gard, M. R. Meier, and A. H. Hansen, "Temporal symmetries during gait initiation and termination in nondisabled ambulators and in people with unilateral transtibial limb loss," (in eng), *J Rehabil Res Dev,* vol. 42, no. 2, pp. 175-82, Mar-Apr 2005, doi: 10.1682/jrrd.2004.03.0038.

[116] D. Novak *et al.*, "Automated detection of gait initiation and termination using wearable sensors," *Med Eng Phys,* vol. 35, no. 12, pp. 1713-20, Dec 2013, doi: 10.1016/j.medengphy.2013.07.003.

[117] F. Zhang, M. Liu, and H. Huang, "Effects of locomotion mode recognition errors on volitional control of powered above-knee prostheses," *IEEE Trans Neural Syst Rehabil Eng,* vol. 23, no. 1, pp. 64-72, Jan 2015, doi: 10.1109/TNSRE.2014.2327230.

[118] B. Su and E. M. Gutierrez-Farewik, "Gait trajectory and gait phase prediction based on an LSTM network," *Sensors (Basel),* vol. 20, no. 24, p. 7127, Dec 12 2020, doi: 10.3390/s20247127.

[119] F. Sup, A. Bohara, and M. Goldfarb, "Design and control of a powered transfemoral prosthesis," *Int J Rob Res,* vol. 27, no. 2, pp. 263-273, Feb 1 2008, doi: 10.1177/0278364907084588.

[120] H. Vallery, E. H. van Asseldonk, M. Buss, and H. van der Kooij, "Reference trajectory generation for rehabilitation robots: complementary limb motion estimation," *IEEE Trans Neural Syst Rehabil Eng,* vol. 17, no. 1, pp. 23-30, Feb 2009, doi: 10.1109/TNSRE.2008.2008278.

[121] C. Ferreira, L. P. Reis, and C. P. Santos, "Review of control strategies for lower limb prostheses," in *Robot 2015: Second Iberian Robotics Conference*, (Advances in Intelligent Systems and Computing: Springer International Publishing, 2016, ch. Chapter 17, pp. 209-220.

[122] Y. Sun *et al.*, "Review of recent progress in robotic knee prosthesis related techniques: Structure, actuation and control," *Journal of Bionic Engineering,* vol. 18, no. 4, pp. 764-785, 2021, doi: 10.1007/s42235-021-0065-4.

[123] N. Hogan, "Impedance control: An approach to manipulation," presented at the 1984 American Control Conference, 1984, 1984. [Online]. Available: https://dx.doi.org/10.23919/acc.1984.4788393.

[124] F. Zhang, M. Liu, and H. Huang, "Investigation of timing to switch control mode in powered knee prostheses during task transitions," *PLoS One,* vol. 10, no. 7, p. e0133965, 2015, doi: 10.1371/journal.pone.0133965.

[125] R. Unal *et al.*, "Modeling of WalkMECH: a fully-passive energy-efficient transfemoral prosthesis prototype," *IEEE Int Conf Rehabil Robot,* vol. 2013, p. 6650406, Jun 2013, doi: 10.1109/ICORR.2013.6650406.

[126] L. Ambrozic *et al.*, "CYBERLEGs: A user-oriented robotic transfemoral prosthesis with whole-body awareness control," *IEEE Robotics & Automation Magazine,* vol. 21, no. 4, pp. 82-93, 2014, doi: 10.1109/mra.2014.2360278.

[127] M. A. Shandiz, F. Farahmand, N. A. A. Osman, and H. Zohoor, "A robotic model of transfemoral amputee locomotion for design optimization of knee controllers," *International Journal of Advanced Robotic Systems,* vol. 10, no. 3, 2013, doi: 10.5772/52855.

[128] G. G. Fiorezi, P. H. F. Ulhoa, A. B. Filho, and R. M. De Andrade, "Digital prototyping of a microprocessor controlled active knee prosthesis," presented at the 2021 Ieee Urucon, 2021, 2021. [Online]. Available: https://dx.doi.org/10.1109/urucon53396.2021.9647069.

[129] E. C. Martinez-Villalpando and H. Herr, "Agonist-antagonist active knee prosthesis: a preliminary study in level-ground walking," *J Rehabil Res Dev,* vol. 46, no. 3, pp. 361-73, 2009, doi: 10.1682/JRRD.2008.09.0131.

[130] R. C. Dorf and R. H. Bishop, *Modern control systems*. Pearson Prentice Hall, 2008.

[131] M. Wojtyra, "Dynamical analysis of human walking," in *15th European ADAMS Conference*, 2000, p. 15.

[132] L. Xinwei, X. Yixuan, H. Chen, H. Bingshan, and Y. Hongliu, "A gait simulation and evaluation system for hip disarticulation prostheses," *IEEE Transactions on Automation Science and Engineering,* vol. 18, no. 2, pp. 448-457, 2021, doi: 10.1109/tase.2020.3035438.

[133] M. R. Williams, S. D'Andrea, and H. M. Herr, "Impact on gait biomechanics of using an active variable impedance prosthetic knee," *J Neuroeng Rehabil,* vol. 13, no. 1, p. 54, Jun 10 2016, doi: 10.1186/s12984-016-0159-0.

[134] A. E. Chisholm, S. Makepeace, E. L. Inness, S. D. Perry, W. E. McIlroy, and A. Mansfield, "Spatial-temporal gait variability poststroke: variations in measurement and implications for measuring change," *Arch Phys Med Rehabil,* vol. 95, no. 7, pp. 1335-41, Jul 2014, doi: 10.1016/j.apmr.2014.02.014.

[135] M. S. Zahedi, W. D. Spence, S. E. Solomonidis, and J. P. Paul, "Repeatability of kinetic and kinematic measurements in gait studies of the lower limb amputee," *Prosthet Orthot Int,* vol. 11, no. 2, pp. 55-64, Aug 1987, doi: 10.3109/03093648709078179.

[136] A. Fanous, M. Botros, H. Gholizadeh, N. Baddour, and E. D. Lemaire, "Design and evaluation of a hip prosthesis simulator: A technical note," (in eng), *Prosthet Orthot Int,* vol. 47, no. 4, pp. 443-446, Aug 1 2023, doi: 10.1097/PXR.0000000000000208.

[137] S. Mroz, N. Baddour, P. Dumond, and E. D. Lemaire, "Design and prototype validation of a laterally mounted powered hip joint prothesis," *J Rehabil Assist Technol Eng,* vol. 11, p. 20556683241248584, Jan-Dec 2024, doi: 10.1177/20556683241248584.

[138] K. Brannen, N. Baddour, L. Cho, D. Langlois, P. Dumond, and E. D. Lemaire, "Development and evaluation of an anteriorly mounted microprocessor-controlled powered hip joint prosthesis," (in eng), *Can Prosthet Orthot J,* vol. 7, no. 2, p. 44494, 2024, doi: 10.33137/cpoj.v7i2.44494.

[139] B. Baker, *Analog and interface guide*: Microchip Technology Inc, 2005. [Online]. Available: https://ww1.microchip.com/downloads/cn/DeviceDoc/cn022032.pdf#page=7.10. Accessed on: 2024.

[140] T. M. Control, "TMC4671 data sheet." [Online]. Available: https://www.analog.com/en/products/tmc4671.html#documentation

[141] R. Lee, P. Pillay, and R. Harley, "D, Q reference frames for the simulation of induction motors," *Electric power systems research,* vol. 8, no. 1, pp. 15-26, 1984.

[142] J. L. Willems, "Generalized clarke components for polyphase networks," *IEEE Transactions on Education,* vol. 12, no. 1, pp. 69-71, 1969, doi: 10.1109/TE.1969.4320448.

[143] R. H. Park, "Two-reaction theory of synchronous machines generalized method of analysis-part I," *Transactions of the American Institute of Electrical Engineers,* vol. 48, no. 3, pp. 716-727, 1929, doi: 10.1109/T-AIEE.1929.5055275.

[144] C. Blambert, "d,q coordinate system superimposed on three-phase system," vol. 431 × 449, ed. Wikimedia Commons: Wikimedia, 2012.

[145] L. Zhou *et al.*, "How we found our IMU: Guidelines to IMU selection and a comparison of seven IMUs for pervasive healthcare applications," *Sensors (Basel),* vol. 20, no. 15, p. 4090, Jul 22 2020, doi: 10.3390/s20154090.

[146] D. M. Henderson, "Shuttle program. Euler angles, quaternions, and transformation matrices working relationships," McDonnell Douglas Tech. Services Co., Inc., NASA-TM-74839, July 1 1977. [Online]. Available: https://ntrs.nasa.gov/citations/19770024290

[147] A. Kontny. "Pelvis 3D model." SketchFab. https://sketchfab.com/3d-models/pelvis-55e3c54dc2e04d23b0cf46da58c71994 (accessed July-11, 2025).

[148] T. Chin, R. Kuroda, T. Akisue, T. Iguchi, and M. Kurosaka, "Energy consumption during prosthetic walking and physical fitness in older hip disarticulation amputees," *J Rehabil Res Dev,* vol. 49, no. 8, pp. 1255-60, 2012, doi: 10.1682/jrrd.2011.04.0067.

[149] D. Boone, "Prosthetists and orthotists: An evolution from mechanic to clinician," *Prosthet Orthot Int,* vol. 44, no. 6, pp. 368-372, Dec 2020, doi: 10.1177/0309364620968643.

[150] B. Engstrom and C. Van de Ven, *Therapy for amputees*, 3rd ed. Edinburgh: Churchill Livingstone, 1999.

[151] H. Devan, A. Carman, P. Hendrick, L. Hale, and D. C. Ribeiro, "Spinal, pelvic, and hip movement asymmetries in people with lower-limb amputation: Systematic review," in *Journal of Rehabilitation Research and Development* vol. 52, ed, 2015, pp. 1-19.

[152] R. S. Gailey *et al.*, "The amputee mobility predictor: an instrument to assess determinants of the lower-limb amputee's ability to ambulate," *Arch Phys Med Rehabil,* vol. 83, no. 5, pp. 613-27, May 2002, doi: 10.1053/apmr.2002.32309.

[153] E. H. Sinitski, E. D. Lemaire, and N. Baddour, "Evaluation of motion platform embedded with dual belt treadmill instrumented with two force plates," *J Rehabil Res Dev,* vol. 52, no. 2, pp. 221-34, 2015, doi: 10.1682/JRRD.2013.11.0244.

[154] S. Hood, M. K. Ishmael, A. Gunnell, K. B. Foreman, and T. Lenzi, "A kinematic and kinetic dataset of 18 above-knee amputees walking at various speeds," *Sci Data,* vol. 7, no. 1, p. 150, May 21 2020, doi: 10.1038/s41597-020-0494-7.

[155] S. Hood and T. Lenzi. *Lower limb kinetic and kinematic data of 18 above knee amputees*, Spring Nature, doi: https://doi.org/10.6084/m9.figshare.c.4962305.v1.

[156] K. O'Sullivan, A. Clifford, and L. Hughes, "The reliability of the CODA motion analysis system for lumbar spine analysis: a pilot study," *Physiotherapy Practice and Research,* vol. 31, no. 1, pp. 16-22, 2010, doi: 10.3233/ppr-2010-31104.

[157] V. J. Eberly, S. J. Mulroy, J. K. Gronley, J. Perry, W. J. Yule, and J. M. Burnfield, "Impact of a stance phase microprocessor-controlled knee prosthesis on level walking in lower functioning individuals with a transfemoral amputation," *Prosthet Orthot Int,* vol. 38, no. 6, pp. 447-55, Dec 2014, doi: 10.1177/0309364613506912.

[158] J. E. Edelstein, "Amputations and prostheses," in *Physical Rehabilitation*, M. H. Cameron and L. G. Monroe Eds. Saint Louis: W.B. Saunders, 2007, pp. 267-299.

[159] S. R. Koehler-McNicholas, R. D. Lipschutz, and S. A. Gard, "The biomechanical response of persons with transfemoral amputation to variations in prosthetic knee alignment during level walking," *J Rehabil Res Dev,* vol. 53, no. 6, pp. 1089-1106, 2016, doi: 10.1682/JRRD.2014.12.0311.

[160] D. W. W. Heitzmann *et al.*, "The influence of hip muscle strength on gait in individuals with a unilateral transfemoral amputation," *PLoS One,* vol. 15, no. 9, p. e0238093, 2020, doi: 10.1371/journal.pone.0238093.

[161] M. Akay, "Wavelets in biomedical engineering," *Ann Biomed Eng,* vol. 23, no. 5, pp. 531-42, Sep-Oct 1995, doi: 10.1007/BF02584453.

[162] G. Chalvatzaki, X. S. Papageorgiou, P. Maragos, and C. S. Tzafestas, "User-adaptive human-robot formation control for an intelligent robotic walker using augmented human state estimation and pathological gait characterization," 2018: IEEE, doi: 10.1109/iros.2018.8594360. [Online]. Available: https://dx.doi.org/10.1109/iros.2018.8594360

[163] A. Ferrari *et al.*, "Quantitative comparison of five current protocols in gait analysis," *Gait Posture,* vol. 28, no. 2, pp. 207-16, Aug 2008, doi: 10.1016/j.gaitpost.2007.11.009.

[164] K. Berner, J. Cockcroft, L. D. Morris, and Q. Louw, "Concurrent validity and within-session reliability of gait kinematics measured using an inertial motion capture system with repeated calibration," *J Bodyw Mov Ther,* vol. 24, no. 4, pp. 251-260, Oct 2020, doi: 10.1016/j.jbmt.2020.06.008.

[165] S. A. Bolink *et al.*, "Validity of an inertial measurement unit to assess pelvic orientation angles during gait, sit-stand transfers and step-up transfers: Comparison with an optoelectronic motion capture system," *Med Eng Phys,* vol. 38, no. 3, pp. 225-31, Mar 2016, doi: 10.1016/j.medengphy.2015.11.009.

[166] M. H. Ebrahimzadeh, A. R. Kachooei, M. R. Soroush, E. G. Hasankhani, S. Razi, and A. Birjandinejad, "Long-term clinical outcomes of war-related hip disarticulation and transpelvic amputation," *J Bone Joint Surg Am,* vol. 95, no. 16, pp. e114(1-6), Aug 21 2013, doi: 10.2106/JBJS.L.01160.

[167] F. Rasheed, S. Martin, and K. M. Tse, "Design, kinematics and gait analysis, of prosthetic knee joints: A systematic review," (in eng), *Bioengineering (Basel),* vol. 10, no. 7, Jun 27 2023, doi: 10.3390/bioengineering10070773.

[168] S. Hood, S. Creveling, L. Gabert, M. Tran, and T. Lenzi, "Powered knee and ankle prostheses enable natural ambulation on level ground and stairs for individuals with bilateral above-knee amputation: a case study," (in eng), *Sci Rep,* vol. 12, no. 1, p. 15465, Sep 14 2022, doi: 10.1038/s41598-022-19701-8.

[169] M. Liu, F. Zhang, P. Datseris, and H. Huang, "Improving finite state impedance control of active-transfemoral prosthesis using Dempster-Shafer based state transition rules," *Journal of Intelligent & Robotic Systems,* vol. 76, no. 3-4, pp. 461-474, 2014/12/01 2013, doi: 10.1007/s10846-013-9979-3.

[170] J. J. Carollo and D. Matthews, "Strategies for clinical motion analysis based on functional decomposition of the gait cycle," *Phys Med Rehabil Clin N Am,* vol. 13, no. 4, pp. 949-77, Nov 2002, doi: 10.1016/s1047-9651(02)00029-3.

[171] L. Frossard, L. Cheze, and R. Dumas, "Dynamic input to determine hip joint moments, power and work on the prosthetic limb of transfemoral amputees: ground reaction vs knee reaction," *Prosthet Orthot Int,* vol. 35, no. 2, pp. 140-9, Jun 2011, doi: 10.1177/0309364611409002.

[172] M. Anand, J. Seipel, and S. Rietdyk, "A modelling approach to the dynamics of gait initiation," *J R Soc Interface,* vol. 14, no. 128, p. 20170043, Mar 2017, doi: 10.1098/rsif.2017.0043.

[173] S. Leteneur, E. Simoneau, C. Gillet, Y. Dessery, and F. Barbier, "Trunk's natural inclination influences stance limb kinetics, but not body kinematics, during gait initiation in able men," *PLoS One,* vol. 8, no. 1, p. e55256, 2013, doi: 10.1371/journal.pone.0055256.

[174] R. E. Seroussi, A. Gitter, J. M. Czerniecki, and K. Weaver, "Mechanical work adaptations of above-knee amputee ambulation," *Arch Phys Med Rehabil,* vol. 77, no. 11, pp. 1209-14, Nov 1996, doi: 10.1016/s0003-9993(96)90151-3.

[175] A. R. De Asha and J. G. Buckley, "The effects of walking speed on minimum toe clearance and on the temporal relationship between minimum clearance and peak swing-foot velocity in unilateral trans-tibial amputees," *Prosthet Orthot Int,* vol. 39, no. 2, pp. 120-5, Apr 2015, doi: 10.1177/0309364613515493.

[176] A. D. Kuo and J. M. Donelan, "Dynamic principles of gait and their clinical implications," *Phys Ther,* vol. 90, no. 2, pp. 157-74, Feb 2010, doi: 10.2522/ptj.20090125.

[177] B. F. Mentiplay, M. Banky, R. A. Clark, M. B. Kahn, and G. Williams, "Lower limb angular velocity during walking at various speeds," *Gait Posture,* vol. 65, pp. 190-196, Sep 2018, doi: 10.1016/j.gaitpost.2018.06.162.

[178] M. Garcia, A. Chatterjee, A. Ruina, and M. Coleman, "The simplest walking model: stability, complexity, and scaling," *J Biomech Eng,* vol. 120, no. 2, pp. 281-8, Apr 1998, doi: 10.1115/1.2798313.

[179] R. L. McGrath, M. L. Ziegler, M. Pires-Fernandes, B. A. Knarr, J. S. Higginson, and F. Sergi, "The effect of stride length on lower extremity joint kinetics at various gait speeds," *PLoS One,* vol. 14, no. 2, p. e0200862, 2019, doi: 10.1371/journal.pone.0200862.

[180] F. Golshan, N. Baddour, H. Gholizadeh, and E. D. Lemaire, "A pelvic kinematic approach for calculating hip angles for active hip disarticulation prosthesis control," *J Neuroeng Rehabil,* vol. 20, no. 1, p. 152, Nov 9 2023, doi: 10.1186/s12984-023-01273-x.

[181] C. Howard, C. Wallace, and D. S. Stokic, "Stride length-cadence relationship is disrupted in below-knee prosthesis users," *Gait Posture,* vol. 38, no. 4, pp. 883-7, Sep 2013, doi: 10.1016/j.gaitpost.2013.04.008.

[182] T. Egerton, M. Danoudis, F. Huxham, and R. Iansek, "Central gait control mechanisms and the stride length - cadence relationship," *Gait Posture,* vol. 34, no. 2, pp. 178-82, Jun 2011, doi: 10.1016/j.gaitpost.2011.04.006.

[183] L. Hak, H. Houdijk, P. J. Beek, and J. H. van Dieen, "Steps to take to enhance gait stability: the effect of stride frequency, stride length, and walking speed on local dynamic stability and margins of stability," *PLoS One,* vol. 8, no. 12, p. e82842, 2013, doi: 10.1371/journal.pone.0082842.

[184] D. W. Grieve and R. J. Gear, "The relationships between length of stride, step frequency, time of swing and speed of walking for children and adults," *Ergonomics,* vol. 9, no. 5, pp. 379-99, Sep 1966, doi: 10.1080/00140136608964399.

[185] Y. Breniere and M. C. Do, "When and how does steady state gait movement induced from upright posture begin?," *J Biomech,* vol. 19, no. 12, pp. 1035-40, 1986, doi: 10.1016/0021-9290(86)90120-x.

[186] E. J. Roth, C. Merbitz, K. Mroczek, S. A. Dugan, and W. W. Suh, "HEMIPLEGIC GAIT: Relationships between walking speed and other temporal parameters," *American Journal of Physical Medicine & Rehabilitation,* vol. 76, no. 2, pp. 128-133, 1997. [Online]. Available: https://journals.lww.com/ajpmr/fulltext/1997/03000/hemiplegic_gait__relationships_between_walking.8.aspx.

[187] T. Kawaguchi, T. Yamada, and K. Iwashita, "Biomechanical gait analysis for a hip disarticulation prosthesis: power source for the swing phase of a hip disarticulation prosthetic limb," (in eng), *J Phys Ther Sci,* vol. 35, no. 5, pp. 361-365, May 2023, doi: 10.1589/jpts.35.361.

[188] S. Blumentritt, "A new biomechanical method for determination of static prosthetic alignment," *Prosthetics and Orthotics International,* vol. 21, no. 2, pp. 107-113, 1997/01/01 1997, doi: 10.3109/03093649709164538.

[189] M. Bellmann, S. Blumentritt, M. Pusch, T. Schmalz, and M. Schönemeier, "The 3D LASAR—a new generation of static analysis for optimising prosthetic and orthotic alignment," *Orthop Tech,* vol. 12, pp. 18-25, 2017.

[190] E. Bergamini, A. Cereatti, and G. Pavei, "Walking symmetry is speed and index dependent," *Scientific Reports,* vol. 14, no. 1, p. 19548, 2024/08/22 2024, doi: 10.1038/s41598-024-69461-w.

[191] J. A. Zeni, J. G. Richards, and J. S. Higginson, "Two simple methods for determining gait events during treadmill and overground walking using kinematic data," *Gait & Posture,* vol. 27, no. 4, pp. 710-714, 2008/05/01/ 2008, doi: https://doi.org/10.1016/j.gaitpost.2007.07.007.

[192] S. Viteckova, P. Kutilek, Z. Svoboda, R. Krupicka, J. Kauler, and Z. Szabo, "Gait symmetry measures: A review of current and prospective methods," *Biomedical Signal Processing and Control,* vol. 42, pp. 89-100, 2018/04/01/ 2018, doi: https://doi.org/10.1016/j.bspc.2018.01.013.

[193] M. Mortezanejad, Z. Ebrahimabadi, A. Rahimi, A. Maleki, A. A. Baghban, and F. Ehsani, "Postural adjustment and muscle activity during each phase of gait initiation in chronic ankle instability: an observational study," *BMC Sports Science, Medicine and Rehabilitation,* vol. 16, no. 1, 2024, doi: 10.1186/s13102-024-01033-x.

[194] A. Saif, R. Francis, J. Sullivan, and I. Sedki, "Factors affecting successful prosthetic use after hemipelvectomy and hip disarticulation amputations: Five-year experience from a tertiary prosthetic rehabilitation center," (in eng), *Prosthet Orthot Int,* vol. 48, no. 1, pp. 20-24, Jan 1 2024, doi: 10.1097/PXR.0000000000000226.

[195] M. J. Highsmith *et al.*, "Correlations between residual limb length and joint moments during sitting and standing movements in transfemoral amputees," *Prosthetics and Orthotics International,* vol. 40, no. 4, pp. 522-527, 2016, doi: 10.1177/0309364614564025.

[196] H. Burger, J. Kuželicki, and C. Marincek, "Transition from sitting to standing after trans-femoral amputation," *Prosthetics and Orthotics International,* vol. 29, no. 2, pp. 139-151, 2005, doi: 10.1080/03093640500199612.

[197] J. Kim, C. L. McDonald, B. J. Hafner, and A. Sawers, "Fall-related events in people who are lower limb prosthesis users: the lived experience," *Disability and Rehabilitation,* vol. 44, no. 15, pp. 3897-3908, 2022, doi: 10.1080/09638288.2021.1891467.

[198] F. Gao, F. Zhang, and H. Huang, "Investigation of sit-to-stand and stand-to-sit in an above knee amputee," (in eng), *Annu Int Conf IEEE Eng Med Biol Soc,* vol. 2011, pp. 7340-3, 2011, doi: 10.1109/iembs.2011.6091712.

[199] L. Yi-Ting and L. Heng-Ju, "Comparison of the lower extremity kinematics and center of mass variations in sit-to-stand and stand-to-sit movements of older fallers and nonfallers," *Archives of Rehabilitation Research and Clinical Translation,* vol. 4, no. 1, p. 100181, 2022/03/01/ 2022, doi: https://doi.org/10.1016/j.arrct.2022.100181.

[200] K. M. Kerr, J. A. White, D. A. Barr, and R. A. B. Mollan, "Analysis of the sit-stand-sit movement cycle in normal subjects," *Clinical Biomechanics,* vol. 12, no. 4, pp. 236-245, 1997/06/01/ 1997, doi: https://doi.org/10.1016/S0268-0033(96)00077-0.

[201] M. J. Highsmith, J. T. Kahle, S. L. Carey, D. J. Lura, R. V. Dubey, and W. S. Quillen, "Kinetic differences using a Power Knee and C-Leg while sitting down and standing up: A Case report," *JPO Journal of Prosthetics and Orthotics,* vol. 22, no. 4, pp. 237-243, 2010, doi: 10.1097/JPO.0b013e3181f46b65.

[202] C. G. Welker, T. K. Best, and R. D. Gregg, "Improving sit/stand loading symmetry and timing through unified variable impedance control of a powered knee-ankle prosthesis," *IEEE Transactions on Neural Systems and Rehabilitation Engineering,* vol. 31, pp. 4146-4155, 2023, doi: 10.1109/TNSRE.2023.3320692.

[203] M. J. Highsmith *et al.*, "Kinetic asymmetry in transfemoral amputees while performing sit to stand and stand to sit movements," *Gait & Posture,* vol. 34, no. 1, pp. 86-91, 2011/05/01/ 2011, doi: https://doi.org/10.1016/j.gaitpost.2011.03.018.

[204] A. M. Simon, S. B. Finucane, A. J. Ikeda, R. J. Cotton, and L. J. Hargrove, "Powered knee and ankle prosthesis use with a K2 level ambulator: a case report," *Frontiers in Rehabilitation Sciences,* vol. 4, 2023, doi: 10.3389/fresc.2023.1203545.

[205] J. H. Carr, "Balancing the centre of body mass during standingup," *Physiotherapy Theory and Practice,* vol. 8, pp. 159-164, 1992.

[206] R. B. Shepherd and A. M. Gentile, "Sit-to-stand: Functional relationship between upper body and lower limb segments," *Human Movement Science,* vol. 13, no. 6, pp. 817-840, 1994/12/01/ 1994, doi: 10.1016/0167-9457(94)90020-5.

[207] Theia3d. "Theia3D documentation." Theia3d. https://www.theiamarkerless.ca/docs/index.html# (accessed 12,16, 2024).

[208] E. S. Grood and W. J. Suntay, "A joint coordinate system for the clinical description of three-dimensional motions: application to the knee," (in eng), *J Biomech Eng,* vol. 105, no. 2, pp. 136-44, May 1983, doi: 10.1115/1.3138397.

Appendix A

This section displays the data acquisition schematics from Chapter 3.3

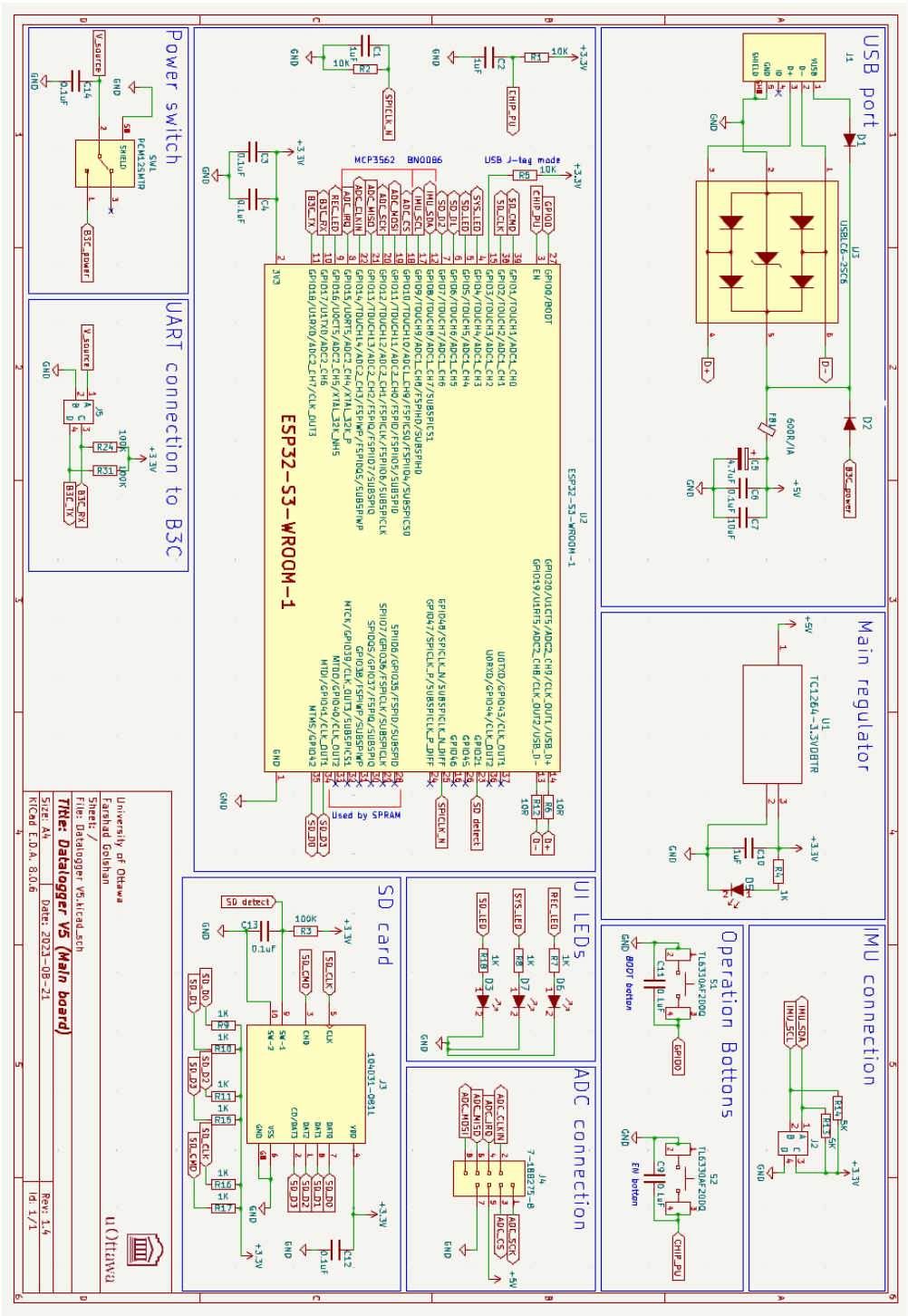

Fig. A.1 Electronics schematic of the main data acquisition board.

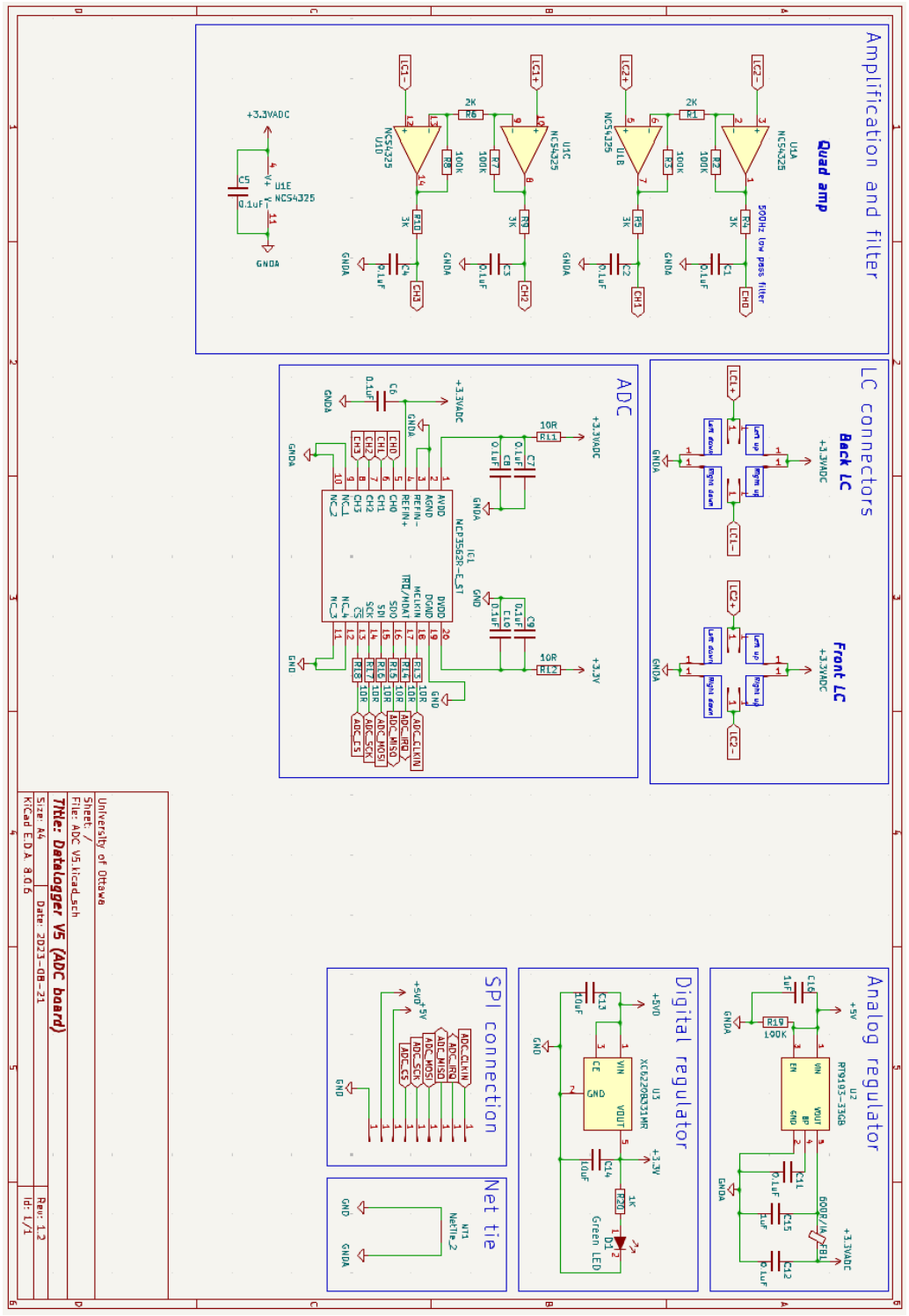

Fig. A.2 Electronics schematics of the load cell ADC board.

Appendix B

Real-time hip angle calculation algorithm

Sequence 1: Foot-strike to pelvic rotation zero-crossing time

$$CH\theta(t) = H\theta_{FS} + (P1\omega_{\alpha} \times t),\ 0 < t \leq PR\tau_{ZC1}$$

where t is the gait time initiated at foot-strike (t=0 is foot-strike instant), CHθ(t) is the calculated hip angle throughout the gait time, $P1\omega_{\alpha}$ is the period 1 calculated constant angular velocity at foot-strike.

$$P1\omega_{\alpha} = \frac{\overline{H\theta}_{ME} - H\theta_{FS}}{\acute{H}\tau_{ME} - \tau_{FS}}$$

where $\overline{H\theta}_{ME}$ is the per-person hip max extension angle constant, $H\theta_{FS}$ is the hip angle at foot-strike, $\acute{H}\tau_{ME}$ is past-stride hip max extension time, and τ_{FS} is the foot-strike time. $\overline{H\theta}_{ME}$ was determined for each participant based on their averaged hip max extension angle across all strides.

Sequence 2: pelvic rotation zero-crossing time to pelvic tilt zero-crossing time

$$CH\theta(t) = CH\theta(PR\tau_{ZC}) + \left(P1\omega_{\beta} \times t\right),\ PR\tau_{ZC1} < t \leq PT\tau_{ZC}$$

where $PR\tau_{ZC}$ is the pelvic rotation first zero-crossing time, $PT\tau_{ZC}$ is the pelvic tilt zero-crossing time, and $P1\omega_{\beta}$ is the calculated period 1 calculated constant angular velocity when $PR\tau_{ZC}$ is achieved.

$$P1_{\omega\beta} = 70 + 2.177 \times \left(\frac{\Delta H\theta}{PR\tau_{ZC} - \tau_{FS}} + P1\omega_{\alpha}\right) \div 2$$

where $P1\omega_{\beta}$ is the calculated constant angular velocity for sequence 2, $P1\omega_{\alpha}$ is the sequence 1 calculated constant angular velocity, τ_{FS} is the foot-strike time, and $PR\tau_{ZC}$ is the pelvic rotation first zero-crossing time.

Constant values (70, 2.177) were obtained from the correlation analysis in thesis Section 4.3.2.

Sequence 3: pelvic tilt zero-crossing time to hip max extension time

$$CH\theta(t) = CH\theta(PT\tau_{ZC}) + \left(P1\omega_{\beta} \times t\right), PT\tau_{ZC1} < t \leq H\tau_{ME}$$

Sequence 4: hip max extension time to stance time

$$CH\theta(t) = CH\theta(H\tau_{ME}) + (P2\omega_{\alpha} \times t),\ H\tau_{ME} < t \leq \tau_{S}$$

where $P2\omega_{\alpha}$ is the calculated constant angular velocity at sequence 4, $H\tau_{ME}$ is the calculated hip max extension time, and τ_S is the foot-off time.

$$P2\omega_{\alpha} = \frac{\overline{H\theta}_{MF} - CH\theta(H\tau_{ME})}{H\tau_{MF\alpha} - H\tau_{ME}}$$

where $\overline{H\theta}_{MF}$ is the per-participant hip max flexion angle constant, $CH\theta(H\tau_{ME})$ is the calculated hip max extension angle at sequence 3, $H\tau_{MF\alpha}$ is the calculated hip max flexion time, and $H\tau_{ME}$ is the calculated hip max extension time.

Sequence 5: Stance time to hip max flexion time

$$CH\theta(t) = CH\theta(\tau_{FO}) + \left(P2\omega_{\beta} \times t\right),\ \tau_{S} < t \leq H\tau_{MF\beta}$$

where $P2\omega_{\beta}$ is the calculated period 2 calculated constant angular velocity when τ_S is achieved, $H\tau_{MF\beta}$ is the hip max flexion time, and τ_{FO} is the foot-off time.

Sequence 6: hip max flexion time to next foot-strike

$$CH\theta(t) = CH\theta\left(H\tau_{MF\beta}\right),\ H\tau_{MF\beta} < t$$

Appendix C

Tuned Power Hip gait control parameters

Finite state machine thresholds:

- $th_1 = -0.9$
- $th_2 = 0.9$
- $th_3 = 0.5$

Hip flexion states parameters:

- $r_{\theta flexion} = 0.4$
- $\theta_{\text{Max ROM}} = 45$
- $S_C = 30$
- $r_{ZC} = 0.3$
- $b_{ZC} = 0.1461$
- $r_{Stance} = 0.3$
- $b_{Stance} = 0.0874$

Hip extension state parameters:

- $r_{ST1\ time} = 0.5$

Table C.1 Impedance-based controller tuned gains for each gait subphase

	GI	**ST1**	**ST2**	**ST3**	**SW1**	**SW2**
K gain	23.0	4.0	20.0	1.0	0.5	6.0
B gain	0.1	2.0	0.0	0.5	0.1	1.0

Appendix D

List of tuned Power Hip sit-to-stand and stand-to-sit control parameters

Tunable control parameters

- $\theta_{ST\_Phase1} = 10$
- $h_{ST\_Phase2} = 10$
- $C_{ST\_Phase2} = 0.6$
- $\omega_{SI\_Phase1} = -10$
- $\theta_{SI\_Phase2} = 30$
- $C_{SI\_Phase3} = 3$
- $h_{SI\_Phase3} = 10$

Table D.2 Impedance-based controller tuned gains for each sit-to-stand and stand-to-sit phases

	Phase 1	**Phase 2**	**Phase 3**	**Phase 4**
Sit-to-stand				
K gain	0.2	5.0	10.0	23.0
B gain	0.0	3.0	0.5	0.0
Stand-to-sit				
K gain	20.0	40.0	2.0	0.0
B gain	1.0	0	1.0	0.0